

**Cell targeting and imaging
using magnetic nanoparticles**

Panagiotis Kyrtatos

**Submitted for the degree of
Doctor of Philosophy in Biophysics**

September 2009

**Royal College of Surgeons Unit of Biophysics,
Institute of Child Health**

and

**Centre for Advanced Biomedical Imaging,
Department of Medicine & Institute of Child Health**

University College London

DECLARATION

I, Panagiotis Kyrtatos, confirm that the work presented in this thesis is my own work, except where acknowledged in the text. This work is based on research that was undertaken by me at University College London, during the period 1st January 2006 to 20th September 2009.

Panagiotis Kyrtatos

7th June 2010

ABSTRACT

BACKGROUND AND AIMS. The success of stem cell therapies partly depends on the ability to deliver the cells to the site of injury. Circulating endothelial progenitor cells (EPCs) are involved in physiological processes such as vascular re-endothelialisation and post-ischaemic neovascularisation and have been utilised in several clinical trials. Superparamagnetic iron oxide particles have previously been used to label and track cells using magnetic resonance imaging (MRI), as well as to magnetically attract drugs and cells to desired sites. The aim of this PhD was to develop a methodology to magnetically attract EPCs, labelled with a clinically approved iron oxide agent, to a site of arterial injury using magnetic fields originating outside the body.

METHODS AND RESULTS. Human EPCs were cultured in the presence of iron oxide superparamagnetic nanoparticles. A labelling method was developed that retained cell survival and differentiation, as indicated by metabolic activity and flow cytometry assays, as well as MRI visibility. Finite element modelling (FEM) computer simulations were performed to investigate the interaction of magnetic forces with hydrodynamic drag forces. FEM indicated successful external magnetic cell targeting from a vessel with flow rate similar to a rat common carotid artery; correspondingly there was a 6-fold increase in cell capture in an *in vitro* flow system. Angioplasty was performed on rat common carotid arteries to denude the endothelium and EPCs were administered with and without the presence of the external magnetic device during a 10 minute period of flow cessation. Targeting enhanced cell retention at the site of injury by 5-fold.

CONCLUSIONS. Using an externally applied magnetic device, it is possible to enhance EPC localisation in a flowing system *in vitro* and to a flow-isolated site of common carotid artery injury *in vivo*, without affecting cell viability or differentiation in culture. This technology could be more widely adapted to localise and monitor cells in other organs and may provide a useful tool for systemic injection of cell therapies.

ACKNOWLEDGEMENTS

First and foremost I am indebted to my close collaborators on this project, Dr Ana Garcia-Prieto and Dr Manfred Junemann-Ramirez. Their presence opened up new frontiers in the development of this truly multi-disciplinary work. Without their help and support, some the studies presented here would have been impossible to surmount.

My supervisors Dr Mark Lythgoe, Professor Quentin Pankhurst and Dr Pauliina Lehtolainen, as well as Professor David Gadian, have provided endless support throughout the project, and have made my PhD studies a truly enjoyable experience, both in and outside of the lab. They have provided a working environment that would be envied by many, such that I will always miss being their student.

Many thanks also go to all the students and post-docs that I had the pleasure to meet and work with throughout my studies, in particular (but in no particular order!) Mankin Choy, Ken Cheung, Jon Orlando Solas Hawke Cleary, Rachael Dobson, Jack Wells, Michael Loebinger, Mathew Kallumadil, Paul Southern, Tamsin Langley, Kim Vigor, Bernard Siow, Martin King, Anthony Price Tatjana Holland and Johannes Riegler. Special thanks to Stuart Ings for his endless help in acquiring blood samples.

I am also especially thankful to Sally Dowsett and Sati Sahota at the RCS Unit of Biophysics in ICH, whose endless assistance has accompanied me since my first hours at the department. There was never a day they did not greet me with a smile.

I am grateful for the financial support provided from the Institute of Child Health Child Health Research Appeal Trust (CHRAT) and the Alexander S. Onassis Public Benefit Foundation, as well as the Biotechnology and Biomedical Sciences Research Council grant. Without them, my endeavours in academic medicine would have been in vain.

Finally, my eternal gratitude to my family, for I am who they made me be.

PUBLICATIONS ARISING FROM THIS THESIS

Kyrtatos PG, Lehtolainen P, Junemann-Ramirez M, Garcia-Prieto A, Price AN, Martin JF, Gadian DG, Pankhurst QA, Lythgoe MF. Magnetic tagging increases delivery of circulating progenitors in vascular injury. *JACC Cardiovasc Interv.* 2009; 2(8):794-802.

Published abstracts:

Kyrtatos P *et al.* Magnetic targeting of stem cells to a site of vascular injury using an MRI contrast agent. *16th Annual Meeting of the International Society for Magnetic Resonance in Medicine (ISMRM)*. May 2008. Toronto, Canada

Kyrtatos P *et al.* Magnetic targeting of stem cells to a site of vascular injury using an MRI contrast agent. *13th Annual Meeting of the British Chapter of the ISMRM*. September 2007. Birmingham, United Kingdom

Kyrtatos P *et al.* Ferumoxide labelling of CD133+ cells for targeted re-endothelialisation. *15th Annual Meeting of the ISMRM*. May 2007. Berlin, Germany

Kyrtatos P *et al.* Magnetic targeting of stem cells for endothelial regeneration using an MRI contrast agent. *16th Annual Nuclear Magnetic Resonance Symposium*. March 2007. Oxford, United Kingdom

THESIS OUTLINE

This thesis deals with the development of a method for magnetic attraction of cells to a desired site in the body, using external magnetic fields. Specifically, endothelial progenitor cells are investigated, as they are thought to play an important role in the vascular healing process. The thesis is comprised of three introductory chapters and four experimental chapters.

Chapter 1 is an introduction to stem cells and cardiovascular disease, in particular atherosclerosis and the role of the endothelial progenitor cells in maintaining the vasculature. Here I present animal studies and clinical trials that investigate the utility of these cells, as well as the need for specific cell targeting and current targeting strategies.

Chapter 2 deals with the current use of superparamagnetic iron oxide particles for cell labelling, particularly in the context of magnetic resonance imaging. In this section I describe the basics of magnetic resonance imaging and generation of image contrast, and review cell labelling methodologies.

Chapter 3 starts with a review of the utility of magnetic targeting in the medical sciences, after which I deal with the basic concepts of magnetism and fluid dynamics used in within the thesis.

In **Chapters 4 and 5** I present the development of a labelling methodology, called “differential labelling”, which is particularly concerned with the maintenance of cell viability after magnetic attraction.

Chapter 6 describes my studies on the development of a suitable magnetic device, computer modelling and *in vitro* testing, in both static and flowing scenarios.

In **Chapter 7** an animal study is presented, which was designed to mimic the current methodology used in clinical trials for the administration of progenitor cells in the heart. In this study I investigated whether magnetic targeting can enhance cell delivery *in vivo*.

TABLE OF CONTENTS

<i>Declaration</i>	- 2 -
<i>Abstract</i>	- 3 -
<i>Acknowledgements</i>	- 4 -
<i>Publications arising from this thesis</i>	- 5 -
<i>Thesis outline</i>	- 6 -
<i>Table of contents</i>	- 7 -
<i>List of figures</i>	- 11 -
<i>List of tables</i>	- 13 -
<i>Abbreviations</i>	- 14 -
CHAPTER 1	- 15 -
<i>Stem cells and cardiovascular disease</i>	- 15 -
1.1 Introduction	- 16 -
1.2 Stem cells – an overview	- 18 -
1.2.1 Embryonic stem cells	- 18 -
1.2.2 Adult stem cells	- 19 -
1.3 Cardiovascular disease	- 24 -
1.3.1 The burden of cardiovascular diseases	- 24 -
1.3.2 Atherosclerosis	- 24 -
1.4 Endothelial progenitor cells in cardiovascular disease	- 37 -
1.4.1 Introduction	- 37 -
1.4.2 Emergence of the term ‘EPC’	- 38 -
1.4.3 Identifying the EPC	- 38 -
1.4.4 Role of the EPC	- 42 -
1.4.5 Mobilisation and homing of EPCs to sites of injury	- 43 -
1.4.6 Enhancing recruitment, homing and retention of EPCs	- 45 -
1.5 Summary	- 48 -
CHAPTER 2	- 50 -
2.1 Introduction	- 51 -
2.2 Basic principles of MRI	- 52 -
2.2.1 The source of the signal that produces the image	- 52 -
2.2.2 Nuclear magnetic resonance	- 52 -
2.2.3 Relaxation	- 55 -
2.2.4 Acquiring the signal	- 57 -
2.2.5 Spatial localisation of the MR signal	- 58 -
2.3 Superparamagnetic MRI contrast agents	- 60 -
2.3.1 Introduction	- 60 -
2.3.2 Endorem for <i>in vivo</i> contrast enhancement in humans	- 62 -

2.3.3 SPIOs for cellular tracking <i>in vivo</i>	- 62 -
2.3.4 <i>In vitro</i> SPIO labelling methods	- 65 -
2.4 Summary	- 66 -
CHAPTER 3	- 67 -
3.1 Introduction	- 68 -
3.2 Magnetic targeting in medicine	- 69 -
3.2.1 Laboratory uses of magnetic targeting	- 69 -
3.2.2 Magnetic drug targeting	- 69 -
3.2.3 Magnetic cell targeting	- 70 -
3.3 Basics of magnetics	- 76 -
3.3.1 Magnetic fields	- 76 -
3.3.2 Magnetisation of materials	- 78 -
3.3.3 Magnetic forces	- 82 -
3.4 Fluid dynamics	- 86 -
3.4.1 Introduction	- 86 -
3.4.2 Basic concepts	- 86 -
3.4.3 Turbulent vs laminar flow	- 87 -
3.4.4 Hydrodynamic drag on a sphere	- 91 -
3.5 Summary	- 93 -
CHAPTER 4	- 94 -
4.1 Chapter overview	- 95 -
4.2 – Part I: Labelling CD133 cells with Endorem®	- 96 -
4.2.1 Background and aims	- 96 -
4.2.2 Methods	- 98 -
4.2.3 Results	- 104 -
4.2.4 Discussion	- 109 -
4.2.5 Conclusions	- 112 -
4.3 – Part II: Magnetic attraction and viability	- 113 -
4.3.1 Background and aims	- 113 -
4.3.2 Methods	- 115 -
4.3.3 Results	- 117 -
4.3.4 Discussion	- 126 -
4.3.5 Conclusions	- 127 -
CHAPTER 5	- 128 -
5.1 Introduction	- 129 -
5.2 Methods	- 130 -
5.2.1 Cell culture and labelling	- 130 -
5.2.2 Viability assay after 10min attraction with stacked magnets	- 130 -
5.2.3 Water evaporation	- 131 -
5.2.4 Growth assay post DfL and magnetic attraction	- 131 -

5.2.5 Apoptosis assays	- 131 -
5.2.6 Flow cytometry for cell differentiation	- 132 -
5.2.7 SQUID for iron quantification	- 133 -
5.2.8 <i>In vitro</i> MRI	- 133 -
5.2.9 Statistical analyses	- 134 -
5.3 Results	- 135 -
5.3.1 Viability assay after 10min attraction with stacked magnets	- 135 -
5.3.2 Cellular growth after DfL and magnetic attraction	- 136 -
5.3.3 Cellular apoptosis after differential labelling	- 137 -
5.3.4 Cellular apoptosis after magnetic attraction	- 138 -
5.3.5 Cell differentiation after differential labelling	- 140 -
5.3.6 Iron quantification using SQUID	- 142 -
5.3.7 Estimation of a cell-safe magnetic force	- 145 -
5.3.8 <i>In vitro</i> MRI	- 146 -
5.4 Discussion	- 147 -
5.4.1 Main findings	- 147 -
5.4.2 Magnetic forces	- 147 -
5.4.3 Cell viability and differentiation	- 148 -
5.5 Conclusions	- 150 -
CHAPTER 6	- 151 -
6.1 Introduction	- 152 -
6.2 Methods	- 153 -
6.2.1 Cell culture	- 153 -
6.2.2 <i>In vitro</i> actuation in a static liquid	- 154 -
6.2.3 Magnetic actuator (Halbach array)	- 154 -
6.2.4 Computer simulations	- 154 -
6.2.5 <i>In vitro</i> flow system	- 155 -
6.2.6 Statistical analyses	- 155 -
6.3 Results	- 156 -
6.3.1 Cell actuation in a static liquid	- 156 -
6.3.2 Design and construction of the magnetic actuator	- 158 -
6.3.3 Effect of the SPIO magnetisation saturation	- 161 -
6.3.4 Consideration of the 'cell-safe' force	- 163 -
6.3.5 Finite element modelling of cell targeting	- 165 -
6.3.6 <i>In vitro</i> flow system	- 167 -
6.4 Discussion	- 173 -
6.4.1 Main findings	- 173 -
6.4.2 Fluid dynamics simulations	- 173 -
6.4.3 <i>In vitro</i> flow system	- 174 -
6.5 Conclusions	- 177 -
CHAPTER 7	- 178 -

7.1 Introduction	- 179 -
7.2 Methods	- 180 -
7.2.1 Cell culture and Endorem® labelling	- 180 -
7.2.2 Vascular injury	- 180 -
7.2.3 Cell administration and magnetic targeting	- 180 -
7.2.4 Confocal microscopy	- 181 -
7.2.5 Quantification of cell engraftment	- 181 -
7.2.6 Statistical analyses	- 181 -
7.3 Results	- 182 -
7.3.1 Methodological setup	- 182 -
7.3.2 CD133 cell engraftment to the rat common carotid artery	- 184 -
7.4 Discussion	- 188 -
7.5 Conclusions	- 190 -
<i>Thesis summary</i>	- 191 -
<i>Bibliography</i>	- 195 -
<u>Appendix A - Methodological developments</u>	- 216 -
<u>Appendix B - Full Tables</u>	- 222 -
<u>Appendix C - MTS assay</u>	- 226 -

LIST OF FIGURES

<i>Figure 1.1 – Prometheus and Atlas, ca. 550 BC</i>	- 17 -
<i>Figure 1.2 – Stem cells and their progeny in adult tissue</i>	- 20 -
<i>Figure 1.3 – Anatomy of the artery</i>	- 26 -
<i>Figure 1.4 – Lesion initiation</i>	- 28 -
<i>Figure 1.5 – Development of the ‘fatty streak’</i>	- 28 -
<i>Figure 1.6 – Advanced lesion</i>	- 30 -
<i>Figure 1.7 – Unstable lesion</i>	- 30 -
<i>Figure 1.8 – PCI. a) PTCA b) PTCA + stenting</i>	- 33 -
<i>Figure 1.9 – In-stent stenosis due to NI formation</i>	- 35 -
<i>Figure 1.10 – Origin and differentiation of the EPC</i>	- 41 -
<i>Figure 1.11 – Mobilisation and homing of EPCs in neo-vascularisation</i>	- 44 -
<i>Figure 2.1 – The source of net magnetisation</i>	- 54 -
<i>Figure 2.2 – Precession and application of a 90° RF pulse</i>	- 54 -
<i>Figure 2.3 – T₁ relaxation</i>	- 56 -
<i>Figure 2.4 – T₂ relaxation</i>	- 56 -
<i>Figure 2.5 – Endorem® structure and superparamagnetism</i>	- 61 -
<i>Figure 2.6 – Contrast enhancement of liver lesions using Endorem®</i>	- 63 -
<i>Figure 2.7 – MR visualisation of CD34+ cells in the mouse bone marrow</i>	- 64 -
<i>Figure 2.8 – MRI of CD133+ cells trafficking to a site of tumour angiogenesis</i>	- 64 -
<i>Figure 3.1 – Magnetic cell spelling</i>	- 72 -
<i>Figure 3.2 – Star formations with magnetic cells</i>	- 72 -
<i>Figure 3.3 – Magnetic field around a moving electron</i>	- 77 -
<i>Figure 3.4 – Magnetic field around a permanent magnet</i>	- 77 -
<i>Figure 3.5 – Magnetisation vs magnetic field strength (M-H) curves</i>	- 81 -
<i>Figure 3.6 – SQUID M-H curve of a sample of Endorem®</i>	- 85 -
<i>Figure 3.7 – Laminar and turbulent flow visualisation</i>	- 88 -
<i>Figure 3.8 – Choice of velocity and length scales used in calculating Re</i>	- 88 -
<i>Figure 3.9 – Parabolic flow between two parallel plates</i>	- 90 -
<i>Figure 3.10 – The relationship between C_D and Re</i>	- 92 -
<i>Figure 3.11 – The Khan and Richardson prediction for C_D</i>	- 92 -
<i>Figure 4.1 – PrB stain of whole d11-CD133 population</i>	- 100 -
<i>Figure 4.2 – PrB stain of adherent d11-CD133s.</i>	- 100 -
<i>Figure 4.3 – PrB positivity of CD133 cell subtypes</i>	- 104 -
<i>Figure 4.4 – Bland-Altman plot of two counts</i>	- 106 -
<i>Figure 4.5 – Labelling timecourse - cellular iron content</i>	- 108 -
<i>Figure 4.6 – Design and construction of the magnetic plate</i>	- 118 -
<i>Figure 4.7 – Particle attraction toward the magnet edges</i>	- 119 -
<i>Figure 4.8 – Placement of cell samples on top of disk magnets</i>	- 120 -
<i>Figure 4.9 – Increase in applied force with stacked configuration</i>	- 121 -
<i>Figure 4.10 – Viability of StL cells following 24h magnetic attraction</i>	- 122 -
<i>Figure 4.11 – Viability following 24h magnetic attraction</i>	- 124 -
<i>Figure 4.12 – Photomicrographs of cells following magnetic actuation</i>	- 125 -

<i>Figure 5.1– MTS assays following 10 min magnetic attraction of DfL cells</i>	- 135 -
<i>Figure 5.2 – Cell proliferation post DfL and magnetic attraction</i>	- 136 -
<i>Figure 5.3 – Apoptosis rates after differential labelling</i>	- 137 -
<i>Figure 5.4 – Apoptosis differences after differential labelling</i>	- 137 -
<i>Figure 5.5 – Apoptosis rates after magnetic attraction</i>	- 138 -
<i>Figure 5.6 – Apoptosis difference after magnetic attraction</i>	- 138 -
<i>Figure 5.7 – Sample cytometry scatterplots for the apoptosis assays</i>	- 139 -
<i>Figure 5.8 – Surface marker expression after DfL</i>	- 140 -
<i>Figure 5.9 – Sample cytometry scatterplots for the CD14 surface marker analysis</i>	- 141 -
<i>Figure 5.10 – SQUID loop of an Endorem® sample at 300K.</i>	- 142 -
<i>Figure 5.11 – Close up of SQUID loop for Endorem® at 300K</i>	- 142 -
<i>Figure 5.12 – Close up of SQUID loop for Endorem® at 10K</i>	- 143 -
<i>Figure 5.13 – Close up of SQUID loop for 5x10⁵ DfL cells at 10K</i>	- 143 -
<i>Figure 5.14 – In vitro MRI phantom of DfL-CD133s</i>	- 146 -
<i>Figure 6.1 – Actuation of Endorem®-labelled MNC in a static suspension</i>	- 157 -
<i>Figure 6.2 – Halbach array</i>	- 159 -
<i>Figure 6.3 - Halbach array versus disk magnets</i>	- 160 -
<i>Figure 6.4 – Magnetic field strength and magnetisation saturation</i>	- 161 -
<i>Figure 6.5 – Selection of force expression</i>	- 162 -
<i>Figure 6.6 – Switch in force expression</i>	- 162 -
<i>Figure 6.7 – Magnetic force on cells: Halbach vs disk magnets</i>	- 164 -
<i>Figure 6.8 – The constructed 5-magnet array</i>	- 164 -
<i>Figure 6.9 – FEM simulation: cell capture at 1mm</i>	- 165 -
<i>Figure 6.10 – Cell capture simulations at 1mm and 5mm</i>	- 166 -
<i>Figure 6.11 – In vitro flow system setup</i>	- 167 -
<i>Figure 6.12 – Cell capture at 1mm, 1ml/min</i>	- 168 -
<i>Figure 6.13 – Forces along 1mm horizontal line</i>	- 170 -
<i>Figure 6.14 – Cell capture at 1mm with 10ml/min flow</i>	- 170 -
<i>Figure 6.15 – Cell capture counts at 1mm with 10ml/min flow</i>	- 171 -
<i>Figure 6.16 – Targeting at 5mm</i>	- 172 -
<i>Figure 7.1 – Methodological setup</i>	- 183 -
<i>Figure 7.2 – Representative CCA confocal scans</i>	- 185 -
<i>Figure 7.3 – Confocal image of a single DfL-CD133</i>	- 186 -
<i>Figure 7.4 – Count of cells adherent on rat CCA lumen</i>	- 187 -
<i>Figure A.1 - Absorbance profile of Prussian Blue</i>	- 217 -
<i>Figure A.2 - Prussian blue with lysis buffer</i>	- 218 -
<i>Figure A.3 – Labelling timecourse - absorbance at 690nm</i>	- 219 -
<i>Figure A.4 – Standard curve for iron quantification</i>	- 220 -
<i>Figure A.5 – Water evaporation in 96-well plates</i>	- 221 -
<i>Figure C.1 – MTS assay absorbance at 490nm</i>	- 227 -

LIST OF TABLES

<i>Table 4.1 – Count-recount of PrB positive cells</i>	- 106 -
<i>Table 4.2 – Comparison of viability after magnetic attraction: StL vs DfL</i>	- 124 -
<i>Table 5.1 – FACS settings</i>	- 132 -
<i>Table 5.2 – Cell proliferation post DfL and magnetic attraction</i>	- 136 -
<i>Table A.1 – Prussian blue with lysis buffer</i>	- 218 -
<i>Table A.2 – Labelling timecourse - absorbance at 690nm</i>	- 219 -
<i>Table A.3 - Labelling timecourse - estimation of cellular iron content</i>	- 220 -
<i>Table A.4 – Water evaporation in 96-well plates</i>	- 221 -
<i>Table B.1 – Full table for Figure 4.5</i>	- 223 -
<i>Table B.2 – Full table for Figure 5.3</i>	- 224 -
<i>Table B.3 – Full table for Figure 5.5</i>	- 224 -
<i>Table B.4 – Full table for Figure 5.8</i>	- 225 -

ABBREVIATIONS

AAD	Aminoactinomycin-D
AMI	Acute myocardial infarction
BM	Bone marrow
BMS	Bare metal stent
BSA	Bovine serum albumin
CABG	Coronary artery bypass graft
CCA	Common carotid artery
CD	Cluster of differentiation
CEC	Circulating endothelial cell
EBM	Endothelial basal medium
EGM	Endothelial growth medium
EPC	Endothelial progenitor cell
ESC	Embryonic stem cell
FcR	Crystallisable fragment receptor
FDA	Food and Drug Administration
FEM	Finite element modelling
FePro	Endorem® + Protamine sulphate
FGF	Fibroblast growth factor
FITC	Fluorescein isothiocyanate
FSC	Forward scatter
GA	Gentamicin amphotericin antibiotic
G-CSF	Granulocyte colony stimulating factor
HCl	Hydrochloric acid
HSC	Haematopoietic stem cell
IGF	Insulin-like growth factor
IL-3	Interleukin 3
ISR	In-stent restenosis
KCN	Potassium ferrocyanide
LDL	Low density lipoprotein
MDT	Magnetic drug targeting
MNC	Mononuclear cell
MRI	Magnetic resonance imaging
NI	Neointima
NO	Nitric oxide
oxLDL	Oxidised LDL
PB-MNC	Peripheral blood MNC
PBS	Phosphate buffered saline
PCI	Percutaneous coronary intervention
PFA	Paraformaldehyde
PLL	Poly-L-lysine
PTCA	Percutaneous transluminal coronary angioplasty
RF	Radio frequency
SCF	Stem cell factor
SDF	Stromal derived factor
SMC	Smooth muscle cell
SPIO	Superparamagnetic iron oxide
SSC	Side scatter
UV	Ultraviolet
VEGF	Vascular endothelial growth factor

CHAPTER 1

STEM CELLS AND CARDIOVASCULAR DISEASE

1.1 Introduction

This chapter will provide a relevant synopsis of stem cells in cardiovascular disease. Stem cells and their properties are briefly presented, followed by a description of atherosclerotic disease processes. The specific relevance of stem cells in cardiovascular disease will be outlined along with a more detailed description of the cells thought to regenerate vascular endothelium, which are the main focus of the thesis.

In ancient Greek mythology, Prometheus, known for his wit, stole fire from the Gods to give it to man. It is said that in so doing he played a critical part in the evolution of humankind. To his demise, he was chain-bound to a rock and condemned to daily attacks by Zeus' eagle, who preyed on his liver (Figure 1.1). However, his liver would regenerate overnight, thus granting Zeus' eagle with limitless food and Prometheus with eternal torture.

In modern medicine, an experimental model that closely resembles this myth is the one developed by Higgins and Anderson in 1931, in which two-thirds of the rat liver are removed. The remaining liver re-grows to full size within one week (Michalopoulos & DeFrances 1997). To date, we are still unsure whether the regenerative capabilities of the liver were known to ancient Greeks, although the evidence tends to point in the opposite direction (Power & Rasko 2008). Despite this, the myth of Prometheus and the notion of *on demand* tissue regeneration remains a very fascinating concept in medicine. It offers a radically expanded range of possibilities for the treatment of human illness, including cardiovascular disease, and a multitude of basic experimental and clinical studies have sought this goal in recent years. Still, the efficacy and feasibility of stem cell therapy remains controversial.



Figure 1.1 – Prometheus and Atlas, ca. 550 BC
[Reproduced with permission]

This kylix (wine plate) is exhibit no. 16592 in the Vatican Museums. Prometheus is depicted on the right, beside his brother Atlas, who was condemned to hold the skies.

1.2 Stem cells – an overview

1.2.1 Embryonic stem cells

Stem cells are immature cells with no specific identity, which are capable of differentiating into mature cell stages of a variety of tissue types, whilst being able to self-regenerate without losing this differentiation potential (Brehm, Zeus, & Strauer 2002; McKay 2000). During early development certain cells in the embryo have been identified that are pluripotent and can form all three germ layers (endoderm, mesoderm, ectoderm), these are known as embryonic stem cells (ESCs). ESCs are channelled down distinct differentiation pathways and eventually lead to the formation of the organism. Human ESCs were first described by Thomson in 1998, and this has been followed by ten years of considerable research and debate regarding their use.

Possibly the most appealing aspect of ESCs is that, given the appropriate cues, they can be induced to differentiate into an array of cell types *in vitro*. For example, human ESCs have been differentiated into cardiomyocytes, haematopoietic cells, endothelial cells, hepatocytes, osteoblasts and several types of neural tissue (Lerou & Daley 2005; Rippon & Bishop 2004). Indicatively, there have been a number of studies showing that ESCs can be differentiated into functional neural cells, integrate into the host tissue and in some cases have improved symptoms of neurodegenerative diseases in animal models (Goldman & Windrem 2006; Lindvall & Kokaia 2006). However, we are still unclear of the exact molecular pathways that define the fate of the cells. Moreover, a lot of investigations have focused on the immune response generated by the host tissue, which may lead to graft rejection, as well as the potential for the transplants to form tumours (Nussbaum et al. 2007; Swijnenburg et al. 2005). Some of these issues can be overcome with the use of immunosuppressants and specific differentiation protocols,

however concerns regarding safety remain. This was exemplified in a recent case of donor-cell derived tumourigenesis in a patient who was treated experimentally with foetal stem cells (Amariglio et al. 2009).

ESC research remains under inquiry also due to the ethical, religious and political dimension of using unwanted human embryos (McKay 2000; Orive et al. 2003). For this reason, researchers are in the search of stem cells that remain in the body following embryonic development and reside within the adult tissues. Harvesting these cells would be more widely accepted than using embryos, with the added benefit of being autologous, thus eliminating the host immune response to transplanted cells.

1.2.2 Adult stem cells

Some cells with regenerative capacity are known to be retained in adulthood and are thought to aid in the restoration of damaged tissue; these are known as adult stem cells and are traditionally thought to be more limited in their differentiation potential. They serve as a local cell pool for the maintenance of adult tissue, such as the haematopoietic system, the cells of the skin and gut, and also part of the nervous system (Bajada et al. 2008). A representative ‘differentiation tree’ is shown in Figure 1.2.

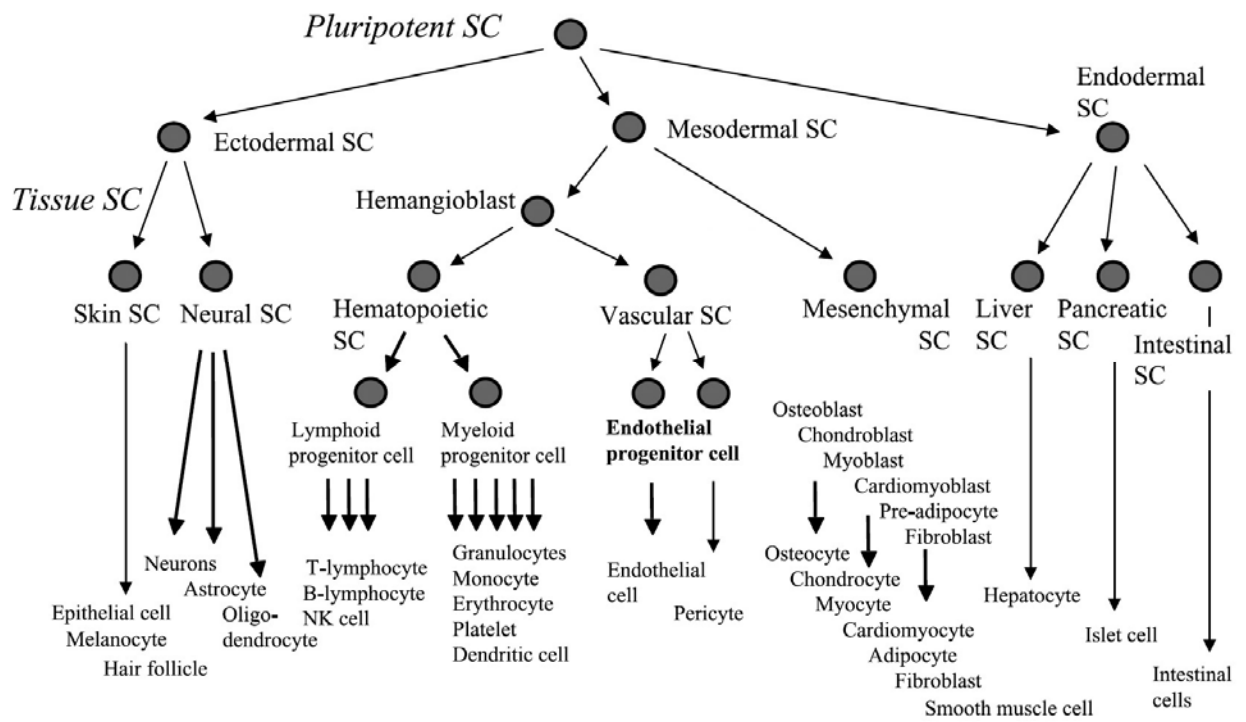


Figure 1.2 – Stem cells and their progeny in adult tissue
 [Adapted from Asahara & Kawamoto 2004]

As in most areas of medicine, the sheer existence of adult stem cells has been highlighted by diseases affecting these cells. Probably the most investigated are the haematopoietic stem cells (HSCs), which reside mainly in the bone marrow and give rise to haematopoietic progenitor cells. These in turn differentiate into the cell lineages of the haematopoietic system: erythrocytes (red cells), megakaryocytes (platelet-forming cells) and leukocytes [white cells, i.e. granulocytes (neutro-, baso- and eosinophils), lymphocytes (T-, B-, and natural killer-cells) and monocytes/macrophages] (Smith 1990). Malignancy in the HSC pool leads to uncontrolled proliferation and diseases such as leukemia, in which there are abnormally high levels of white cells in the blood. Similarly, a complete eradication of the HSC pool, will lead to aplastic anemia, in which case there are insufficient numbers of circulating red and white cells (Lerou & Daley 2005).

The regenerative potential of HSCs is the basis of a well established stem cell therapy regime, bone marrow transplantation. This is the preferred therapy for certain types of immunodeficiency disorders and leukemias (Duncombe 1997). During the procedure, bone marrow cells, including ~1 in 10,000 HSCs, are infused in a patient who has had a complete eradication of their bone marrow cells using chemo/radio-therapy. The infused HSCs then reconstitute the entire haematopoietic system. The success of this treatment clearly exemplifies the main characteristics of stem cells; self renewal and ability to form multilineage progeny.

In addition to HSCs, a multitude of other stem cells exist in the adult body. For example, mesenchymal stem cells in the bone marrow can give rise to cartilage, bone and adipose tissue; neural stem cells in the nervous system differentiate into neurones, oligodendrocytes and astrocytes (Alison & Islam 2009). In fact, most organs such as the

musculoskeletal system, the heart, the lung, kidney, digestive tract, gonads and skin are believed to have some residing progenitor cell that aids in tissue regeneration.

Recent evidence shows that adult stem cells may, in fact, have more potential to trans-differentiate between tissue types, and behave like embryonic stem cells if given the right cues. This has resulted in a lot of hype (McKay 2000), because an adult pluripotent cell, being autologous, would diminish the immunocompatibility issues found with ESCs and also bypass the ethical obstacle of using human embryos. For example, there are several reports on subsets of HSCs that can form tissues from all three germ layers (Ratajczak et al. 2008). Several names have been coined for these cells, such as *multipotent adult progenitor cells* (MAPC), *marrow-isolated adult multilineage inducible cells* (MIAMI), *multipotent adult stem cells* (MACS) and *very small embryonic-like cells* (VESL). It is likely that these recent studies are describing overlapping cell populations, and that the pluripotent adult stem cell is yet to be defined.

In addition, recently a methodology was described, whereby pluripotency is induced in somatic adult cells through the overexpression of certain transcription factors (Klimanskaya, Rosenthal, & Lanza 2008; Ratajczak et al. 2008). This has been achieved both for mouse and human cells, with different combinations of transcription factors such as Oct4, Sox2, Nanog and Lin28. In mouse models, these induced pluripotent (iPS) cells could generate cells from all three germ lines and form chimeric mice.

However, the use of viruses in iPS cell formation, as well as the yet unknown fate of these cells, are likely to be obstacles in clinical translation. In addition, even if success with adult pluripotent cells is shown in animal models, it is believed that these cells will be rare and difficult to isolate, which may, practically and economically, hamper

expansion to large cell numbers for transplantation and organ regeneration. The success of cellular therapies will therefore require strategies to ‘accurately deliver and/or home the cells or their derivatives to the injury site’ (Stocum & Zupanc 2008). Meanwhile, it is important to keep in mind that, despite any possible excitement in the media and the possibility of business opportunities for stem cell therapy companies, the characterisation of stem cells still remains in its infancy. The following sections will focus on the current role of cellular therapies in cardiovascular disease, and in particular the capacity of the cells thought to regenerate endothelium, the ‘endothelial progenitor cells’, for vascular repair.

1.3 Cardiovascular disease

1.3.1 The burden of cardiovascular diseases

Cardiovascular diseases are the number one cause of death globally (W.H.O. 2007). They comprise a group of diseases of the heart and vasculature, including coronary artery disease (the vessels that ‘crown’ the heart and supply it with blood), cerebrovascular disease and peripheral arterial disease. Coronary artery disease and stroke alone were the cause of one quarter of all deaths in 2005.

The primary cause of coronary artery disease and stroke is atherosclerosis, a disease of the large arteries. There are several major risk factors for the development of atherosclerosis, which include a high-fat diet, lack of exercise and smoking tobacco. These risk factors are descriptive of the lifestyle of Westernised world, which has led atherosclerosis to be the cause for half of the deaths in these societies (Lusis 2000).

1.3.2 Atherosclerosis

1.3.2.1 Etymology

Atheroma in Greek means *lump of goat*, essentially porridge; *sclerosis* means *hardening*. *Atherosclerosis* thus describes a condition in which the arteries are hardened due to the presence of a porridge-like lump. This section will outline the normal anatomy and physiology of the artery, along with the pathophysiology and the management of atherosclerosis.

1.3.2.2 Anatomy and physiology of the artery

The arterial system is a high-pressure tubing system that carries the blood from the heart to the various organs in the body (Oliver, Entman, & Jacob 2009). The wall of these

tubes is a very complex structure; it provides elasticity and mechanical support, active contractile control and a smooth non-thrombogenic surface. At the same time there are mechanisms in place for the timely plugging and repair of this wall in case of a breach (such as in trauma). Due to their vast cellular and molecular complexity, only a brief account of these functions will be considered here.

The arterial wall is comprised of three major layers (Figure 1.3); the innermost and thinnest is the intima, which is made of extracellular connective tissue matrix. This is covered with a layer of tightly joined endothelial cells on the luminal side and bound by a layer of elastic fibres, the internal elastic lamina, around its periphery. The endothelium normally serves multiple roles. For example, apart from a non-adherent surface for circulating cells, it provides a permeability barrier for nutrients and fluid, regulates the vascular tone by release of constrictive or dilatory molecules (such as the dilatory nitric oxide, NO) and also forms and maintains the matrix on which it lies (Ross 1995). This intimal matrix contains collagen and is pro-thombogenic; which is essential for the prompt termination of bloodflow in case of injury.

Surrounding the intima is the media, made of smooth muscle cells (SMCs), which control the contractility of the vessel. It has been shown that with age SMCs slowly migrate into the intima of some areas and create small thickenings. It is in these areas that atherosclerotic lesions develop further (Ross 1995).

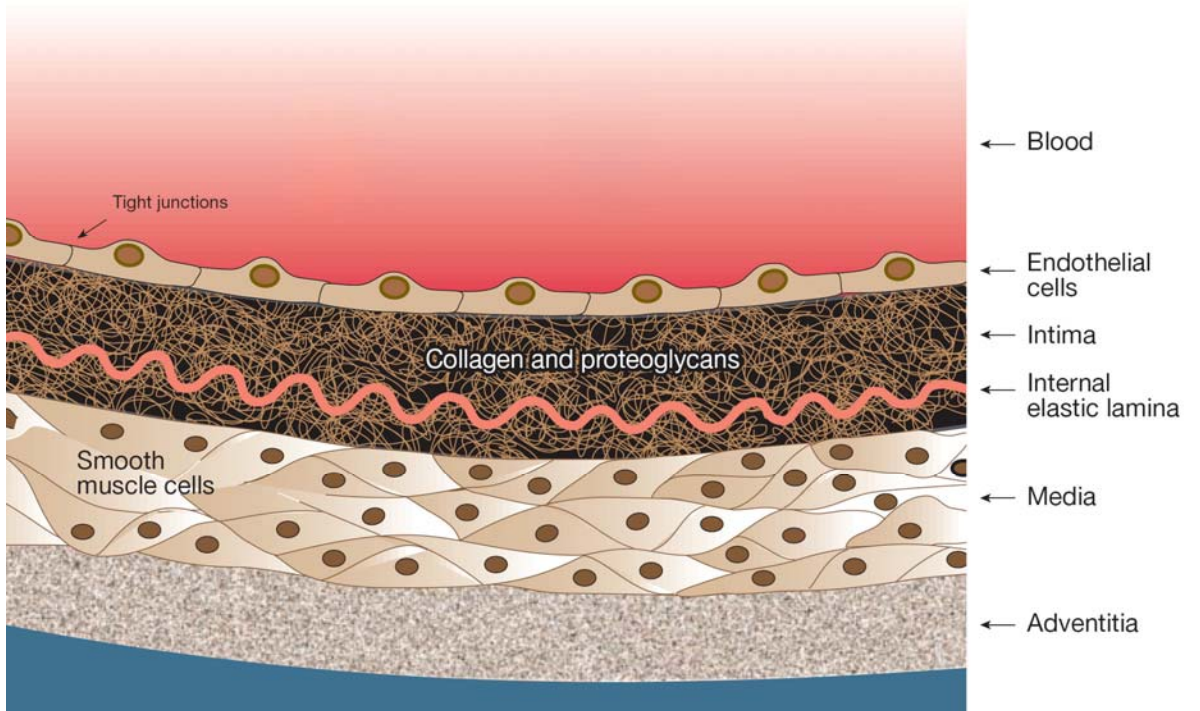


Figure 1.3 – Anatomy of the artery
[Adapted from Lusis 2000]

The whole structure is bound by the adventitia, a connective tissue layer containing SMCs and fibroblasts, the role of which is mainly to provide structural support and protect the artery from over-expansion. Traditionally, the pathophysiology of atherosclerosis is not thought to be associated with this layer, which is also evident by its name; *adventicius* in Latin means *foreign*, thus the adventitial layer is, at least by nomenclature, thought to be unrelated to the rest of the artery. However, there is emerging evidence for the importance of the adventitia in atherosclerosis (Maiellaro & Taylor 2007).

1.3.2.3 Pathophysiology of atherosclerosis

Atherosclerosis is considered to be a chronic, progressive, inflammatory response to endothelial injury or dysfunction (Goldschmidt-Clermont et al. 2005; Ross 1999). It is characterised by the accumulation of lipids and fibrous components, recruitment of circulating lymphocytes and monocytes, and SMC proliferation. Possible factors that can be insulting to the endothelium include high blood cholesterol levels, in particular the cholesterol-carrying molecule low density lipoprotein (LDL), free radicals produced by cigarette smoking, high blood pressure, raised blood glucose such as in diabetes mellitus, infectious agents such as herpesviruses and several genetic factors. Of importance is also the blood flow pattern; the structure and function of endothelial cells is dependent on the stresses experienced, and arterial branching points, having high turbulence and low shear stress, are prone to atherogenesis (Gimbrone et al. 2000).

The notion that endothelial injury, followed by inflammation and a proliferative response within the artery, precedes the degeneration found in advanced atherosclerotic lesions, was first suggested by Rudolph Virchow in the mid-1850s (Ross, Glomset, & Harker 1977). This progression can be divided in four arbitrary stages (Figures 1.4-1.7).

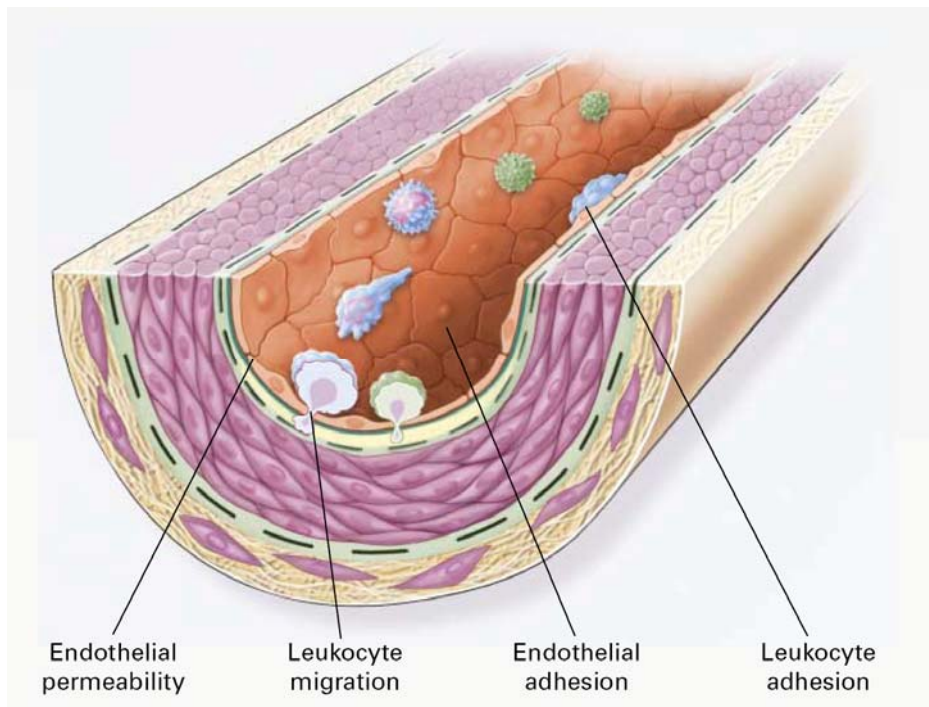


Figure 1.4 – Lesion initiation
[From Ross 1999]

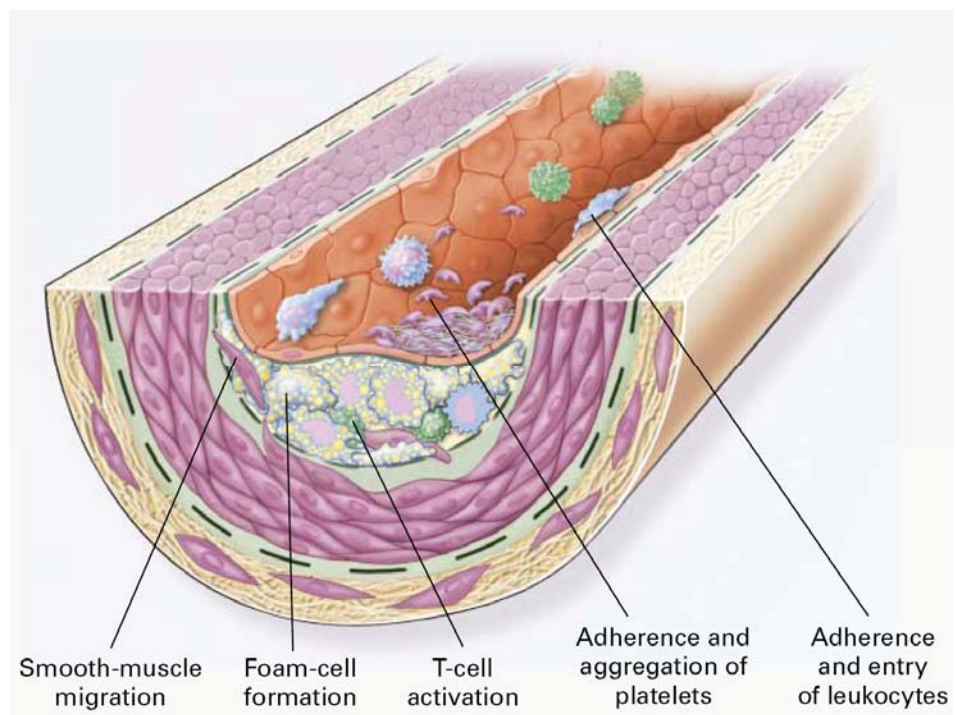


Figure 1.5 – Development of the ‘fatty streak’
[From Ross 1999]

During lesion initiation, the insulted endothelium becomes more permeable to macromolecules such as LDL, which accumulate in the sub-endothelial space and become oxidised (oxLDL). This causes an insult to the endothelium and an inflammatory response is initiated; the endothelium exhibits increased adhesiveness to leukocytes (Figure 1.4). The leukocytes migrate to the intima, T-cells become activated and monocytes differentiate into macrophages, ingesting the accumulated oxLDL and forming lipid-rich 'foam cells'. Thus a 'fatty streak' is developed (Figure 1.5). The removal of oxLDL by macrophages is a normal response that protects the endothelium and underlying SMCs. Fatty streaks are not clinically significant and are normally present in most adults from adolescence onwards.

Continued accumulation of oxLDL causes an increase in the size of the lesion, as more foam cells are formed, get trapped and begin to form a necrotic core. Continued insult to the endothelial cells, coupled with insufficient endogenous repair of the endothelial layer, causes endothelial dysfunction; this includes increased adhesiveness to platelets and reduced production of NO with a corresponding increase in vascular tone. In addition, as a result of the inflammatory mediators released by the endothelium and activated leukocytes, SMCs start to migrate into the intima and proliferate, depositing extracellular matrix and forming a fibrous cap which protrudes in the lumen of the vessel (Figure 1.6). The stability of this fibrous plaque is a complex interplay between the strength of the fibrous cap, calcification and neovascularisation within the core. If there is plaque rupture, the pro-thrombotic matrix of the intima becomes exposed to the blood, and a thrombus forms (Figure 1.7). This results in partial or total occlusion of the vessel and tissue ischaemia, such as myocardial ischaemia, acute myocardial infarction (AMI) or stroke.

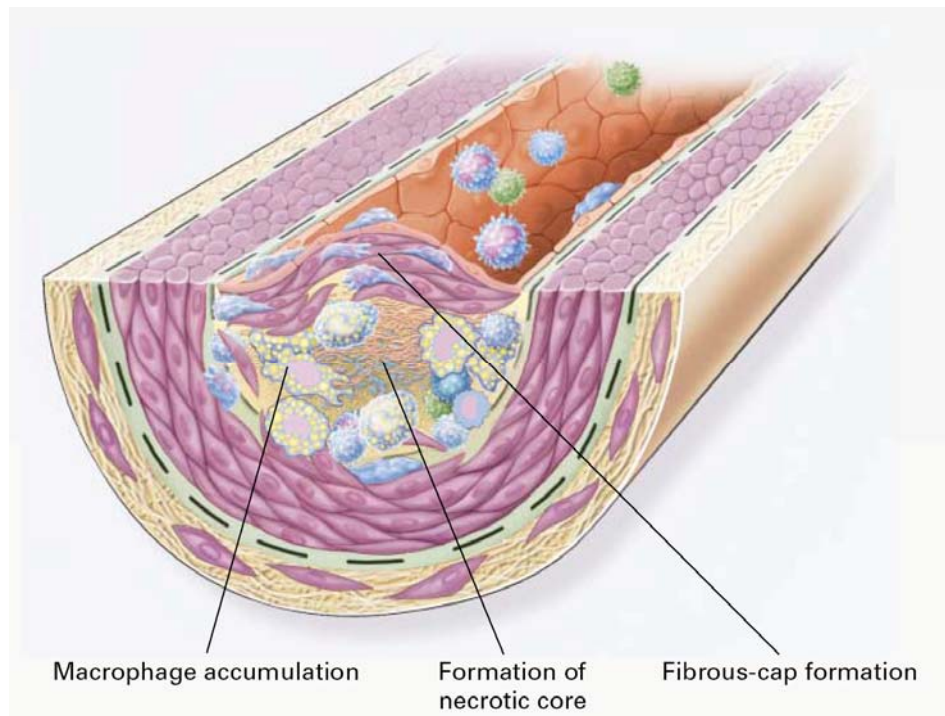


Figure 1.6 – Advanced lesion
[From Ross 1999]

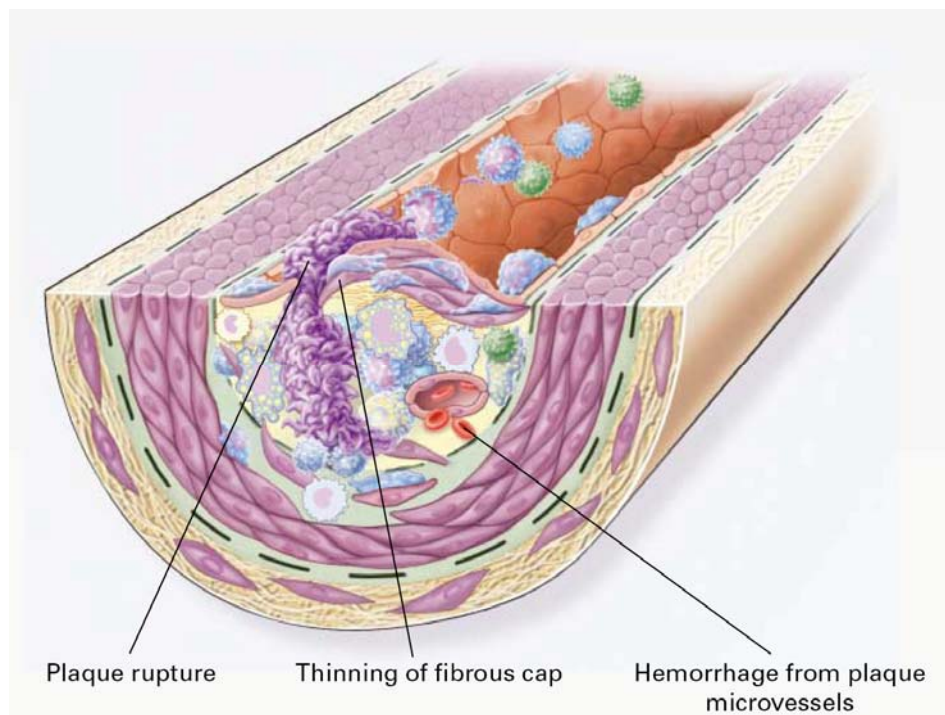


Figure 1.7 – Unstable lesion
[From Ross 1999]

1.3.2.4 Non-surgical management of atherosclerosis

Pharmacological and lifestyle management is aimed at reducing the risk factors in those at high-risk, those with recognised arterial atherosclerotic stenoses and those who have already had a cardiovascular episode (ischaemia, AMI, stroke etc).

Statins are a class of commonly used drugs that are particularly helpful in reducing blood LDL levels by inhibiting LDL production in the liver; they are associated with a 30% reduction in clinical events and mortality from atherosclerosis (Vaughan, Gotto, & Basson 2000). Anti-hypertensive drugs are used to control blood pressure; lifestyle changes include cessation of cigarette smoking, increased levels of exercise, a low-cholesterol diet and better diabetes management.

1.3.2.5 Surgical management of atherosclerosis

1.3.2.5.1 Introduction

In the heart, surgical management takes the form of either percutaneous coronary intervention (PCI), or coronary artery bypass graft surgery (CABG) (Gunn & Taggart 2003). In PCI, a catheter is inserted in a peripheral artery and advanced to the coronary arteries under radiological guidance. The catheter is tipped with a inflatable balloon that is used to open up the stenosed section. This may be accompanied by intraluminal implantation of a metallic mesh (a stent) to act as a supporting scaffold. In CABG, the diseased coronary vessels are replaced with vein grafts, usually from the leg. CABG, which will not be discussed further, is reserved for either chronic total occlusions or multiple vessel disease; in other cases PCI is preferred.

1.3.2.5.2 *Balloon angioplasty*

PCI is a general term that encompasses percutaneous transluminal coronary angioplasty (PTCA, balloon angioplasty, Figure 1.8a), with the further use of stents (Figure 1.8b) or other atheroma-cutting devices. The term *angioplasty* literally means *moulding of the arteries* in Greek. The first PTCA procedures were performed in the late 1970s (Serruys, Kutryk, & Ong 2006). PTCA is associated with restenosis, defined as the arterial healing response after injury incurred during transluminal coronary revascularisation (Lowe, Oesterle, & Khachigian 2002). This restenosis is attributable to elastic recoil, constrictive remodelling (arterial shrinkage), thrombus at the site of injury, proliferation of SMCs and deposition of extracellular matrix. The latter two processes contribute to the formation of a thick layer known as the neo-intima (NI) (Hoffmann & Mintz 2000; Lowe, Oesterle, & Khachigian 2002). The endothelium plays a role in the modulation of this NI formation: with injury and denudation of only a small area of endothelium, minimal NI is observed, which is increased when larger areas are affected (Kipshidze et al. 2004). In the rat for example, SMCs appear in the intima only in areas that are not re-endothelialised seven days after injury (Haudenschild & Schwartz 1979).

1.3.2.5.3 *Stent implantation following PTCA*

Metallic stents were introduced in 1986 to reduce the acute recoil and post-injury arterial shrinkage associated with PTCA, and the BENESTENT and STRESS clinical trials in 1994 showed a reduction in restenosis rates by approximately 30% with the use of a stent (Fischman et al. 1994; Serruys et al. 1994). By 1999, stenting comprised 85% of all PCI and in 2006 this figure had risen to 90-95% (Serruys, Kutryk, & Ong 2006). Interestingly, PTCA is now sometimes performed where pharmacological treatment alone could produce the same result (Fox 2009).

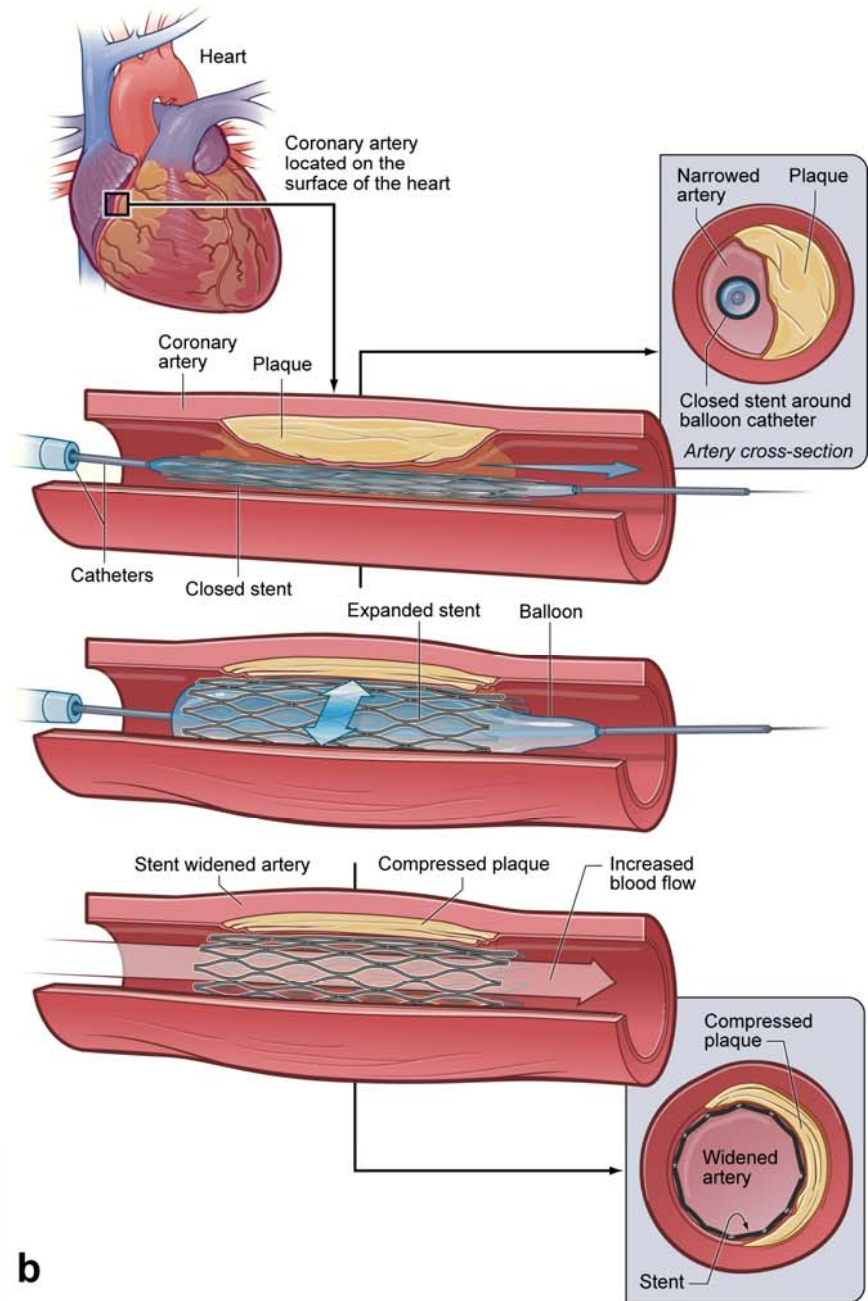
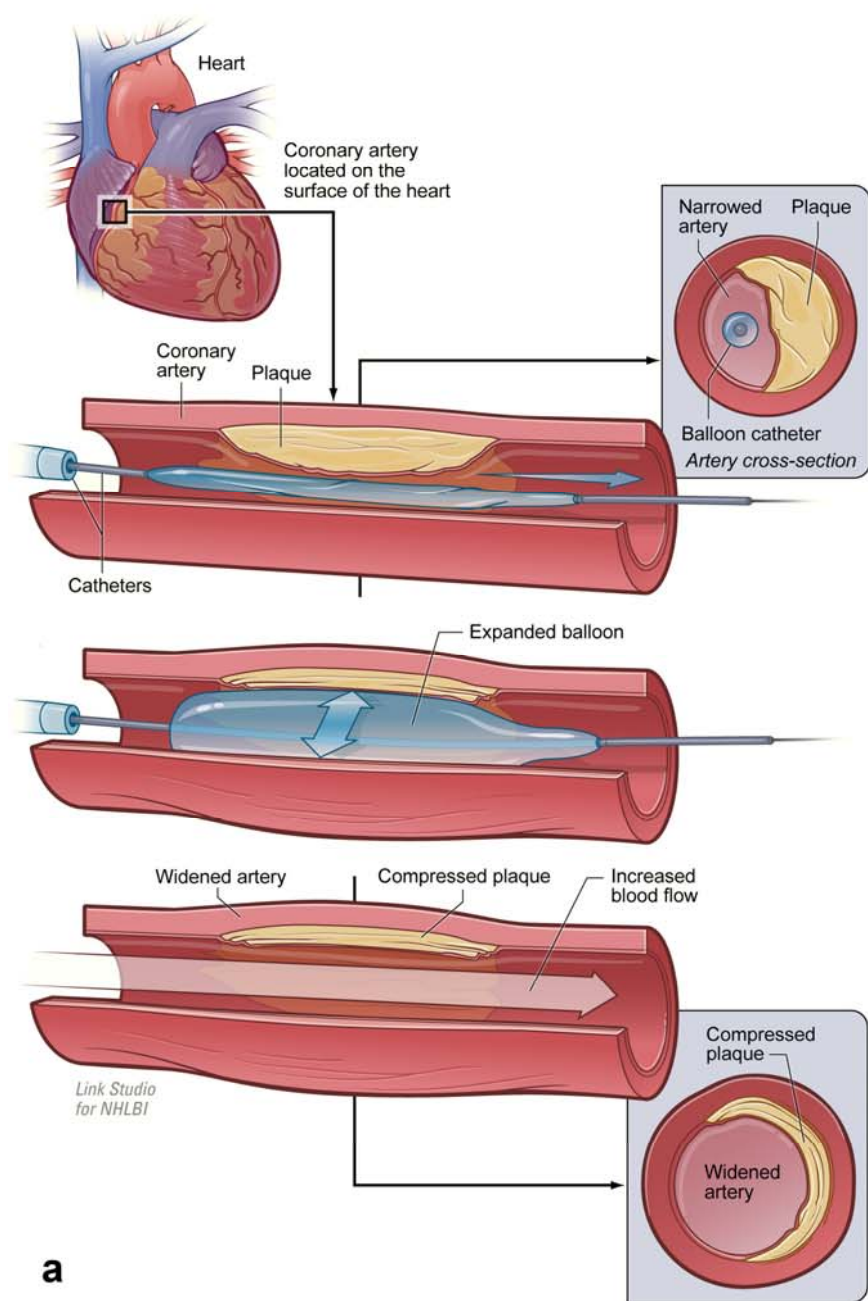


Figure 1.8 – PCI. a) PTCA b) PTCA + stenting
 Adapted from original kindly provided by the U.S. National Heart Lung and Blood Institute

Even though stents eliminated vessel remodelling and recoil, they were associated with thrombogenicity and did not abolish re-stenosis attributable to NI formation. Dual antiplatelet therapy consisting of aspirin and a thienopyridine such as clopidogrel resulted in reduction of stent thrombosis; in addition, stents coated with heparin provided a further reduction (Gupta et al. 2004). However, in-stent-restenosis (ISR, Figure 1.9a) due to NI hyperplasia remained a considerable problem, occurring in 10%-50% of cases (Hoffmann & Mintz 2000; Lowe, Oesterle, & Khachigian 2002). This may be explained by the endothelial damage caused by the metallic stent, which would be associated with increased endothelial dysfunction (van Beusekom et al. 1998). The treatment of choice for ISR in 2000 was repeat PTCA; however, despite temporary dilatation of the vessel and amelioration of symptoms, it was commonly associated with re-invasion with NI and decreased lumen diameter.

As attempts to deliver systemic medications to limit proliferation of SMCs at the lesion site were not successful (Takahashi, Letourneur, & Grainger 2007), in the last few years there have been efforts to develop stents that can locally and slowly release anti-proliferative agents to inhibit NI hyperplasia and ISR; these are known as drug-eluting stents (DES). The two main drugs used are sirolimus (Cypher® stent) and paclitaxel (Taxus® stent) in various stent strut forms; they act by arresting the cell cycle and thus reducing the proliferation and migration of SMCs. Because they markedly decreased NI hyperplasia (Figure 1.9) compared with the previously used bare-metal stents (BMS), they gained Food and Drug Administration (FDA) approval in 2003 and 2004 respectively (Serruys, Kutryk, & Ong 2006).

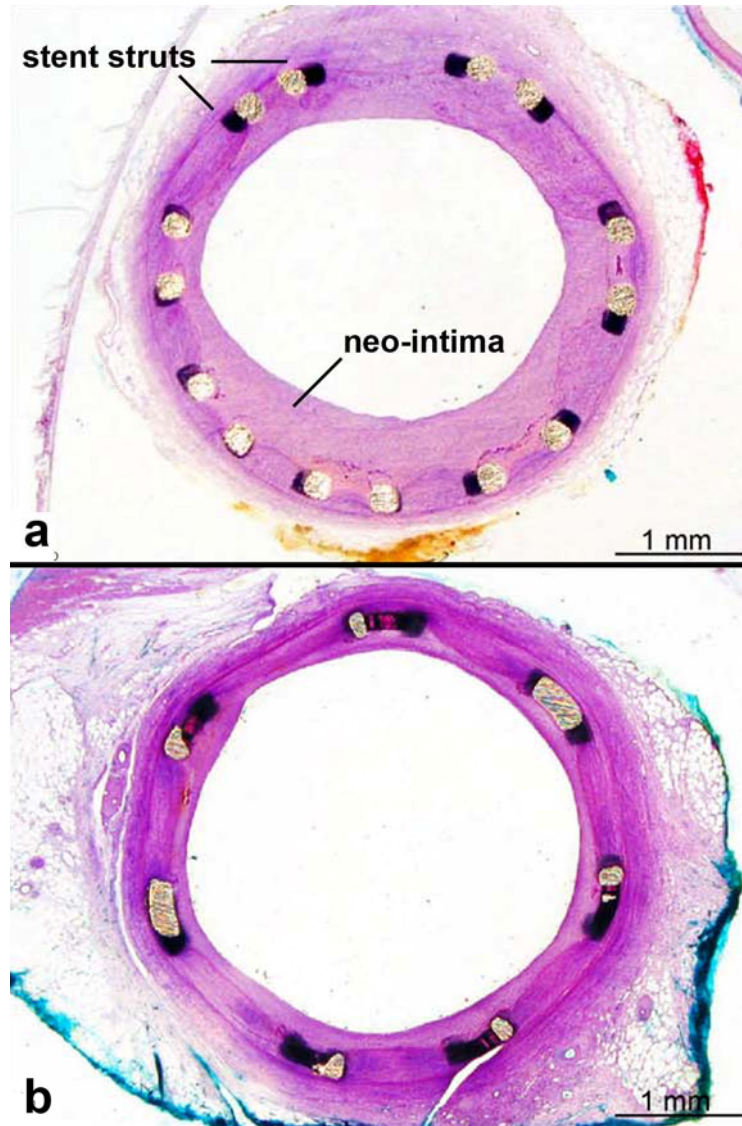


Figure 1.9 – In-stent stenosis due to NI formation
a) BMS and b) sirolimus DES 30, days after implantation in porcine coronary arteries
[Adapted from Carter et al. 2004]

However, in the last two years there has been increasing concern regarding the safety of DES, particularly regarding the occurrence of late stent thrombosis, which can occur months or years following implantation (Lemesle et al. 2008; Stahli, Camici, & Tanner 2009). Although the rate of thrombosis is only about 0.5% per year higher than BMS, it is associated with 20% - 30% mortality and 60% non-fatal MI (Jaffe & Strauss 2007). Since sirolimus and paclitaxel do not act in a cell-specific manner, it was assumed that re-endothelialisation may be impaired in the presence of a DES, exposing the pro-thrombogenic stent strut to the blood for prolonged periods of time. There is evidence for delayed endothelial function as late as 2 years post-implantation (van Beusekom et al. 2007) and human autopsy studies have confirmed impaired re-endothelialisation at sites of DES compared with BMS (Stahli, Camici, & Tanner 2009).

Thus, despite their differences in causality, *de novo* atherosclerotic lesions, ISR following PCI, and possibly DES thrombosis, share a common pathophysiological feature: endothelial cell damage with subsequent delay or impairment in re-endothelialisation. There is, therefore, a need for the development of strategies that enhance vascular endothelialisation following injury. The next section will focus on the cells that are thought to give rise to endothelium in the adult, the endothelial progenitor cells, and their relationship with cardiovascular disease.

1.4 Endothelial progenitor cells in cardiovascular disease

1.4.1 Introduction

Apart from the recognised benefit of PTCA, stenting with/out DES, in parallel with pharmacological therapy with anti-thrombotic drugs and statins, recent years have seen increased interest in the usage of various types of BM-derived stem cells in ischaemic heart disease (Dimmeler, Zeiher, & Schneider 2005). This interest was partly sparked by reports concluding that there is significant contribution of donor stem cells in the muscle of transplanted hearts (Quaini et al. 2002) and that BM-derived cells can regenerate the heart muscle (Orlic et al. 2001).

A large number of pilot clinical trials have since been conducted; these have shown a small but consistent increase in cardiac function following cell transplantation and, most importantly, the safety of the procedure in the case of the human heart (Abdel-Latif et al. 2007). However, the exact mechanism underlying the observed changes became disputed (Chien 2004; Orlic 2005). For example, several reports have shown that BM cells do not differentiate into heart muscle (Balsam et al. 2004; Murry et al. 2004) or improve heart function (Carr et al. 2008). It has been suggested that, depending on the particular cell type used, augmentation of the function of existing cells via paracrine mechanisms or neovascularisation leading to increased oxygen delivery to the ischaemic area may play an important role (Hristov & Weber 2006; Welt & Losordo 2006). Yet the cellular and molecular basis of the functional improvement remain incompletely understood despite the numerous types of cells, isolation and implantation procedures implemented (Segers & Lee 2008) –or, perhaps, precisely because of this diversity.

What is of particular relevance to this thesis is the paradigm of some clinical trials, that the administered endothelial progenitor cells (EPCs) would aid in neovascularisation of the ischaemic tissue. The identity and role of these cells in both the neovascularisation of ischaemic areas and arterial re-endothelialisation will be the focus of the last sections of this chapter.

1.4.2 Emergence of the term ‘EPC’

Traditionally, despite circumstantial evidence dating to 1932 (Ribatti 2007), it was thought that the repair of injured arteries is dependent on proliferation of neighbouring mature, differentiated endothelial cells (Ross, Glomset, & Harker 1977). Similarly, in contrast with stem-cell mediated blood vessel formation in the embryo (vasculogenesis), postnatal neovascularisation (angiogenesis) was believed to be dependent on the proliferation of pre-existing endothelium (Murohara 2001). However, following the differentiation of endothelial cells from circulating cells *in vitro* (Asahara et al. 1997; Shi et al. 1998), in the last decade the concept of the adult ‘endothelial progenitor’ cell has arisen, which is thought to reside in the bone marrow and circulate in small numbers in the circulation, playing an important role in processes such as post-ischaemic neovascularisation, tumour angiogenesis, and re-endothelialisation (Gulati, Lerman, & Simari 2005). For example, observational investigations in humans have shown that mobilisation of EPCs is a natural response in myocardial injury (Shintani et al. 2001) and the clinical outcome is correlated to the degree of mobilisation (Werner et al. 2005).

1.4.3 Identifying the EPC

The term ‘EPC’ has been used widely to represent a variety of cells that can form endothelial-like cells *in vitro*, and the true identity of the EPC remains elusive, as there

is no marker specific to this cell type (Roncalli et al. 2008). Initially the term was assigned to an unknown population of cells within the peripheral blood mononuclear cell (PB-MNC) fraction, which consists of leukocytes with a single nuclear lobe (lymphocytes and monocytes/ macrophages, but not granulocytes). The PB-MNC fraction was enriched for CD34 -a HSC cluster of differentiation marker also expressed on some mature cells- and cultured from 7 to 10 days on fibronectin-coated plates. Adherent cells with characteristics similar to mature endothelial cells formed, which incorporated into sites of angiogenesis in a hindlimb ischemia model (Asahara et al. 1997). Similar results were published shortly after for CD34+ purified cells (Shi et al. 1998).

Culture of the whole PB-MNC fraction in endothelial-promoting medium, without CD34 enrichment or isolation, was proposed as an alternative method for deriving EPCs (Kalka et al. 2000) and was adopted by other groups (Murohara et al. 2000; Vasa et al. 2001b). These EPCs were subsequently shown to express markers of the monocytic lineage such as CD14 (Rehman et al. 2003). It was considered that these were monocytic cells with capacity to differentiate into endothelial cells under the pressure of the cultivation media; they were called culture-modified mononuclear cells (CMMC).

To further complicate matters, in the same year as the initial description by Asahara, a novel differentiation marker was found, CD133 (Yin et al. 1997). This marker recognises a form of the membrane protein prominin-1, which is only expressed in undifferentiated, pluripotent-like cell types such as HSCs, fetal brain stem cells, myogenic stem cells and certain tumours (Shmelkov et al. 2005); it was therefore postulated that it would constitute a better marker for identification of true progenitors. EPCs were eventually characterised on the basis of CD133 expression (Gehling et al.

2000; Peichev et al. 2000; Quirici et al. 2001; Reyes et al. 2002) and were shown to be upregulated by 50-fold within 12h after vascular trauma secondary to burn injury or CABG surgery (Gill et al. 2001).

Longer term culture was also proposed to select for more proliferative EPCs from whole PB-MNC fractions and included a pre-plating step to remove differentiated monocytes and mature endothelial cells, which rapidly adhere to culture plates (Hill et al. 2003; Lin et al. 2000). Extended MNC culture for 2-4 weeks resulted in an outgrowth of cells (termed endothelial outgrowth cells, EOC) that were distinctly more proliferative than CMMC and had an endothelial-like phenotype (Khakoo & Finkel 2005). These EOCs have also recently been shown to include cells of monocytic origin (Rohde et al. 2006; Rohde et al. 2007). Both CMMCs and EOCs have the capacity to incorporate into the vasculature and enhance neovascularisation and re-endothelialisation (Hristov & Weber 2004).

The actual identity of circulating EPCs may cross the boundaries of pure 'endothelial' or 'monocytic' populations. That is, if an identifiable, single, specific 'EPC' exists at all. Monocytes have been shown to express both endothelial and macrophagocytic markers (Schmeisser et al. 2001) and incorporate in newly formed blood vessels *in vivo* (Urbich et al. 2003). CD14⁺ cells can also re-endothelialise denuded arteries and inhibit neointimal hyperplasia (Fujiyama et al. 2003). Thus EPC populations are heterogeneous and may express an array of progenitor markers such as CD133 / CD34, monocytic markers such as CD11b / CD14 and endothelial markers such as VE-cadherin (Hristov & Weber 2008; Urbich & Dimmeler 2004). The mainstay is that, *in vivo*, EPCs originate in the BM from a CD133⁺/CD34⁺ cell, which is released in the circulation in small numbers and can differentiate into endothelial cells *in vitro* under endothelial-

specific media; thus state-of-the-art protocols necessitate isolation from peripheral blood using CD133 antigens (Zammaretti & Zisch 2005).

An outline of the origin and differentiation of EPCs is given in Figure 1.10. Regardless of their exact origin, the regenerative capacity of EPCs has been utilised in various scenarios; these are summarised in the next section.

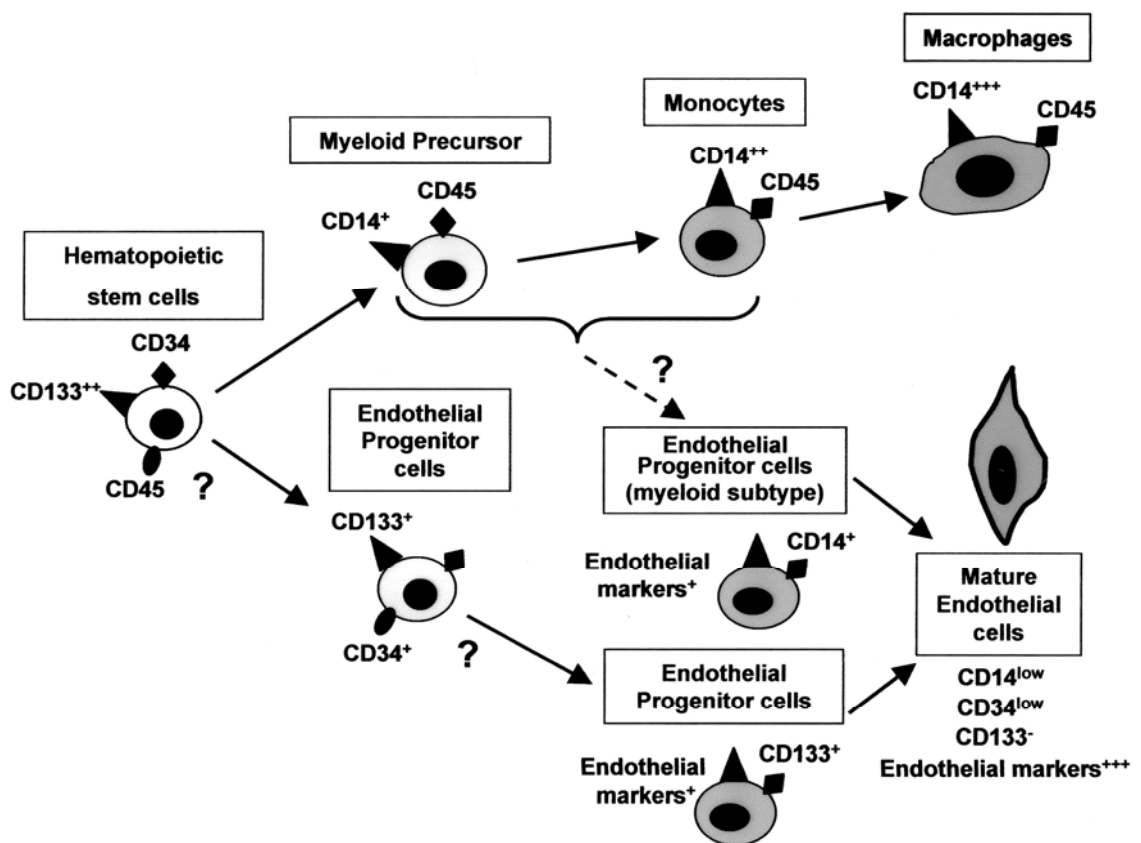


Figure 1.10 – Origin and differentiation of the EPC
[Adapted from Urbich & Dimmeler 2004]

1.4.4 Role of the EPC

EPCs were originally used in the context of neovascularisation for ischemia; a number of studies focused on the improvement in perfusion in ischaemic hindlimbs in animal models (Asahara et al. 1999; Asahara et al. 1997; Kalka et al. 2000; Murohara et al. 2000) and humans (Inaba, Egashira, & Komori 2002; Tateishi-Yuyama et al. 2002). Evidence for beneficial involvement of EPCs in myocardial ischaemia (Kawamoto et al. 2001; Kocher et al. 2001) eventually led to the first clinical trials in humans (Erbs et al. 2005; Losordo et al. 2007; Schachinger et al. 2004; Stamm et al. 2007).

It is also well established that EPCs play a significant role in the pathogenesis of atherosclerosis. They have been shown to re-endothelialise artificial grafts (Shi et al. 1998) and sites of injury caused by balloon angioplasty in animal models, reducing neointima formation (Friedrich et al. 2006; Fujiyama et al. 2003; Griese et al. 2003; Gulati et al. 2003; Kong et al. 2004; Walter et al. 2002; Wang et al. 2008; Werner et al. 2003; Werner et al. 2002). To date there have not been any clinical trials investigating the potential of EPCs to reduce post-PTCA NI hyperplasia and ISR (Kawamoto & Losordo 2008), although some preliminary trials are underway (see section 1.4.6)

Most of the risk factors for atherosclerosis have been related to circulating EPC availability and function (Hill et al. 2003; Urbich & Dimmeler 2005; Vasa et al. 2001b; Werner & Nickenig 2006). This is in concordance with the notion that the balance of endothelial damage versus re-endothelialisation is impaired in the development of atherosclerotic lesions (section 1.3.2.3). Furthermore, there has been a number of studies indicating that statins augment EPC mobilisation from the bone marrow, enhance their proliferation and differentiation and prevent their apoptosis, increasing re-endothelialisation and decreasing NI formation in animal models and humans

(Dimmeler et al. 2001; Vasa et al. 2001a; Walter et al. 2002; Walter, Zeiher, & Dimmeler 2004; Werner et al. 2002).

1.4.5 Mobilisation and homing of EPCs to sites of injury

EPCs are mobilised from the bone marrow, where they are normally in a quiescent state and associated with the stromal tissue (Khakoo & Finkel 2005; Urbich & Dimmeler 2004). Cytokines such as vascular endothelial growth factor (VEGF) and stromal cell derived factor 1 alpha (SDF-1 α), which are upregulated in response to hypoxia or arterial injury (Gill et al. 2001; Hristov & Weber 2008), are thought to activate matrix metalloproteinases in the bone marrow. These proteinases cleave the adhesions between stem cells and stromal tissue, increasing their mobility; this allows the cells to transfer to the more vascular sinusoidal zone of the bone marrow, favouring mobilisation into the peripheral circulation and the initiation of differentiation (Zampetaki, Kirton, & Xu 2008). A potent mobiliser is granulocyte-colony stimulating factor (G-CSF) (Korbling et al. 2006), which mobilises the whole HSC pool and has been used clinically for HSC mobilisation in the context of BM transplantation (section 1.2.2). Other mobilisers include erythropoietin, exercise, estrogens and statins (section 1.4.4).

The recruitment, adhesion, transmigration and final differentiation of EPCs at sites of damage or ischaemia is an interplay between attractive chemokines such as VEGF or SDF-1 α and adhesion molecules (Figure 1.11). For example, the receptor for SDF-1 α is expressed in EPCs and promotes homing along hypoxic gradients; in addition, blockade of this receptor reduces their adhesion to sites of arterial injury (Hristov et al. 2007a).

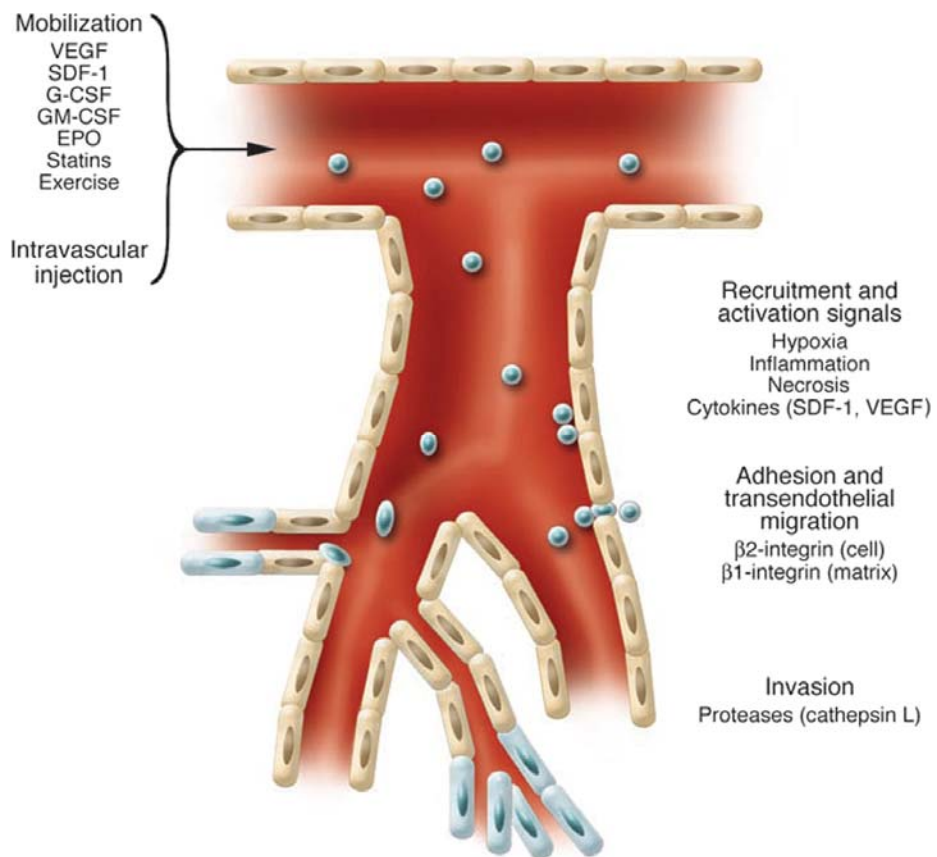


Figure 1.11 – Mobilisation and homing of EPCs in neo-vascularisation
[Adapted from Dimmeler, Zeiher & Schneider 2005]

Adherence of platelets on the exposed subendothelial matrix of the injured vessel wall has recently been shown to be an important part of this SDF-1 α -mediated recruitment (Massberg et al. 2006; Rafii et al. 2008). Firm attachment of EPCs is thought to be mediated by adhesion molecules, initially E- and P-selectin and subsequently integrins (Hristov et al. 2007b); one such example is the $\alpha 1\beta 4$ integrin, the most common integrin on CD34+ cells, which mediates attachment to vascular endothelial adhesion molecule 1 (VCAM-1, expressed on inflamed endothelium) and cellular fibronectin (Jin et al. 2006). Final differentiation into mature ECs is the result of interactions which are still poorly understood; these include circulating growth factors as well as locally secreted factors by SMCs, platelets, and the existing endothelium. VEGF, SDF-1 α and the mechanical force of blood flow (shear stress) are thought to play a primary role here (Zampetaki, Kirton, & Xu 2008).

1.4.6 Enhancing recruitment, homing and retention of EPCs

1.4.6.1 Introduction

Prior to the discovery of endothelial progenitors, there had been attempts to enhance re-endothelialisation by seeding the vessels with mature ECs. These methods were faced with weak adherence of the cells to the vessel wall, which necessitated prolonged seeding time and cessation of flow. Clinically, an important problem was the sourcing of sufficient numbers of non-proliferative autologous ECs, which would require sacrifice of other vessels (Gulati, Lerman, & Simari 2005; Gulati & Simari 2004; Kipshidze et al. 2004).

Studies attempting to enhance re-endothelialisation and neovascularisation have also been faced with some of these issues; namely the low availability of these cells, which

can be improved by expansion in culture (although this may be an issue for subsequent administration to humans), and the low uptake at the site of injury. For example, based on animal experiments it has been estimated that in the context of critical limb ischaemia in humans, 12 litres of blood would be necessary to harvest sufficient numbers of EPCs for an effective intravenous infusion (Iwaguro et al. 2002). There have been attempts with several techniques to overcome these hurdles; these include local delivery, increasing mobilisation and potency by gene therapy, seeding of grafts prior to implantation and recruitment of endogenous EPCs. Some of these techniques are considered next.

1.4.6.2 Local delivery of EPCs to sites of injury

Most of the clinical trials aiming neovascularisation in the heart have implemented delivery in the form of intracoronary injection, delivering the cells where they are most likely to be effective in their role (Hristov & Weber 2006). To increase adherence and extravasation of the cells, the arterial flow is halted for multiple periods of 2-4 minutes, alternated with short periods of reflow to avoid ischaemia. However, even in these favourable conditions, very few of the administered cells actually remain on site; for example, following intracoronary PB-MNC injection with 3 minutes flow-stop, 2.6% of cells remain in the heart of rats (Hou et al. 2005). The vast majority escape and get trapped in the lung, liver and spleen. Similar results have been shown in humans (Hofmann et al. 2005).

1.4.6.3 EPC mobilising agents

A way to increase the yield of EPCs for cell culture is to amplify the numbers of circulating cells by use of exogenous mobilising agents (section 1.4.5). This has been implemented successfully. The next logical step was to increase the endogenous EPC

numbers and attempt neovascularisation with the infusion of a mobilising agent, but without harvesting the EPCs. Although there were some positive results with cytokines such as G-CSF and SDF-1 α in animals (Laflamme & Murry 2005; Orlic 2005; Srinivas, Anversa, & Frishman 2009) the improvement was not coherent among animal models and, despite successful CD34⁺ mobilisation, did not work in humans (Abdel-Latif et al. 2008; Ince et al. 2008; Zohlnhofer et al. 2008). The exact reasons for which this treatment was not effective has not been elucidated; possibly part of the cause is that G-CSF mobilised cells are mainly committed monocytes and granulocytes, rather than EPCs, so selection for EPCs and expansion in culture may be necessary. Furthermore, G-CSF is known to be involved in the cleavage of the SDF-1 α receptor on EPCs, which may lead to impairment of their homing capacity (Zohlnhofer et al. 2008).

1.4.6.4 Gene transfer

An alternative strategy is to artificially enhance the numbers or the repair capacity of EPCs using gene transfer protocols. Plasmids encoding for VEGF successfully increased circulating EPC levels in humans after intramuscular injection in ischaemic lower limbs (Freedman 2002). Furthermore, *ex vivo* VEGF gene transfer into EPCs not only increased their integration in vasculature of ischaemic mouse hindlimbs, but also increased the endogenous neovascularisation, leading to increased limb salvation (Iwaguro et al. 2002). In an attempt to increase re-endothelialisation and prevent ISR, VEGF-eluting stents have been developed (Walter et al. 2004). However, recently it has been shown that local over-expression of VEGF can recruit leukocytes and cause plaque vulnerability in advanced atherosclerotic plaques (Lucerna et al. 2007).

1.4.6.5 EPC-capturing stents

Finally, the most recent advance aiming to increase EPC recruitment has been the clinical implementation of a stent coated with anti-CD34 antibodies, which causes rapid attachment of EPCs and re-endothelialisation following stent placement (Aoki et al. 2005; Co et al. 2008). Nonetheless, in a manner analogous to G-CSF-induced mobilisation (section 1.4.6.3), this approach non-specifically recruits all HSCs bearing the CD34 antigen, including potential progenitors for SMCs. This may lead to increased NI formation (Rotmans et al. 2005). Indeed, CD34-capturing stents have not managed to resolve the ISR seen after BMS implantation (Pompilio et al. 2009), and only after a handful of small trials, the first reports of CD34-stent thrombosis have started to emerge (Rossi et al. 2009).

Overall, these approaches, despite some of their negative aspects, serve to stimulate further research into the exact characteristics of EPCs and improved targeting strategies.

1.5 Summary

Atherosclerosis is an inflammatory process that affects a massive part of the population on a clinical level (1.3.1). Although the ageing of the arteries is a natural phenomenon, several factors serve to increase the risk of further complications, which eventually lead to occlusive events such as stroke and myocardial infarction, with considerable associated morbidity and mortality. The human body has an innate repair mechanism to fight the progression of atherosclerosis, the malfunction of which is linked to atherosclerotic progression (1.3.2.3). This repair mechanism may involve vascular progenitors that can accelerate or decelerate the progression of the lesions; these include the endothelial progenitor cells, which play a fundamental role in the repair of

endothelium and formation of new blood vessels, and have received considerable attention in the last decade (1.4.2). A rapid response by endothelial progenitors with complete re-endothelialisation is thought to be a primary factor in vessel protection after injury (1.3.2.5.2), which can be either endogenous or iatrogenic, such as after balloon angioplasty and stenting (1.3.2.5.3). Finally, although multiple strategies have focused on targeting these cells to the sites of damage (1.4.6), arterial stenosis is still a significant problem, the *Achilles' tendon* of interventional cardiology. Quoting Roncalli (2008):

Although the role of EPCs [...] is well established, the challenge for the next decade is to identify and evaluate methods that increase EPC homing and incorporation, thereby enabling targeted delivery of EPCs to a site of interest.

CHAPTER 2

MRI AND SUPERPARAMAGNETIC IRON OXIDE

2.1 Introduction

Magnetic resonance imaging (MRI) is an imaging technique based on the nuclear magnetic resonance phenomenon. It has gained popularity in the last 20 years, due to its ability to non-invasively image living beings with good tissue contrast and minimal energy deposition; this in contrast to modalities such as computed tomography, which utilises x-rays. These benefits are further enhanced by the use of contrast agents, that not only allow improved tissue contrast, but can also give information on pathological and metabolic states. As increasing numbers of MRI scanners are being used in hospitals and research laboratories around the world, it is a field that engages physicists, computer programmers, electrical and electronic engineers, clinicians, basic biologists and people across many more scientific disciplines.

With the recent advances in stem cell therapies, in the last ten years there has also been much interest in the use of iron oxide contrast agents for tracking the fate of transplanted cells in the body. It is these iron particles that have also been used in magnetic targeting applications, as described in Chapter 3. A great advantage of iron oxide particles is their multimodality, which allows for both magnetic targeting and imaging with a single agent. This chapter will therefore provide a background necessary to understand the basis of MRI and how superparamagnetic iron oxide particles help improve image contrast, as well as cell labelling techniques and the utility of MRI-based cell tracking.

2.2 Basic principles of MRI

2.2.1 The source of the signal that produces the image

In conventional MR imaging, the actual source of the signal comes from the magnetic moment of hydrogen nuclei inside a sample and is picked up by the receiving coil, which can be thought of as a radio antenna. Hydrogen is the predominant source of the MRI signal because of its high magnetic moment and relative abundance in living tissue such as water and fat. For example, an animal is comprised of tissue, which contains water molecules (Figure 2.1a). These water molecules have one oxygen and two hydrogen atoms. In simple terms, the hydrogen nucleus is comprised of a single unpaired charged proton possessing a spin; this moving charge creates a magnetic moment which behaves like a small dipole magnet (Westbrook, Roth, & Talbot 2005).

In the absence of any applied external magnetic field, the magnetic moments are randomly orientated and cancel each other out (Figure 2.1b), but in the presence of a large external field, such as that of an MRI scanner (B_0), they align parallel to it, and either with or against its direction. A higher percentage align with B_0 than against it, giving the tissue a small net magnetisation in the direction of the external field.

2.2.2 Nuclear magnetic resonance

Although the net magnetisation is parallel to and in the direction of B_0 , the individual moments that comprise it are actually rotating around the axis of B_0 , which is arbitrarily said to be the 'z' axis (Figure 2.2a). This rotation is called *precession* and has a specific frequency, the *Larmor frequency* (ω_0), for a given B_0 and a given atom:

$$\omega_0 = \gamma B_0 \quad , \quad \text{Equation 2.1}$$

where γ is a property of the specific nucleus and is called the gyromagnetic ratio. This is also called the *resonance* frequency, because energy can be transferred to the precessing moments if applied at this frequency.

The net tissue magnetisation cannot be measured directly. It is parallel to and much smaller than B_0 . However, it is possible to give it energy and ‘flip’ it to the side using a radiofrequency (RF) pulse at Larmor frequency, so that it transiently points toward a plane transverse to the external magnetic field (the ‘xy’ plane), in which case it can be picked up by the receiver coil (Figure 2.2b). If the RF pulse has exactly enough energy to tip the magnetisation from M_z to M_{xy} , it is called a 90° RF pulse. The instant after the pulse is applied, M_z is zero and M_{xy} is at its maximum, precessing around the xy plane. The receiver coil can only measure the magnetisation along this xy plane. Once the RF pulse is turned off, the magnetisation gradually returns to its previous state, or relaxes, and the received signal decays over time. There are two distinct processes during this relaxation period, the T_1 or ‘spin-lattice’ relaxation, and the T_2 or ‘spin-spin’ relaxation; these will be described in the next section.

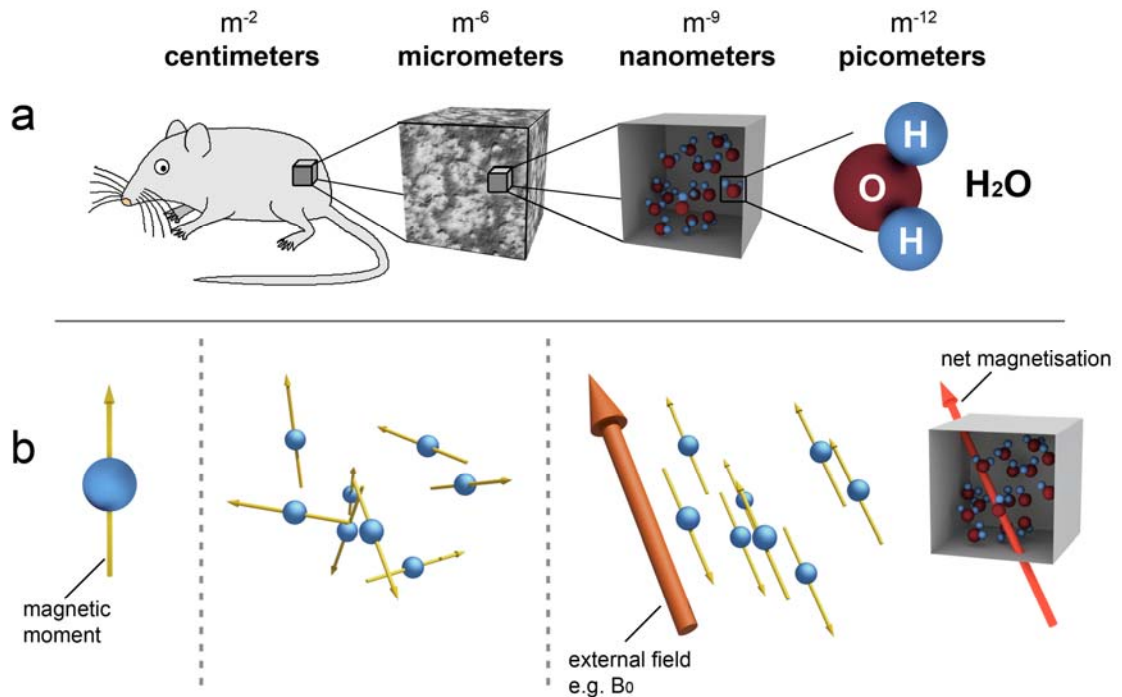


Figure 2.1 – The source of net magnetisation

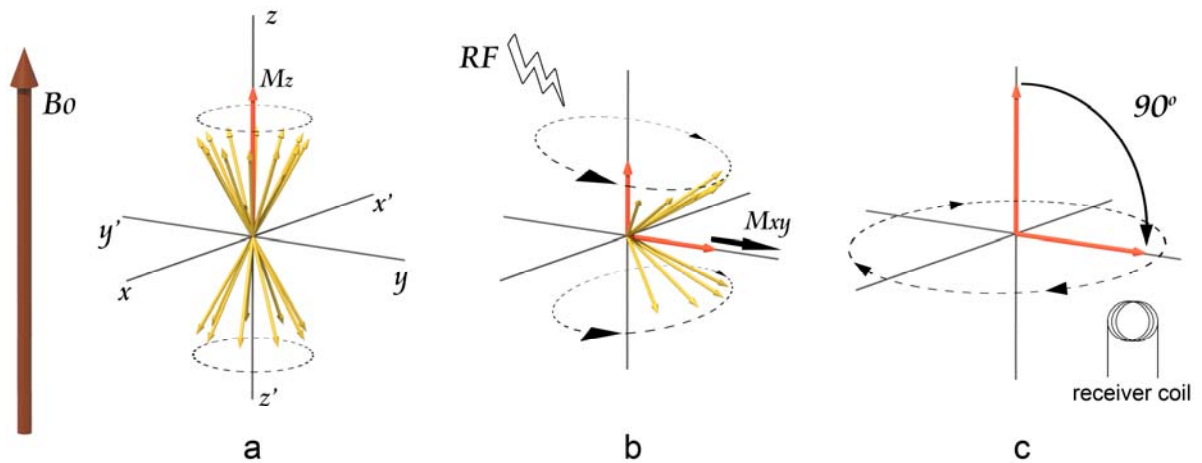


Figure 2.2 – Precession and application of a 90° RF pulse

Application of B_0 results in alignment and precession of the magnetic moments with the axis of B_0 , creating a net tissue magnetisation M_z (Figure 2.1b, Figure 2.2a). Application of an RF pulse leads to precession phase coherence and tilting of the precession axis, causing a drop in M_z and an increase in M_{xy} (Figure 2.2b). This is represented as tilting of the magnetisation from the z axis to the xy plane (Figure 2.2c). The rotating magnetisation causes a sinusoidal current in the receiver coil. This is the signal, whose intensity depends on the magnitude of the net xy magnetisation.

2.2.3 Relaxation

The so-called T_1 relaxation is the gradual increase in longitudinal magnetisation M_z following the RF pulse, as the magnetic moments reach equilibrium again; this commonly takes between 1 and 5 seconds to occur. The time constant T_1 is the time it takes for 63% of the recovery to occur; following a 90° pulse, M_z at time (t) is given by the following equation (Figure 2.3):

$$M_z(t) = M_{z,eq} \left(1 - e^{-t/T_1}\right) , \quad \text{Equation 2.2}$$

where $M_{z,eq}$ is the equilibrium magnetisation in the z axis (100%). For $t=T_1$:

$$M_z(T_1) = M_{z,eq} \left(1 - e^{-T_1/T_1}\right) = M_{z,eq} (1 - 1/e) \cong M_{z,eq} \times 0.63$$

T_2 relaxation is the decrease in M_{xy} following the RF pulse; this process occurs faster than T_1 ; $T_2 < T_1$. T_2 is less than T_1 because the net magnetisation in the xy plane, as described in the previous section, is also dependent on the phase coherence of the individual magnetic moments in that voxel. The RF pulse causes the moments to precess in phase with each other as a single magnetic moment, resulting in a measurable M_{xy} . Once the RF is switched off, each magnetic moment is free to precess at its own Larmor frequency, which is affected by the magnetic field it is experiencing. Due to local field inhomogeneities, the magnetic moments start to lose their phase coherence, eventually cancelling each other out and bringing M_{xy} to zero, even before M_z has reached its maximum. Thus T_2 is shorter than T_1 . The time after which M_{xy} has reached 37% of its original value is called T_2 ; following a 90° pulse, M_{xy} at time (t) is given by the following equation (Figure 2.4):

$$M_{xy}(t) = M_{xy,0} \times e^{-t/T_2} , \quad \text{Equation 2.3}$$

where $M_{xy,0}$ is the magnetisation in the xy plane immediately after the RF application.

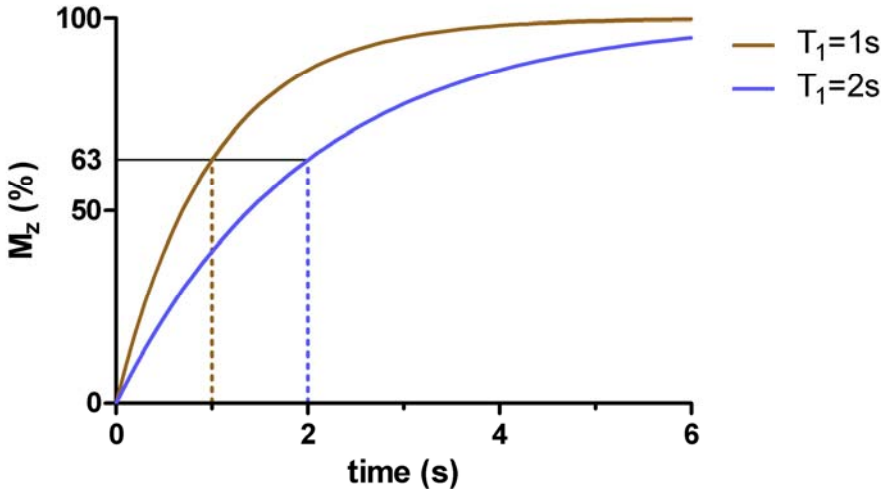


Figure 2.3 – T_1 relaxation

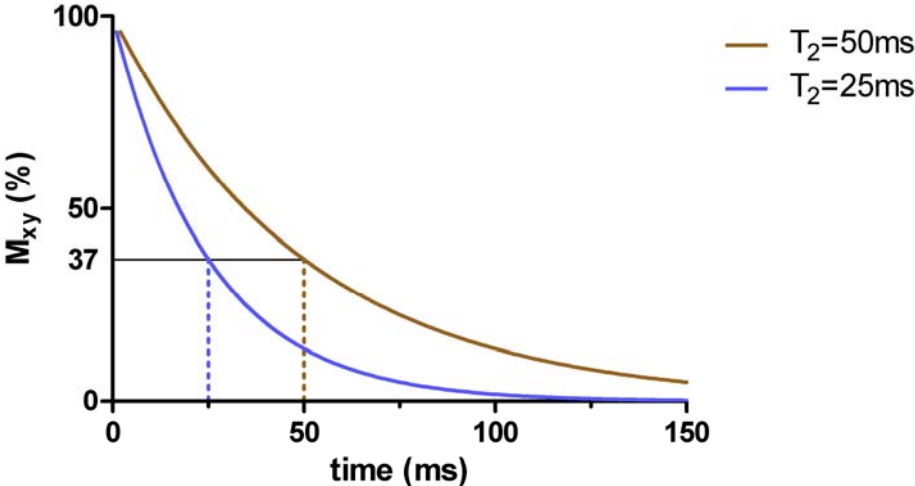


Figure 2.4 – T_2 relaxation

For $t=T_2$:

$$M_{xy}(T_2) = M_{xy,0} \left(e^{-T_2/T_2} \right) = M_{xy,0} (1/e) \cong M_{xy,0} \times 0.37$$

Assuming perfect 90° tilting $M_{xy,0}$ is also equal to $M_{z,eq}$.

In a system with no field inhomogeneities and if the magnetic moments experience the same external field over time, T_2 would be equal to T_1 . However, this does not occur in practice. There are differences in the local field of each moment, which occur due to: i) any spatial variations in B_0 ii) any local magnetic source in the tissue iii) the interaction with neighbouring magnetic moments. The tissue compartment affects (iii); a more fluidic environment will cause random interactions between the moments and a slower decrease in M_{xy} ; therefore a longer T_2 .

Presence of SPIO causes a local magnetic field and affects the moments in its vicinity, causing a lot of variation in the frequency with which they precess and thus a drop in M_{xy} , a decrease in T_2 , and faster loss of signal.

The differences in T_1 and T_2 within the tissue are what provides tissue contrast in MRI, by employing specific imaging techniques like T_2 -weighted sequences, which are sensitive to differences in T_2 .

2.2.4 Acquiring the signal

As previously discussed, only the magnetisation in the xy plane can be measured by the receiver coil. However, the dephasing of the magnetic moments can cause the signal to drop within microseconds. This is commonly overcome with the use of an additional 180° pulse, which flips the spins across to the other side of the xy plane, so that they

start to ‘travel back’ along the path they had travelled since the 90° pulse. Eventually they become coherent again (before dephasing in the other direction), giving a measurable signal, the *echo*. The time after the 90° pulse at which the echo occurs is the time-to-echo (TE), which is double the time between the 90° and 180° pulse. More 180° pulses can be applied to get multiple echoes from one 90° excitation, before all of the magnetisation on the xy plane has diminished. This happens due to two reasons: the return of the magnetisation to the z axis (which occurs slowly), and the presence of local field inhomogeneities that are varying in time, and thus affect the frequency of the magnetic moments differently between the pulses, causing a less accurate re-phasing and a decrease in the net xy magnetisation at the time of the echo.

The magnitude of M_{xy} when the echo occurs is directly correlated to the current induced in the receiver coil and the signal intensity (SI) that is attributed to the specific voxel. If TE is long, time-varying field inhomogeneities have more opportunity to affect the phase coherence of the moments in an irreversible way, and SI is lower. In general, SI is related to TE according to the following equation:

$$SI = M_{xy,0} \times e^{-TE/T_2} \quad , \quad \text{Equation 2.4}$$

which is essentially the same as Equation 2.3; $SI = M_{xy}$ at $t = TE$.

T₂-weighted sequences have long TE’s to give the time-varying inhomogeneities more chance to affect the magnetic moments, producing lower signal intensities from tissues with shorter T₂ values.

2.2.5 Spatial localisation of the MR signal

In the absence of any additional intervention, all the above processes would produce a concurrent echo from all the voxels in the sample, which would not be of interest for

imaging. To discriminate between the voxels, additional magnetic fields are superimposed on B_0 on all three axes. These fields are not homogeneous like B_0 ; instead they have a known spatial field gradient (usually linear) and are applied at specific times throughout the RF excitation and acquisition cycle. The slice-select gradient is applied during the 90° pulse. It works by inducing a range of Larmor frequencies along its direction, allowing the RF pulse to couple with and tilt the magnetisation of only the required plane of voxels, the slice.

The phase- and frequency-encoding gradients are applied in the other two directions before and during acquisition. These gradients change the precession frequency of magnetic moments along one axis, and timing of the echo along the other axis. Thus, the signal from each region in a sample will have a specific frequency, depending on the particular location of that voxel in the plane of the excited slice. The acquired signal is decoded using a mathematical process called Fourier transform, and the image corresponding to the particular slice of tissue is reconstructed. The intensity of each pixel in the image, usually in grayscale, is defined by the average signal intensity that originated in that region. Thus, the MR image is generated.

2.3 Superparamagnetic MRI contrast agents

2.3.1 Introduction

Superparamagnetic materials are magnetised when in a magnetic field, but lose this magnetisation once the field is removed. Superparamagnetic iron oxide (SPIO) nanoparticles can be used as MRI contrast agents because they acquire a magnetic moment inside the MRI scanner. This causes a lot of local field inhomogeneity in the tissue surrounding the particles, leading to loss of phase coherence of the magnetic moments of the tissue following RF excitation and a decrease in SI (section 2.2.4). In this way, tissues containing SPIOs appear darker on T2 and T2* MR images (Fahlvik, Klaveness, & Stark 1993; Nelson & Runge 1995).

Several SPIO particles exist for MR imaging applications, each exhibiting different biodistribution. A well-known SPIO nanoparticle is AMI-25, commercially known as *Endorem*® in Europe and *Feridex*® in the U.S.A, whose diameter is 80-150nm and it is comprised of magnetite crystals (each 4.8-5.6 nm in diameter) enclosed in dextran, a glucose polysaccharide (Wang, Hussain, & Krestin 2001) (Figure 2.5).

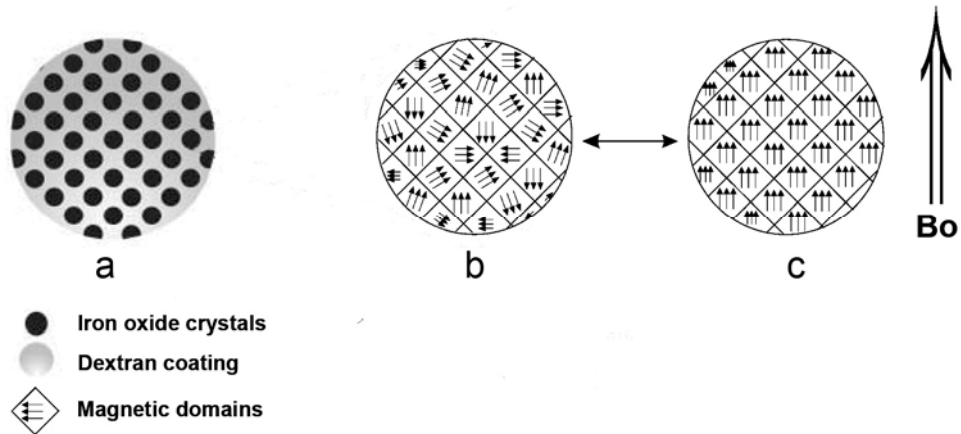


Figure 2.5 – Endorem® structure and superparamagnetism
 [Adapted from Wang, Hussain & Krestin 2001]

Each Endorem® particle is 80-150 nm in diameter and consists of iron crystals enclosed in dextran (a). In the absence of an external magnetic field, the magnetic domains of SPIO are orientated randomly (b), but will align parallel to the B_0 field once inside an MRI scanner and thus give the particle its own magnetisation (c).

2.3.2 Endorem for *in vivo* contrast enhancement in humans

Endorem® has been licensed by the Food and Drug Administration (FDA) for MRI of the liver. Following injection in the peripheral circulation, the iron particles are rapidly phagocytosed by the reticuloendothelial system in the liver (blood half-life: 6h), causing a decrease in signal intensity of the liver parenchyma. The signal intensity of lesions that do not contain phagocytic cells, such as metastatic tumours, remains unaffected; this increases tumour-to-liver contrast and lesion detectability (Reimer & Tombach 1998)(Figure 2.6). Endorem® has been shown to be fully biocompatible following intravenous injection; the particles are broken down intracellularly in the liver and the iron is eventually incorporated in erythrocyte haemoglobin (Weissleder et al. 1989).

2.3.3 SPIOs for cellular tracking *in vivo*

Apart from the usual usage of SPIOs, with the advent of cell therapies it is becoming ever more important to be able to monitor stem cell migration and trafficking (Bulte & Kraitchman 2004). In the cardiovascular system, SPIO-labelled MSCs have been tracked in the heart of rats, pigs and dogs for up to 7 weeks after peripheral or intracardiac injection (Chemaly et al. 2005). Following peripheral injection, MSCs have also been tracked in the spleens of rats (Arbab et al. 2004a). These are only a few examples of the multitude of research that has focused on SPIO-based cell tracking. More importantly for this thesis, CD34⁺ cells (Figure 2.7) and CD133⁺ cells (Figure 2.8) have been previously labelled with SPIO. This has allowed single CD34⁺ cell visualisation in the bone marrow of immunodeficient mice (Lewin et al. 2000) and CD133⁺ cell incorporation into sites of neovascularisation of tumours implanted in mice (Arbab et al. 2008; Arbab et al. 2006; Rad et al. 2009). For a discussion of the latter studies with CD133⁺ cells see section 4.2.4.2.

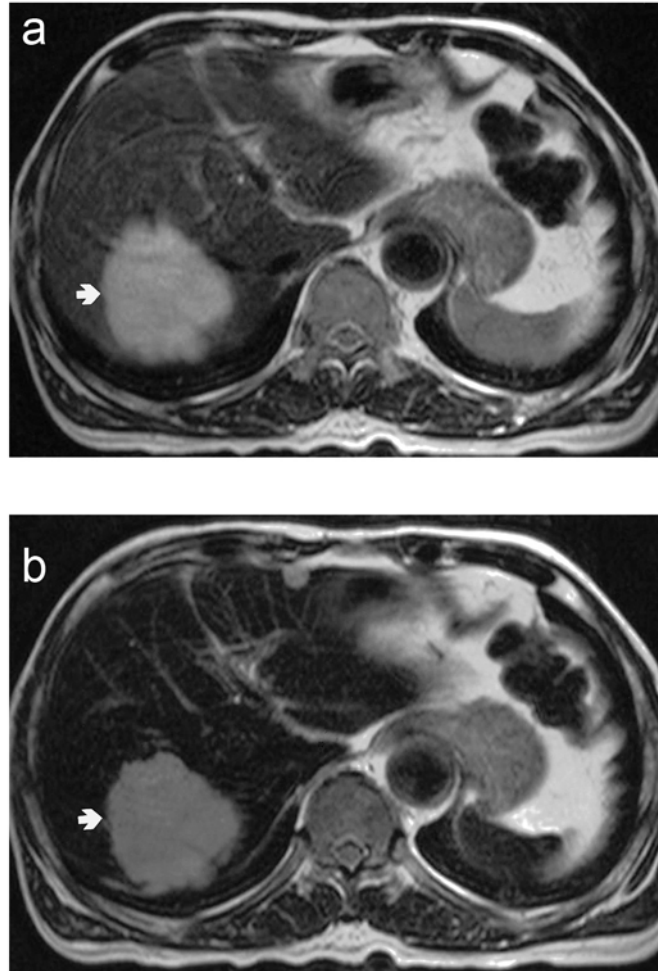


**Figure 2.6 – Contrast enhancement of liver lesions using Endorem®
a: pre-contrast, b: post-contrast
[Adapted from Lee et al. 2003]**

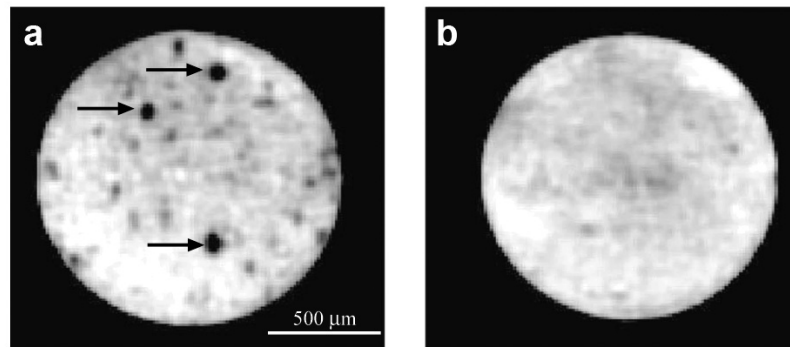


Figure 2.7 – MR visualisation of CD34+ cells in the mouse bone marrow
[Adapted from Lewin et al. 2000]

Ex vivo MR images of immunodeficient mouse bone marrow 24 hours after injection of (a) SPIO-labelled and (b) unlabelled CD34+ cells. Acquired at 14T.

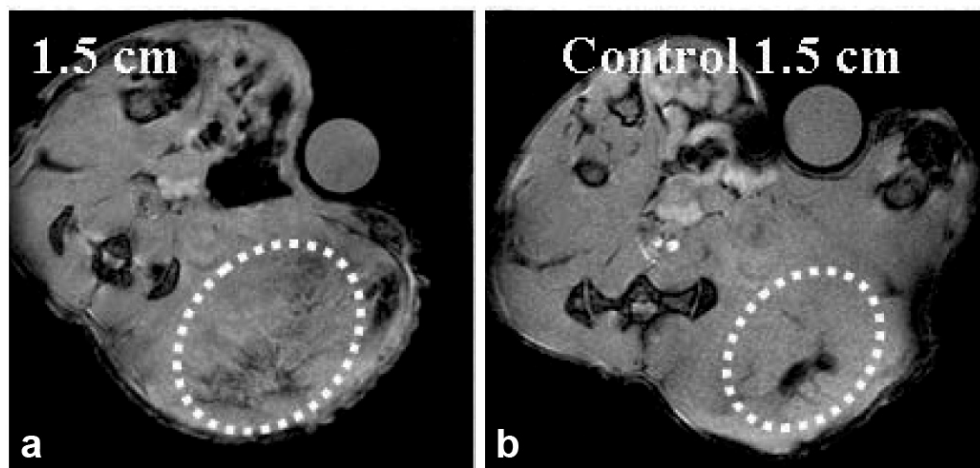


Figure 2.8 – MRI of CD133+ cells trafficking to a site of tumour angiogenesis
[Adapted from Arbab et al, 2006]

Approximately 2 weeks after peripheral injection, SPIO-labelled CD133+ cells were visualised as a diffuse hypointensity at the tumour site (a). Only a dark central area of necrosis can be seen in the control tumours (b).

2.3.4 *In vitro* SPIO labelling methods

The first reports on labelling non-phagocytic cells with MR contrast agents *in vitro* date to the early 1990's, in which mouse neural transplants were labelled with iron oxide (Hawrylak et al. 1993). SPIOs have since been used to label a variety of cells, including lymphocytes, leucocytes, monocytes and neural, mesenchymal and haematopoietic stem cells (Bulte & Kraitchman 2004). Several groups used SPIOs without modifying the dextran coating, thus depending on non-specific endocytosis-mediated uptake, which generally resulted in low iron uptake in non-phagocytic cells. Initial efforts to increase uptake, which included enclosing the iron oxide in liposomes (Bulte et al. 1993) or using lectins (Bulte et al. 1996), led to moderate success.

Markedly increased intracellular incorporation was first achieved in 1999 by modification of the dextran coating of the particles to utilise specific receptor-mediated endocytosis pathways. One method involved conjugating the dextran with the HIV tat-1 peptide (Josephson et al. 1999; Lewin et al. 2000). This peptide contains a signal that causes membrane translocation, thus aiding the incorporation of the particles into the cell. The other method involved conjugation of the mouse antibody for transferring receptor 'OX-26' with the dextran coating, which caused receptor-mediated endocytosis via the transferrin receptor situated on the cell membrane (Bulte et al. 1999). Other attempts included conjugating particles with polymeric dendrimers, producing 'magneto-dendrimers' (Bulte et al. 2001) or manufacturing dextran-free anionic particles (Billotey et al. 2003; Wilhelm et al. 2003a).

A method that has gained in popularity is the combination of SPIOs with transfection agents through electrostatic interactions (Kalish et al. 2003). Promising results have been obtained using high molecular weight poly-L-lysine (PLL) (Anderson et al. 2004; Arbab et al. 2003b; Arbab et al. 2003a; Cahill et al. 2004; Frank et al. 2003; Frank et al.

2002; Kraitchman et al. 2003) and SPIO-protamine sulphate complexes (FePro). The latter has been shown to yield better results, both in terms of labelling efficiency and cell viability (Arbab et al. 2005; Arbab et al. 2004b; Panizzo et al. 2009). Despite being efficient in labelling, all of the above methods have the obvious disadvantage of being custom-made in the laboratories, not commercially available, and lacking FDA approval. For example, there have been reports of impaired differentiation capacity following labelling with the combination of Feridex® and PLL (Kostura et al. 2004). However, there are no reports of decreased viability or differentiation when Endorem® (or Feridex®) alone were used. To date, there has been only one clinical study of MR-based cell tracking in humans using MRI (de Vries et al. 2005). In this study, the cells were labelled with Endorem® alone.

Previous work with haematopoietic cells has included labelling with micron-sized iron oxide particles (Hinds et al. 2003), SPIO-PLL (Arbab et al. 2003a) and SPIO-protamine sulphate complexes (Arbab et al. 2008; Arbab et al. 2006; Arbab et al. 2005; Arbab et al. 2004b; Rad et al. 2009). Cellular iron content in these experiments ranged from 10-30pg/cell. All studies reported good cell viability using preliminary assays such as trypan blue exclusion and metabolic activity assays and undisturbed differentiation. In general, adherent cells are easier to label than cells in suspension; the mechanism responsible for this observation has not been elucidated (Arbab et al. 2003a).

2.4 Summary

MRI is an anatomical imaging technique based on the magnetisation of tissue. This magnetisation can be disturbed by the presence of iron, and this effect has been utilised to non-invasively track cells labelled with iron oxide agents. Despite the numerous labelling protocols available, their clinical use has possibly been hampered by the implementation of non-approved manufacturing protocols and transfection agents.

CHAPTER 3

MAGNETIC TARGETING

3.1 Introduction

This chapter will provide an outline of the current state of magnetic targeting in medicine. Following that, I will present the essential background to magnetism and fluid dynamics for the understanding of the studies within the thesis.

The Greek philosopher *Thales of Miletus* (600BC) described magnetic rocks as stones with a soul, in one of the first written accounts of magnetism (Meyer 1972; Mourino 1991). This remote force has opened a new frontier for targeted delivery of magnetically tagged molecules and cells in modern medicine. The ability to localise the desired entity to a specific site from the peripheral circulation could offer increased efficiency due to a decrease in initial dosage, a decrease in non-specific distribution and side-effects, and maximum delivery to the target site (Lübbe, Alexiou, & Bergemann 2001).

As concluded in Chapter 1, there is a need for stem cell targeting strategies. Although magnetic drug targeting has been extensively studied in the last two decades, cell targeting has only just picked up and is still very much in its infancy.

3.2 Magnetic targeting in medicine

3.2.1 Laboratory uses of magnetic targeting

Since the 1980s there has been an increase in the use of magnetic carriers for biomedical applications. Perhaps the most widespread use is found in cell sorting equipment, where a magnetic bead conjugated to an antibody is used to separate the desired cell type by application of a magnetic force (Chalmers et al. 1998); for example, this immunomagnetic separation method has been used to select CD133+ cells from peripheral blood or bone marrow aspirates for EPC cultivation. Magnetic plates are also commonly used to increase transfection of cells with magnetically labelled DNA (Schillinger et al. 2005).

3.2.2 Magnetic drug targeting

Drug targeting to specific locations would be of great interest, particularly in the case of cancer, as anti-cancer medications have considerable side-effects. Magnetic drug targeting (MDT) was first suggested in the late 1970s. Since then many research groups have attempted MDT for cancer in various animal models, including mice and rats, with promising results such as enhanced tumour regression (Dobson 2006). Two Phase I/II clinical trials have been conducted so far, which confirmed the feasibility and safety of targeting magnetic carriers bound to anti-cancer medication (Lübbe, Alexiou, & Bergemann 2001; Wilson et al. 2004).

An important issue that has hampered the transition from animal models to humans is the scale-up of the magnetic forces, which have to be sufficient to withstand the fluid forces in the circulation. The majority of investigations have considered the application of external magnets; in humans this translates to very weak forces in deeper regions.

There have been several attempts to model and ascertain the relationship between particle size, iron content, and magnetic and fluid forces, for iron oxide particles ranging from 10nm to 2 μ m (Chen et al. 2008; Cregg, Murphy, & Mardinoglu 2008; Furlani & Furlani 2007; Grief & Richardson 2005; Min-Cheol et al. 2006; Ritter et al. 2004; Voltairas, Fotiadis, & Michalis 2002). The details of these reports are beyond the scope of this text as they have dealt with relatively small carriers with high iron content, which is a scenario not applicable to targeting of cells. However, the consensus is that magnetic targeting using external magnets will be most effective in regions close to the surface of the body. It is not possible to ‘focus’ the force to a deeper region; the area closer to the magnetic source will always experience a stronger force.

To allow for targeting of deeper regions within the body, there have been some invasive attempts to embed metallic implants in the tissue that cause a local magnetic force; these take the form of needles, stent-like wires and seeds (Avilés, Ebner, & Ritter 2008; Forbes et al. 2003; Forbes et al. 2008; Iacob et al. 2004; Yellen et al. 2005). For example, *in vivo* studies have suggested that magnetic implants can successfully target drugs in deep regions of the body. In 2000, Kubo and colleagues showed that implantation of a permanent magnet to a tumour site increased magnetic liposome delivery by four-fold (Kubo et al. 2000). In addition, magnetic stent-like structures have been shown to enhance drug delivery in flowing circulations, both *in vitro* (Avilés, Ebner, & Ritter 2008) and *in vivo* (Forbes et al. 2008).

3.2.3 Magnetic cell targeting

Targeting cells from the peripheral circulation to a site of interest would have the obvious advantage of decreasing the number of cells needed for treatment and

concentrating the cells to the injury site. It has now been a decade since the first magnetic cell targeting report (Consigny, Silverberg, & Vitali 1999). In this time, few studies have looked into the possibility of targeting cells to specific locations within the body. However, the increasing interest in stem cells has caused a rise in cell targeting investigations, particularly in the last two years.

In vitro application of a magnetic field on cells via small magnets under the culture plate has been shown to concentrate cells in the area directly above the magnet. This has been shown using mature ECs labelled with 4.5µm-diameter beads (Consigny, Silverberg, & Vitali 1999), SPIO-PLL labelling of MSCs (Arbab et al. 2004a) and extracellular labelling of neural progenitor cells with integrin-binding microbeads (Hamasaki et al. 2005). Movement of macrophages in a field gradient has also been recorded with speeds up to 40µm/sec (Wilhelm, Gazeau, & Bacri 2002). Perhaps the most unusual aspect of the recent interest in magnetic cell targeting is creating cell patterns (Frasca, Gazeau, & Wilhelm 2009; Ho et al. 2009; Ino, Ito, & Honda 2007) (Figure 3.1 and Figure 3.2).

There have been limited *in vivo* cell targeting studies to date. In 1999, Consigny and co-workers used labelled and unlabelled mature circulating endothelial cells (CECs) in a rabbit iliac artery injury model. In their hands, catheter-delivered unlabelled CECs are pulled by gravity and only attach to the lower side of the lumen in the absence of flow. By using a combination of labelled and unlabelled CECs, an external magnet attached on top of the artery, and axial rotation of the animal, they achieved near-circumferential attachment of CECs.

Although this study by Consigny is a proof of concept, there are several issues that could be improved upon. Firstly, mature, non-proliferative CECs were used, which would possibly fail to multiply and re-endothelialise the artery following attachment.

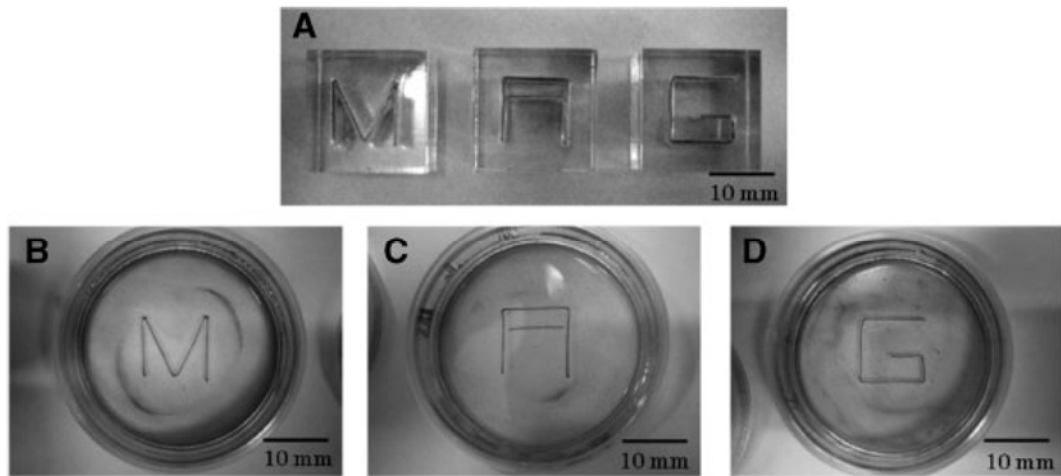


Figure 3.1 – Magnetic cell spelling
[From Ino, Ito and Honda 2007]

A metallic strip was embedded in a laser cut block (A) to spell out M,A,G (B-D).

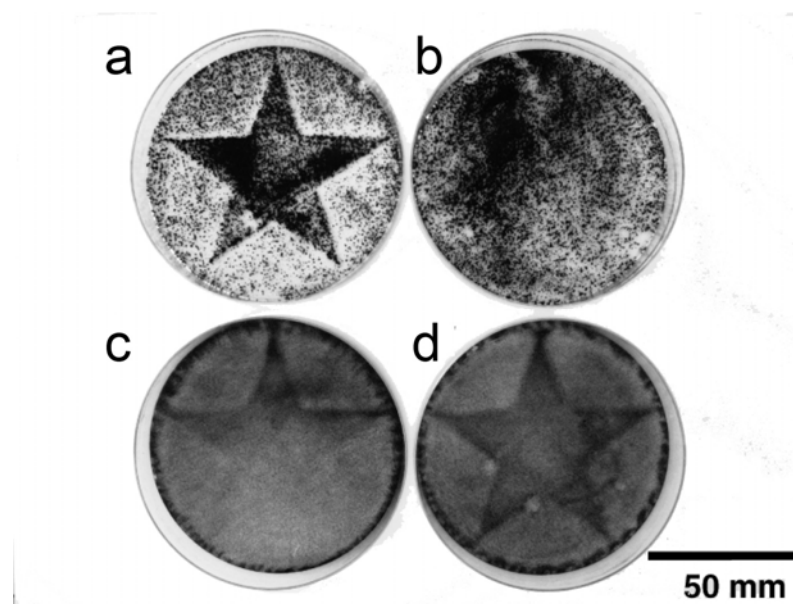


Figure 3.2 – Star formations with magnetic cells
[Adapted from Ho *et al* 2009]

A star-shaped magnetic device under the culture plate resulted in formation of a star-shaped cell colony (a), which did not form in the absence of the magnetic device (b). Interestingly, the stars formed even in the absence of iron oxide in the cells! (c and d).

A long-term investigation of re-endothelialisation was not performed; on the contrary the arteries were excised immediately after cell delivery and were investigated in only two animals. Finally, the beads used were micron-sized and not biodegradable; in addition was no investigation of the effect of the beads themselves, or of magnetic attraction, on cell viability. Later studies improved on some of these issues.

A few years later, SPIO-PLL labelled MSCs were targeted to the rat liver by using an external magnet (Arbab et al. 2004a). The doubling in cell number was attributed to the magnet and confirmed using histology and MRI. Although stem cells were used in this study, the clinical applicability of MSC targeting to the liver is limited and not discussed in the paper. SPIO labelling was shown not to affect the cell's viability; however any effect of the magnetic forces was not examined. Finally, the authors used PLL to transfect the cells, which is not optimal with regard to cell safety (section 2.3.4).

In 2006, endothelial outgrowth cells (EOCs) labelled with non-biodegradable micron-sized SPIO beads were injected in a carotid/femoral artery injury model in the absence of flow. In an attempt to increase the magnetic force locally, a magnetic wire (in the form of a stent) was implanted and this increased cell adhesion following 24h of reperfusion (Pislaru et al. 2006b). Although adhesion at 24h is, in effect, an indication of good viability after the application of the magnetic force, again this was not thoroughly examined in this study. Furthermore, attraction was not performed by using an external magnet but required an insertion of a custom-made permanent device.

Two more reports appeared in 2008. In the first, monocytes were labelled with magnetic particles available from the company Sigma-Aldrich, and targeted to the post-capillary venules of tumours using external magnets; the authors suggested that in the future this

may be used to deliver genes that can cause tumour cell death (Muthana et al. 2008). The other study used a magnetisable intravascular stent and external magnetic fields to generate high forces and target mature endothelial cells, labelled with custom-made iron particles, to carotid arteries (Polyak et al. 2008). For the first time, in these two studies the *in vivo* data were accompanied with *in vitro* data showing magnetic capture of cells within a flowing vessel at the appropriate flow speeds.

Finally, since the beginning of 2009, another two studies have been published. The first successfully targeted lentiviral vectors and umbilical vein endothelial cells to murine large arteries by implanting small strong magnets adjacent to the vessel wall (Hofmann et al. 2009). In the second, the authors managed to increase the numbers of hepatoma cells trafficking to murine livers by using an external magnet (Luciani et al. 2009). The clinical applicability of targeting cancer cells to the liver is questionable; despite this, as with Arbab (2004), this shows it is possible to target deeper regions in the body.

In summary, magnetic cell targeting is still limited to animal models. This may be attributable to two factors: 1) the problems associated with scaling up the magnetic forces to human distances, and 2) the widespread use of non-approved agents and devices, which make targeting easier due to higher iron content and applied magnetic forces, but at the same time may well be an obstacle to clinical translation. For structures close to the skin and slower flow speeds, external magnets are generally used, which would not require approval. Efforts on cell targeting in the arterial circulation have necessitated the use of large non-biodegradable micron-sized beads (Consigny, Silverberg, & Vitali 1999; Pislaru et al. 2006b; Pislaru et al. 2006a) or nanoparticle composites fabricated in-house (Polyak et al. 2008), and in most cases the additional

introduction of permanent metallic devices not currently approved for human use (Hofmann et al. 2009; Pislaru et al. 2006b; Pislaru et al. 2006a; Polyak et al. 2008).

Furthermore, the effect of applying a magnetic field or force on the viability of labelled cells remains largely unknown; interestingly, it has been observed that under a magnetic field, endosomes containing SPIOs elongate, align along the field lines and may fuse, due to the acquisition of magnetic dipole moment (Wilhelm et al. 2003b). Whether such organelle re-arrangements are harmful is not known.

3.3 Basics of magnetics

3.3.1 Magnetic fields

The source of all magnetic fields is a moving electrical charge (Schmitt 2002). This can be the spatial movement of a charged particle such as an electron (Figure 3.3), or the spin of a particle around its axis (as it happens in the case of the hydrogen protons that give the MRI signal, section 2.2.1). Permanent magnets have an ordered crystalline structure with aligned magnetic moments, giving the material a magnetic field (Figure 3.4). One of the strongest magnetic materials for permanent magnet design are ‘rare earth’ alloys such as neodymium iron boron ($\text{Nd}_2\text{Fe}_{14}\text{B}$) magnets, which are available commercially at various grades.

Using mathematical notation, the magnetic field at a specific location can be represented by a vector, which has both a magnitude and a direction (polarity). In this thesis vectors are represented by a bold character. The magnitude of the vector is represented by a non-bold character (e.g. $H=||\mathbf{H}||$). Two notations used to describe magnetic fields are the magnetic field strength \mathbf{H} (in amperes per meter, A/m), and the magnetic induction \mathbf{B} (in Tesla, T). \mathbf{B} can be thought of as the magnetic field induced in (and felt by) a material, when an external field \mathbf{H} is applied to the material. \mathbf{B} and \mathbf{H} are the same only in free space, and connected by the equation $\mathbf{B} = \mu_0\mathbf{H}$, where $\mu_0 = 4\pi \times 10^{-7}$ (in Tm/A, SI units) is the magnetic permeability of free space. However, the atomic structure of matter responds to \mathbf{H} , changing the field \mathbf{B} within the material; this effect will be considered next.

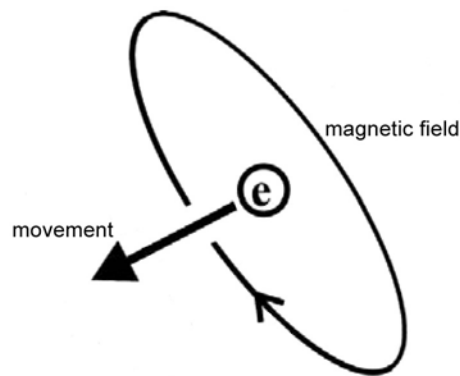


Figure 3.3 – Magnetic field around a moving electron
[Adapted from Schmitt 2002]

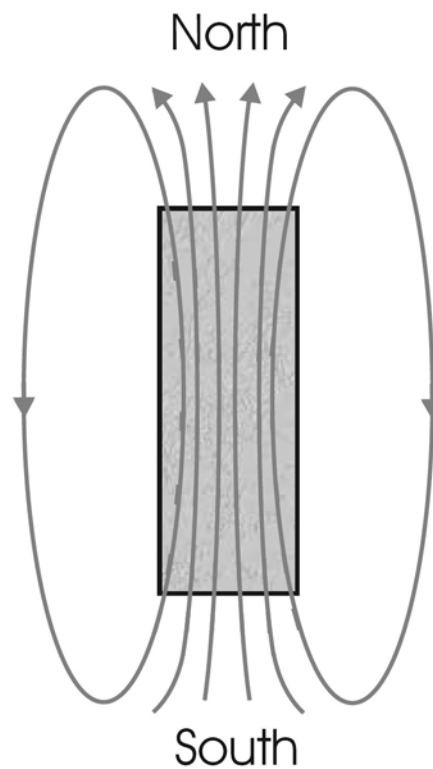


Figure 3.4 – Magnetic field around a permanent magnet
[From Schmitt 2002]

Permanent magnets tend to align with the Earth's magnetic field; they have a 'North' and a 'South' pointing pole. The material's magnetic field is due to the ordered crystalline structure with aligned magnetic moments (e.g. ferromagnetic materials).

3.3.2 Magnetisation of materials

When a material is placed in an applied magnetic field, a magnetic dipole moment \mathbf{m} (in Am^2 , SI units) is induced in the material. The way the material reacts, i.e. the direction and magnitude of the dipole moment, depends on the structure of the material. According to the way materials react, they can be classified into diamagnetic, paramagnetic, ferromagnetic and superparamagnetic (Pankhurst et al. 2003; Schmitt 2002).

The vector sum of the dipole moments in a volume of the material (V_m , in m^3) is the magnetisation \mathbf{M} , given by $\mathbf{M} = \mathbf{m}/V_m$ (A/m). If a material is placed in a magnetic field of strength \mathbf{H} , the magnetic field induced within the material (\mathbf{B}) is given by

$$\mathbf{B} = \mu_0(\mathbf{H} + \mathbf{M}) \quad . \quad \text{Equation 3.1}$$

In turn, \mathbf{M} is dependent on \mathbf{H} ; for moderate magnetic field strengths, the change in magnetisation is proportional to the material's magnetic susceptibility (χ), which is dimensionless in SI units:

$$\mathbf{M} = \chi\mathbf{H} \quad . \quad \text{Equation 3.2}$$

In diamagnetic materials (e.g. copper), a very weak magnetisation is induced that opposes the applied magnetic field. This is an intrinsic phenomenon in nature, whereby the motion of electrons orbiting around the nucleus changes in order to oppose the effect of the applied magnetic field. Although all materials have this diamagnetic component, only materials with no unpaired electrons exhibit diamagnetism.

In paramagnetic materials (e.g. aluminium), unpaired electrons exist. The spin of these electrons around their own axis creates an additional magnetisation, which in this case aligns with \mathbf{H} so that \mathbf{B} is now increased within the material; this magnetisation over

comes the diamagnetic component but is also quite weak, so paramagnetic materials have a small positive susceptibility.

Ferromagnetism is responsible for the existence of permanent magnets. Ferromagnetic materials (e.g. iron) have ordered clusters of magnetic dipole moments (domains), which align with the applied H-field. The difference between paramagnetic materials and ferromagnetic materials, is that in ferromagnetic materials the entire domain will align with application of an external H-field. As a result, the susceptibility of these materials is much higher; \mathbf{M} can typically be 10^4 times higher than in paramagnetic materials, and the resulting B-field is correspondingly increased. These materials exhibit memory (hysteresis); once the H-field is removed the domains remain partly aligned, giving the materials a remanent magnetisation (M_r). Another thing to note is that at H-fields of high magnitude, \mathbf{M} reaches a saturation value (M_s) as the domains are maximally aligned with the H-field; in this case

$$\mathbf{M} = M_s \mathbf{H}/H \quad . \quad \text{Equation 3.3}$$

For the sake of simplicity, it is common to define two limiting scenarios (Hayden & Hafeli 2006):

- i) the unsaturated response, in which \mathbf{M} changes proportionally to \mathbf{H} ($\mathbf{M} = \chi\mathbf{H}$)
- ii) the saturated response, in which \mathbf{M} is independent of \mathbf{H} ($\mathbf{M} = M_s \mathbf{H}/H$)

Two classes of material similar to ferromagnets are ferrimagnets and antiferromagnets; these materials have more complex structures and magnetic ordering within the material. One example is magnetite (Fe_3O_4), in which the Fe ions occupy two distinct interlaced sublattices. The magnetic Fe atoms in the two sublattices point in opposite directions and they are slightly different in size. Thus there is a net magnetisation

overall and magnetite behaves similarly to a ferromagnetic material. In antiferromagnets such as haematite ($\alpha\text{-Fe}_2\text{O}_3$), the magnetic moments on the two sublattices are the same size and cancel each other, thus there is no net magnetisation.

Superparamagnetic materials behave similarly to ferro/ferrimagnetic materials and attain large M values; however the particle size allows for the magnetic moment of the entire particle to rapidly fluctuate between energy minima in the absence of an H-field, so that they do not show hysteresis and thus do not remain magnetised once the H-field is removed. This property of superparamagnetic materials is dependent on the size of the particle and a critical temperature, the blocking temperature T_B , below which the material exhibits hysteresis.

M-H curves of materials (e.g. iron oxide solutions) and biological samples (e.g. cells) can be obtained using a superconducting quantum interference device (SQUID) (Hautot, Pankhurst, & Dobson 2005). The susceptibility χ , remanent magnetisation M_r and saturation magnetisation M_s can be derived from these curves (Figure 3.5).

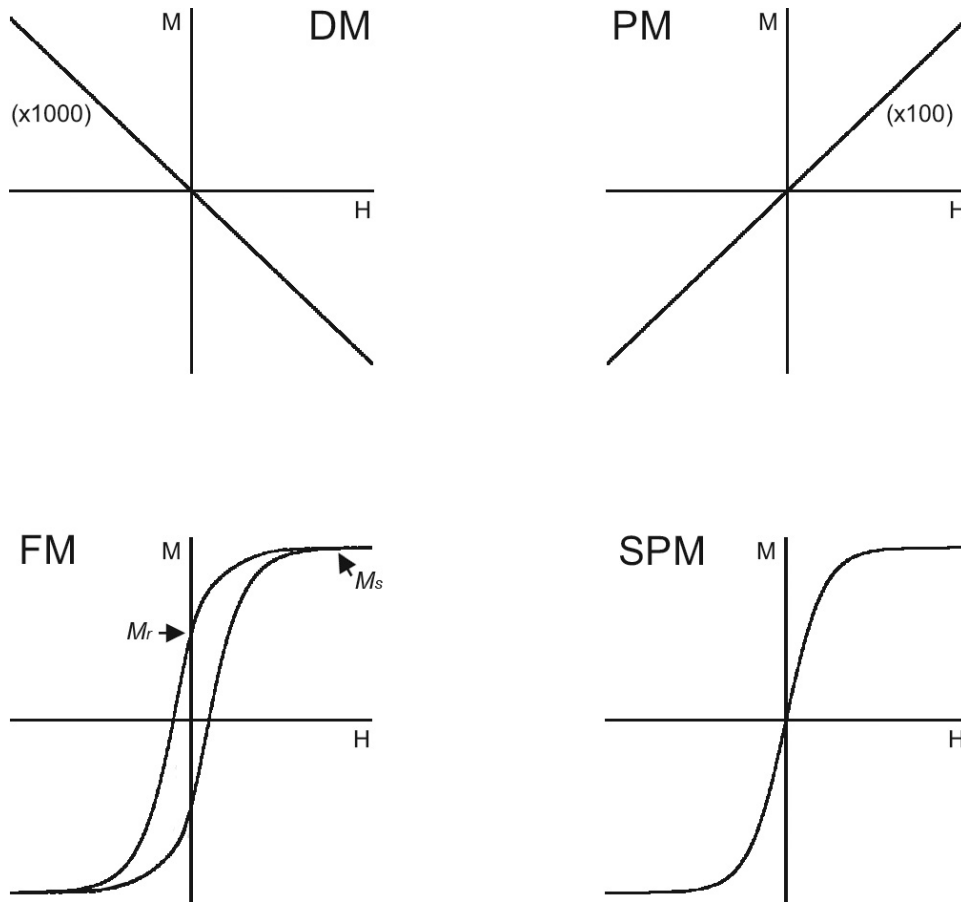


Figure 3.5 – Magnetisation vs magnetic field strength (M-H) curves
[From Pankhurst *et al* 2003]

Diamagnetic (**DM**) materials exhibit a very weak net magnetisation in the opposite direction of the applied H-field. Paramagnetic (**PM**) materials exhibit a weak magnetisation in the direction of the H-field. Note that since $\mathbf{M} = \chi\mathbf{H}$, the magnetic susceptibility χ is the slope of the M-H curve. Ferromagnetic (**FM**) materials have much increased net magnetisation and exhibit hysteresis; following removal of the H-field these materials remain magnetised with $M=M_r$. At high field strengths, the magnetisation reaches a saturation value $M=M_s$. Superparamagnetic (**SPM**) materials do not exhibit hysteresis.

3.3.3 Magnetic forces

Magnetic actuation of an element refers to movement of that element under the influence of a magnetic force. This force is the result of the presence of a magnetic field and also a gradient in that field, i.e. the rate at which the field strength is changing in space (Jiles 1998; Pankhurst et al. 2003). The force \mathbf{F}_m (measured in Newtons, N) acting on a magnetic particle with point-like dipole moment \mathbf{m} in a static, non-homogeneous field \mathbf{B} is defined as (Pankhurst et al. 2003):

$$\mathbf{F}_m = (\mathbf{m} \cdot \nabla) \mathbf{B} \quad , \quad \text{Equation 3.4}$$

where $\nabla = \frac{\partial}{\partial x} \mathbf{i} + \frac{\partial}{\partial y} \mathbf{j} + \frac{\partial}{\partial z} \mathbf{k}$ is the gradient operator, $\mathbf{m} = m_x \mathbf{i} + m_y \mathbf{j} + m_z \mathbf{k}$, $\mathbf{B} = B_x \mathbf{i} + B_y \mathbf{j} + B_z \mathbf{k}$ and \mathbf{i}, \mathbf{j} and \mathbf{k} are unit vectors in 3-dimensional Cartesian coordinate system.

Within this thesis, the magnetic forces on SPIO-labelled cells have been modelled using computer software. Due to the way these programs operate, it is necessary to express the force in terms of magnetic susceptibility of the cells. The forces on each axis must also be calculated in terms of the xyz components of the H-field vector, before calculating the total magnitude of the force. This is achieved as follows:

Assuming the cells are suspended in water, the magnetisation of the water is negligible and $\mathbf{B} = \mu_0 \mathbf{H}$ (from Equation 3.1) Also, $\mathbf{m}_c = V_c \mathbf{M}_c$ (the ‘c’ subscript denotes ‘cell’).

In the unsaturated case, $\mathbf{M}_c = \chi_c \mathbf{H}$ (Equation 3.2) and Equation 3.4 becomes:

$$\mathbf{F}_{m,unsat} = \mu_0 \chi_c V_c (\mathbf{H} \cdot \nabla) \mathbf{H} \quad . \quad \text{Equation 3.5}$$

Thus the force is higher with higher magnetic susceptibility of the cell (more iron content), and is dependent both on the magnetic field strength and also its gradient, i.e.

the rate with which the magnitude of \mathbf{H} ($\|\mathbf{H}\|=H$) is changing. The fast drop-off of magnetic field and field gradient at increasing distances is the main reason the scale-up of magnetic drug targeting from small animal models to humans has been so challenging, so magnetic devices have to be designed carefully.

To define the force in terms of the xyz components of the H-field vector, we have

$$(\mathbf{H} \cdot \nabla) = H_x \frac{\partial}{\partial x} + H_y \frac{\partial}{\partial y} + H_z \frac{\partial}{\partial z} \quad \text{and} \quad \mathbf{H} = H_x \mathbf{i} + H_y \mathbf{j} + H_z \mathbf{k} . \quad \text{Thus:}$$

$$(\mathbf{H} \cdot \nabla)\mathbf{H} = H_x \left(\frac{\partial H_x}{\partial x} \mathbf{i} + \frac{\partial H_y}{\partial x} \mathbf{j} + \frac{\partial H_z}{\partial x} \mathbf{k} \right) + H_y \left(\frac{\partial H_x}{\partial y} \mathbf{i} + \frac{\partial H_y}{\partial y} \mathbf{j} + \frac{\partial H_z}{\partial y} \mathbf{k} \right) +$$

$$H_z \left(\frac{\partial H_x}{\partial z} \mathbf{i} + \frac{\partial H_y}{\partial z} \mathbf{j} + \frac{\partial H_z}{\partial z} \mathbf{k} \right)$$

Because $\mathbf{F} = F_x \mathbf{i} + F_y \mathbf{j} + F_z \mathbf{k}$, the force component of each of the three axes is:

$$F_{x,unsat} = \mu_0 \chi_c V_c \left(H_x \frac{\partial H_x}{\partial x} + H_y \frac{\partial H_x}{\partial y} + H_z \frac{\partial H_x}{\partial z} \right)$$

$$F_{y,unsat} = \mu_0 \chi_c V_c \left(H_x \frac{\partial H_y}{\partial x} + H_y \frac{\partial H_y}{\partial y} + H_z \frac{\partial H_y}{\partial z} \right)$$

$$F_{z,unsat} = \mu_0 \chi_c V_c \left(H_x \frac{\partial H_z}{\partial x} + H_y \frac{\partial H_z}{\partial y} + H_z \frac{\partial H_z}{\partial z} \right)$$

The magnitude of the force vector is then $\|\mathbf{F}_{m,unsat}\| = F_{m,unsat} = \sqrt{F_x^2 + F_y^2 + F_z^2}$.

In the case of 2-dimensional modelling $H_z = F_z = 0$.

In the saturated case, the magnetic force is independent of the magnitude of \mathbf{H} (but still dependent on the gradient of \mathbf{H}). From Equation 3.3 and Equation 3.4 it follows that

$$\mathbf{F}_{m,sat} = \mu_0 M_{s,c} V_c (\mathbf{H}/H \cdot \nabla)\mathbf{H} = \mu_0 M_{s,c} V_c (\mathbf{H} \cdot \nabla) \frac{\mathbf{H}}{H} , \quad \text{Equation 3.6}$$

where $M_{s,c}$ is the saturation magnetisation of the cell and $\frac{1}{H} = \frac{1}{\|\mathbf{H}\|} = \frac{1}{\sqrt{H_x^2 + H_y^2 + H_z^2}}$.

The forces in each direction then become:

$$F_{x,sat} = \mu_0 M_s V \frac{1}{H} \left(H_x \frac{\partial H_x}{\partial x} + H_y \frac{\partial H_x}{\partial y} + H_z \frac{\partial H_x}{\partial z} \right)$$

$$F_{y,sat} = \mu_0 M_s V \frac{1}{H} \left(H_x \frac{\partial H_y}{\partial x} + H_y \frac{\partial H_y}{\partial y} + H_z \frac{\partial H_y}{\partial z} \right)$$

$$F_{z,sat} = \mu_0 M_s V \frac{1}{H} \left(H_x \frac{\partial H_z}{\partial x} + H_y \frac{\partial H_z}{\partial y} + H_z \frac{\partial H_z}{\partial z} \right)$$

These forces will be more accurate in cases where the cells are in a magnetic field of high magnitude.

The susceptibility of the cell χ_c is the susceptibility of the iron oxide the with which it is loaded $\chi(Fe_3O_4)$ scaled to the volumetric amount of Fe_3O_4 in a single cell. The susceptibility of the iron oxide $\chi(Fe_3O_4)$ can be estimated from SQUID M-H curve of a sample (Figure 3.6). The susceptibility of the cell χ_c can be estimated from the M-H curve of a cell sample or calculated from the volume-per-volume loading of the cell with Fe_3O_4 (L_c), if $\chi(Fe_3O_4)$ is known:

$$\chi_c = \chi_{Fe_3O_4} \times L_c \quad , \quad \text{Equation 3.7}$$

$$L_c = \frac{V_{Fe_3O_4}}{V_c} = \frac{m_{Fe_3O_4} / \rho_{Fe_3O_4}}{\frac{\pi}{6} D_c^3} \quad , \quad \text{Equation 3.8}$$

where m is the mass of Fe_3O_4 in the cell, ρ is the Fe_3O_4 density and D_c the cell diameter.

The saturation magnetisation $M_{s,c}$ can be estimated from the SQUID M-H curve of a cell sample or scaled volumetrically from the saturation of Fe_3O_4 .

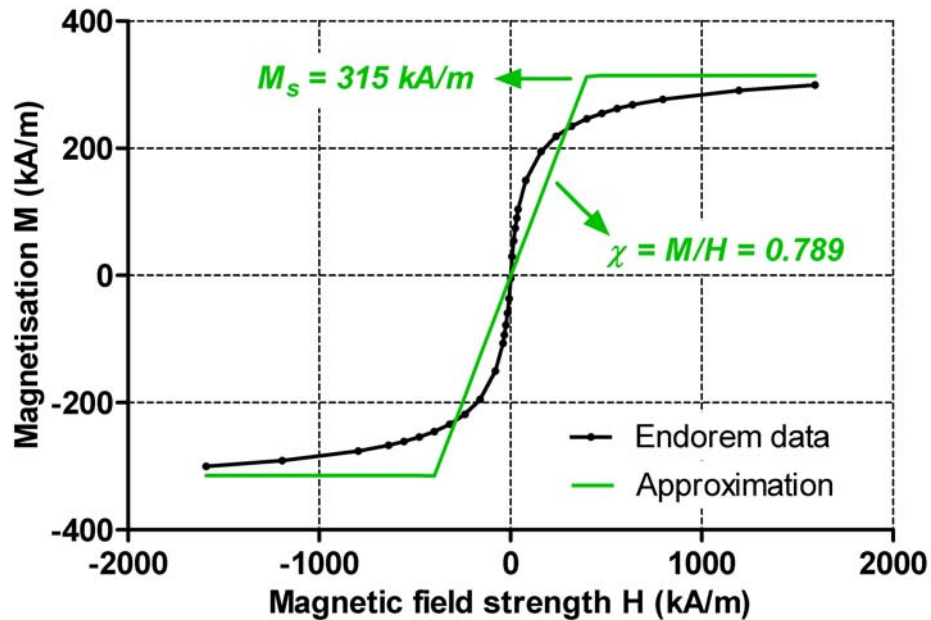


Figure 3.6 – SQUID M-H curve of a sample of Endorem®

The measured magnetisation is shown in black. For force calculations it is common to distinguish between two limiting approximate cases (green). That for which M increases in proportion to H ($\mathbf{M}=\chi\mathbf{H}$) and that in which the magnetisation reaches a saturation value M_s . The saturation limit is defined arbitrarily. Here $\chi=0.789$ up to $H=398$ kA/m ($B=0.5T$ in free space or weakly diamagnetic medium such as water). For $H>398$ kA/m ($B>0.5T$), the forces should be calculated using the expressions for the saturated case. Note that because the calculation of χ for Endorem® is made based on the arbitrary selection of the saturation limit, all further calculations are based on this approximation. This data was acquired by Dr Ana Garcia-Prieto as part of this project.

3.4 Fluid dynamics

3.4.1 Introduction

Fluid dynamics is the study of flowing liquids and gases (fluids). In the case of magnetic targeting, it is easy to appreciate that the success of cell capture within a flowing circulation will depend on the ability of the magnetic force to drag the cells through the moving liquid, overcoming the drag forces acting on the cells from the liquid. This relationship is considered in Chapter 6 of this thesis. This introductory section will briefly describe the theory on which Chapter 6 is based (Fay 1994; Nakayama & Boucher 1999; Shaughnessy, Katz, & Schaffer 2005).

3.4.2 Basic concepts

While the classification of a substance into a gas or a liquid is straightforward, the boundary between liquids and solids is less clear. For example, materials such as porridge, paint and toothpaste lie somewhere between a solid and a liquid, and behave in a complex way when a force is applied on their surface. Such semi-fluids are called non-Newtonian. In contrast, all gases and most common liquids, such as water, are called Newtonian.

The governing equations that describe the behaviour of a Newtonian fluid are called the Navier-Stokes equations. These equations are complicated, but can be simplified in a number of ways that make them easier to solve in each specific application (Shaughnessy, Katz, & Schaffer 2005). One such simplification is the case of fluid that is incompressible (i.e. has constant density), which is a valid approximation for all liquids. The Navier-Stokes equations can be applied to a large number of fluid dynamics problems under turbulent or laminar flow.

3.4.3 Turbulent vs laminar flow

Turbulent flow is the chaotic behaviour of the fluid that results from large inertial forces. Whether fluid flow is turbulent or laminar (Figure 3.7) depends on the dimensionless Reynolds number, which is essentially a ratio of the inertial versus viscous forces in the fluid:

$$Re = \frac{\rho u L}{\mu} \quad , \quad \text{Equation 3.9}$$

where ρ is the fluid density (kg/m^3), u is flow velocity (m/s), L is a characteristic length scale (m) and μ is the fluid viscosity (kg/ms) (Figure 3.8). Thus higher Re results in more turbulence.

Low Re values result in laminar flow; this means that the flow occurs in parallel layers (laminae) that do not get disturbed (Figure 3.7). For example, pipe flows with $Re < 2300$ are almost always laminar. Flow with $Re < 1$ is called *creeping* or *Stokes* flow. It has to be noted that the transition Re , above which flow starts to become turbulent, can be very different depending on whether the flow under consideration is internal (e.g. flow in a pipe) or external (e.g. flow around a sphere); see Figure 3.8.

Only laminar flows will be considered from this point onwards.

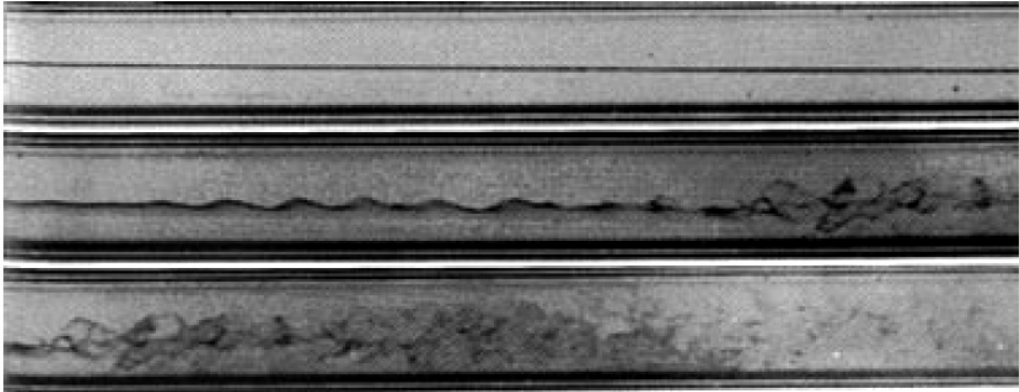


Figure 3.7 – Laminar and turbulent flow visualisation
[From Shaughnessy, Katz, & Schaffer 2005]

Side view a parallel chamber with flow from left to right. Dye injected in slow, laminar flow travels in a single streamline (top image). The flow becomes turbulent with increasing fluid velocity (middle and bottom).

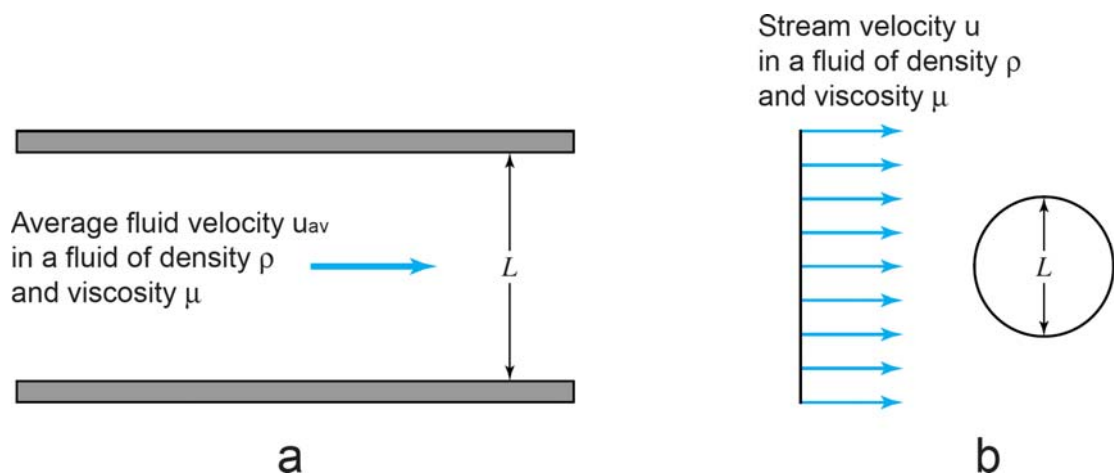


Figure 3.8 – Choice of velocity and length scales used in calculating Re
a: internal flow, b: external flow
[Adapted from Shaughnessy, Katz, & Schaffer 2005]

At boundaries with solids, the surface is so rough at a molecular level that there is no relative motion between the fluid and solid particles. This creates a boundary layer with zero velocity and what is known as a “no-slip” condition. In laminar flow, the velocity then progressively increases, so that at the centre of the flow field the velocity reaches a maximum (Figure 3.9). The velocity across a pipe has a parabolic flow profile; at any point of the pipe radius r , the velocity u is given by:

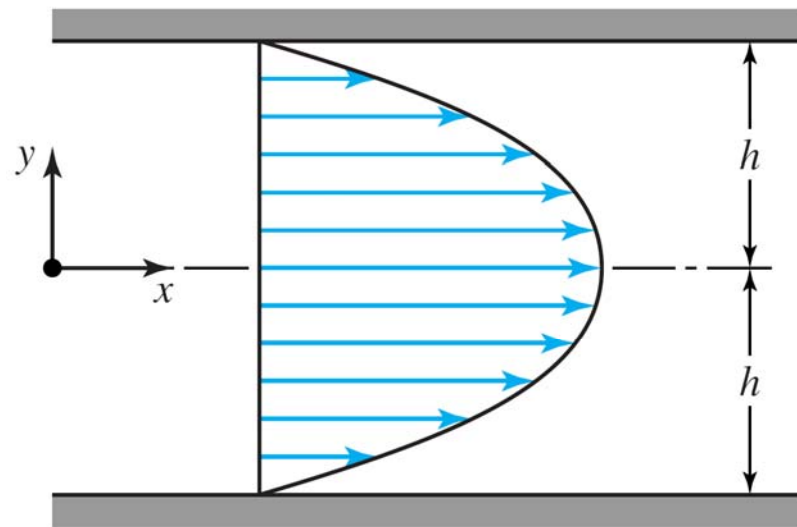
$$\mathbf{u}(r) = \mathbf{u}_{max} \left[1 - \left(\frac{r}{R} \right)^2 \right] , \quad \mathbf{u}_{max} = 2\mathbf{u}_{av} \quad \text{Equation 3.10}$$

where R is the radius of the pipe. The average velocity \mathbf{u}_{av} related to the average flow rate Q and the tube cross-sectional area A : $\mathbf{u}_{av} = Q/A$. In computer modelling, it is simpler to model the flow through parallel plates in 2 dimensions. The velocity field is then given by:

$$\mathbf{u}(y) = \mathbf{u}_{max} \left[1 - \left(\frac{y}{a} \right)^2 \right] , \quad \mathbf{u}_{max} = \frac{3}{2} \mathbf{u}_{av} , \quad a = \frac{h}{2} \quad \text{Equation 3.11}$$

where h is the distance between the plates and $y=0$ is the mid-plane between the plates (Figure 3.9).

Laminar flow with a parabolic profile is the model of choice in magnetic drug targeting simulations (Avilés, Ebner, & Ritter 2008; Chen et al. 2008; Cregg, Murphy, & Mardinoglu 2008; Forbes et al. 2003; Furlani & Furlani 2007; Grief & Richardson 2005; Voltairas, Fotiadis, & Michalis 2002; Wang, Liu, & Xu 2008).



$$u(y) = u_{\max} \left[1 - \left(\frac{y}{h} \right)^2 \right]$$

Figure 3.9 – Parabolic flow between two parallel plates
[From Shaughnessy, Katz, & Schaffer 2005]

3.4.4 Hydrodynamic drag on a sphere

Hydrodynamic drag is the force that a moving fluid exerts on an immersed body. For a sphere of radius r (m), in a fluid of density ρ and velocity u this force is given by:

$$\mathbf{F}_d = C_D \frac{1}{2} \rho A u^2 \quad , \quad \text{Equation 3.12}$$

where $A = \pi r^2$ (m²) is the maximum cross-sectional area of the sphere and C_D is a drag coefficient. This drag coefficient is a function of the Reynolds number around the sphere, and thus depends on the fluid velocity and density, as well as the sphere diameter. From Equation 3.9:

$$Re_{sphere} = \frac{\rho u D}{\mu} \quad , \quad D = 2r_{sphere} \quad \text{Equation 3.13}$$

The relationship between C_D and Re is not straightforward and is based on experimental observations (Figure 3.10). For Stokes flow around the sphere ($Re < 1$), the relationship is linear, and $C_D \approx 24/Re$. The drag on a sphere with such low Re values is known as Stokes drag, and Equation 3.12 can be simplified to:

$$\mathbf{F}_d = 6\pi\mu u r \quad . \quad \text{Equation 3.14}$$

This is an acceptable approximation, given that $Re < 1$, and is therefore acceptable for spheres in slow fluid velocity. Indeed, the above equation is used in the vast majority of MDT simulations in the literature. However, from Re values of 1 and more, significant error exists; for example at $Re = 0.2$ the error is already 4% (Khan & Richardson 1987). There have been several attempts to derive a single function that describes C_D across a wide range of Re numbers. One such function is that calculated by Khan and Richardson (1987), according to which:

$$C_D = \left(1.84 Re^{-0.31} + 0.36 Re^{0.06} \right)^{3.45} \quad . \quad \text{Equation 3.15}$$

This function approximates C_D for a range of Re values between 10^{-2} and 10^5 with average error of 5% (Figure 3.11).

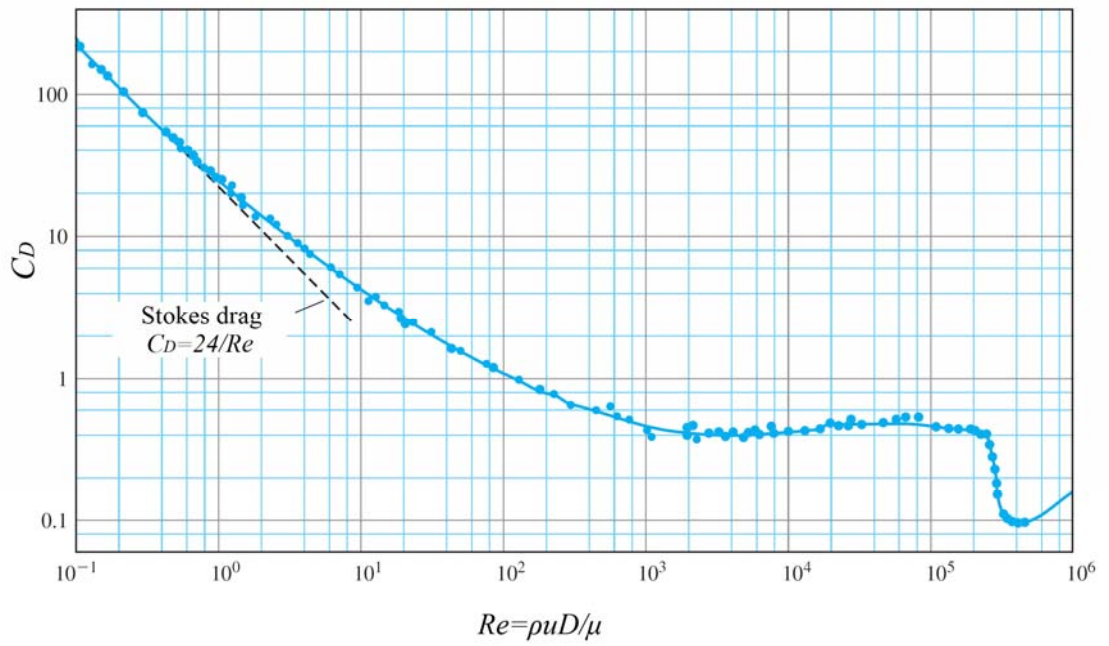


Figure 3.10 – The relationship between C_D and Re
 [Adapted from Shaughnessy, Katz, & Schaffer 2005]

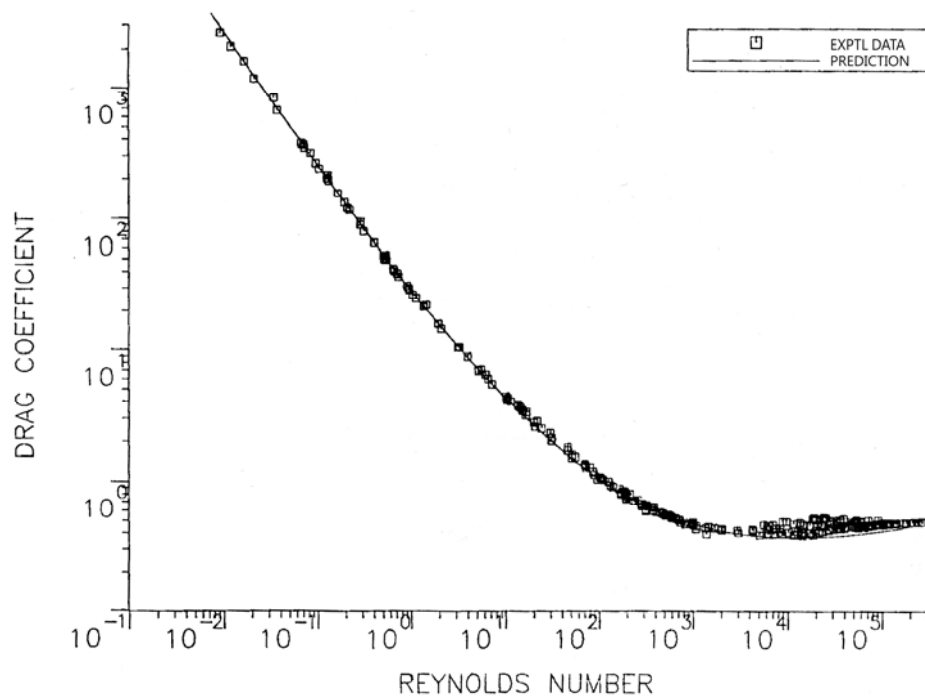


Figure 3.11 – The Khan and Richardson prediction for C_D
 [Adapted from Khan and Richardson 1987]

3.5 Summary

The properties of magnets have been known to humans for thousands of years. Advances in drug technology have required more specific targeting, particularly in the context of cancer treatment, where a decrease in non-specific distribution and side effects is desirable. Drug targeting via magnetic interactions with an applied magnet or implanted magnetic material is being considered in clinical trials as a way to physically guide the drug to a desired site. In the context of stem cell therapy, a similar approach could be employed to increase cell homing and retention at a desired site. This notion seems to be gaining in popularity, however there have been limited investigations and the effect of magnetic forces on cells has not been elucidated.

Magnetic drug targeting investigations have commonly been accompanied by some form of theoretical analysis; however this has largely been absent from the cell targeting field. The success of targeting will depend on the ability of a magnetic source to apply a force large enough to withstand fluid forces or at least deflect the cells in a flowing circulation. Therefore, the characteristics of the magnetic source, the cells and those of the flowing medium need to be considered, and theoretical calculations can inform the design of the targeting system.

CHAPTER 4

DEVELOPMENT OF DIFFERENTIAL LABELLING

4.1 Chapter overview

This chapter deals with my initial studies on CD133 cell labelling and magnetic attraction. For clarity, I have divided the chapter in two parts, each with separate methods, results, discussion and conclusions.

The first part deals with cell labelling. As CD133 cells in culture can be either adherent to the culture plate or in suspension, the primary objective was to ascertain any differences in SPIO uptake between the adherent and suspension cell fractions. The second undertaking in this part of the chapter was to investigate the relationship between the time of incubation with SPIO and the amount of iron uptake.

Part II deals with cell viability following magnetic attraction. First, the development of a magnetic device to perform viability tests is described. This is followed by the results of these tests, and the subsequent development of the “differential labelling” method.

4.2 – Part I: Labelling CD133 cells with Endorem®

4.2.1 Background and aims

CD133s remain in suspension when freshly isolated but become adherent over time in culture (Gehling et al. 2000; Quirici et al. 2001). As mentioned in the introduction (2.3.4), some reports have documented a decreased labelling efficiency with premature and non-adherent cell types. We have also seen in section 2.3.4 that various conjugation methods have previously been used in the past to increase SPIO uptake in such problematical situations. Near 100% labelling has been achieved with CD133 cells using FePro conjugates (Arbab et al. 2008; Arbab et al. 2006; Rad et al. 2009). However, these customised methods may be an obstacle to clinical translation; to date there has only been one clinical cell tracking study, which used the SPIO agent Endorem® without any transfection agents (de Vries et al. 2005).

In this study, the aim was to:

- i) Label CD133 cells with Endorem® and investigate if there are differences in iron uptake between adherent and suspension cells.
- ii) Investigate the ability of CD133 cells to be magnetically attracted.
- iii) Investigate the relationship of labelling time to iron oxide uptake.

The main findings of this study were as follows:

- i) Adherent cells label more readily than suspension cells.
- ii) 65% of suspension cells can be magnetically separated following labelling, which means they can be magnetically attracted.
- iii) SPIO uptake is time-dependent. It is faster during the first hours of labelling.

The main purpose of this study was to confirm previous results regarding the ability of cultured EPCs to be labelled with Endorem®. In the literature there are also unclear suggestions that adherent cells incorporate Endorem®, as well as the notion that uptake slows down as time progresses. Importantly, this was the first attempt to quantify the difference in uptake between suspension and adherent cells. Furthermore, the suggestion regarding time-varying rate of uptake was confirmed; this effect was used in the development of the differential labelling method.

4.2.2 Methods

4.2.2.1 Cell culture

Human mononuclear cells (MNCs) were collected by leukapheresis from peripheral blood of G-CSF-stimulated donors (Korbling et al. 2006). Blood samples were obtained under consent and approval by the local ethics committee. CD133⁺ cells were isolated using anti-human CD133 (epitope 1) magnetic microbeads (*Miltenyi Biotech GmbH*). These beads are biodegradable and typically disintegrate after a few days in culture. Each isolation provided approximately 5×10^5 cells. The culture medium was based on previous studies on EPC differentiation from CD133⁺ cells (Gehling et al. 2000; Quirici et al. 2001). $2-6 \times 10^5$ cryopreserved or fresh CD133⁺ cells per well were cultured in fibronectin-coated 24-well plates (BD) for 3 days in EGM-2 medium (EBM-2 with EGF, IGF, FGF, GA, ascorbic acid and heparin, *Lonza*) containing 20% FBS, 20mM HEPES and supplemented with FLT-3 ligand 50ng/ml, IL-3 10ng/ml, SCF 100ng/ml and rhVEGF165 25 μ g/ml (*R&D systems*). The cells were then cultured in similar FLT-3 / IL-3 / SCF free medium for a further 7 days. Fresh medium (200 μ L) and VEGF was added every 2-3 days for the duration of the culture.

4.2.2.2 Cell labelling

For labelling with Endorem® [*Guerbet Laboratories Ltd*, 11.2mg/ml iron (Fe)], the whole cell population was incubated for 1, 12 or 24 hours in the presence of the Endorem® suspension, as stated in sections 4.2.2.3 and 4.2.2.6.3, using 500 μ g/ml Fe (equivalent to 690 μ g/ml Fe₃O₄). Day9-CD133s were used unless otherwise stated. After labelling, cells were dissociated with 300 μ L dissociation buffer (*Sigma*) for 15mins and washed 3 times in 15mL PBS by centrifuging 12mins (250g, low brake).

4.2.2.3 Prussian Blue stain for microscopy

Iron uptake was visualised with Prussian Blue (PrB) staining. D9-CD133 cells were labelled with Endorem® for 24 hours. Three samples of 2.5×10^4 labelled d10-CD133s were then incubated for 24 hours in 100 μ L medium in wells of a 96-well plate, to allow the adherent fraction to adhere to bottom of the wells. Control wells contained unlabelled cells. After adherence, the whole d11-CD133 population was washed *in situ* (see below), fixed in 4% PFA for 20 mins, washed again, incubated in PrB staining solution (1% w/v KCN and 100mM HCl) for 30mins, washed and stored in PBS. The *in situ* washing step in each case involved filling the wells to the top (300 μ L) with PBS, spinning the whole 96-well plate at 200g for 2 minutes with no break to bring the suspension cells to the bottom of the well, carefully removing the top 260 μ L from the wells and repeating 4 times. There was no dissociation/trypsinisation step. Thus both adherent and suspension fractions were stained without removing them from their original wells.

4.2.2.4 Microscopy

Following PrB staining, the plate was spun one final time to bring all suspension cells to the bottom. Phase contrast microscopy images were taken using a 20x objective, a 10x eyepiece and a standard grayscale CCD camera; four random fields from each of the six wells were captured (e.g. Figure 4.1). The wells were then rinsed with PBS to remove the suspension cells, and images of the adherent cells alone were captured after finding the same fields of view (Figure 4.2). Cells that stained dark with PrB throughout were regarded 'Prb positive'. Partially dark cells were regarded ambiguous and counted as negative. The counts of PrB positive cells of four fields from each well were averaged and the percentage of PrB positive cells was calculated for each of the three groups (suspension population, adherent population, unlabelled control).

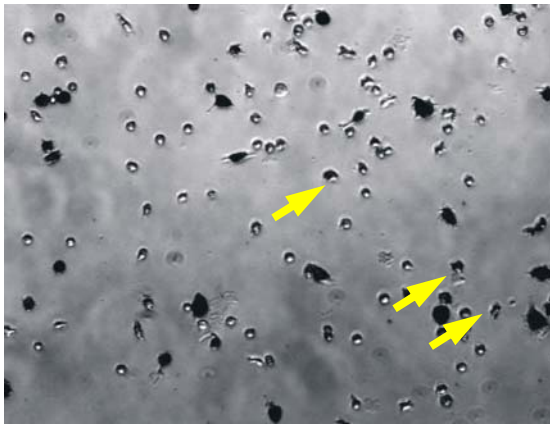
Whole population

Figure 4.1 – PrB stain of whole d11-CD133 population. Partially dark cells (arrows) were regarded ambiguous and counted as negative.

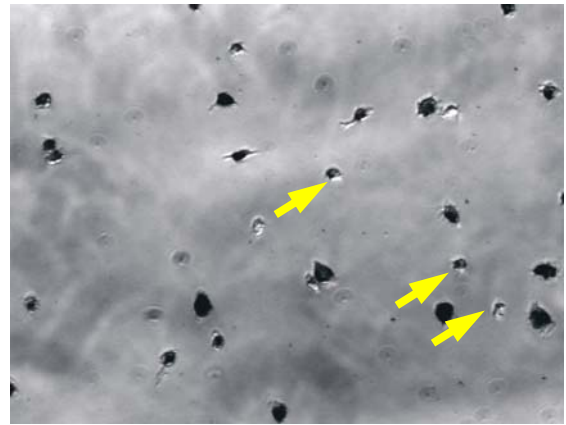
Adherent population

Figure 4.2 – PrB stain of adherent d11-CD133s. This figure and Figure 4.1 on the left are the same field of view.

A second count of PrB positive cells was repeated on images from 6 wells, at least 4 weeks later, to assess the repeatability of the counting method.

4.2.2.5 Magnetic separation

For a better estimation of the labelling efficiency of suspension cells, suspension d10-CD133s, labelled for 24h, were passed through a magnetic separation column (*Miltenyi Biotech GmbH*). Retained and non-retained cells were counted and expressed as a percentage. The experiment was repeated 3 times.

4.2.2.6 Dependence of iron oxide uptake on incubation time

In these experiments the aim was to investigate whether SPIO uptake is dependent on the time of incubation. Cellular iron content was quantified based on staining the cell lysate for iron using prussian blue, and measuring a peak absorbance photometrically (4.2.2.6). This method has been used previously (Rad et al. 2007) and was optimised here for the specific available equipment. The results of this methodological optimisation are given in Appendix A.

4.2.2.6.1 Method optimisation - absorbance spectrum of Prussian Blue

To determine the absorbance at which the PrB stain exhibits increased absorbance using the available microplate reader and filters (GENios, *Tecan*), the following three 100 μ L samples were analysed in triplicate. **i) PrB staining solution + SPIO:** 0.4 μ g Fe₃O₄ were mixed with 100 μ L PrB staining solution, resulting in a light-blue mixture. **ii) SPIO only:** 0.4 μ g Fe₃O₄ in PBS. **iii) PrB staining solution only.** The absorbance of these samples was then measured at the wavelength of the available filters (405, 450, 490, 560, 595, 690 and 900nm). The expected maximum is ~700nm (Rad et al. 2007).

4.2.2.6.2 *Method optimisation - effect of the cell lysis buffer on the PrB reaction*

To determine whether the cell lysis buffer, used to dissolve the cells and release the iron, has itself an effect on the PrB reaction, mixture (i) above was prepared in the presence of 10 μ L of the buffer (7M urea, 2M thiourea, 4% 3-[(3-cholamidopropyl)-dimethylammonio]-1-propanesulfonate) or 10 μ L PBS as a control, in triplicate. Absorbance at 690nm (defined by the experiment above) was measured every 14 seconds for 6 minutes. The maximum absorbance reached was recorded. A 400-segment cubic spline curve was fitted to interpolate the data and the time to reach the half-maximum was estimated.

4.2.2.6.3 *SPIO labelling timecourse*

To determine whether cellular SPIO uptake is dependent on time length of labelling, samples of 4.5×10^5 d10-CD133 adherent cells were labelled with 0.5mg/ml SPIO for 24h, 12h, 1 hour or were left unlabelled. Specifically, d9 cells were labelled for 24h, d9.5 for 12h and d10 for 1h. Samples were dissociated and washed twice in 15mL PBS, pelleted and lysed in 10 μ L lysis buffer. The lysate was suspended in 300 μ L PBS containing 1% KCN and 1.7% 6M HCl. The mixture was transferred to a 96-well plate in triplicate 100 μ L aliquots. The final contents of each well were a mixture of lysate from 1.5×10^5 cells, 3.3 μ L lysis buffer and 100 μ L PrB staining solution. Three extra wells contained 100 μ L PrB and 3.3 μ L lysis buffer, without cells, as a control. Absorbance at 690nm was measured after 5 minutes.

4.2.2.6.4 *Method optimisation – derivation of a standard curve*

Five wells in triplicate were prepared containing dilutions of Endorem® (0, 3.4, 6.7, 13.4, 26.9 μ g Fe₃O₄ / ml) in 100 μ L PrB staining solution and 3.3 μ L lysis buffer. The

absorbance at 690nm was measured after 5 minutes and a 400-segment cubic spline curve was fitted to interpolate the mean data.

4.2.2.7 Statistical analyses

Data were processed with SPSS for Windows v11.5.1 (*SPSS Inc*) or with Prism for Windows v4.02 (*GraphPad Software Inc*). All p-values reported are two-tailed and were considered statistically significant at the 5% level ($p < 0.05$). Data were inspected visually and with the Shapiro-Wilk test for small samples to test for normality. The homogeneity of variance assumption was evaluated with Levene's test. When ANOVA was performed and significant differences were found between groups, Tukey's test was used when comparing all groups between them and Dunnett's multiple comparison test was used when it was sufficient to compare all groups to a single control group. Other statistical tests are identified in context.

4.2.3 Results

4.2.3.1 SPIO uptake and PrB staining of adherent and suspension cells

The majority of adherent cells (80.3%) were PrB positive (Figure 4.3). On the contrary, the majority of the suspension cells were PrB negative (86.6%). No cells stained in unlabelled controls (cell count = 0). In addition, in studies unrelated to this project, PrB staining was not positive when ferritin expression was upregulated, indicating that endogenous iron storage is not sufficient to cause false-positive results.

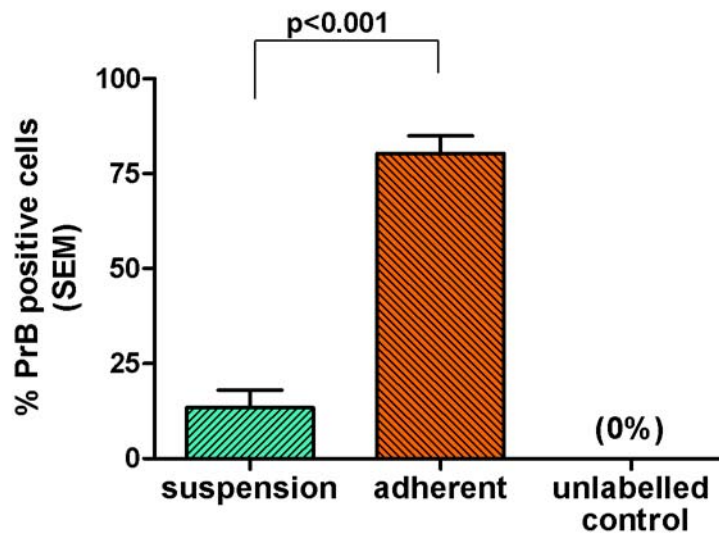


Figure 4.3 – PrB positivity of CD133 cell subtypes

*The mean percentage of PrB positive adherent cells was $80.3 \pm 4.7\%$, whereas that of suspension cells was $13.4 \pm 4.7\%$. The mean difference between the suspension and adherent populations was 66.9% (95% CI for the difference 48.4% to 84.3% , $p < 0.001$, unpaired *t*-test). SEM: standard error of the mean, $n=6$.*

4.2.3.2 Repeatability of the cell counting method

To assess the repeatability of the cell count, PrB positive cells in images from six random wells were re-counted at least 4 weeks after the first count. Only these six wells were re-counted.

Table 4.1 is a summary of the repeatability analysis. Figure 4.4 is the Bland-Altman plot.

The first and second counts were within the 95% limits of agreement (approximately $\pm 7\%$) and had a small negative bias (-1%). These values are small compared to the actual differences between the groups (66.9%, section 4.2.3.1). Therefore, the cell count was considered repeatable.

Table 4.1 – Count-recount of PrB positive cells

	1 st count	2 nd count	Difference
	157	160	3
	72	75	3
	199	195	-4
	107	102	-5
	172	168	-4
	86	83	-3
Bias	-1.67		
SD of bias	3.67		
95% limits of agreement	-8.86 to 5.53		

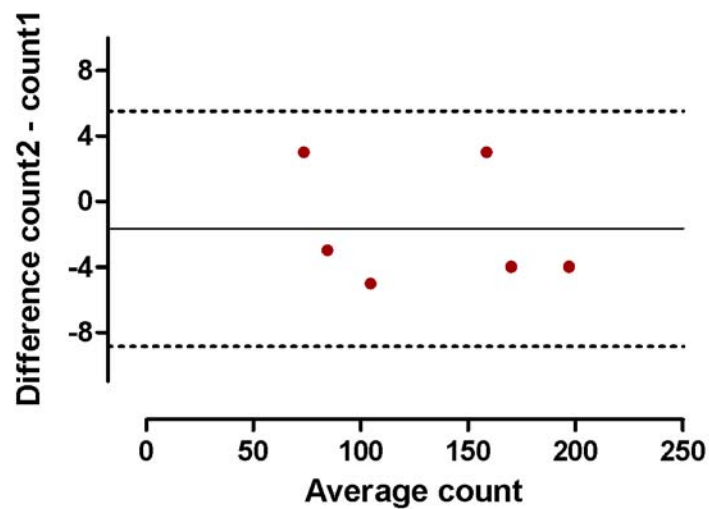


Figure 4.4 – Bland-Altman plot of two counts

Figure 4.4 is a Bland-Altman plot of the two counts used to test repeatability. The solid line is the bias (average difference). The dotted lines are the 95% limits of agreement ($\text{bias} \pm 1.96 \text{ SD}$). All the differences between the counts fall inside the 95% limits of agreement (-8.86 to 5.53). There was a negative average bias (-1.67).

4.2.3.3 Ability of CD133 cells to be magnetically attracted

The ability of CD133 cells to be magnetically attracted was tested based on their ability to be retained inside a magnetic separation column.

On visual inspection of Prussian Blue staining, the majority of suspension cells (86.6%) did not stain positively (section 4.2.3.1). However, 64% (± 5.6) of suspension cells were retained in the separation column. This means that, despite the decreased SPIO uptake compared with adherent cells, the majority of suspension cells have enough iron oxide to be pulled with a magnet inside the separation column.

Adherent cells stained positively throughout the cell with Prussian Blue. It was assumed that this level of iron content would be sufficient to keep them retained in the separation column, therefore the magnetic separation experiment was not performed on adherent cells.

4.2.3.4 Dependence of iron oxide uptake on incubation time

4.2.3.4.1 *Methodological developments*

For a full description of the methodological developments that were necessary for the derivation of the following results, please refer to Appendix A.

4.2.3.4.2 *Iron oxide uptake with increasing incubation time*

Cells were labelled with SPIO for 0h (control), 1h, 12h or 24 hours. Iron uptake was measured using an photometric absorbance assay (Appendix A). There was a notable increase in SPIO uptake with increasing labelling time. A large proportion of the uptake (45%) occurred during the first hour of labelling (Figure 4.5). For the full table of differences and pairwise comparisons see Appendix B.

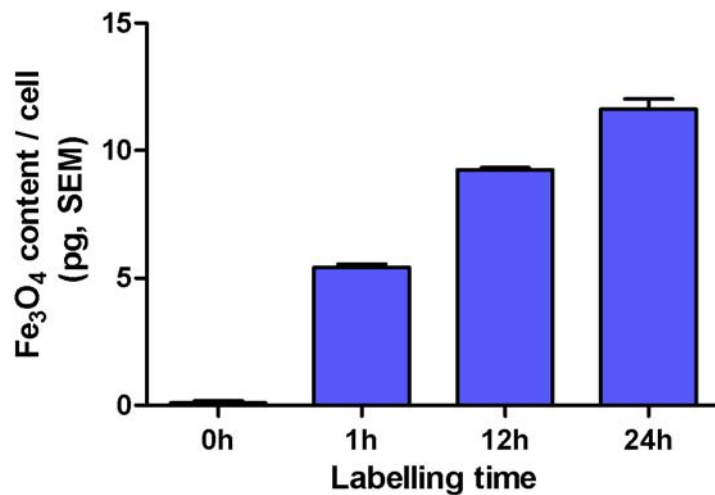


Figure 4.5 – Labelling timecourse - cellular iron content

The differences between all timepoints were significant (one-way ANOVA with Tukey's post-hoc multiple comparison test, $p < 0.001$ for all comparison pairs, $n=3$). A large proportion of the iron oxide uptake (~45%) took place during the first hour of labelling.

4.2.4 Discussion

4.2.4.1 Main findings

- i) Adherent cells label more readily than suspension cells.
- ii) Even though suspension cells do not label readily and are hard to visualise with the prussian blue stain, approximately 65% of suspension cells incorporate enough iron oxide to be magnetically attracted.
- iii) SPIO uptake is time-dependent. It is faster during the first hours of labelling.

4.2.4.2 Adherent cells label more readily than suspension cells

In these experiments it was found that adherent d10-CD133s take up iron oxide more readily than suspension cells (Figure 4.3).

One possible explanation for such a difference could be that the adherent cells have an inherent increased ability to take up SPIO. During the presented experiments it was noted that adherent cells have more proliferative capacity than suspension cells. It has previously been reported that SPIO particles are endocytosed faster by rapidly dividing cell types (Arbab et al. 2003a). Therefore, the increased activity of the cells may account for the increase in uptake. Furthermore, receptor-mediated endocytosis via the scavenger receptor SR-A1 has been shown to be involved in SPIO uptake in macrophages (Raynal et al. 2004). Interestingly, CD133 cells may express this receptor as they become more differentiated (Voo et al. 2008). The transition from suspension to adherent cells may thus coincide with an upregulation of this receptor.

A second factor that may contribute to an increased uptake by adherent cells is the higher concentration of particles at the bottom of the wells, sedimenting under the

influence of gravity. It has been noted that an increased concentration of particles in the medium will lead to higher uptake rate (Sun et al. 2005).

The SPIO uptake of suspension CD133 cells in this study was quite low, compared to other studies that have labelled CD133 cells with 100% efficiency (Arbab et al. 2008; Arbab et al. 2006; Rad et al. 2009). The important finding regarding suspension cells was that, although they do not stain strongly with Prussian Blue, the majority contain enough iron to keep them inside a magnetic separation column. Therefore they can be magnetically attracted, which is a prerequisite for the purposes of this project. Thus both adherent and suspension cells were used in future studies.

The lower labelling efficiency observed in this study compared to the literature may be attributed to several factors. First, the use of a transfection agent in published studies is likely to have increased the labelling efficiency, by increasing cell-particle interactions and promoting endocytosis (Arbab et al. 2003a; Panizzo et al. 2009). Secondly, the specific culture conditions used in some previous reports (Arbab et al. 2008; Arbab et al. 2006; Rad et al. 2009) are likely to have increased the inherent endocytotic ability of the cells: the *StemSpan* and *Stemline II* media used in these studies are normally aimed at numeric expansion of the entire HSC pool and can lead to differentiation towards the erythroid and myeloid lineages (Lam et al. 2001; Schipper et al. 1998). More importantly, the media in these studies were supplemented with thrombopoietin, which upregulates adhesion molecules (Cui et al. 1997; Gotoh et al. 1997). This would render the majority of the cells adherent, increasing the labelling efficiency.

4.2.4.3 Dependency of iron uptake on incubation time with the particles

The dependency of iron uptake on the concentration of iron oxide in the culture medium is well established in the literature (Bulte & Kraitchman 2004; Matuszewski et al. 2005; Sun et al. 2005) and was not investigated as part of this study. Higher iron concentration in the culture medium leads to faster uptake rate. It is also generally accepted that longer incubation time leads to higher intracellular iron concentration; however, few investigations explicitly report on this time dependency (Arbab et al. 2003a; Arbab et al. 2004b; Sun et al. 2005).

Within the literature available, there exist observations of higher iron uptake rate during the first hours of incubation. Specifically, Sun and co-workers (2005) report that **i**) their cells were clearly labelled after 20 minutes of incubation with SPIO, **ii**) the cellular iron content rose sharply during the first 2h and **iii**) continued to increase, however at a slower rate. In the presented data, it was observed that a large proportion (~45%) of the iron uptake of adherent CD133 cells occurs during the first hour of labelling (Figure 4.5). The cells continued to endocytose iron for the next 24h, however this occurred at a slower rate. This finding, which is in accordance with Sun (2005), was fundamental to the development of the differential labelling method, as described in Part II of this chapter.

4.2.4.4 Choice of iron quantification assay

The photometric assay employed in this chapter was a relatively simple method of assessing iron content. It has been previously used by Rad (2007), who dried the cells instead of using a lysis buffer. In my hands, cell drying resulted in an inhomogeneous mixture with high non-specific absorbance (data not included in thesis). Instead, a lysis buffer was used, which may also have introduced some measurement error (see

Appendix A for details). To avoid these errors, in future studies a more accurate method for iron quantification was used; this will be introduced in Chapter 5.

4.2.5 Conclusions

From this study it can be concluded that:

- i) Adherent cells label more readily than suspension cells. Suspension cells do not take up enough iron to be easily visualised with prussian blue stain but
- ii) 65% of suspension cells can be magnetically separated following labelling, which means they can be magnetically attracted.
- iii) SPIO uptake is time-dependent. It is faster during the first hours of labelling.

4.3 – Part II: Magnetic attraction and viability

4.3.1 Background and aims

Magnetic forces can affect intracellular structures (Wilhelm et al. 2003b). However, there have not been any studies to ascertain whether a magnetic force is sufficient to affect cell viability (3.2.3). Furthermore, as described in section 3.3.3, the magnetic force depends on both the magnitude of the applied magnetic field and also the gradient of this field. The force distribution around a magnet will therefore be dependent not only on the magnetic material, but also on magnet shape. Therefore, to perform magnetic attraction viability experiments, it was necessary to design a magnetic device for the application of a magnetic force on cells. This force should be applied uniformly across a population of cells, in order to achieve reproducible viability results.

The design and construction of such a device, named “**magnetic plate**”, was the first aim of this study. Cell viability tests were then conducted using this plate. The results of these tests led to the development of the “differential labelling” method (**DfL**).

In this study, the aim was to:

- i) Build a magnetic plate to apply a homogeneous force on a cell sample.
- ii) Investigate the effect of magnetic force on cell viability.

It was found that:

- i) Using the magnetic plate, it is possible to apply a force with limited variation (15%) in magnitude across a cell sample.
- ii) An excessive magnetic force can cause cell death, but by using DfL the amount of iron in the cell is decreased and cell viability can be maintained.

Two important findings were established with the studies of Part II of this chapter. Firstly, for the first time, a custom-made magnetic plate was designed and constructed in order to perform viability tests. The selected design decreased the applied force variation across a cell sample to 15%, as compared to 755% that would otherwise be encountered.

Secondly, using this magnetic plate it was found that magnetic attraction of cells for prolonged periods of time has the potential to compromise viability. This has not been reported before. A novel labelling method (DfL) was used to solve this problem and maintain cell viability.

4.3.2 Methods

4.3.2.1 Magnet modelling

Opera 2d (*Vectorfields*) was used to model Nd₂Fe₁₄B N35SH magnets (*Magnetic Applications Ltd*) for the design of a suitable platform. Dr Ana Garcia-Prieto provided initial models and guidance on how to use the software. For the purposes of this study, forces were modelled for an arbitrary 100nm iron particle with susceptibility $\chi = 0.2$; this was an arbitrary value and does not compare with the forces on cells. Conformity of the magnets chosen (see section 4.3.3.1 below) to the computer model was tested by placing a modelled magnet directly beneath a 3cm culture plate containing 250 μ g/ml Endorem® in PBS for 15 minutes, to allow the particles to sediment at the area of maximum force. The effect of vertical piling of two magnets was also considered, in an attempt to increase the magnitude of the applied force.

4.3.2.2 Platform and magnetic attraction

Following computer modelling of magnets (Results, section 4.3.3.1), the purpose-built platform base was constructed by aligning four of the chosen Nd₂Fe₁₄B grade N35SH disk magnets (1.195T, 22mm diameter x 8mm height) on top of the four corners of a 96-well plate. The 96-well plate containing the cells to be examined was placed on top of this base, so that the bottom of each corner well, i.e. the cells, was 1mm from the magnet surface (1mm is the thickness of the plastic of the plate base). Magnetic cell attraction (against the restraint of the well bottom) was preceded by centrifugation of the cell-containing plate at 200g for 2mins with no brake to bring all the cells to the bottom of the plate. The attraction lasted 24 hours and was followed by the viability assays in the same 96-well plate.

4.3.2.3 Cell culture and labelling

Cells were cultured as previously described (4.2.2.1); d9-CD133s were used. For standard labelling (StL) the whole cell population was labelled for 24h with Endorem® (500 µg/ml Fe). For differential labelling (DfL), the suspension d9-CD133 fraction was separated and labelled for 22h followed by additional labelling for 2h with the adherent fraction (24:2 DfL) or 23h and 1h respectively (24:1 DfL). Cells were washed three times in 15mL PBS to remove unbound iron.

4.3.2.4 Viability assay

The CellTiter 96® AQueous One Solution Assay (Promega) was performed after 24h of magnetic attraction of labelled CD133⁺ cells. The tetrazolium compound in this assay undergoes reduction to a coloured formazan product by viable cells, primarily mediated by NAD(P)H (Berridge & Tan 1993). Spectrophotometric quantification of viability of samples of 3×10^4 CD133⁺ cells was performed using the same microplate reader as in Part I (GENios, Tecan) (490 nm, at 4h). Absorbance at 690nm was measured as a reference for non-specific absorbance and subtracted from the 490nm value as per manufacturer guidelines. For the assay, cells were cultured in medium lacking ascorbic acid (see Appendix C for rationale). Sample activity was normalised to the mean absorbance of control (no magnet). Four experimental groups were examined: **i**) standard labelling (StL) without magnetic attraction, **ii**) StL with 24h attraction, **iii**) 24:2 DfL with 24h attraction, **iv**) 24:1 DfL with 24h attraction. Values were normalised by setting the mean of the control as 100% viability. For positive controls see Appendix C. Phase contrast microscopy photographs for **(i)**, **(ii)** and **(iv)** were taken to assess any differences in the visual appearance of the cells.

4.3.2.5 Statistical analyses

The results were analysed as described in 4.2.2.7. Tamhane's T2 post hoc test for ANOVA was used when the variances were not homogeneous (Levene's test, $p < 0.05$).

4.3.3 Results

4.3.3.1 Design and construction of the magnetic plate

The magnetic plate was constructed using disk magnets 22mm in diameter (11mm radius) and 8mm in height (Figure 4.6). According to the computer model, the force maximum of these 22mm x 8mm magnets were predicted to occur at the magnet edges. The forces were predicted to be most homogeneous above the magnet central area. This prediction was confirmed by placing SPIO particles on top of the magnet and leaving them to accumulate at the area of maximum force (Figure 4.7).

Therefore, the cells under investigation should be confined to the central area of the magnet, where the forces are more homogeneous. To achieve this, the magnets were placed so that they were centered beneath a culture well of a 96-well plate, which is 6mm in diameter (3mm radius) (Figure 4.8). The force variation across the cell sample in this well was calculated to be 15%.

Finally, an alternative magnet configuration was modelled, in an attempt to increase the applied magnetic force without increasing the variation across the cell sample. Disk magnets 22mm in diameter and 8mm in height were stacked vertically, to produce a magnet stack 22mm in diameter and 16mm in height. This doubled the applied force, and also decreased the variation across the cell sample from 15% to 7% (Figure 4.9).

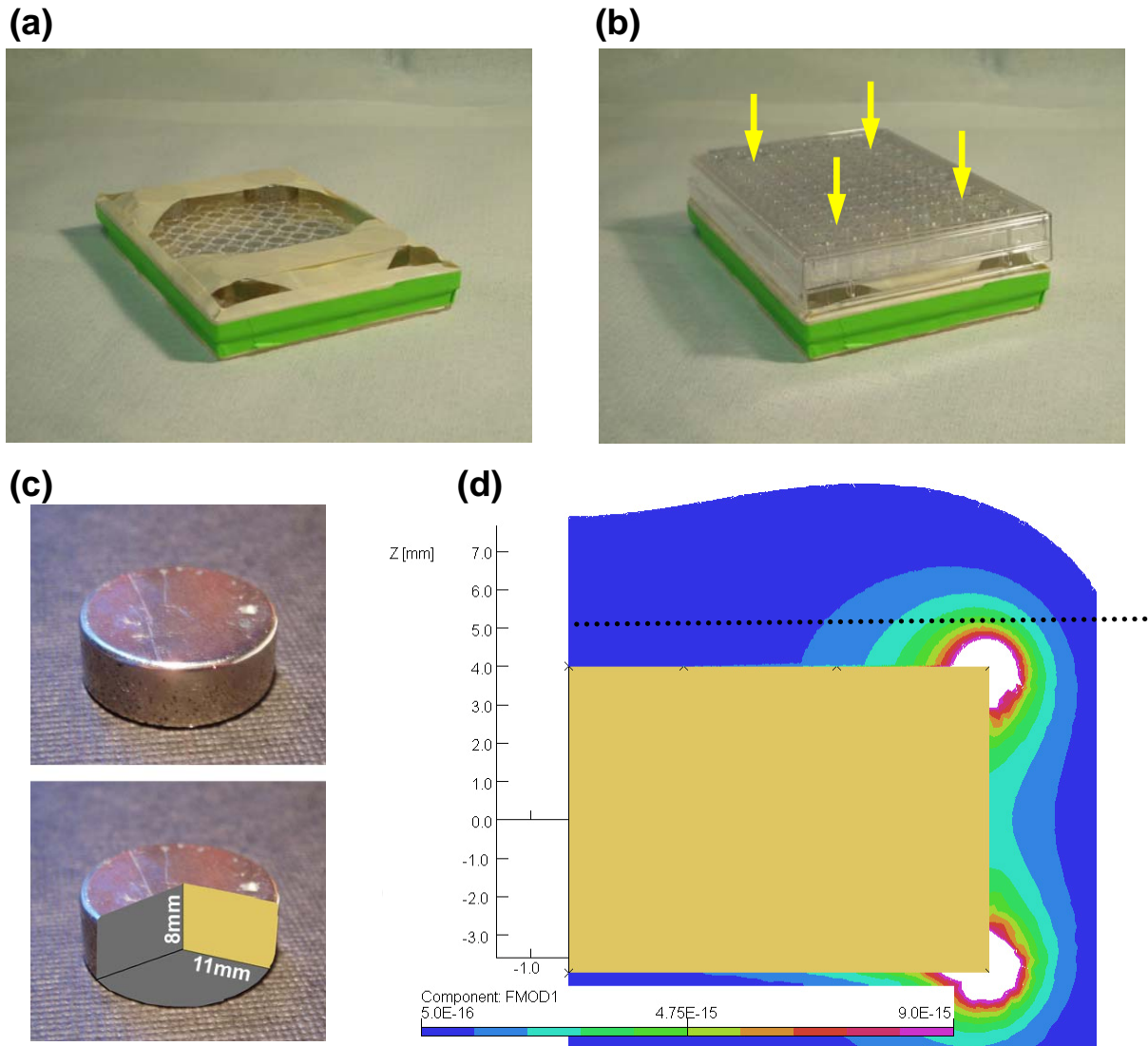


Figure 4.6 – Design and construction of the magnetic plate

Four disk magnets, 22mm in diameter and 8mm in height were used to construct the magnetic plate (a). The cell-containing 96-well plate was placed on top of the magnetic plate (b). There are four wells that contain cell samples (arrows). A photograph of one of these magnets is shown in (c). The yellow rectangle represents the modelled area, seen in (d). The computer model shows colour-coding of the force magnitude (Equation 3.5) increasing from blue to white. The black dotted line signifies the 1mm distance from the magnet surface, the distance where the cell samples are placed (the well bottom). This distance was used for the force calculations in Figure 4.8.

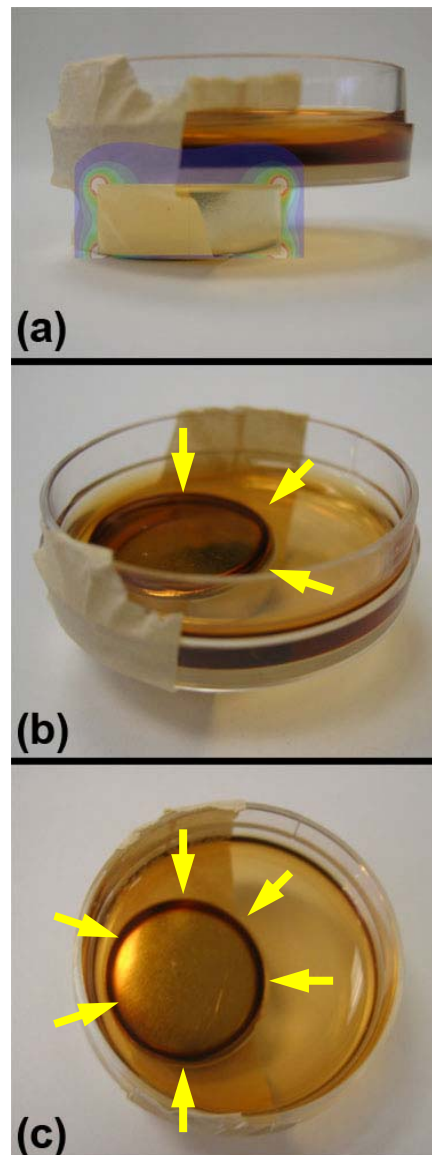


Figure 4.7 – Particle attraction toward the magnet edges

To confirm the computer model prediction for the areas of maximum force, SPIO particles were placed in a culture dish, 1mm from the magnet surface. **a)** side view of culture dish with magnet on its underside (force model superimposed). The particles were allowed to accumulate at the area of maximum attractive force from the magnet. **b,c)** top views showing particles attracted toward the the upper rim of the magnet (dark ring, arrows), which is in accordance with the computer model.

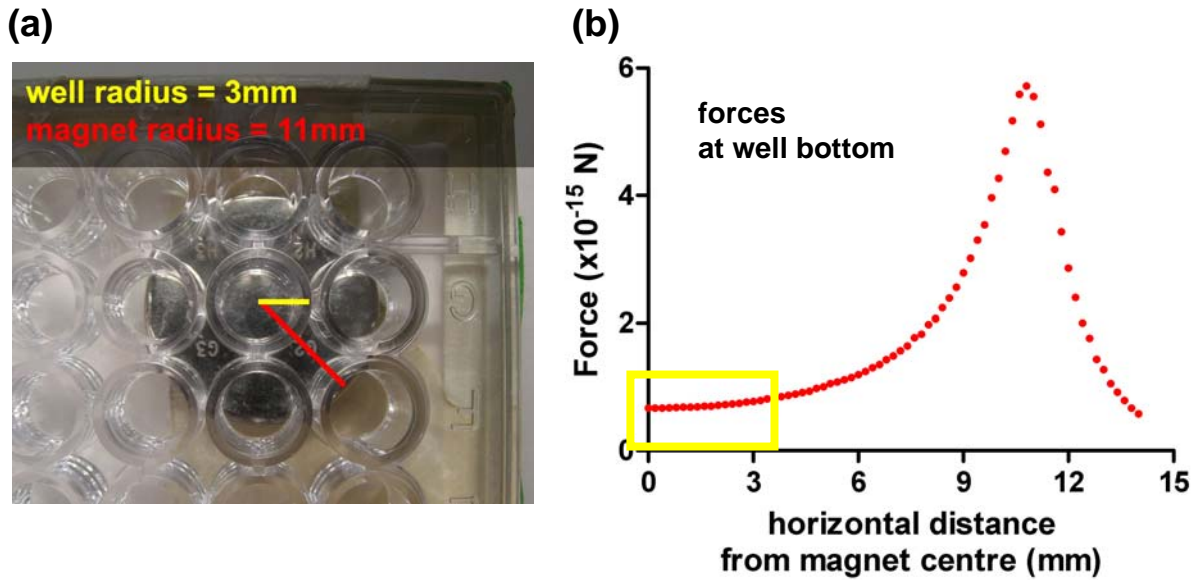


Figure 4.8 – Placement of cell samples on top of disk magnets

a) Photograph of 22mm diameter disk magnet beneath 96-well plate. The cells under investigation are confined to the central area of the magnet, up to 3mm away from the magnet centre (yellow line). The force magnitude was investigated to ascertain the homogeneity of the forces at 1mm distance above the magnet surface (b). This distance is denoted with a black dotted line on Figure 4.6-d. The force maximum occurs at the magnet edge (11mm from the centre). The cells under investigation are confined to the area bounded by the yellow square. The variation in force magnitude in this area was 15%. In contrast, the variation in force along the entire face of the magnet is 755%. Force magnitude was calculated for an arbitrary SPIO particle with $\chi=0.2$.

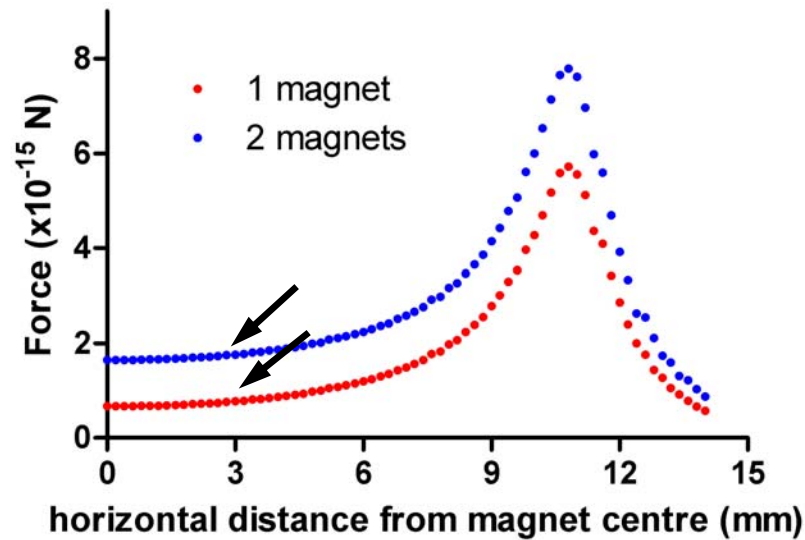


Figure 4.9 – Increase in applied force with stacked configuration

The effect of stacking magnets on top of each other was investigated in an attempt to increase the force magnitude without decreasing the homogeneity of the force. Placing two magnets on top of each other increased the maximum force experienced per particle by 2.3-fold, from 7.74×10^{-16} to 1.76×10^{-15} N, at 3mm from the centre (black arrows). It also decreased the '0mm \rightarrow 3mm' variability across each well from 15% to 7%. This stacked configuration was used in the studies presented in Chapter 5.

4.3.3.2 Viability after magnetic attraction (single magnet configuration)

Cells were labelled with Endorem for 24 hours ('standard labelling', StL). After a further 24 hours of magnetic attraction, there was a 72.5% decrease in cell viability (Figure 4.10).

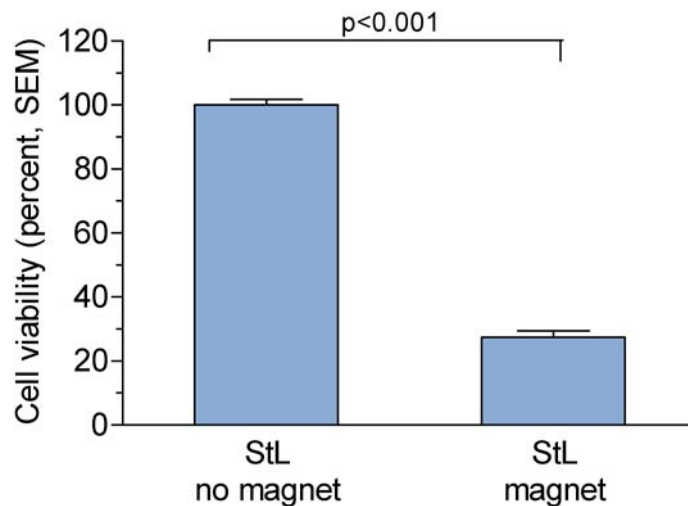


Figure 4.10 – Viability of StL cells following 24h magnetic attraction

Figure 4.10 displays the viability of magnetically attracted StL-CD133 cells compared to control cells (standard labelling, no magnetic force). There was a significant decrease in viability ($p < 0.001$, unpaired *t*-test). Viability was investigated using the MTS assay, normalised to the control cells and expressed as a percentage.

SEM: standard error of the mean, $n=4$.

4.3.3.3 Development of the differential labelling method (DfL)

It has already been mentioned that **i)** adherent cells take up iron more readily than suspension cells, and more notably in the first hours of labelling (Part I of this chapter) and **ii)** endocytosed SPIO can induce a force and change the shape of endosomes when an external magnetic field is applied (Wilhelm et al. 2003b). Based on these facts I hypothesised that the observed decrease in viability was due to mechanical damage of the adherent cell fraction, due to excessive magnetic forces. The differential labelling method was devised to solve this problem, whereby adherent cells were only labelled for 1 hour (**24:1 DfL**) or 2 hours (**24:2 DfL**). The suspension cells were labelled for 24 hours to preserve their SPIO content.

Figure 4.11 displays the comparison of cell viability after magnetic attraction for standard labelling (StL), 2 hours differential labelling (24:2 DfL) and 1 hour differential labelling (24:1 DfL). Both differential labelling methods increased viability.

With StL there was a 72.5% decrease in viability following 24h of magnetic attraction (reproduction of the data in Figure 4.10). With 24:2 DfL there was a 20.8% decrease in viability. For 24:1 DfL there was no evidence to support a decrease in viability. Table 4.2 summarizes these results.

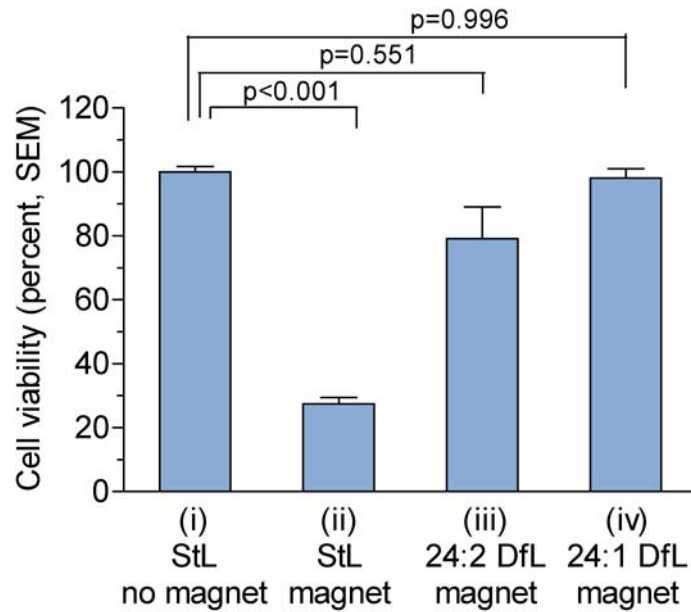


Figure 4.11 – Viability following 24h magnetic attraction: StL vs DfL

Table 4.2 – Comparison of viability after magnetic attraction: StL vs DfL

Group (n=4)	Mean viability % (SEM)	Compared groups ¹	Mean % difference	95% CI difference ¹	p-value ¹
(i) StL no magnet (control)	100 (1.8)	(i) vs (ii)	72.5	62.1 to 82.9	<0.001
(ii) StL magnet	27.5 (2.0)	(i) vs (iii)	20.8	-37.8 to 79.4	0.551
(iii) 24:2 DfL magnet	79.2 (9.9)	(i) vs (iv)	2.0	-13.1 to 17.0	0.996
(iv) 24:1 DfL magnet	98.1 (3.0)	(iii) vs (iv)	13.4	-73.7 to 35.9	0.627

¹ One-way ANOVA with Tamhane's T2 multiple comparison test

Differential labelling improved viability after magnetic attraction, compared to standard labelling. With StL there was a 72.5% significant decrease in viability ($p < 0.001$). With 24:2 DfL there was a non-significant 20.8% decrease in viability. With 24:1 DfL there was no evidence to support a difference to the control samples (StL without magnet). Viability was analysed using an MTS assay and is normalised to the the control samples. SEM: standard error of the mean, $n=4$ for each group.

4.3.3.4 Histology following magnetic attraction

The cells' visual appearance was different between the labelling methods after the cells had been magnetically attracted (Figure 4.12). With standard labelling and magnetic attraction, the cells did not look normal. With differential labelling, the cell appearance was similar to the control.

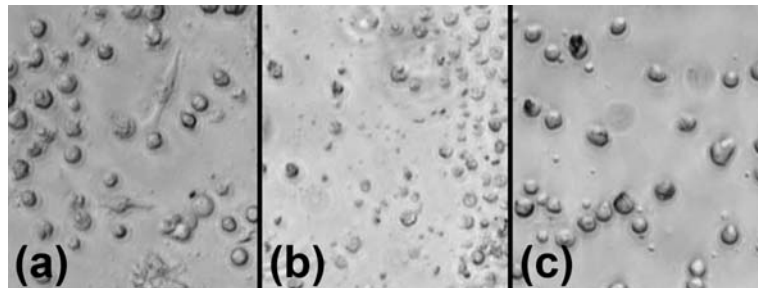


Figure 4.12 – Photomicrographs of cells following magnetic actuation
a) StL (no magnet), b) StL + magnet, c) 24:1 DfL + magnet

Cells labelled with the standard method (a) appeared normal when no magnet was used. Cell fragments were observed in the 'StL + magnet' samples (b), which paralleled the observed decrease in viability. 24:1 DfL cells appeared normal following magnetic attraction (c). Scale: each cell is approximately 10 μ m in diameter.

4.3.4 Discussion

4.3.4.1 Main findings

- i) Using the magnetic plate, it is possible to apply a force with limited variation (15%) in magnitude across a cell sample.
- ii) An excessive magnetic force can cause cell death, but by using DfL the amount of iron in the cell is decreased and cell viability can be maintained.

4.3.4.2 Design of the magnetic plate

In the first part of this study, a magnetic plate was designed for subsequent use in viability experiments. The plate was designed to provide homogeneity of the applied force across the diameter of a well. As shown in Figure 4.6, disk magnets have an inhomogeneous force distribution around them, which could influence reproducibility of results and subsequent interpretation. Using the magnetic plate presented there was 15% variation in force across a cell sample. This variation was, arbitrarily, considered sufficient for the purposes of the study. It was not investigated whether a decrease in variation would give better reproducibility of results. In Chapter 5, the stacked configuration was used i) to increase the applied force and ii) decrease the force magnitude variation to 7%. An additional advantage of the 96-well plate design was the possibility of direct use in the microplate reader for the MTS viability assay. This helped to decrease variation in the results that may be caused by additional cell handling and pipetting between the magnetic attraction phase and the MTS assay.

An alternative design would be the construction of an electromagnetic plate, in which case the forces applied could be varied, allowing a broader range of force application. However, this option was not considered practical at this stage, as alterations to an incubator would be necessary in order to provide power supply to the platform.

4.3.4.3 Cell viability after magnetic attraction

The effect of magnetic attraction of cells has not previously been examined, apart from investigations on non-fatal deformations of endosomes (Wilhelm et al. 2003b). In this study it was found that that a magnetic force can cause cell death. This result, in conjunction with the observed increased uptake of iron oxide by adherent cells as found in Part I, meant that decreasing the amount of iron in adherent cells alone could restore viability. Differential labelling was developed in an attempt to decrease the amount of iron in adherent cells, without compromising the suspension cell SPIO uptake. This restored viability, and 24:1 DfL was selected as the labelling method of choice for magnetic attraction experiments, as it did not cause a decrease in viability.

For the computer modelling in this study, an arbitrary iron particle was modelled to compare the different magnets and the force variation near the magnet surface. The actual magnitude of the magnetic forces on cells were not calculated as part of this study. Such a calculation would require knowledge of the magnetic susceptibility of the cells in each group examined, which was not estimated at this stage. However, the maximum force that can be exerted on 24:1 DfL cells without effects on viability would be a necessary ‘safety’ marker for the design of subsequent experiments. This ‘cell-safe’ maximum force will be dealt with in Chapter 5.

4.3.5 Conclusions

From this study it can be concluded that:

- i) Using disk magnets with diameter four times larger than the cell sample, it is possible to apply a force with 15% variation in magnitude across the sample.
- ii) An excessive magnetic force can cause cell death, but by decreasing the amount of iron in the cell, cell viability can be maintained.

CHAPTER 5

FURTHER INVESTIGATION OF DIFFERENTIAL LABELLING

5.1 Introduction

In Chapter 4, we saw how the concept of differential labelling was developed in order to maintain viability after magnetic attraction. In this chapter I will describe some steps that I considered necessary for the validation of this labelling method. In short, the post-attraction viability had to be confirmed at later timepoints. I also quantified the amount of iron in the cells for magnetic force calculations, and confirmed that the cells can be visualised using MRI.

By the time these experiments were conducted, there was a plan in place for some *in vivo* work (Chapter 7). This entailed application of a magnet for only 10 minutes. Therefore, the magnetic attraction period was reduced from 24h to 10min in the studies presented here, to be directly applicable to the *in vivo* experiments. Because of the decreased magnet application time, the cells would possibly withstand a higher force, so I used stacked instead of single magnets (Figure 4.9) to increase the force magnitude in all of the magnetic attraction experiments presented in this chapter. Finally, water evaporation from the culture plate affected the viability results of preliminary experiments (not presented here). The method used to minimise evaporation is presented in the methods of this chapter and the validation is outlined in Appendix A.

In this study, the aim was to:

- i) Investigate cell viability, growth and apoptosis following DfL and magnetic attraction using stacked magnets.
- ii) Investigate cell differentiation following DfL.
- iii) Quantify the iron content per cell and calculate the magnetic forces.
- iv) Verify visibility of cells using MRI.

It was found that:

- i) Cell viability, growth and apoptosis is normal following DfL and magnetic attraction using stacked magnets.
- ii) Cell differentiation is normal 10 days post-labelling.
- iii) Cells contain on average 3.9pg iron oxide / cell. A force of 9.3pN per cell is safe with regard to (i) above.
- iv) Cells are visible using MRI and readily create signal voids *in vitro*.

The studies in this chapter concentrated on validating the differential labelling method. This was achieved with analysis of cell viability, growth, apoptosis and differentiation. In addition, in order to calculate 'safe' magnetic forces, the amount of iron oxide per cell was calculated. This calculation of safe forces has not been attempted in the past. Finally, visibility of cells with MRI was confirmed; although this is not a novel finding, I considered it a necessary step in validating the labelling method.

5.2 Methods

5.2.1 Cell culture and labelling

Cells were obtained and cultured as previously described (4.2.2.1) and were labelled using the 24:1 DfL method (4.3.2.3). For simplicity, 'DfL' alone will refer to 24:1 DfL of day10 cells, which was the labelling method of choice (Chapter 4). 24:2 DfL was not investigated further.

5.2.2 Viability assay after 10min attraction with stacked magnets

The MTS assay was repeated as described before (4.3.2.4), on cells that had been on stacked magnets for 10 minutes, 24h after the magnetic attraction.

5.2.3 Water evaporation

These experiments (Appendix A) were performed to investigate if there is significant water evaporation from 96-well plates despite the plate cover, which would affect viability results. Two 96-well plates were kept in an incubator for 48h. In each plate, the 4 corner wells and the 4 centre wells were filled with 100 μ L PBS. In one of the plates, the inter-well spaces were flooded with PBS to saturate the atmosphere around the wells with water vapour and attempt to decrease evaporation (total=10mL). Subsequent to the results of this experiment, all culture plates were flooded in the same way.

5.2.4 Growth assay post DfL and magnetic attraction

Sixteen samples of either (i) control, unlabelled d10-CD133s or (ii) DfL-CD133s magnetically attracted for 10 minutes with stacked magnets, were plated in a 96-well plate (total wells= 32). 5×10^3 cells cultured in each well with 100 μ L medium. The growth of the cells was investigated by performing the MTS assay as previously described (4.3.2.4) on quadruplicate samples at four timepoints (24h, 48h, 96h, 192h). Data was normalised to the control samples at 24h and is presented as relative absorbance units. 10 μ L fresh medium was added to the wells every two days. A PBS-filled well served as an evaporation gauge to adjust the addition of fresh medium, so that wells contained 100 μ L medium when the MTS assay was to be performed.

5.2.5 Apoptosis assays

Cell apoptosis was analysed using an Annexin-V-FITC/Propidium Iodide (A-V/PI) flow cytometric assay (ApoTarget™, Invitrogen). In combination with propidium iodide, Annexin-V can distinguish between normal, early apoptotic, late apoptotic and necrotic cells (Vermees et al. 1995). $3-4 \times 10^4$ cells were incubated in 150 μ L medium in wells of a

96-well plate for 24, 48 or 120 hours. On the day of the measurement, cells were collected, washed once in warm PBS, resuspended in 100 μ L of the supplied buffer and incubated with 5 μ L Annexin-V and 10 μ L PI for 15mins before another 400 μ L buffer was added. FACS analysis was done on the FACScan cytometer (BD) with the starting settings shown in Table 5.1. The % apoptotic and necrotic cells was calculated.

Table 5.1 – FACS settings

PARAMETER	VOLTAGE	GAIN	SCALE
FSC	E-1	7.01	Lin
SSC	287	3.17	Lin
FL1 (A-V)	509	1	Log
FL2 (PI)	498	1	Log
Threshold: 35 - FL1 Comp: 5.3% FL2 - FL2 Comp: 29% FL1			

Three groups were examined: (i) unlabelled, control d10-CD133s, (ii) DfL-CD133s and (iii) DfL-CD133s with magnetic attraction.

5.2.6 Flow cytometry for cell differentiation

The immunophenotypic characteristics of d21-DfL-CD133 cells labelled with SPIO at day 10, were analysed using flow cytometry (FACSCalibur, BD). Cells pre-treated with FcR blocking reagent (Miltenyi Biotech) were stained using the following anti-human antibodies: phycoerythrin (PE)-CD304 BDCA-4/Neuropilin-1(n=6)(Fons et al. 2004), biotin-CD144 / VE-Cadherin (n=6) (Bender MedSystems) with Streptavidin-FITC for endothelial differentiation; PE-CD14 (n=6) and CD11b (n=3) (BD Pharmingen) for monocytic differentiation. Fluorochrome- and dose-matched isotypes were used as controls. Cells were suspended in 20mM HEPES/0.5% BSA/PBS containing 10 μ g/ml

7-aminoactinomycin D (7-AAD, Sigma Aldrich). 7-AAD positive, nonviable cells were excluded and 1×10^4 viable cells were scored per analysis (CellQuestPro, BD).

5.2.7 SQUID for iron quantification

A superconducting quantum interference device (SQUID) (Hautot, Pankhurst, & Dobson 2005) was used to measure the amount of Fe_3O_4 in the cells. The data acquisition was performed by Dr Ana Garcia-Prieto. 5×10^5 DfL cells were placed in a glycine capsule. $15 \mu\text{L}$ of 11.2 mg Fe/ml Endorem® were measured for standardisation ($15 \mu\text{L} = 168 \mu\text{g Fe} = 233 \mu\text{g Fe}_3\text{O}_4$). To separate SPIO signal from background signal coming from the cells and media, measurements were performed at 10K (-263°C). This is below the blocking temperature of Endorem® (60K). The cell sample was saturated in an applied field of 2 Tesla, which was subsequently removed to leave the SPIO particles in a remanently magnetised state. Comparison of this remanent signal with that of the undiluted Endorem® sample allowed quantification of Fe_3O_4 per cell. This then allowed calculation of the magnetic force acting on the cells in the viability assays.

5.2.8 In vitro MRI

DfL-CD133 cells were embedded in low melting point agarose (0.5%, 37°C) at concentrations of approximately 750, 166, 50, 16 and 0 cells $\times 10^3/\text{ml}$ in $250 \mu\text{L}$ eppendorf tubes and were cooled to 4°C . Suspension in agarose allowed for homogeneous distribution of the cells. The tubes were secured in a 4% agarose phantom and were imaged in a 9.4T horizontal bore Varian (VNMRs) MRI system using a 39mm RF coil (RAPID Biomedical GmbH, Germany). T_2^* weighted images were acquired using a spoiled gradient echo sequence ($\text{TE}=25\text{ms}$, $\text{TR}=200\text{ms}$, $\text{FA}=30$, 512^2 matrix, 0.5mm slice). T_2^* maps were obtained from 20 echo times (TE 2.5-30ms,

TR=200ms, FA=30, 256² matrix, 0.5mm slice). These were produced using the ImageJ MRI Analysis Calculator plugin (Schmidt, K., ImageJ, U. S. National Institutes of Health, MA USA) by fitting the decay of signal intensity with increasing echo time (Equation 2.4) on a pixel-by-pixel basis.

5.2.9 Statistical analyses

For the repeated MTS assays, two-way ANOVA was used with no *post hoc* test. For the growth, and differentiation assays, the null hypothesis was that there would not be a difference. A qualitative comparison was considered sufficient for the purposes of these studies. In the apoptosis assays it was possible to employ equivalence testing. The two one-sided t-test (TOST, Schuirmann's test) approach was used with a 3% equivalence limit at the 0.05 level (Cribbie, Gruman, & Arpin-Cribbie 2004). A maximum acceptable difference of 3% was set *a priori* based on 24hr serum deprived positive control cells (3% mean increase in early apoptosis, 16% increase in late apoptosis).

5.3 Results

5.3.1 Viability assay after 10min attraction with stacked magnets

Stacked magnets were used to double the applied force, compared to the force used in Chapter 4 (Figure 4.10). Cell viability following 24:1 differential labelling and 10 minutes of magnetic attraction was investigated in triplicate. Figure 5.1 displays the results from these experiments. Cell viability was similar between the non-magnet control and the magnet groups, for all three experiments.

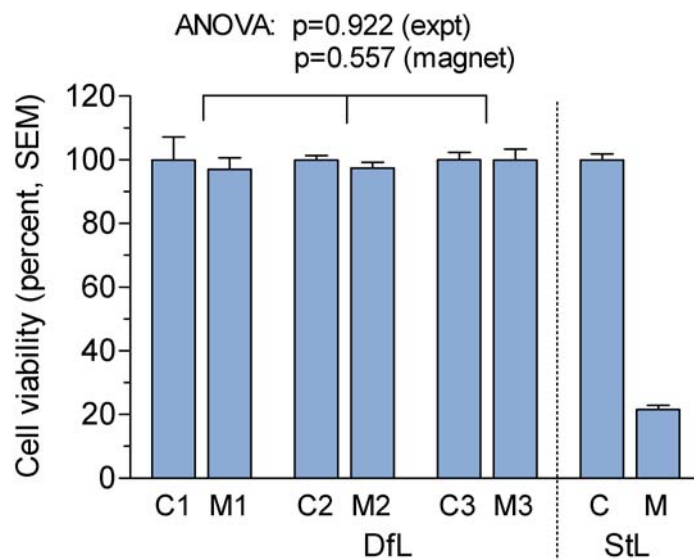


Figure 5.1– MTS assays following 10 min magnetic attraction of DfL cells

Three experiments (1-3) were conducted comparing no-magnet control (C) to 10 minutes of magnetic attraction (M). The effect of standard labelling is shown for reference (from Figure 4.10). There was no evidence to support a difference between control and magnet groups (C1 vs M1, C2 vs M2, C3 vs M3, $p=0.557$, two-way ANOVA). SEM: standard error of the mean, $n=4$ per group.

5.3.2 Cellular growth after DfL and magnetic attraction

There were no differences in cellular growth rate between the unlabelled control and DfL + magnet cells. The data from the MTS assay is presented in Table 5.2 and Figure 5.2 as absorbance units relative to unlabelled control at 24h. The increase in cell number as the cells multiply leads to higher absorbance values.

Table 5.2 – Cell proliferation post DfL and magnetic attraction

	Relative absorbance units (SEM)			
	24h	48h	96h	192h
Unlabelled control	1.0 (0.09)	1.3 (0.06)	1.9 (0.09)	2.7 (0.04)
DfL+ magnet	1.1 (0.08)	1.3 (0.05)	1.9 (0.05)	2.8 (0.10)

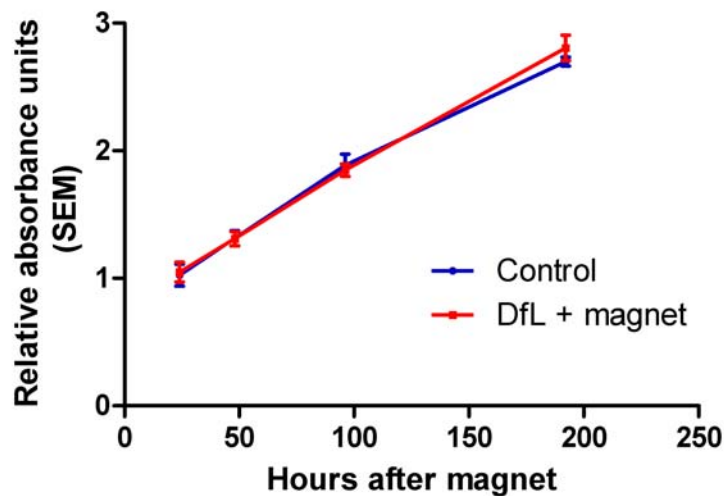


Figure 5.2 – Cell proliferation post DfL and magnetic attraction

Increased cell number due to proliferation leads to more formazan product produced in the 4 hours the MTS assay is allowed to react with the cells. This leads to higher absorbance values. Figure 5.2 shows the increase in absorbance over a period of 8 days (192 hours) for unlabelled control (blue) and cells that were differentially labelled and exposed to the stacked magnets for 10 minutes (red), with n=4 at each timepoint.

5.3.3 Cellular apoptosis after differential labelling

Figure 5.3 displays the early apoptosis (EA), late apoptosis (LA) and necrosis (N) rates of unlabelled control and DfL cells, at 24 and 72 hours after labelling. There were no differences in cellular apoptosis between unlabelled control and DfL cells. All groups passed equivalence testing, apart from early apoptosis at 24hrs, in which apoptosis was less for the labelled group (mean difference = 1.6%, $p < 0.05$). For a full table see Appendix B. These results can be further summarised by calculating the mean difference ‘labelled minus control’ and 95% confidence interval (CI) for this difference, for each timepoint pair (Figure 5.4).

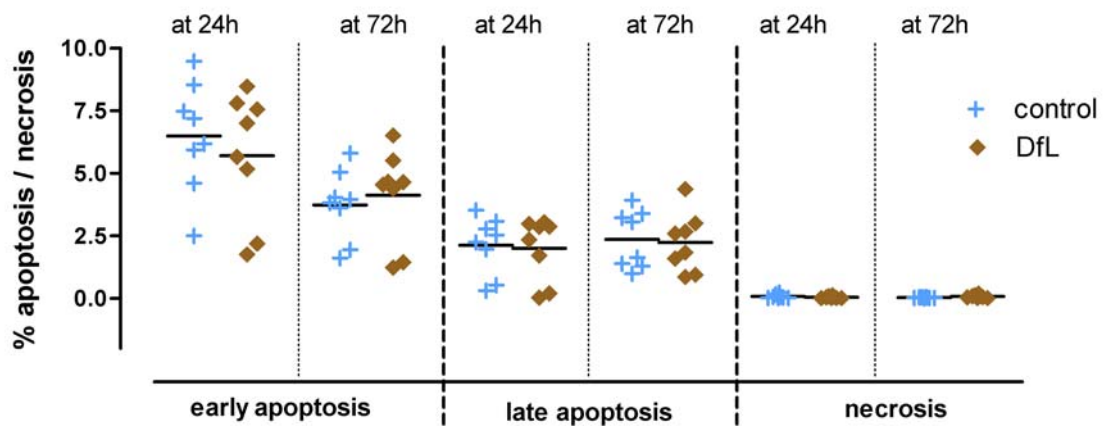


Figure 5.3 – Apoptosis rates after differential labelling

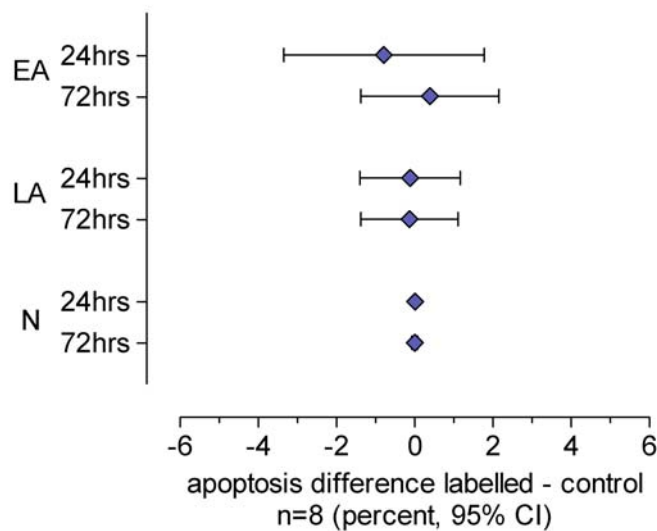


Figure 5.4 – Apoptosis differences after differential labelling

5.3.4 Cellular apoptosis after magnetic attraction

Figure 5.5 displays the apoptosis/necrosis rates at 24h, 48h and 120h after 10min magnetic attraction. Figure 5.6 displays the mean difference and 95% CI for each group pair. There was no increase in cellular apoptosis after magnetic attraction. All groups passed equivalence testing. For a full table see Appendix B. Figure 5.7 displays sample flow cytometry data from the apoptosis assays below and the previous section (5.3.3).

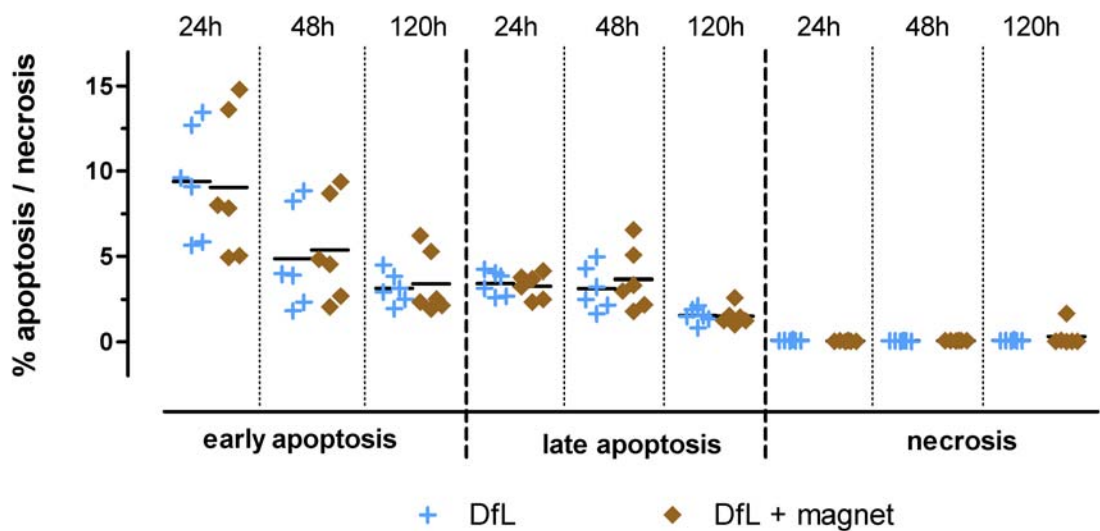


Figure 5.5 – Apoptosis rates after magnetic attraction

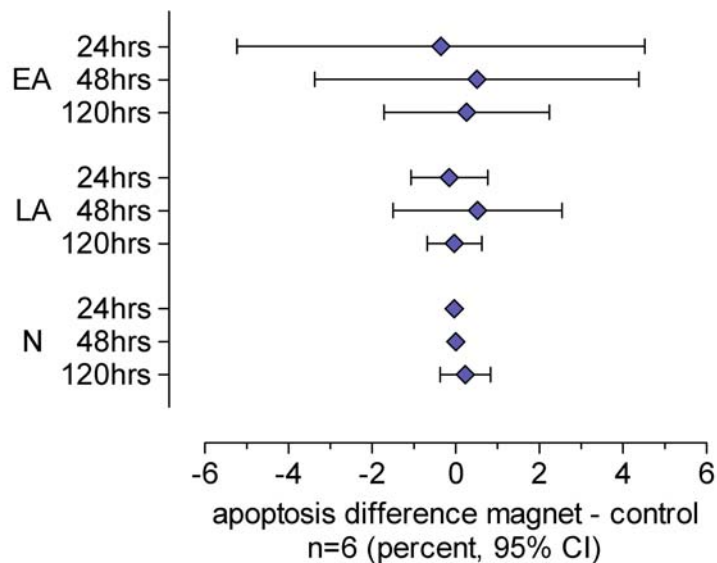


Figure 5.6 – Apoptosis difference after magnetic attraction

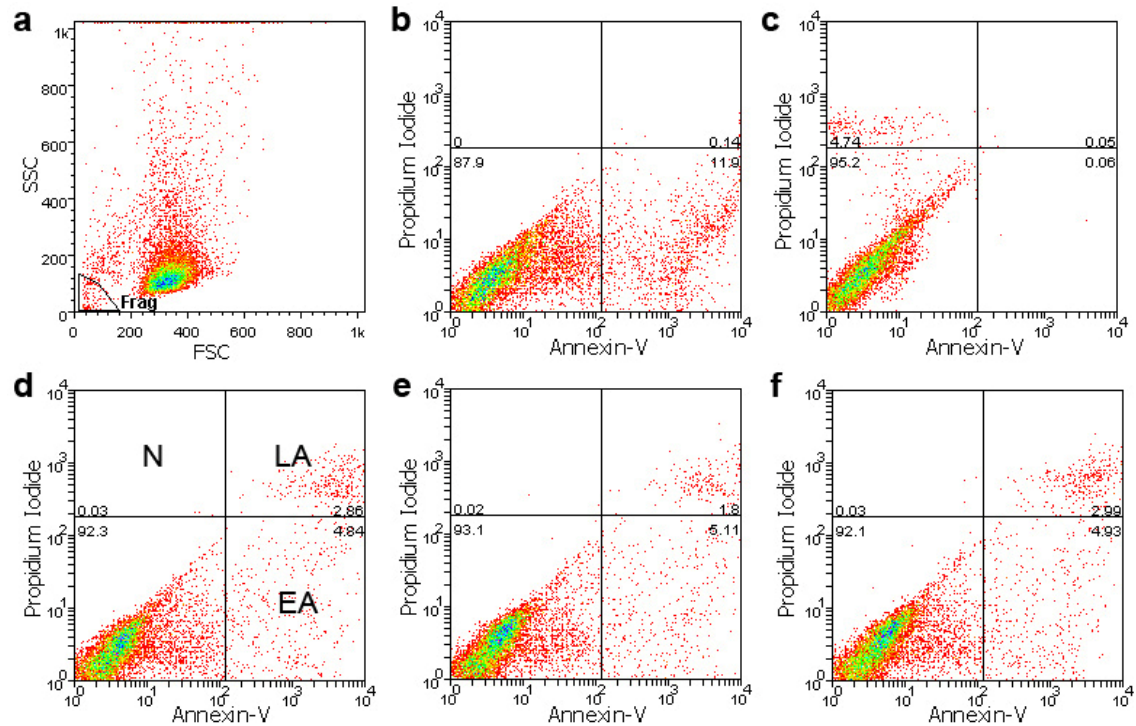


Figure 5.7 – Sample cytometry scatterplots for the apoptosis assays

All cells were included on the analysis, apart from cell fragments based on FSC and SSC (a). (b) and (c) show representative scatterplots for Propidium Iodide and Annexin-V negative controls, respectively. Early apoptotic cells (EA) are only positive for A-V. Doubly positive cells are late apoptotic (LA). Necrotic cells (N) stain only with PI. Unlabelled (d), differentially labelled (e) and DfL cells exposed to the magnetic force (f) had similar rates of apoptosis.

5.3.5 Cell differentiation after differential labelling

Figure 5.8 displays the surface marker expression ten days post-labelling. There was similar expression of endothelial (VE-Cadherin, CD304/NP-1) and monocytic (CD14, CD11b) markers of differentiation between labelled and non-labelled cells. For a full table of the surface marker expression values see Appendix B. Figure 5.9 displays sample flow cytometry data for the CD14 marker analysis.

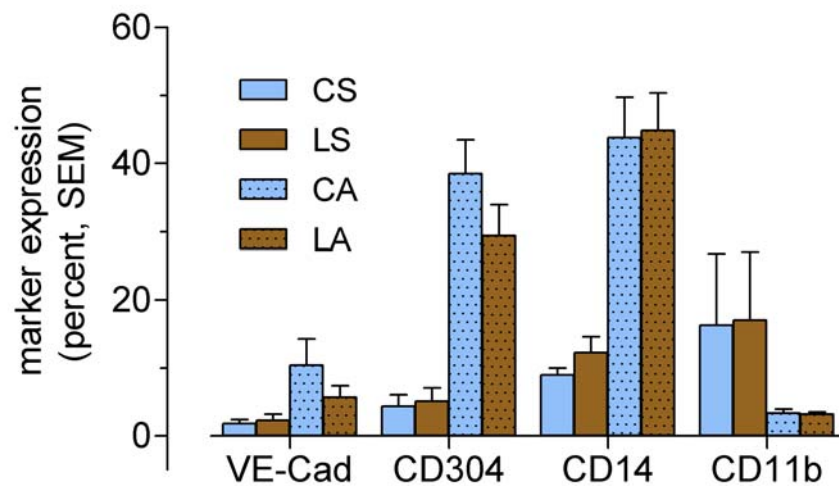


Figure 5.8 – Surface marker expression after DfL

Graph displays the percentage of live cells expressing the markers VE-Cadherin (VE-Cad), neuropilin-1 (CD304), CD14 and CD11b. Unlabelled samples are shown in blue, labelled samples are shown in brown. Suspension cells (clear bars) and adherent cells (dotted bars) were analysed separately. CS: Control non-labelled Suspension fraction; LS: SPIO-Labelled Suspension fraction; CA: Control non-labelled Adherent fraction; LA: SPIO-Labelled Adherent fraction. There was similar expression of differentiation markers between unlabelled and labelled cells (CS vs LS, CA vs LA). SEM: standard error of the mean. CD11b: n=3, all others: n=6.

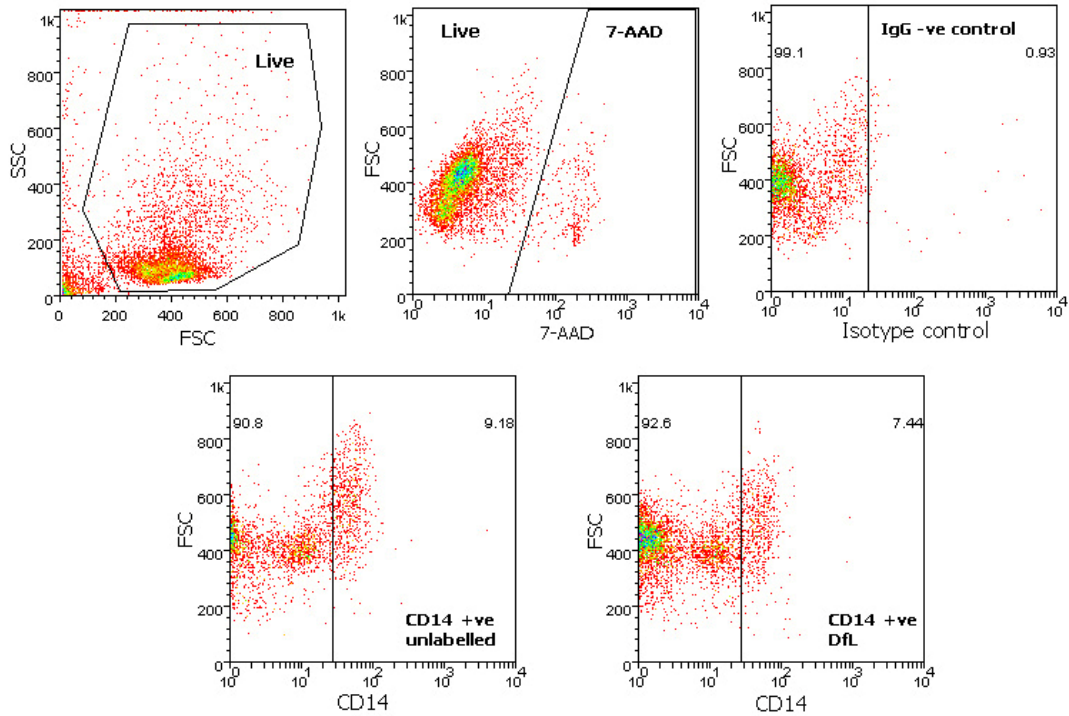


Figure 5.9 – Sample cytometry scatterplots for the CD14 surface marker analysis

Live cells were selected based on gating forward and side scatter (a) and 7-aminoactinomycin D (7-AAD) (b). Laser intensity adjustments were based on dose-matched negative controls (c). In these samples, unlabelled control (d) and Endorem®-labelled cells (e) had similar amounts of CD14 expression.

5.3.6 Iron quantification using SQUID

The amount of iron oxide (Fe_3O_4) per cell was calculated to be 3.9pg per cell. The following is a description of the results that were used for this calculation.

The SQUID measures the magnetic moment of a sample, in Am^2 . Figure 5.10 displays the data from a 15 μL Endorem® sample (233 μg Fe_3O_4), measured at 300K (27°C). Figure 5.11 displays a close-up of the sample behaviour near the zero applied H field at this temperature, to examine whether there is hysteresis. No hysteresis was observed and at zero applied field there was no remanent magnetisation. This occurred because the iron oxide is superparamagnetic. For a synopsis of the relevant theory see section 3.3.2.

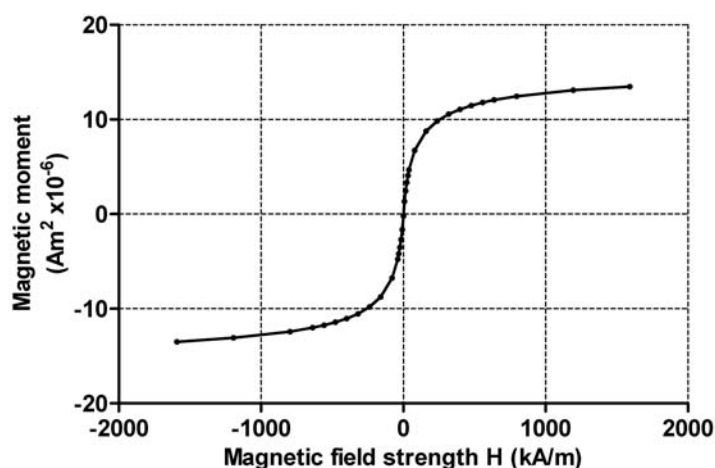


Figure 5.10 – SQUID loop of an Endorem® sample at 300K.

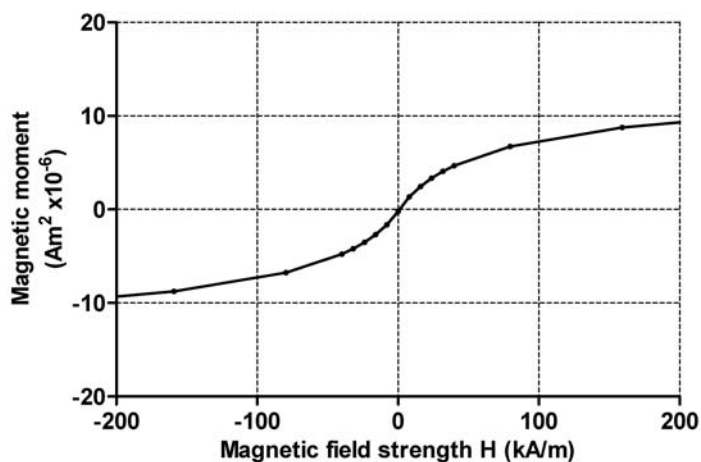


Figure 5.11 – Close up of SQUID loop for Endorem® at 300K

At 10K the sample lost its superparamagnetism and exhibited hysteresis (Figure 5.12). There was remanence at zero field. A sample of 5×10^5 DfL cells was measured in the same way (Figure 5.13). This remanence was used to quantify the amount of iron oxide per cell.

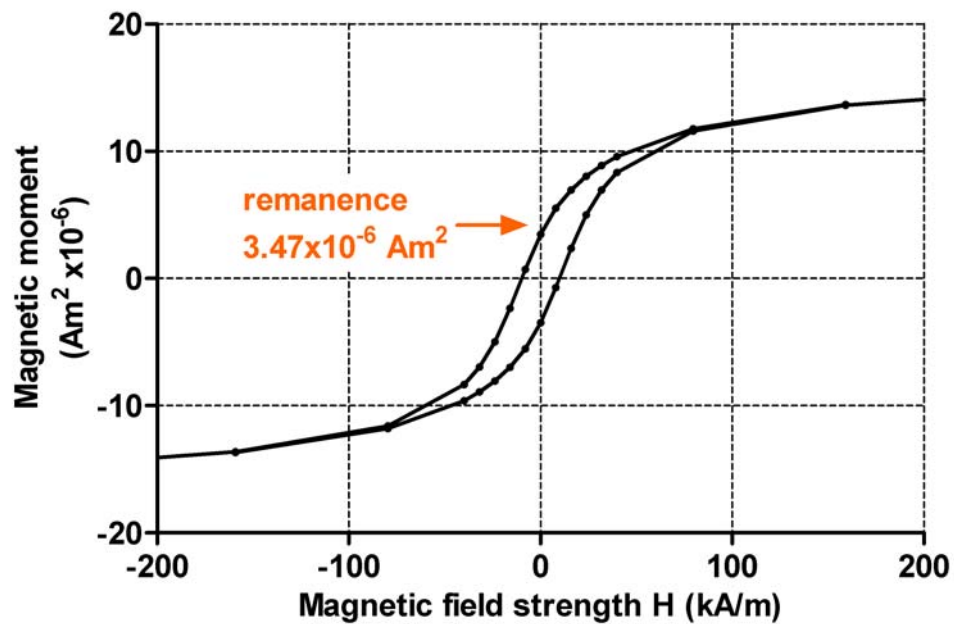


Figure 5.12 – Close up of SQUID loop for Endorem® at 10K

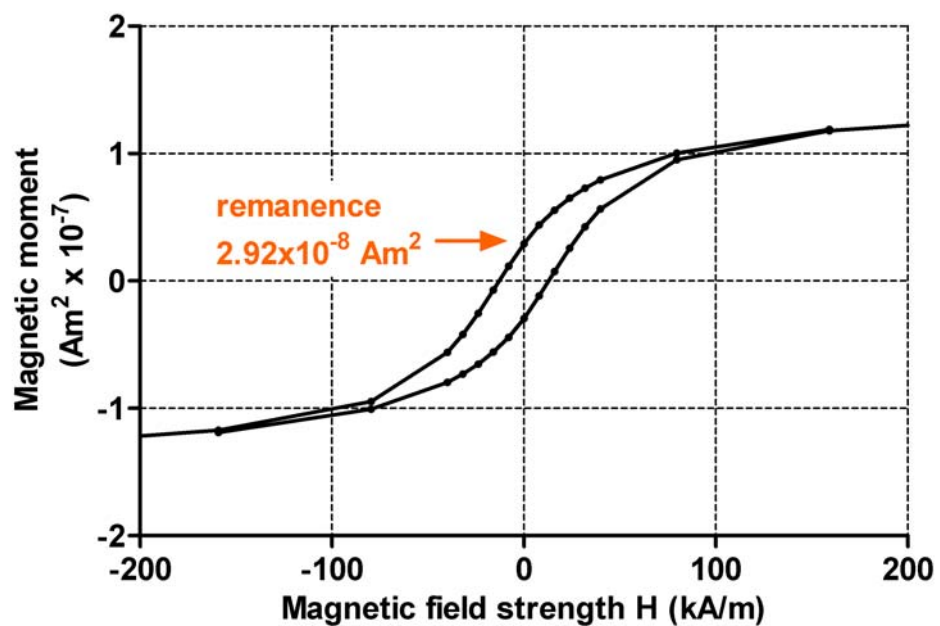


Figure 5.13 – Close up of SQUID loop for 5×10^5 DfL cells at 10K

Knowing the amount of iron oxide in the Endorem® sample ($15\mu\text{L} = 233\mu\text{g Fe}_3\text{O}_4$) the the remanence of Fe_3O_4 per gram was calculated:

$$\frac{3.47 \times 10^{-6}}{233} \times 10^6 = 14.87 \times 10^{-3} \text{ Am}^2/\text{g} \quad .$$

The remanence attributable to each cell is: $\frac{2.92 \times 10^{-8}}{5 \times 10^5} = 5.84 \times 10^{-14} \text{ Am}^2/\text{cell} \quad .$

Thus from the ratio of the two remanences, the ammount of Fe_3O_4 per cell was found:

$$\text{Fe}_3\text{O}_4 \text{ content} = \frac{\text{cell remanence} [\text{Am}^2 / \text{cell}]}{\text{Fe}_3\text{O}_4 \text{ remanence} [\text{Am}^2 / \text{g}]} = 3.92 \text{ pg} / \text{cell} .$$

The cell sample examined in these experiments were heterogeneous; thus the iron content quoted above is likely to be an underestimate for adherent cells and an overestimate for suspension cells.

5.3.7 Estimation of a cell-safe magnetic force

The maximum force that was applied on DfL-CD133⁺s during the viability tests in this chapter, with which there were no notable cellular effects was calculated to be 9.3 pN per cell. This is the ‘cell-safe’ magnetic force, and was calculated as follows.

As described in Figure 3.6, a linear magnetisation response for $|H| \leq 398$ A/m ($|B| \leq 0.5$ T) can be assumed. From the Endorem® M-H loop the magnetic susceptibility of Fe₃O₄ can be approximated [$\chi(Fe_3O_4)=0.789$]. The susceptibility of the cell χ_c will depend on the susceptibility of the iron oxide with which it is loaded $\chi(Fe_3O_4)$ (Equation 3.6) and can be calculated from the volume-per-volume loading of the cell with Fe₃O₄ (L_c) (Equation 3.7):

$$\chi_c = L_c \times \chi_{Fe_3O_4} \qquad L_c = \frac{V_{Fe_3O_4}}{V_c} = \frac{mass_{Fe_3O_4} / \rho_{Fe_3O_4}}{\frac{\pi}{6} \times D_c^3} .$$

Based on the 3.9pg loading of a 10µm-diameter cell, L_c was calculated:

$$L_c = \frac{3.9 \times 10^{-15} \text{ kg} / 5.21 \times 10^{+3} \text{ kg/m}^3}{5.24 \times 10^{-16} \text{ m}^3} = 1.44 \times 10^{-3} \text{ or } 0.14\%$$

The susceptibility of each cell (χ_c), necessary for the calculation of the force, is:

$$\chi_c = 1.44 \times 10^{-3} \times \chi_{Fe_3O_4} = 1.13 \times 10^{-3} .$$

Given a CD133⁺ cell diameter of 10µm (confocal data, Chapter 7) and viability tests at maximum tested $(\mathbf{H} \cdot \nabla)\mathbf{H} = 1.25 \times 10^{13} \text{ A}^2/\text{m}^3$ at $H=350\text{kA/m}$ (stacked magnets for 10 minutes), the cell-safe force is calculated using the unsaturated force expression (Equation 3.5) and is: $F_{max} = \mu_0 V_c \chi_c (\mathbf{H} \cdot \nabla)\mathbf{H} = 9.3\text{pN}$ per cell, against the restraint of the culture plate. Magnetic forces will be considered in more detail in Chapter 6.

5.3.8 *In vitro* MRI

At this stage I also investigated whether the cells contain enough iron to be visualised using MRI *in vitro* (Figure 5.14). Cells were visible as areas of hypointensity (signal voids) on T2*-weighted images from 25 cells/mm² (**a**, tube C) and caused a decrease in T2* from 8 cells/mm² (**b** and **c**, tube B).

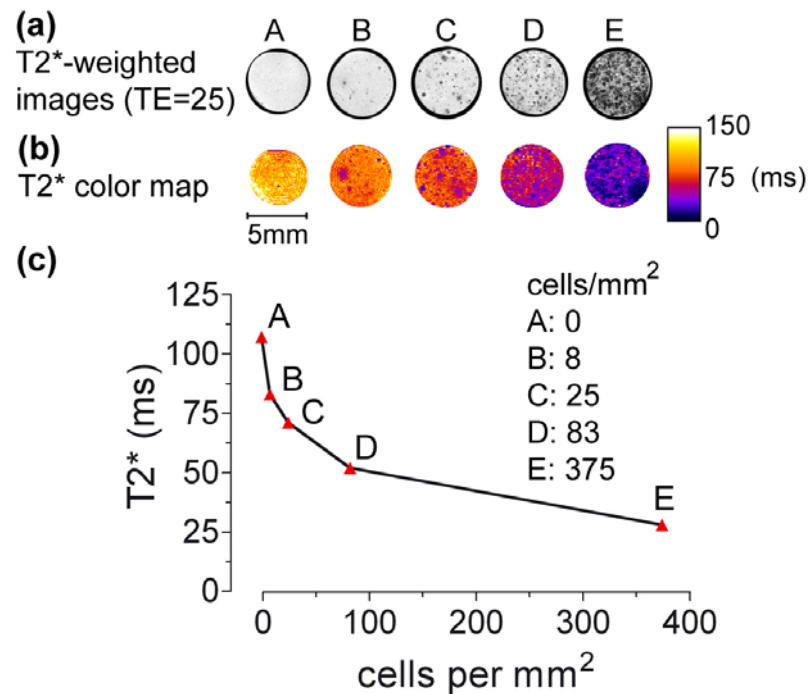


Figure 5.14 – *In vitro* MRI phantom of DfL-CD133s

Tubes A to E contain increasing amounts of cells. The cell concentration in ml was divided by 2 to give the in-plane cell content of the 0.5mm slice in mm². T2*-weighted images are shown in (a). T2* maps and the corresponding T2* values are shown in (b) and (c).

5.4 Discussion

5.4.1 Main findings

In these studies, it was found that:

- i) Cell viability, growth and apoptosis is normal following DfL and magnetic attraction using stacked magnets.
- ii) Cell differentiation is normal 10 days post-labelling.
- iii) Cells contain on average 3.9pg iron oxide / cell. A force of 9.3pN per cell is safe with regard to (i) above.
- iv) Cells are visible using MRI and readily create signal voids *in vitro*.

5.4.2 Magnetic forces

This chapter focused on the validation of the differential labelling method, mostly with regard to cell safety with SPIO labelling and magnetic attraction. As we saw in Chapter 4, a magnetic force has the potential to cause cell damage; this effect can be controlled by decreasing SPIO uptake. In this chapter, the force was applied for a shorter period of time (10 minutes instead of 24 hours), to match the *in vivo* scenario (Chapter 7). It was hypothesised that the force could correspondingly be increased. Subsequent to iron quantification, a cell-safe force was estimated to be 9.3pN per cell. Even with this force, in Figure 5.1 there is an insignificant decrease in viability in groups M1 and M2. However, no difference was observed on the growth and apoptosis assays. The effect of an even higher force, applied for 10 minutes, was not considered a priority at this stage and was not investigated further.

Regarding the iron quantification itself, the SQUID is a precise instrument that can allow detection of down to 1ng of iron oxide without the need for a chemical assay

(Hautot, Pankhurst, & Dobson 2005). Because it is relatively easy to use, it was considered a better option than the chemical assay used in Chapter 4. The 3.9pg/cell iron oxide estimated using SQUID compares well with the 5.4pg/cell seen for adherent cells in Chapter 4 (Figure 4.12). An important drawback with SQUID was the large number of CD133 cells that were needed for measurements. For this reason, only the mean cell content of a mixture of suspension and adherent cells was estimated. This is likely to have led to an underestimation of the magnetic force applied on adherent cells.

There are limited studies that have investigated the magnitude of the force necessary to rupture a cell membrane; these mainly focus on the force needed to withdraw molecules from the membrane, and estimates between 100pN and 800pN are quoted (Afrin, Yamada, & Ikai 2004; Benoit et al. 2000). These forces are larger than the observed 9.3pN force that is regarded as the maximum safe force in the presented studies.

However, in the above studies investigating rupture, forces are applied for a timespan of seconds to minutes, and it is noted that the rupture force decreases with increasing force application time (Marrink et al. 1998). Moreover, forces as low as 2pN can distort the intracellular cytoskeleton (Jiang et al. 2003). These facts, together with the likely underestimation of the forces applied on adherent cells, can explain the fact that in my experiments, above average forces 9.3pN per cell, some cell death was observed.

5.4.3 Cell viability and differentiation

I could not find any reported cell toxicity when Endorem® or Feridex® have been used to label cells without additional transfection agents. Although the general consensus is that SPIO labelling in general is not harmful (Bulte & Kraitchman 2004), adding a transfection agent has been reported to affect the cell differentiation (Kostura et al.

2004). In MRI studies where a transfection agent has been used, typically 20-30pg of iron oxide per cell is achieved (Bulte & Kraitchman 2004). In this study, the iron content was lower than that. However, as previously discussed, adding a transfection agent may be an obstacle to clinical translation, and more importantly, was not necessary in the context of these studies, as it would increase the force. However, because of the lower iron content, the visibility of the cells using MRI needed to be investigated. Using a T2*-weighted sequence, it was possible to visualise the cells, at least *in vitro*. This indicates that the multi-modality of using an SPIO agent, both for targeting and imaging, is retained.

A variety of assays were used to confirm that the labelling method itself, i.e. the process of separating the cells as well as the uptake of SPIO, does not increase apoptosis (Figure 5.3) or affect differentiation in culture (Figure 5.8). Furthermore, immediate (Figure 5.1) post-attraction viability was shown to be normal, as well as cell growth up to 192h (Figure 5.2) and apoptosis up to 120h after attraction (Figure 5.5). The success of these assays was very dependent on the amount of water evaporation. This effect of evaporation was only recently reported in the literature, in a study that showed the same spatial differences within the plate as described in the Appendix (Figure A.5), and also concluded that the plate should be filled with water to limit the evaporation (Patel, Tuckerman, & Dong 2005).

5.5 Conclusions

In these studies, it was found that:

- i) Cell viability, growth and apoptosis is normal following DfL and magnetic attraction using stacked magnets.
- ii) Cell differentiation is normal 10 days post-labelling.
- iii) Cells contain on average 3.9pg iron oxide / cell. A force of 9.3pN per cell is safe with regard to (i) above.
- iv) Cells are visible using MRI and readily create signal voids *in vitro*.

CHAPTER 6

MAGNETIC ACTUATION *IN VITRO*

6.1 Introduction

Magnetic actuation refers to the movement of an entity under the influence of a magnetic force. This chapter will focus on theoretical modelling and *in vitro* experiments of CD133-derived, Endorem®-labelled cells. The aim of these experiments was to examine the feasibility of external targeting of cells to a site of rat common carotid artery (CCA) injury. Results using an *in vivo* rat CCA injury model are presented in Chapter 7. Here, static and fluid dynamic problems will be considered in simulations and *in vitro*.

As outlined in section 3.2.2, magnetic targeting has mainly been exploited in the context of drug targeting. Several theoretical models have been developed, which focus on laminar flows in liquids such as water. Targeting of cells only recently gained interest alongside the advent of stem cell therapies. A variety of magnetic targeting methods have been utilised for cells (section 3.2.3). As previously mentioned, these are not directly applicable to a clinical scenario. Moreover, so far there have not been any theoretical models of cell targeting.

An important consideration in the common carotid artery (CCA) model is that the artery is a non-superficial structure approximately 5mm from the skin, in which there are large hydrodynamic forces acting on the cells, with peak systolic blood flow rate up to 10mL/min (maximum velocity 40cm/s) (Garcia-Villalon et al. 1992; Miyashiro, Poppa, & Berk 1997). However, there is a rapid decline of magnetic force at increased target tissue distances, which in general poses a challenge to magnetic targeting using external devices *in vivo* (Dobson 2006; Pankhurst et al. 2003). To overcome this issue, a permanent magnetic actuator configuration was chosen which increases the force magnitude at large distances (Halbach array) (Häfeli et al. 2007; Mallinson 1973).

In this study, the aim was to:

- i) Magnetically actuate cells in the absence of external flow *in vitro*.
- ii) Model and construct an external magnetic actuator for *in vivo* targeting, which would not exceed the cell-safe force.
- iii) Model magnetic targeting of cells in a flowing vessel using this actuator.
- iv) Magnetically attract cells from a flowing vessel *in vitro* using this actuator.

It was found that:

- i) Endorem®-labelled cells are readily actuated in a static liquid.
- ii) The Halbach array constructed leads to higher forces than single or stacked disk magnets, without exceeding the cell-safe force at 5mm distance.
- iii) Cells can be theoretically captured from a 10mL/min flow using the array.
- iv) Cells can be captured *in vitro*. The capture efficiency is less than predicted using the theoretical model.

6.2 Methods

6.2.1 Cell culture

Because of the limited availability of CD133 cells, in these experiments human mononuclear cells (MNCs) were used. These were collected by leukapheresis from peripheral blood of G-CSF-stimulated donors. MNCs were grown for 2h in serum-free DMEM medium (Gibco) followed by removal of non-adherent cells and culture of adherent fraction in 10%FBS/DMEM. MNCs were labelled by incubating 12 hours in

0.5 mg/ml Endorem® or 36 hours in 0.1 mg/ml, resulting in 7.9pg Fe₃O₄/cell or 3.5pg Fe₃O₄/cell, respectively, as measured using the SQUID (see section 5.2.7).

6.2.2 *In vitro* actuation in a static liquid

To investigate whether the forces applied on Endorem®-labelled cells are in the order of magnitude necessary to move them through a liquid, 1×10^4 MNCs (7.9pg iron oxide per cell) were placed in a suspension of PBS on a glass slide under a phase contrast microscope. The movement of the cells were captured on video using a 20x objective and a standard CCD camera, while a single 22mm x 8mm disk magnet was placed 5mm away from the suspension edge.

6.2.3 Magnetic actuator (Halbach array)

The array was constructed using five $10 \times 10 \times 25 \text{mm}^3$ Nd₂Fe₁₄B grade N35 magnet blocks in a configuration of rotating magnetisation, whereby the magnetisation direction rotates 90° for every block. This type of configuration exhibits destructive and constructive superposition of magnetisation on its two sides, resulting in a preferentially one-sided flux and force higher than that of a single magnet (Hafeli et al. 2007; Mallinson 1973). Because of the repulsive forces between the blocks, they were attached together inside a machined aluminium casing.

6.2.4 Computer simulations

Magnet designs were modelled using Opera 2D and 3D (Vector Fields Inc, IL USA) and COMSOL Multiphysics 3.1 (COMSOL Inc, MA USA). The single and stacked magnets used in Chapter 4 were compared to the Halbach array. Fluid dynamics simulations were run using COMSOL, on a 4x2GHz quad-core MacPro workstation

with 8Gb RAM. The Khan and Richardson force and the magnetic force from the array were considered, in parabolic non-pulsatile laminar flow of water (density=997kg/m³, viscosity=8.9x10⁻⁴ Pa·s) with maximum velocity 40cm/s. This is equivalent to 10mL/min flow in a 1mm diameter vessel. Simulated cells were 10µm in diameter, 3.9pg Fe₃O₄ / cell. Cell capture was defined as approximation and contact with the vessel wall within the 50mm length of the array. Theoretical capture efficiency for a 3-dimensional vessel was based on capture toward the 1/3 of the vessel periphery closest to the magnet, taking in account the parabolic flow profile in the vessel.

6.2.5 *In vitro* flow system

The array described above was assessed in an *in vitro* flow system by placing 1x10⁶/ml SPIO-labelled blood MNCs (3.5pg Fe₃O₄/cell) in peristaltic pump - driven flow (1-10 ml/min, max velocity 40 cm/s) using biocompatible (ISO 10993) 1mm internal diameter Tygon® S-54 elastic microtubing (Saint-Gobain Performance Plastics, France). The array was placed at 1mm and 5mm distance from the tubing. Cells were washed using cell dissociation buffer (Sigma), stained with Trypan Blue, and the mean of 5 haemocytometer counts of captured cells was calculated for each experiment. Digital images were acquired using a standard dissection microscope and a digital camera.

6.2.6 Statistical analyses

As in 4.2.2.7. The homogeneity of variance assumption was evaluated with Levene's test, and Welch's correction for two-sample t-tests was used where the variances were significantly different (Levene's test for equality of variance p<0.05).

6.3 Results

6.3.1 Cell actuation in a static liquid

Magnetic attraction caused movement of SPIO-labelled MNC (Figure 6.1). As well as being attracted to the magnet, the cells experienced inter-cell attraction, and entered the field of view in aggregates. This led to an increase in cell count rate between 5s – 10s. The cell count rate subsequently decreased (10s - 20s) as the suspension volume closest to the magnet was depleted of cells. The average velocity of two single cells was 150 $\mu\text{m}/\text{sec}$.

To compare the actual cell velocity to the theoretical velocity these cells could achieve, the force on these cells was calculated using Equation 3.5. The force when the cells are 5mm away from the magnet corner was 19pN. Substituting this value in Equation 3.12 and ignoring friction with the glass slide, the theoretical velocity of single spherical cells in a suspension of water is 215 $\mu\text{m}/\text{sec}$. As the cells move closer to the magnet, this theoretical velocity increases. For example, within the 200 μm distance travelled in Figure 6.1, the magnetic force per cell would increase to 19.5pN and the velocity to 220 $\mu\text{m}/\text{sec}$. Given that these values ignore friction with the glass slide, they compare well with the measured velocity of 150 $\mu\text{m}/\text{sec}$.

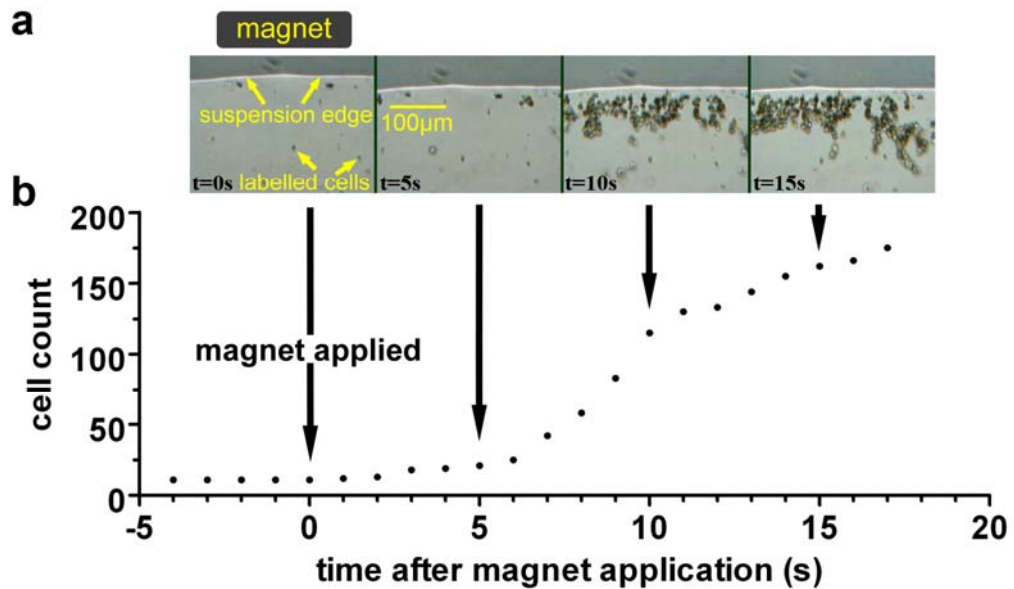


Figure 6.1 – Actuation of Endorem®-labelled MNC in a static suspension

(a) Video frames for $t=0$ (application of magnet), 5, 10 and 15 seconds after exposure to the magnet. Relative position of a 22mm diameter \times 8mm height disk magnet is displayed for $t=0$ (not to scale). (b) Count of cells in field of view.

6.3.2 Design and construction of the magnetic actuator

An actuator design of rotating magnetisation was chosen (Halbach array) (Figure 6.2). The rotating magnetisation should result in a preferentially one-sided magnetic field density and magnetic force magnitude (Hafeli et al. 2007). This was confirmed in the computer modelling (Figure 6.2-a). The force maxima were predicted to occur at the junctions between the magnet blocks and at the corners of the array. Figure 6.2-b is an orientation summary for the modelling and *in vitro* studies presented in this chapter; it describes the two distances along the length of the array (1mm and 5mm horizontal lines), as well as the vertical central and junction lines used for analysis of the forces.

In order to compare the field strength and gradient of the Halbach array to the single and stacked magnets used in Chapter 4 and 5, $(\mathbf{H} \cdot \nabla)\mathbf{H}$ was calculated for the central line of these disk magnets. Assuming constant cell iron content, the magnetic force on the cells will be directly proportional to $(\mathbf{H} \cdot \nabla)\mathbf{H}$ (section 3.3.3). A shorter 3-magnet Halbach array was also simulated. The data for the central line of the disk magnets and the Halbach arrays is presented in Figure 6.3. Note that the Halbach arrays have higher $(\mathbf{H} \cdot \nabla)\mathbf{H}$ at the junctions (Figure 6.2-b); the force on top of these junctions is considered later.

The Halbach array was predicted to have higher $(\mathbf{H} \cdot \nabla)\mathbf{H}$ than the disk magnets. At 1mm along the central line, the $(\mathbf{H} \cdot \nabla)\mathbf{H}$ of the 5-magnet array is approximately double that of the stacked disk magnets, and 10% higher than a 3-magnet array. From the data in Figure 6.3 it can also be observed that stacking the disk magnets effectively doubles the available $(\mathbf{H} \cdot \nabla)\mathbf{H}$ at 1mm; this in turn doubles the force, which was discussed in Chapter 4 (Figure 4.9).

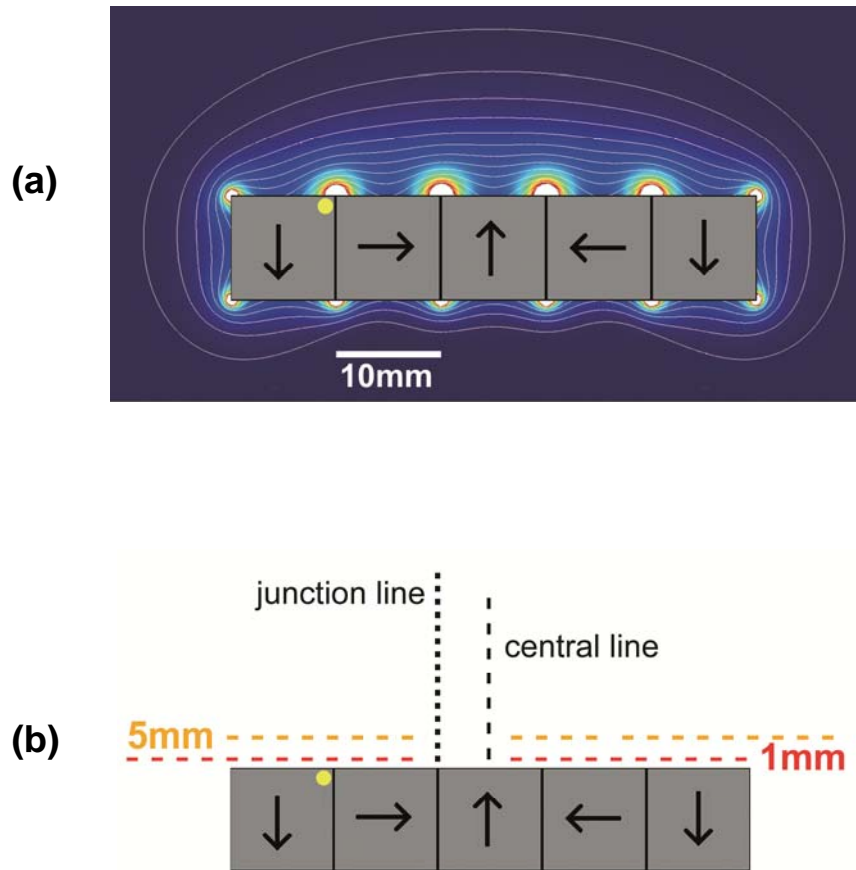


Figure 6.2 – Halbach array

a) Computer model of the Halbach array, with lines of equal magnetic flux density (white lines) and colour coding of force magnitude increasing from blue to white. Black arrows display the magnetisation direction of each magnet block. **b)** Orientation image showing the two distances (1mm and 5mm) and the central line and junction line referred to in this chapter. Yellow mark in left-most block placed for orientation (also in Figure 6.9).

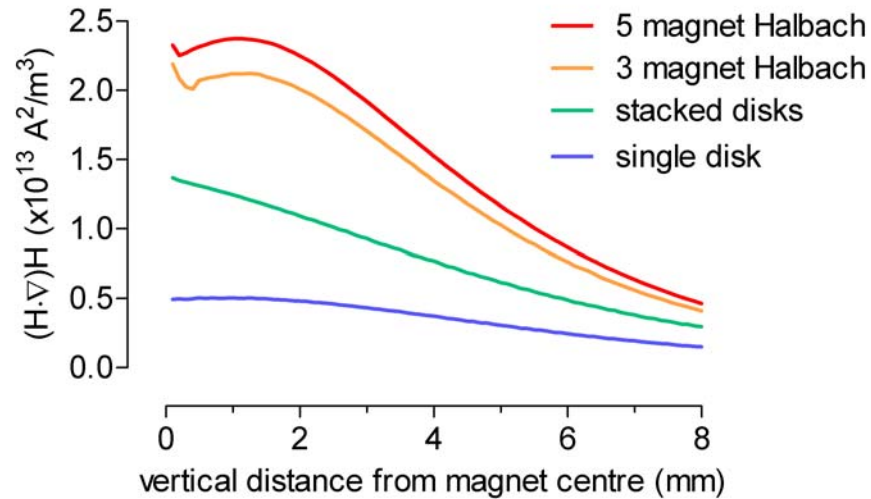


Figure 6.3 - Halbach array versus disk magnets

Figure 6.3 displays the theoretical $(\mathbf{H} \cdot \nabla)\mathbf{H}$ values along the central line, for two Halbach arrays and the single and stacked disk magnets. At 1mm vertical distance, the 5-magnet array can provide a 2-fold stronger force than the stacked magnets. As the distance increases, there is a decline in $(\mathbf{H} \cdot \nabla)\mathbf{H}$, which leads to a decline in available force for magnetic attraction.

6.3.3 Effect of the SPIO magnetisation saturation

A more detailed comparison of the magnetic forces created by these magnets requires consideration of the saturation of the SPIO magnetisation, because the forces are calculated with a different expression if the magnetisation is saturated (section 3.3.3). As shown in Figure 3.6, for the case of Endorem® a saturation limit can be selected at 398 kA/m based on SQUID data. Below 398 kA/m, the magnetic force was calculated using Equation 3.5; above 398 kA/m, Equation 3.6 was used. As seen in Figure 6.4, only the Halbach arrays exceed this limit. For example, for the 5-magnet array, the 398 kA/m limit is reached 2.4mm vertical distance from the magnet centre. Using the unsaturated force expression when $H > 398$ kA/m would thus result in an overestimation of the applicable force (Figure 6.5), so the force expressions were ‘switched’ at the SPIO saturation limit (Figure 6.6).

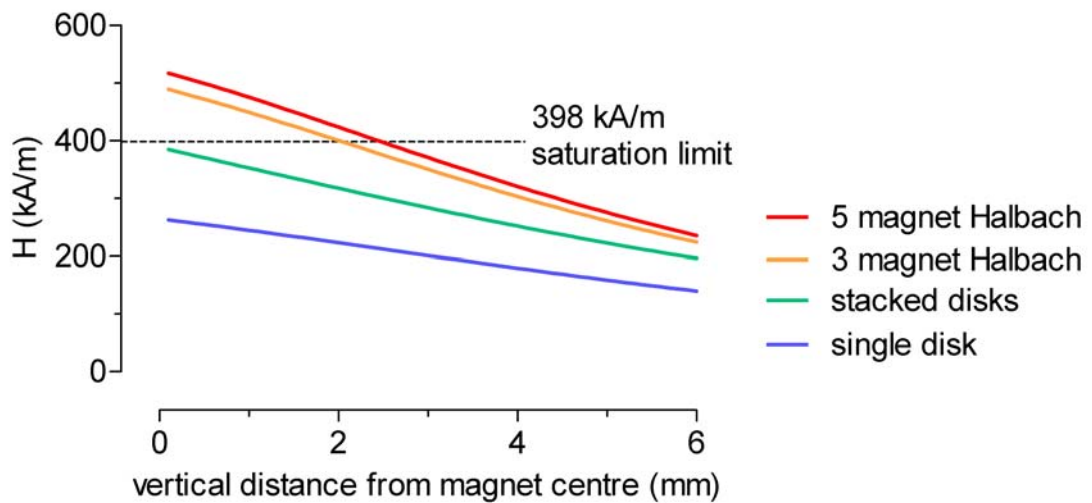


Figure 6.4 – Magnetic field strength and magnetisation saturation

For the 5-magnet array, the 398 kA/m limit is reached at 2.4mm vertical distance from the magnet centre. For the 3-magnet array, this limit is reached at 2mm distance. With the disk magnets, the limit is not reached; the magnetisation of the SPIO particles does not become saturated. Thus the unsaturated force expression was used for the disk magnets.

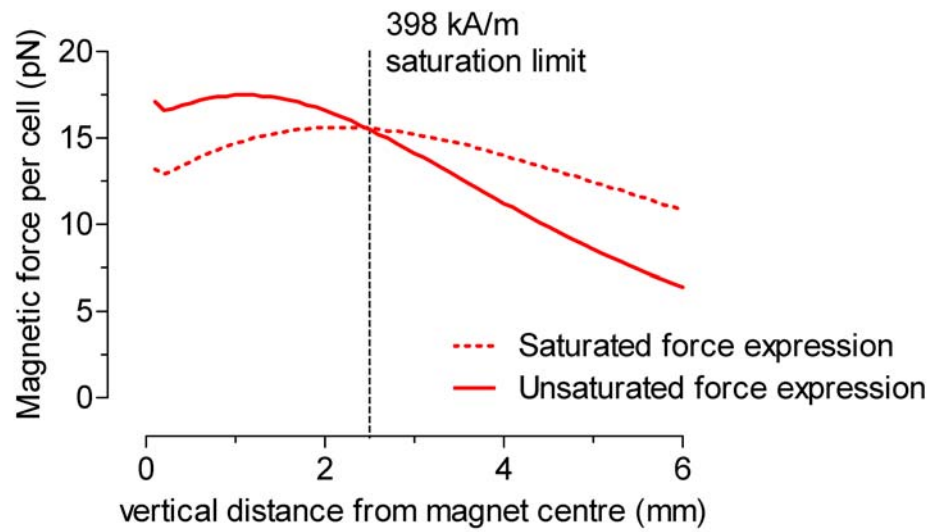


Figure 6.5 – Selection of force expression

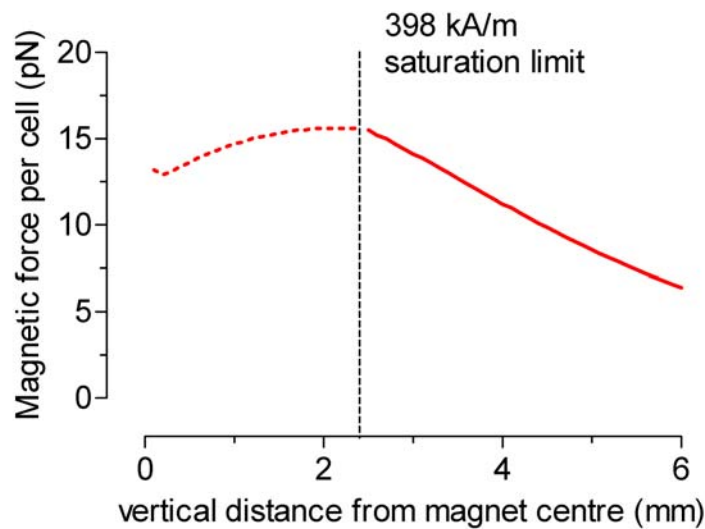


Figure 6.6 – Switch in force expression

Figure 6.5: The magnetic force can be calculated either with the ‘unsaturated magnetisation’ force expression (Equation 3.5) or the ‘saturated magnetisation’ force expression (Equation 3.6). Figure 6.6: The force expression was switched at the 398 kA/m limit. Below 398 kA/m, the magnetic force was calculated using Equation 3.5; above 398 kA/m, Equation 3.6 was used. Forces calculated for 3.9pg Fe_3O_4 / cell.

6.3.4 Consideration of the ‘cell-safe’ force

The Halbach array was constructed to achieve the ‘cell-safe’ magnetic force (Chapter 5) *in vivo*; the force applied on cells in the rat CCA, when the Halbach array is placed on the skin, should not exceed the ‘cell-safe’ magnetic force of 9.3pN. The distance of the skin from the rat CCA is 5mm, measured on rat neck MR images from a study that is not included in this thesis. Figure 6.7 displays the magnetic forces on cells using the disk magnets and the Halbach arrays. The central line is used as before, taking into account the switch in force expression.

For the viability assays, the stacked magnets were used at 1mm distance (Chapters 4 and 5). The cell-safe force using the stacked disks at 1mm distance is 9.3pN per cell, as calculated in Chapter 5 (left vertical dashed line and horizontal line on Figure 6.7). The 5-magnet array exhibits an 8.7pN force on cells at 5mm (right vertical dashed line), which is less than the cell-safe force. The 5-magnet array was chosen over the 3-magnet array, as it provides marginally higher but still safe forces at 5mm. It also allows application of the force along a longer segment (because it is 2 magnet blocks, i.e. 20mm, longer). The array was constructed from five blocks attached together in an aluminum casing (Figure 6.8).

There is an additional set of data on Figure 6.7 (black line). These are the forces on the vertical line above the left central junction of the 5-magnet array, instead of the central line (see Figure 6.2-b for orientation). This set of data was investigated because the forces above the magnet junctions are higher than above the center of the blocks (Figure 6.2-a), and thus may exceed the cell-safe force. The force at 5mm vertical distance from this junction is 9pN, less than the cell-safe force. At closer distances, the force exceeds the cell-safe force (60pN at 1mm, 800pN at 0.1mm).

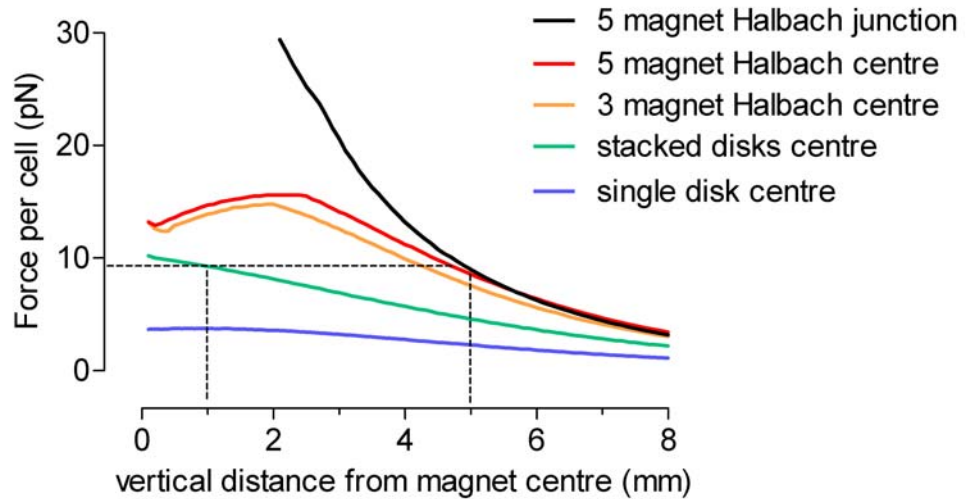


Figure 6.7 – Magnetic force on cells: Halbach vs disk magnets

Figure 6.7 displays the estimated force per cell ($3.9\text{pg Fe}_3\text{O}_4$ per cell) for the disk magnets and the Halbach arrays. The horizontal dashed line is the cell-safe magnetic force; this is reached at 1mm using the stacked magnets, which is the distance the cells were placed from the magnets during the viability tests (left vertical dashed line). Using the 5-magnet Halbach array, this force is not exceeded at 5mm distance (right vertical dashed line) from the 5-magnet array centre (red line) or junction (black line).

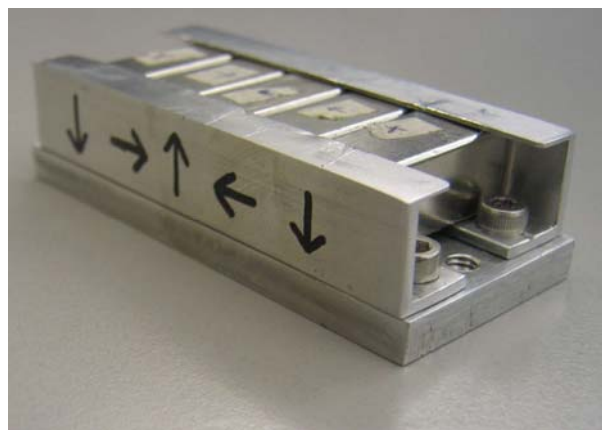


Figure 6.8 – The constructed 5-magnet array

The 5-magnet Halbach array was constructed using 5 magnet blocks in a configuration of rotating magnetisation, inside an aluminium casing. The black arrows represent the magnetisation direction of each block.

6.3.5 Finite element modelling of cell targeting

This section will describe the computer simulations of cell targeting from a flowing vessel using the 5-magnet Halbach array. Two scenarios were considered for the finite element modelling (FEM) fluid dynamics simulations; the vessel was placed either 1mm away or 5mm away from the Halbach array. The purpose of these simulations was to investigate the theoretical feasibility of targeting cells with 3.9pg iron oxide / cell, from a 10mL/min flow. Cell capture was possible at both distances. Figure 6.9 displays FEM of cell targeting to the wall of a vessel placed 1mm from the actuator. As the fluid drag force diminished near the vessel wall, the cells approached with increasing angle.

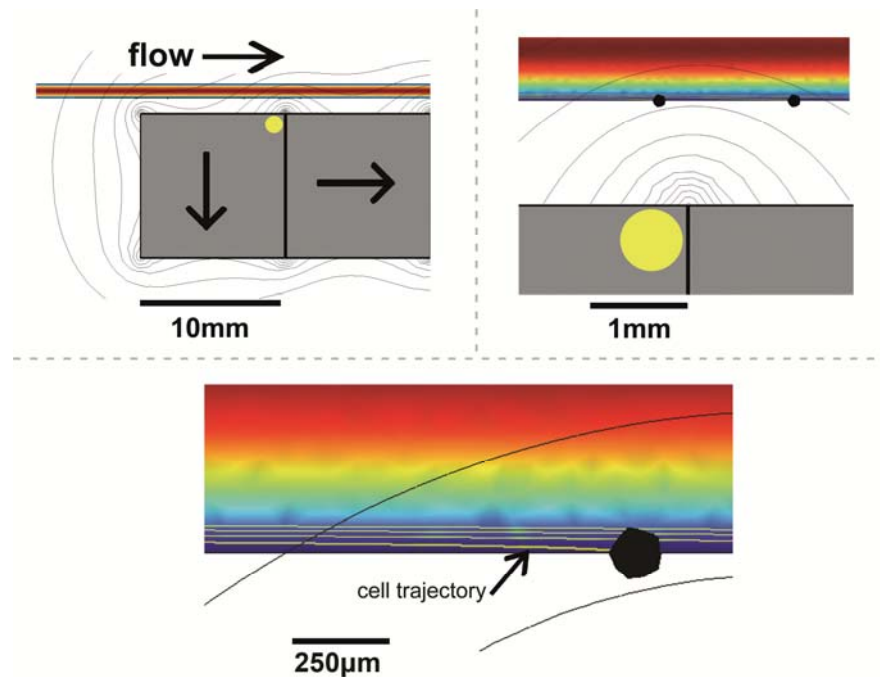


Figure 6.9 – FEM simulation: cell capture at 1mm

The fluid velocity is colour-coded and increases from blue to red. The laminar flow model resulted in a parabolic velocity profile with velocity highest at the centre of the vessel (red, 40cm/s) and minimal near the vessel wall (blue). Targeted cells (black spheres, not to scale) are shown on the vessel wall; the thin yellow lines (bottom image, arrow) are the cells' predicted intraluminal trajectories.

Cell capture was defined as contact with the vessel wall within the 50mm length of the actuator. Due to the laminar flow, successful targeting was dependent on the initial vertical distance of the cells from the vessel wall (Figure 6.10). Cells close to the vessel wall adjacent to the array were captured. Cells near the centre of the vessel, and those near the far side of the vessel, did not get captured within the 50mm length of the array.

Furthermore, the cell capture was dependent on the distance of the vessel from the magnetic array. Cell capture was theoretically possible at both distances. When the array was placed 1mm away from the vessel, cells initially up to 170 μm away from the vessel wall were captured. This represents 11% capture efficiency of flowing cells at each pass. At 5mm, cells up to 70 μm were targeted, which represents a capture efficiency of 2.3%.

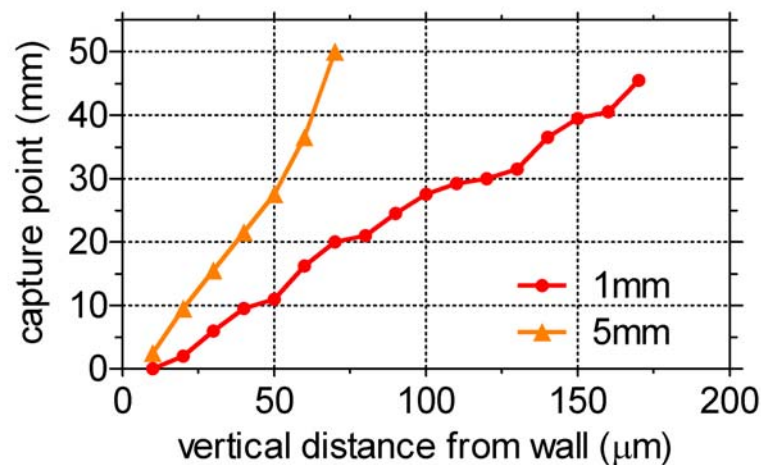


Figure 6.10 – Cell capture simulations at 1mm and 5mm

The graph is a plot of the initial vertical distance of the cells from the vessel wall upon release, against the distance travelled prior to capture. Cells near the centre of the vessel move faster than those near the wall and did not get captured within the 50mm length of the array.

6.3.6 *In vitro* flow system

6.3.6.1 System setup

Subsequent to the finite element modelling simulations, the targeting ability of the 5-magnet Halbach array was investigated *in vitro* at the two distances (1mm and 5mm, see Figure 6.2), using a 10mL/min flow system (Figure 6.11).

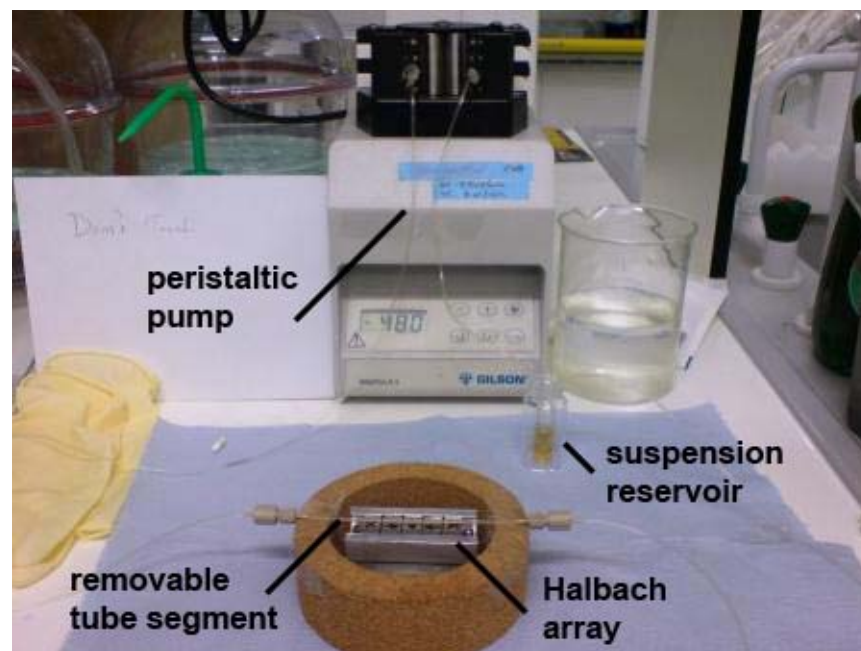


Figure 6.11 – *In vitro* flow system setup

Figure 6.11 is a photograph of the *in vitro* flow system setup. The system was comprised of a reservoir containing a suspension of cells, a peristaltic pump, the Halbach array at 1mm or 5mm and a tube segment above the array that could be removed to quantify the capture. The tubing was attached to a cork ring, which could be elevated with spacers to increase the distance of the tube to the Halbach array.

6.3.6.2 Proof of principle – cell capture at 1ml/min

As a proof of principle, cells were circulated in the system at a flow rate of 1ml/min and 1mm distance from the Halbach array. The slow flow rate and 1mm distance were chosen in order to decrease the hydrodynamic drag force and increase the magnetic force for this proof of principle experiment. A large number of cells accumulated on top of the array within 5 minutes (Figure 6.12).

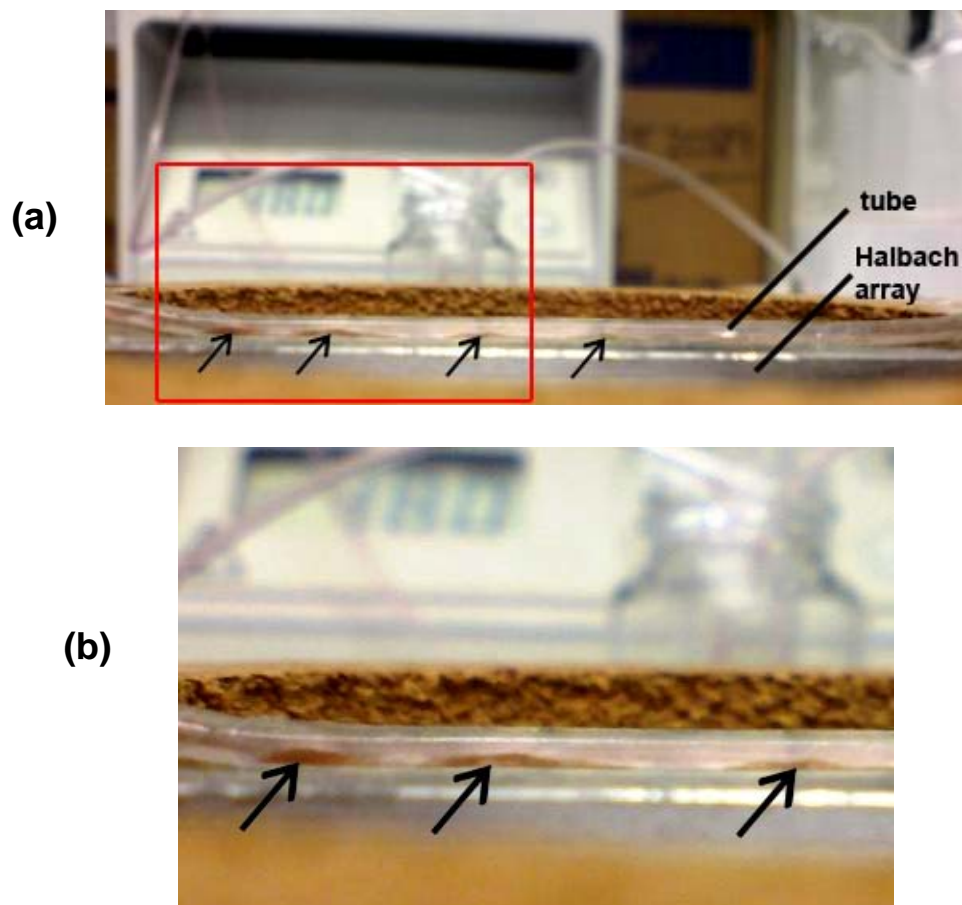


Figure 6.12 – Cell capture at 1mm, 1ml/min

Figure 6.12-**a** is a photograph taken from the side of the cork ring. Cell aggregates were readily visible inside the tube (black arrows). The flow direction was from left to right; correspondingly, the aggregates formed first on the left side. Aggregation was more pronounced on top of the magnet array junction points. The area bounded by the red box is magnified in (b).

6.3.6.3 Cell capture at 10ml/min

Subsequent to the proof of principle experiment and because of the preferential accumulation of the cells above the junction points, it was considered appropriate to examine the forces on the cells along the length of the Halbach array in more detail (see horizontal lines on Figure 6.2 for orientation). The forces along the 1mm and 5mm distances were investigated.

Figure 6.13 shows the forces on cells along the 1mm horizontal line above the array. There are sharp force peaks on top of the magnet junction points. Cells accumulated above these points of predicted maximum force within 1 minute after initiation of 10ml/min flow; Figure 6.14 is a top view photograph of the cell aggregation.

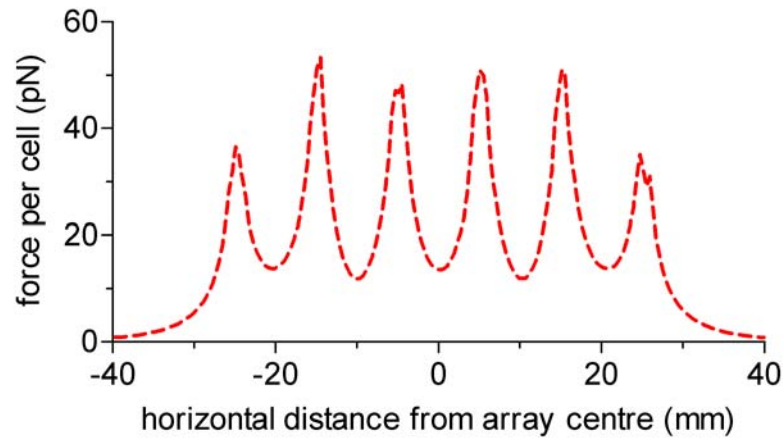


Figure 6.13 – Forces along 1mm horizontal line

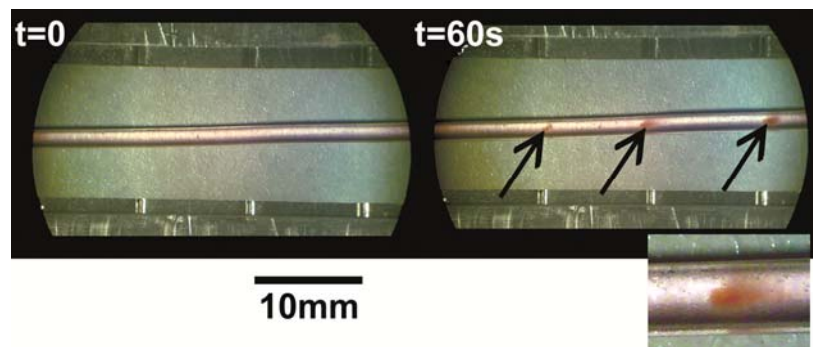


Figure 6.14 – Cell capture at 1mm with 10ml/min flow

Figure 6.13 shows the forces on cells using the saturated force expression (because $H > 398 \text{ kA/m}$ from -30mm to $+30\text{mm}$). The force peaks correspond to the magnet block junctions. Figure 6.14 is a photograph of the cell aggregation (black arrows and magnification inset) 1 minute after initiation of 10ml/min flow. Only three of the six aggregates are visible due to limited field of view. It is important to note that the cell aggregates dissociated a few seconds after removal of the array.

Targeting with the array for 15 minutes at 1mm resulted in 252-fold increase in capture (Figure 6.15). The mean cell count with targeting was $41 \times 10^3 \pm 6 \times 10^3$ cells, compared to 163 ± 41 cells without targeting. Given a circulating cell number of 1×10^6 cells, the capture efficiency with targeting was 4%. The capture efficiency without targeting was 0.02%. Notably, the Trypan Blue dye did not detect any decrease in viability, despite the higher forces. This is discussed later.

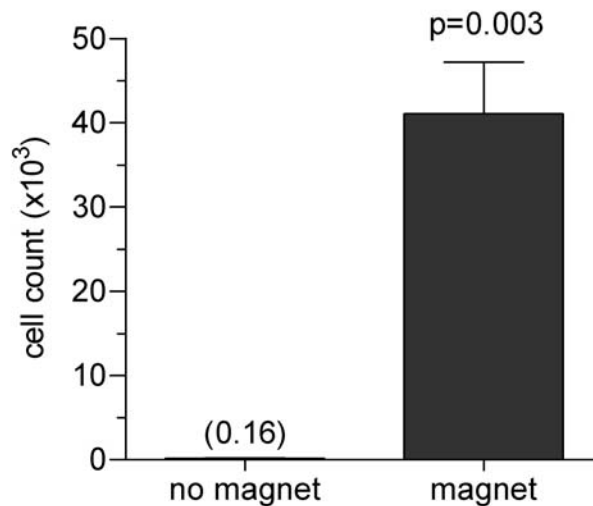


Figure 6.15 – Cell capture counts at 1mm with 10ml/min flow

*The graph shows the captured cell count (in 1000s) following 15 minutes of targeting at 1mm distance and 10ml/min flow rate. There was a 252-fold increase in targeting (mean = $41 \times 10^3 \pm 6 \times 10^3$ cells) compared to control (mean = 163 ± 41 cells). The mean difference was 41×10^3 cells with 95% CI for the difference 24×10^3 to 58×10^3 cells ($p=0.003$, $n=3$, unpaired *t*-test). Error bars are the standard error of the mean.*

Finally, the forces along the 5mm horizontal line were examined; these were 5.5-fold weaker than at 1mm and did not have prominent peaks (Figure 6.16-a). At this distance, no cell aggregates were visualised. However, there was a 6-fold increase cell count after 1 hour of flow (Figure 6.16-b). The mean cell count with targeting was 1630 ± 276 cells, compared to 281 ± 21 cells without targeting. The capture efficiency with targeting was 0.2%.

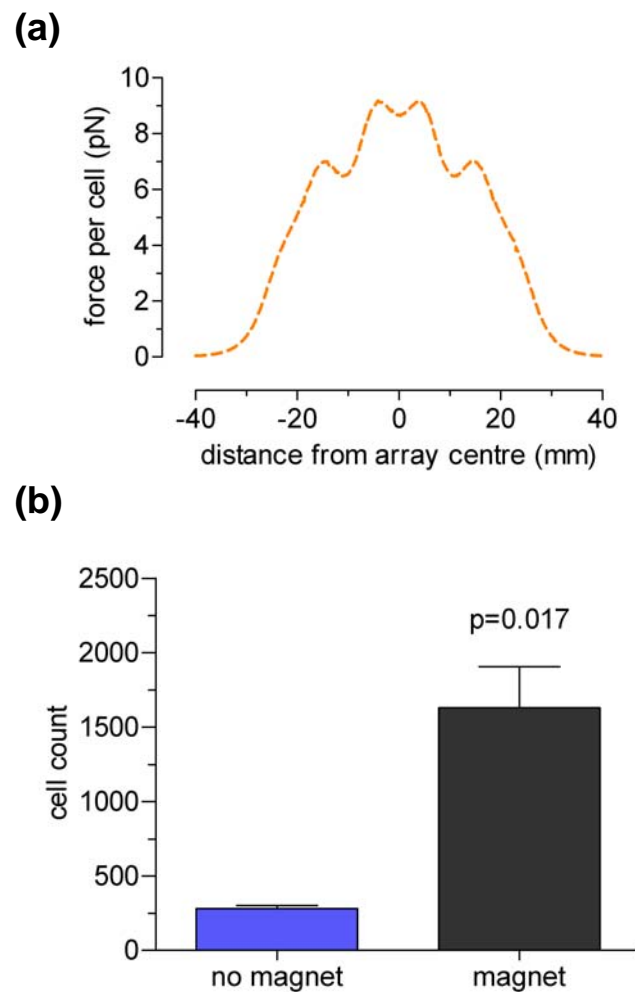


Figure 6.16 – Targeting at 5mm

a) Unsaturated forces on cells at the 5mm line. **b)** Increase in capture with targeting at 5mm distance compared to non-targeted controls after 1 hour of 10ml/min flow. The mean difference was 1350 cells, with 95% CI for the difference 468 to 2230 cells ($p=0.017$, $n=4$, unpaired t -test with Welch's correction). Error bars are the SEM.

6.4 Discussion

6.4.1 Main findings

In this study, it was found that:

- i) Endorem®-labelled cells are readily actuated in a static liquid.
- ii) The Halbach array constructed leads to higher forces at large distances, without exceeding the cell-safe force at 5mm distance.
- iii) Cells can be theoretically captured from a 10ml/min flow using the array at 1mm and 5mm distance.
- iv) Cells can be captured *in vitro* at both distances. The capture efficiency is less than predicted using the theoretical model.

6.4.2 Fluid dynamics simulations

Despite the recent interest in magnetic cell targeting applications (3.2.3), to date there has not been an attempt to develop a theoretical model. The models that exist are focused on drug targeting, as outlined in section 3.2.2 (Chen et al. 2008; Cregg, Murphy, & Mardinoglu 2008; Furlani & Furlani 2007; Grief & Richardson 2005; Min-Cheol et al. 2006; Ritter et al. 2004; Voltairas, Fotiadis, & Michalis 2002). These reports have focused on small magnetic carriers, and are not directly applicable to cells. For example, the assumption of Stokes drag, which is universally used in drug targeting models ($Re < 1$, see section 3.4.4), may be violated when considering a cell moving in arterial flow rates (e.g. maximum $Re=4$ for water). For this reason, the Khan and Richardson (1987) approximation was used in the FEM simulation (Equation 3.15).

The model presented here is simplified in comparison to the real scenario of cell targeting from flowing blood. It does not take into account the blood plasma viscosity

(which is higher than water) and collisions with blood cells, both of which increase the effective drag from the blood and will decrease capture efficiency. It also assumes that cells are captured upon contact with the vessel wall, and does not take into account the rolling of the cells on the artery and their potential to escape the magnetic field in this manner. This would also lead to overestimation of the capture efficiency.

On the other hand, the presented model simulated a continuous 10ml/min flow, which is an extreme scenario, given that the rat CCA has peak systolic flow up to 10ml/min (Garcia-Villalon et al. 1992; Miyashiro, Poppa, & Berk 1997). During the diastolic phase the hydrodynamic drag would decrease, and thus in a pulsating circulation with 10ml/min peak flow, the capture efficiency will be higher than in the modelled continuous 10ml/min flow. Moreover, the model ignores changes in hydrodynamic drag force due to perturbation of the flow by the cells and interactions between the cells and the vessel wall, which are expected to increase the capture efficiency by creating a vertical lift toward the wall (Forbes et al. 2003). The model also ignores magnetic interactions between cells, which as seen in Figure 6.1 are quite marked, and are also expected to increase the capture efficiency (Forbes et al. 2003). This is because the hydrodynamic drag force scales with surface area and the magnetic force scales with volume; cell aggregation changes the ratio of these two forces in favour of magnetic targeting.

6.4.3 *In vitro* flow system

In this study, an external magnet array was used to capture cells in a 1mm tube with 10ml/min flow, giving an average fluid velocity 20cm/sec and maximum fluid velocity at the tube centre 40cm/sec. Cell targeting was possible at both 1mm and 5mm distances, but was more pronounced at 1mm. The capture efficiency was less than

predicted by the theoretical model. It was 3-fold lower at 1mm (4% actual versus 11% theoretical) and 10-fold lower at 5mm (0.2% actual versus 2.3% theoretical). These differences can be attributed to one of the assumptions in the theoretical model that cannot be applied to the *in vitro* system:

The theoretical model assumes cell capture upon contact with the vessel wall. Immediate cell capture is unlikely to happen in a plastic tube *in vitro*, unless the magnetic force is large enough to withstand the fluid force. This is more likely to occur at closer distances and on top of the magnet junctions. Indeed, the cells were visualised to completely arrest on top of the magnet junctions at the closer 1mm distance (Figure 6.14). The cells that are found at increased distances from the actuator, experience smaller magnetic forces and may roll on the tube wall and escape. *In vivo*, this capture process could be amplified by adhesive ligands at the site of injury (1.4.5), which would help arrest the targeted cells on the vessel wall.

In the literature, only two studies have explicitly investigated magnetic capture of cells in flow. Previous *in vitro* flowing experiments using external magnets have only been attempted by Muthana et al (2008). Using a single magnet and a flow rate of 1.9ml/min in parallel plates to match the flow speed of post-capillary venules, the authors increased cell adherence to an endothelial monolayer by approximately 50-100 fold. These results are hard to compare to the current study, because the iron oxide concentration per cell is not presented in the paper, and there is no clear description of the strength of the disk magnet; therefore the magnetic forces on the cells cannot be calculated. The average flow velocity in a venule is 0.1-0.2cm/sec (Embury et al. 1999). This is ten times lower than the average flow velocity used in my studies; yet the capture efficiency in the studies by Muthana et al is less. Assuming the cellular iron

oxide content in my studies is less than those of Muthana, the remaining explanation is that the decreased capture efficiency is attributable to weaker magnetic forces as a result of using a single magnet with weak field strength and gradients, and possibly also due to a larger distance of their magnet to the flowing cells.

In another study, Polyak (2008) could capture up to 20% of circulating cells using an intravascular metallic mesh in a 30ml/min flow system. The captured cells in this study are reported to contain 200pg of particles made in-house; this was calculated using fluorescence of a cell sample. However, based on their presented SQUID data, it can be estimated that the cells contain approximately 25pg of particles instead. Given this disparity, and the unknown iron oxide content of their particles, it was not possible to estimate the iron oxide content of the cells for comparison. Furthermore, the magnetic forces acting on the cells are not presented, and neither is the size of the vessel for the flow system. Given the additional fundamental difference of using an intravascular device for the capture, it was not possible to compare the current study to that of Polyak et al.

A point to be made regarding the presented flow system is that at 1mm the forces far exceed the 'cell-safe' magnetic force (Figure 6.13). Cell viability post-capture was not investigated in depth as part of this study, although the cells appeared normal on visual assessment of the Trypan Blue dye during the haemocytometer counting (images not presented). It is possible that such high forces will be detrimental to the cells; in contrast these forces need only be applied for a very brief amount of time (<15mins) to achieve significant cell capture, so viability may remain unaffected. Indeed, it may be the case in the presented experiments. Additional studies using more sensitive viability tests were not performed because the 1mm distance would not be considered *in vivo*.

Finally, the presented results give some insight to a key issue regarding external targeting; invariably, cells flowing in vessels closer to the magnetic source than the target tissue will also be targeted (section 3.2.2). However, such cells should be released following removal of the magnetic source in the absence of an underlying biological mechanism to keep them engrafted, as visually observed with the cell aggregates after removal of the magnetic array.

6.5 Conclusions

In this study, it was found that:

- i) Endorem®-labelled cells are readily actuated in a static liquid.
- ii) The Halbach array constructed leads to higher forces at large distances, without exceeding the cell-safe force at 5mm distance.
- iii) Cells can be theoretically captured from a 10ml/min flow using the array at 1mm and 5mm distance.
- iv) Cells can be captured *in vitro* at both distances. The capture efficiency is less than predicted using the theoretical model.

CHAPTER 7

MAGNETIC TARGETING IN AN ANIMAL MODEL

7.1 Introduction

There is a pressing need for stem cell targeting strategies (section 1.5). Limited studies have investigated the possibility of magnetic targeting of cells to specific locations *in vivo* (3.2.3). Despite the fact that drug targeting moved quickly into the clinic for feasibility and safety studies (3.2.2) and that SPIO agents have previously been used to track cells in humans (2.3.4), magnetic cell targeting has remained a laboratory endeavour. This could be due to the use of iron oxide preparations not approved by the FDA or the use of customised internal devices, also not approved for clinical use.

The aim of this study was to combine the knowledge obtained from the studies in Chapters 4-6 and demonstrate magnetic targeting of Endorem®-labelled CD133-derived EPCs to a site of rat CCA injury using and an externally applied force obtained with the Halbach array. The targeting was assisted by a 10-minute flow stasis period, similar to the 'flow-stop' protocols used in clinical trials (1.4.6.2).

It was found that magnetic targeting can increase cell adherence to the injured arteries by 5-fold. Targeting did not increase adherence to non-injured arteries.

The study presented in this chapter is a collaboration between Dr Manfred Junemann-Ramirez and myself. Dr Ramirez developed the animal model and confocal microscopy protocols and performed the tissue microscopy. Tissue preparation and analysis of results was done jointly, however with less input on my part. I was responsible for cell culture/ labelling and the development and use of reflectance confocal imaging.

7.2 Methods

7.2.1 Cell culture and Endorem® labelling

Day 10 CD133s were cultured and labelled using 24:1 DfL as previously described.

7.2.2 Vascular injury

Male Sprague-Dawley rats (n=15, Charles River UK, 380-420g) were anaesthetised using midazolam (625µg/100g) and fentanyl (40µg/100g) supported by halothane at 0.5-2% at 2 L/min oxygen. The left CCA was exposed at the bifurcation to the external and internal carotid artery and a 2F embolectomy catheter (Edwards Lifesciences Corp, CA USA) was advanced proximally through an arteriotomy into the CCA. The catheter was inflated with 100µl of air and rotated while retracting to denude the endothelium (Santiago et al. 2007).

7.2.3 Cell administration and magnetic targeting

SPIO-labelled CD133⁺ cells were labelled with 5µM CellTracker Green CMFDA (Invitrogen-Molecular Probes). This dye is activated by intracellular esterases and only stains viable cells. 5×10^5 cells were administered in the injured CCA, which was temporarily clamped for 10 minutes with the Halbach array placed at approximately 5mm distance from the CCA on the ventral aspect of the animal. The circulation was restored and the array was removed after a further 2 minutes of magnetic attraction (n=5). Two types of controls were used: i) CCA injury was performed and labelled cells were injected without magnetic actuation (n=6) and ii) magnetic attraction of labelled cells was performed on uninjured vessels (n=2). Tissues were retrieved 24h later and fixed with 1% PFA/PBS. All experimental procedures complied with the institutional guidelines for animal experiments.

7.2.4 Confocal microscopy

Arteries were opened longitudinally, counterstained with DAPI (Vector Labs, CA) and mounted on glass slides with anti-fading media (CitiFluor, Leicester, UK). Total arterial surface confocal microscope images were acquired using a Leica TCS SP2 confocal microscope equipped with an automated movable stage, an 488nm laser and a UV 348nm laser. Reflectance scanning was used to detect intracellular SPIO (Green, Holloway, & Walker 2001). The 488nm excitation laser was used and the pinhole closed to Airy 0.75. The light collection was adjusted to 10nm above and below the excitation line, to acquire signal reflected by the iron oxide nanoparticles.

7.2.5 Quantification of cell engraftment

Image processing was performed using the Volocity® software (Improvision). A rolling ball algorithm (ImageJ, National Institutes of Health, MA USA) was used for background correction. Signal outliers were removed by application of a despeckle median filter (Rasband, W.S., ImageJ). To analyze cell engraftment, *xyz* scans were rendered into a 3D vector graphic format; this enabled quantification of the total volume of adherent CellTracker-labelled cells per artery. Cell counts were calculated based on a 10µm cell diameter and are presented per mm² of arterial surface area.

7.2.6 Statistical analyses

As previously described. Data were inspected visually and with the Shapiro-Wilk test for small samples to assess normality. Medians are quoted with the interquartile range (IQR). The Wilcoxon-Mann-Whitney exact test was used. P-values reported are two-tailed and were considered statistically significant at the 5% level ($p < 0.05$).

7.3 Results

7.3.1 Methodological setup

SPIO-labelled CD133⁺ cells were labelled with 5 μ M CellTracker Green CMFDA. Cells were administered in the injured CCA, which was temporarily clamped for 10 minutes with the Halbach array placed at approximately 5mm distance from the CCA on the ventral aspect of the animal (Figure 7.1-a). After 24 hours, the arteries were excised and stained for confocal microscopy (Figure 7.1-b).

The entire face of the luminal side of the artery was scanned using an automatic movable stage, by acquiring 72 separate images and tiling them together. A sample single tile is shown in Figure 7.1-c. For the quantification of cell engraftment, the total volume of CellTracker label was estimated for each artery. A sample screenshot from the volume quantification is shown in Figure 7.1-d.

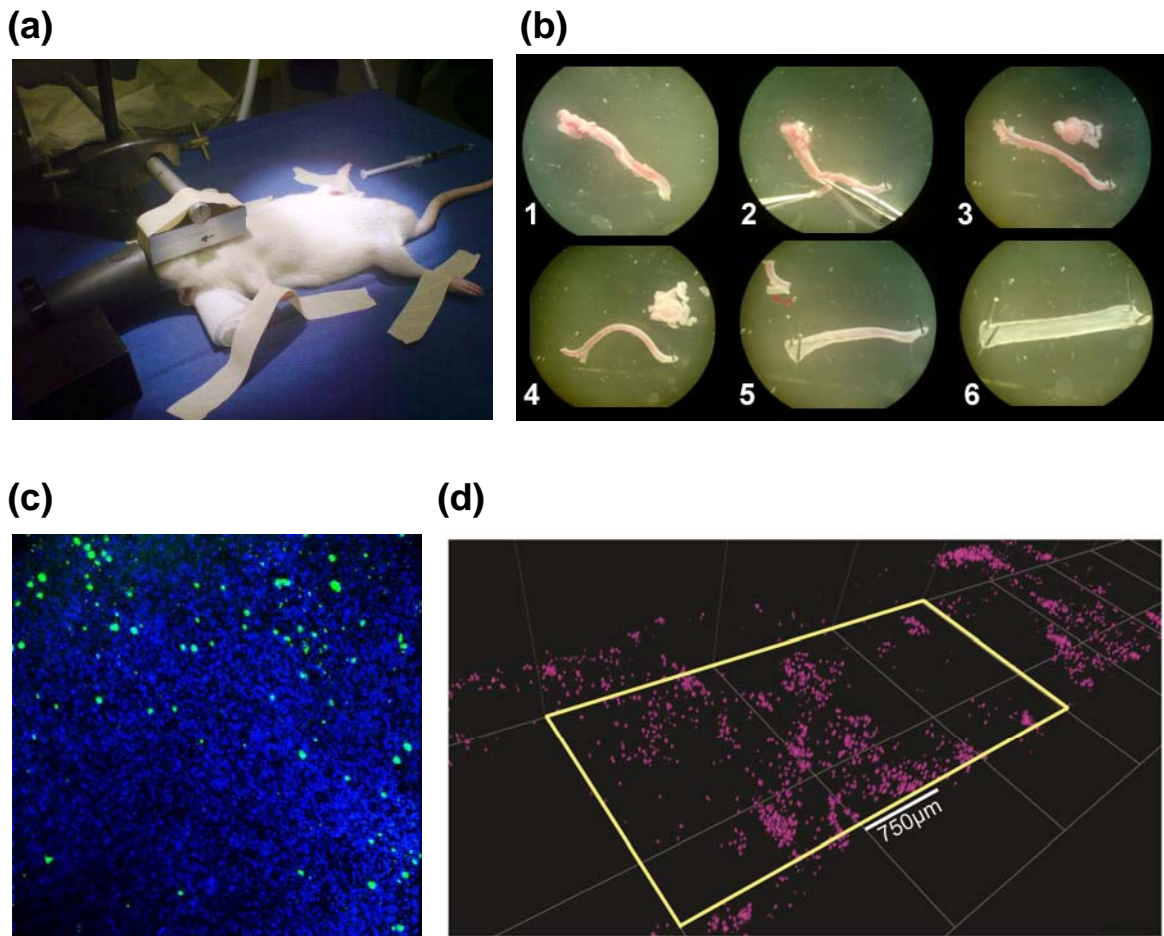


Figure 7.1 – Methodological setup

a) Halbach array on ventral aspect of animal's neck. **b)** Arterial specimen preparation, series of photographs taken through an operating microscope. The specimen is approximately 2cm long. The specimen was first cleared of all surrounding tissue (**1-4**). The specimen was then cut longitudinally (**5**) and opened with the luminal side facing upward (**6**). This side was stained with DAPI and scanned with a confocal microscope. **c)** Sample confocal image. SPIO-labelled cells are green (CellTracker dye); cells of the arterial wall are blue (DAPI). SPIO-labelled cells also stained with DAPI (not visible at this magnification). The image size is $750\mu\text{m}^2$. **d)** Sample 3D volume render used for quantification of cell engraftment. The selected volumes are shown in purple. The yellow rectangle is placed for orientation with Figure 7.2.

7.3.2 CD133 cell engraftment to the rat common carotid artery

On visual inspection of the entire injured arterial specimens, SPIO-CD133 cells had engrafted to the CCA lumen, both in the absence of magnetic targeting (injured control) and following magnetic targeting (Figure 7.2). There were notably more engrafted cells in the targeted group. The cell engraftment in both groups was non-preferential and was distributed throughout the entire vessel.

Following magnetic targeting without CCA injury (non-injured control), no SPIO-CD133 cells were visualised.

High power 3D scans confirmed that the green signal originated from nucleated cells and also confirmed the presence of intracellular clusters of iron oxide (Figure 7.3).

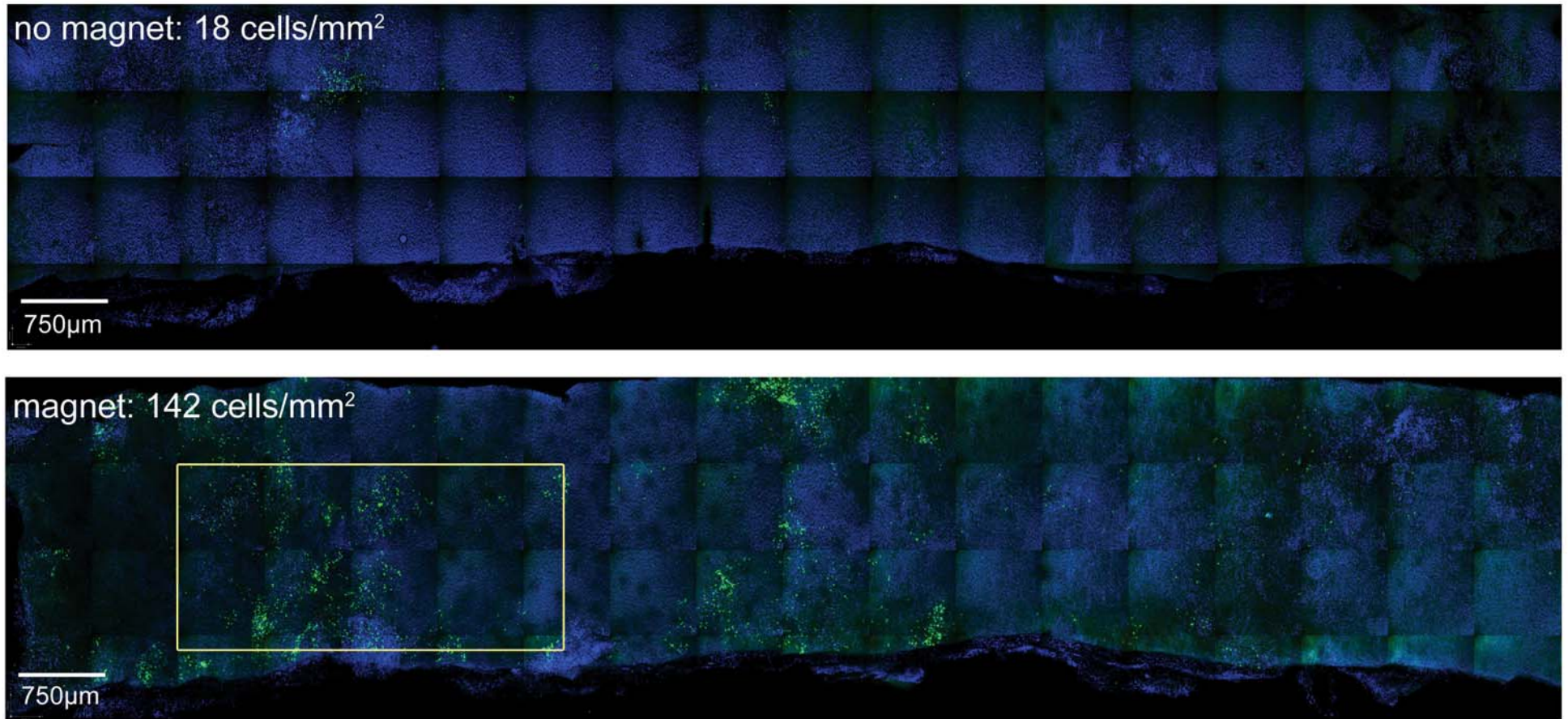


Figure 7.2 – Representative CCA confocal scans

Representative 2D tiled confocal scans of the entire luminal arterial surface 24 hours after cell delivery. The blue signal is DAPI staining of cell nuclei. The green signal is the CellTracker dye in the cytoplasm of SPIO-CD133s. The yellow square is placed for orientation with Figure 7.1-d.

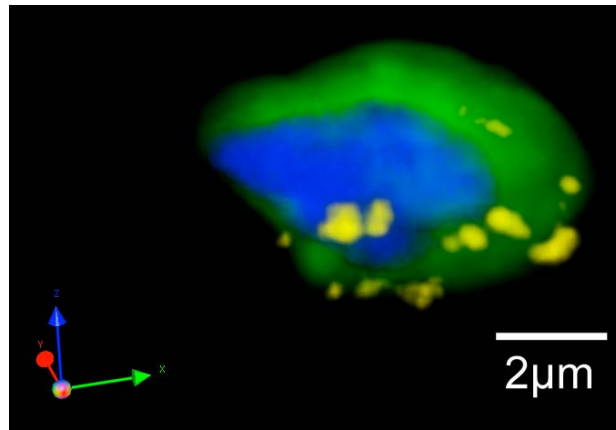


Figure 7.3 – Confocal image of a single DfL-CD133

High magnification confocal scan of an SPIO-labelled CD133 cell (green cytoplasm, CellTracker dye). The cell nucleus is visible (blue, DAPI stain). Clusters of SPIO nanoparticles (yellow) were visualised using reflectance scanning.

Following quantification of the cellular engraftment, there was a notable increase in cell retention with magnetic targeting. Application of an external magnetic force using the magnet array during and after cell delivery increased d10-DfL-CD133 cell engraftment to the injured vascular surface by a factor of 5.4 (Figure 7.4). Targeted samples had median cell count 134 cells/mm². Non-targeted samples had median cell count 25 cells/mm². In the absence of vascular injury (non-injured control) no cells engrafted to the endothelial surface when the magnetic force was applied (cell count=0).

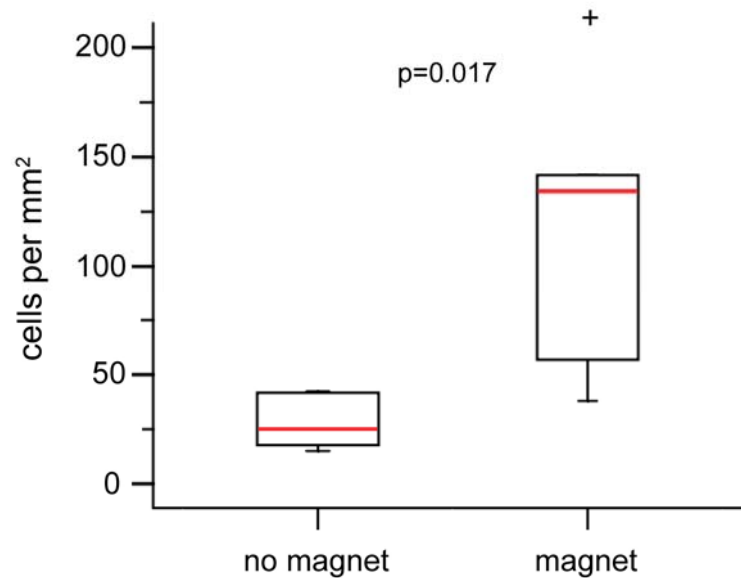


Figure 7.4 – Count of cells adherent on rat CCA lumen

Targeted samples had median cell count = 134 cells/mm² (IQR 47 to 362, n=5). Non-targeted samples had median cell count = 25 cells/mm² (IQR 17 to 42, n=6). This represented a 5.4-fold increase in cell count ($p=0.017$, Wilcoxon-Mann-Whitney exact test). Medians are highlighted in red. Boxes represent the quartiles and whiskers extend to the last value within 1.5 IQR from the quartiles. Cross represents a value at 581 cells/mm².

7.4 Discussion

To investigate the *in vivo* feasibility of magnetic targeting using external magnets, this study aimed to increase Endorem®-labelled CD133 cell engraftment to a site of rat CCA injury by placing an external magnet adjacent to the ventral aspect of the animal's neck. The increase in engraftment was 5-fold compared to control (non-targeted) arteries.

EPCs have recently been utilised for cardiac neovascularisation in clinical trials (Bartunek et al. 2005; Erbs et al. 2005; Losordo et al. 2007; Schachinger et al. 2004; Stamm et al. 2007). In the majority of these and other studies on cardiac regeneration, cells were administered via intracoronary injection with 'flow-stop' periods of several minutes to increase engraftment; yet it has been shown that despite this manoeuvre only 1-3% of the cells remain on site (Charwat et al. 2008; Hristov & Weber 2006), and there is a pressing need for targeting strategies (Roncalli et al. 2008). In contrast to the presented study, previous investigations on magnetic cell targeting have used methods not directly applicable to a clinical setting, as they have used materials not approved for human use.

A flow interruption period was implemented in the present study, similar to those employed in clinical trials. Despite this manoeuvre, the increase in cell engraftment following magnetic targeting was only 5-fold, from 25 cells/mm² to 134/mm². This is attributable to the successful cell engraftment on the non-targeted control specimens, which is a result of the flow interruption period. Future studies aiming to assess EPC engraftment in a variety of flowing conditions following peripheral intravenous injection *in vivo* are likely to observe less cellular engraftment in both in control and targeted specimens. In the presence of high flow rates at the target area, few cells should

be captured under non-targeted conditions, as suggested by the computer simulations and *in vitro* data presented in Chapter 6. This could amplify the increase in capture efficiency observed with magnetic targeting.

One advantage of the quantification method used in this study is that, although the cell count is somewhat arbitrary (as it is based on an average cell volume), it is possible to compare this count to other studies investigating EPC targeting strategies to injured vessels that present sufficient data for such a comparison. For example, Werner found that following intravenous infusion of EPCs the cell count was 100 cells / mm² (Werner et al. 2003). Gulati observed a 1.2-fold increase in adherent EPCs at 4 weeks post local delivery (Gulati et al. 2003). It has also been found that statin administration enhances endogenous EPC homing by 5-fold, from 4 EPCs/mm² to 20/mm², resulting in acceleration in re-endothelialisation (Walter et al. 2002). Oestrogen delivery enhanced EPC delivery by 2-fold (Strehlow et al. 2003). Finally, the use of an intravascular metallic mesh, has led to a relative 7-fold increase in EPC adhesion (Polyak et al. 2008). All of these numbers compare very favourably with the data presented in this study.

Furthermore, from Figure 7.1-a it is evident that the magnetic force was not applied circumferentially; in one external targeting investigation this problem was partially circumvented by axial rotation of the animal (Consigny, Silverberg, & Vitali 1999). Despite this fact, in the presented results there was no consistent preferential targeting of the cells to one side of the arterial specimens. This may be due to a combination of factors.

Firstly, the broad distribution of magnetic targeting forces due to the large size of the magnetic actuator compared to the artery (at least 100° arc of the arterial

circumference) is likely to disperse the targeted cells. Small within-vessel variations in the extent of damage, unrelated of the direction of the magnetic force, could further facilitate non-directional engraftment. The role of gravity is also important here; some cells on the far side of the artery may experience a small net downward force, despite the presence of the magnetic actuator on the opposite side (based on force calculations, not shown). This will be particularly pronounced in cells that have not taken up a lot of Endorem®. Finally, the flow during the 24-hour recirculation period may enable cells to migrate away from the targeted regions, possibly to areas of more pronounced damage. Indeed, in one recent magnetic targeting study, despite the presence of an intravascular permanently magnetised device for 24 hours, iron-labelled cells were present in the damaged areas adjacent to the device, as well as on it (Pislaru et al. 2006b).

The results from the magnetically targeted, non-injured control group (zero cell count) also complement those from Chapter 6 regarding the fate of targeted cells in the absence of an innate adherence mechanism to keep them in place after removal of the magnetic force. Therefore, the perceived problem regarding accumulation of cells in unwanted areas is not a serious issue in this context, unless it leads to total occlusion of the vessel with targeted cells and subsequent infarction.

7.5 Conclusions

In this study, it was demonstrated that magnetic targeting can increase EPC engraftment to a site of rat CCA injury in the absence of flow. Targeting does not increase cell engraftment in non-injured vessels.

THESIS SUMMARY

Atherosclerosis is a disease with considerable morbidity and mortality and can lead to occlusive events such as myocardial infarction or stroke (Chapter 1). The human body has an innate repair mechanism, the endothelial progenitor cells, which play an important role both in the progression of the disease and in the revascularisation of infarcted tissue. A rapid response by endothelial progenitors with complete re-endothelialisation is thought to be a central factor in vessel protection after injury. At the same time, clinical studies on stem cell transplantation for myocardial infarction have been faced with poor retention of the administered cells. Therefore, there exists a need to develop strategies for targeting and monitoring cell trafficking.

Superparamagnetic iron oxide nanoparticles (SPIO) offer an attractive possibility in this realm as they can be incorporated into cells affording a controllable means of ‘tagging’. These particles can be visualised non-invasively using MRI, and cell monitoring using the FDA-approved SPIO Endorem® has already entered the clinic (Chapter 2). Furthermore, SPIO particles can be manipulated by a magnetic field, which opens up the potential of remote spatial control of the living cells. To date, the focus has mainly been on drug delivery, including drug targeting in humans (Chapter 3). Cell targeting has been limited to animal studies; to achieve cell capture these studies have necessitated the use of large non-biodegradable micron-sized beads (Consigny, Silverberg, & Vitali 1999; Pislaru et al. 2006b; Pislaru et al. 2006a) or nanoparticle composites fabricated in-house (Polyak et al. 2008), and in most cases the additional introduction of permanent intravascular metallic devices not currently approved for human use (Pislaru et al. 2006b; Pislaru et al. 2006a; Polyak et al. 2008). The targeted delivery of progenitor cells using external magnetic devices and clinically approved iron-bearing agents has not yet been accomplished.

In the presented studies, CD133-derived EPCs were labelled with Endorem® (Chapter 4, Part I). The particular agent was chosen to facilitate the possibility of transition to clinical work. During initial work, I noted that the application of a large magnetic force for 24 hours had the potential to compromise cell viability, an effect that was dependent on the extent of iron loading (Chapter 4, Part II). By controlling iron uptake, viability was restored. The differential labelling method was developed, which did not affect cell growth, apoptosis, differentiation, or the ability to visualise the cells using MRI, at least *in vitro* (Chapter 5).

A rat CCA injury model was selected, as localisation of EPCs to sites of vascular damage, whether primary or post-PCI (iatrogenic), is considered a key event in the prevention of atherosclerosis progression and neointima formation. To test the feasibility of targeting the Endorem®-DfL-labelled cells to such a high flow vessel, both mathematical simulations and *in vitro* flow models were developed (Chapter 6). A magnetic device was constructed to allow increased forces at the large distances expected in the animal, between the external magnet and the CCA. The results of these studies indicated that targeting is feasible despite the high blood flow of a rat CCA.

Finally, in Chapter 7, an attempt was made to target cells within an injured rat artery. This study only went as far as to demonstrate increased adherence of cells in a flow-stop scenario, similar to those utilised in clinical studies. However, the results from Chapter 6 indicate that targeting in a flowing carotid artery should be possible.

Long-term animal studies beyond 24 hours were not conducted within the studies presented in this thesis; these will eventually be necessary to investigate the retention of the cells at the site of engraftment, their ability to survive in the longer term, proliferate

and cover the artery with a functional endothelium, and thus bolster the fact that magnetic targeting can lead to a functionally beneficial acceleration in healing.

The magnetic control of cells inside the vasculature is a fascinating and promising concept. This thesis has outlined the studies on the feasibility of external targeting of EPCs using a clinical-grade agent. However, the implications of magnetic control of cells stretch far beyond EPCs and arterial repair; this technology can encompass the entire premise of stem cell therapeutic strategies and I hope that the work presented herein will, in one way or another, one day prove useful in human applications.

BIBLIOGRAPHY

- Abdel-Latif, A., Bolli, R., Tleyjeh, I. M., Montori, V. M., Perin, E. C., Hornung, C. A., Zuba-Surma, E. K., Al-Mallah, M., & Dawn, B. 2007, "Adult bone marrow-derived cells for cardiac repair: a systematic review and meta-analysis", *Arch.Intern.Med.*, vol. 167, no. 10, pp. 989-997.
- Abdel-Latif, A., Bolli, R., Zuba-Surma, E. K., Tleyjeh, I. M., Hornung, C. A., & Dawn, B. 2008, "Granulocyte colony-stimulating factor therapy for cardiac repair after acute myocardial infarction: a systematic review and meta-analysis of randomized controlled trials", *Am.Heart J.*, vol. 156, no. 2, pp. 216-226.
- Afrin, R., Yamada, T., & Ikai, A. 2004, "Analysis of force curves obtained on the live cell membrane using chemically modified AFM probes", *Ultramicroscopy*, vol. 100, no. 3-4, pp. 187-195.
- Alison, M. R. & Islam, S. 2009, "Attributes of adult stem cells", *J.Pathol.*, vol. 217, no. 2, pp. 144-160.
- Amariglio, N., Hirshberg, A., Scheithauer, B. W., Cohen, Y., Loewenthal, R., Trakhtenbrot, L., Paz, N., Koren-Michowitz, M., Waldman, D., Leider-Trejo, L., Toren, A., Constantini, S., & Rechavi, G. 2009, "Donor-Derived Brain Tumor Following Neural Stem Cell Transplantation in an Ataxia Telangiectasia Patient", *PLoS.Med.*, vol. 6, no. 2, p. e29.
- Anderson, S. A., Shukaliak-Quandt, J., Jordan, E. K., Arbab, A. S., Martin, R., McFarland, H., & Frank, J. A. 2004, "Magnetic resonance imaging of labeled T-cells in a mouse model of multiple sclerosis", *Ann.Neurol.*, vol. 55, no. 5, pp. 654-659.
- Aoki, J., Serruys, P. W., van, B. H., Ong, A. T., McFadden, E. P., Sianos, G., van der Giessen, W. J., Regar, E., de Feyter, P. J., Davis, H. R., Rowland, S., & Kutryk, M. J. 2005, "Endothelial progenitor cell capture by stents coated with antibody against CD34: the HEALING-FIM (Healthy Endothelial Accelerated Lining Inhibits Neointimal Growth-First In Man) Registry", *J.Am.Coll.Cardiol.*, vol. 45, no. 10, pp. 1574-1579.
- Arbab, A. S., Bashaw, L. A., Miller, B. R., Jordan, E. K., Bulte, J. W., & Frank, J. A. 2003a, "Intracytoplasmic tagging of cells with ferumoxides and transfection agent for cellular magnetic resonance imaging after cell transplantation: methods and techniques", *Transplantation.*, vol. 76, no. 7, pp. 1123-1130.
- Arbab, A. S., Bashaw, L. A., Miller, B. R., Jordan, E. K., Lewis, B. K., Kalish, H., & Frank, J. A. 2003b, "Characterization of biophysical and metabolic properties of cells labeled with superparamagnetic iron oxide nanoparticles and transfection agent for cellular MR imaging", *Radiology.*, vol. 229, no. 3, pp. 838-846.
- Arbab, A. S., Frenkel, V., Pandit, S. D., Anderson, S. A., Yocum, G. T., Bur, M., Khuu, H. M., Read, E. J., & Frank, J. A. 2006, "Magnetic resonance imaging and confocal microscopy studies of magnetically labeled endothelial progenitor cells trafficking to sites of tumor angiogenesis", *Stem Cells*, vol. 24, no. 3, pp. 671-678.
- Arbab, A. S., Janic, B., Knight, R. A., Anderson, S. A., Pawelczyk, E., Rad, A. M., Read, E. J., Pandit, S. D., & Frank, J. A. 2008, "Detection of migration of locally implanted AC133+ stem cells by cellular magnetic resonance imaging with histological findings", *FASEB J.*, vol. 22, no. 9, pp. 3234-3246.

- Arbab, A. S., Jordan, E. K., Wilson, L. B., Yocum, G. T., Lewis, B. K., & Frank, J. A. 2004a, "In vivo trafficking and targeted delivery of magnetically labeled stem cells", *Hum. Gene Ther.*, vol. 15, no. 4, pp. 351-360.
- Arbab, A. S., Yocum, G. T., Kalish, H., Jordan, E. K., Anderson, S. A., Khakoo, A. Y., Read, E. J., & Frank, J. A. 2004b, "Efficient magnetic cell labeling with protamine sulfate complexed to ferumoxides for cellular MRI", *Blood.*, vol. 104, no. 4, pp. 1217-1223.
- Arbab, A. S., Yocum, G. T., Rad, A. M., Khakoo, A. Y., Fellowes, V., Read, E. J., & Frank, J. A. 2005, "Labeling of cells with ferumoxides-protamine sulfate complexes does not inhibit function or differentiation capacity of hematopoietic or mesenchymal stem cells", *NMR Biomed.*, vol. 18, no. 8, pp. 553-559.
- Asahara, T. & Kawamoto, A. 2004, "Endothelial progenitor cells for postnatal vasculogenesis", *Am.J.Physiol Cell Physiol*, vol. 287, no. 3, p. C572-C579.
- Asahara, T., Masuda, H., Takahashi, T., Kalka, C., Pastore, C., Silver, M., Kearne, M., Magner, M., & Isner, J. M. 1999, "Bone marrow origin of endothelial progenitor cells responsible for postnatal vasculogenesis in physiological and pathological neovascularization", *Circ.Res.*, vol. 85, no. 3, pp. 221-228.
- Asahara, T., Murohara, T., Sullivan, A., Silver, M., van der, Z. R., Li, T., Witzenbichler, B., Schatteman, G., & Isner, J. M. 1997, "Isolation of putative progenitor endothelial cells for angiogenesis", *Science*, vol. 275, no. 5302, pp. 964-967.
- Avilés, M. O., Ebner, A. D., & Ritter, J. A. 2008, "Implant assisted-magnetic drug targeting: Comparison of in vitro experiments with theory", *Journal of Magnetism and Magnetic Materials*, vol. 320, no. 21, pp. 2704-2713.
- Bajada, S., Mazakova, I., Richardson, J. B., & Ashammakhi, N. 2008, "Updates on stem cells and their applications in regenerative medicine", *J.Tissue Eng Regen.Med.*, vol. 2, no. 4, pp. 169-183.
- Balsam, L. B., Wagers, A. J., Christensen, J. L., Kofidis, T., Weissman, I. L., & Robbins, R. C. 2004, "Haematopoietic stem cells adopt mature haematopoietic fates in ischaemic myocardium", *Nature*, vol. 428, no. 6983, pp. 668-673.
- Bartunek, J., Vanderheyden, M., Vandekerckhove, B., Mansour, S., De, B. B., De, B. P., Van, H., I, Lootens, N., Heyndrickx, G., & Wijns, W. 2005, "Intracoronary injection of CD133-positive enriched bone marrow progenitor cells promotes cardiac recovery after recent myocardial infarction: feasibility and safety", *Circulation*, vol. 112, no. 9 Suppl, pp. I178-183.
- Benoit, M., Gabriel, D., Gerisch, G., & Gaub, H. E. 2000, "Discrete interactions in cell adhesion measured by single-molecule force spectroscopy", *Nat. Cell Biol.*, vol. 2, no. 6, pp. 313-317.
- Berridge, M. V. & Tan, A. S. 1993, "Characterization of the cellular reduction of 3-(4,5-dimethylthiazol-2-yl)-2,5-diphenyltetrazolium bromide (MTT): subcellular localization, substrate dependence, and involvement of mitochondrial electron transport in MTT reduction", *Arch.Biochem.Biophys.*, vol. 303, no. 2, pp. 474-482.

- Billotey, C., Wilhelm, C., Devaud, M., Bacri, J. C., Bittoun, J., & Gazeau, F. 2003, "Cell internalization of anionic maghemite nanoparticles: quantitative effect on magnetic resonance imaging", *Magn Reson.Med.*, vol. 49, no. 4, pp. 646-654.
- Brehm, M., Zeus, T., & Strauer, B. E. 2002, "Stem cells--clinical application and perspectives", *Herz*, vol. 27, no. 7, pp. 611-620.
- Bulte, J. W., Douglas, T., Witwer, B., Zhang, S. C., Strable, E., Lewis, B. K., Zywicke, H., Miller, B., van, G. P., Moskowitz, B. M., Duncan, I. D., & Frank, J. A. 2001, "Magnetodendrimers allow endosomal magnetic labeling and in vivo tracking of stem cells", *Nat.Biotechnol.*, vol. 19, no. 12, pp. 1141-1147.
- Bulte, J. W. & Kraitchman, D. L. 2004, "Iron oxide MR contrast agents for molecular and cellular imaging", *NMR Biomed.*, vol. 17, no. 7, pp. 484-499.
- Bulte, J. W., Laughlin, P. G., Jordan, E. K., Tran, V. A., Vymazal, J., & Frank, J. A. 1996, "Tagging of T cells with superparamagnetic iron oxide: uptake kinetics and relaxometry", *Acad.Radiol.*, vol. 3 Suppl 2:S301-3., p. S301-S303.
- Bulte, J. W., Ma, L. D., Magin, R. L., Kamman, R. L., Hulstaert, C. E., Go, K. G., The, T. H., & de, L. L. 1993, "Selective MR imaging of labeled human peripheral blood mononuclear cells by liposome mediated incorporation of dextran-magnetite particles", *Magn Reson.Med.*, vol. 29, no. 1, pp. 32-37.
- Bulte, J. W., Zhang, S., van, G. P., Herynek, V., Jordan, E. K., Duncan, I. D., & Frank, J. A. 1999, "Neurotransplantation of magnetically labeled oligodendrocyte progenitors: magnetic resonance tracking of cell migration and myelination", *Proc.Natl.Acad.Sci.U.S.A.*, vol. 96, no. 26, pp. 15256-15261.
- Cahill, K. S., Gaidosh, G., Huard, J., Silver, X., Byrne, B. J., & Walter, G. A. 2004, "Noninvasive monitoring and tracking of muscle stem cell transplants", *Transplantation.*, vol. 78, no. 11, pp. 1626-1633.
- Carr, C. A., Stuckey, D. J., Tatton, L., Tyler, D. J., Hale, S. J., Sweeney, D., Schneider, J. E., Martin-Rendon, E., Radda, G. K., Harding, S. E., Watt, S. M., & Clarke, K. 2008, "Bone marrow-derived stromal cells home to and remain in the infarcted rat heart but fail to improve function: an in vivo cine-MRI study", *Am.J.Physiol Heart Circ.Physiol.*, vol. 295, no. 2, p. H533-H542.
- Carter, A. J., Aggarwal, M., Kopia, G. A., Tio, F., Tsao, P. S., Kolata, R., Yeung, A. C., Llanos, G., Dooley, J., & Falotico, R. 2004, "Long-term effects of polymer-based, slow-release, sirolimus-eluting stents in a porcine coronary model", *Cardiovasc.Res.*, vol. 63, no. 4, pp. 617-624.
- Chalmers, J. J., Zborowski, M., Sun, L., & Moore, L. 1998, "Flow through, immunomagnetic cell separation", *Biotechnol.Prog.*, vol. 14, no. 1, pp. 141-148.
- Charwat, S., Gyongyosi, M., Lang, I., Graf, S., Beran, G., Hemetsberger, R., Nyolczas, N., Sochor, H., & Glogar, D. 2008, "Role of adult bone marrow stem cells in the repair of ischemic myocardium: current state of the art", *Exp.Hematol.*, vol. 36, no. 6, pp. 672-680.

- Chemaly, E. R., Yoneyama, R., Frangioni, J. V., & Hajjar, R. J. 2005, "Tracking stem cells in the cardiovascular system", *Trends Cardiovasc.Med.*, vol. 15, no. 8, pp. 297-302.
- Chen, H., Kaminski, M. D., Pytel, P., Macdonald, L., & Rosengart, A. J. 2008, "Capture of magnetic carriers within large arteries using external magnetic fields", *Journal of Drug Targeting*, vol. 16, no. 4, pp. 262-268.
- Chien, K. R. 2004, "Stem cells: lost in translation", *Nature*, vol. 428, no. 6983, pp. 607-608.
- Co, M., Tay, E., Lee, C. H., Poh, K. K., Low, A., Lim, J., Lim, I. H., Lim, Y. T., & Tan, H. C. 2008, "Use of endothelial progenitor cell capture stent (Genous Bio-Engineered R Stent) during primary percutaneous coronary intervention in acute myocardial infarction: intermediate- to long-term clinical follow-up", *Am.Heart J.*, vol. 155, no. 1, pp. 128-132.
- Consigny, P. M., Silverberg, D. A., & Vitali, N. J. 1999, "Use of endothelial cells containing superparamagnetic microspheres to improve endothelial cell delivery to arterial surfaces after angioplasty", *J.Vasc.Interv.Radiol.*, vol. 10, no. 2 Pt 1, pp. 155-163.
- Cregg, P. J., Murphy, K., & Mardinoglu, A. 2008, "Calculation of nanoparticle capture efficiency in magnetic drug targeting", *Journal of Magnetism and Magnetic Materials*, vol. 320, no. 23, pp. 3272-3275.
- Cribbie, R. A., Gruman, J. A., & Arpin-Cribbie, C. A. 2004, "Recommendations for applying tests of equivalence", *J.Clin.Psychol.*, vol. 60, no. 1, pp. 1-10.
- Cui, L., Ramsfjell, V., Borge, O. J., Veiby, O. P., Lok, S., & Jacobsen, S. E. 1997, "Thrombopoietin promotes adhesion of primitive human hemopoietic cells to fibronectin and vascular cell adhesion molecule-1: role of activation of very late antigen (VLA)-4 and VLA-5", *J.Immunol.*, vol. 159, no. 4, pp. 1961-1969.
- de Vries, I., Lesterhuis, W. J., Barentsz, J. O., Verdijk, P., van Krieken, J. H., Boerman, O. C., Oyen, W. J., Bonenkamp, J. J., Boezeman, J. B., Adema, G. J., Bulte, J. W., Scheenen, T. W., Punt, C. J., Heerschap, A., & Figdor, C. G. 2005, "Magnetic resonance tracking of dendritic cells in melanoma patients for monitoring of cellular therapy", *Nat.Biotechnol.*, vol. 23, no. 11, pp. 1407-1413.
- Dimmeler, S., Aicher, A., Vasa, M., Mildner-Rihm, C., Adler, K., Tiemann, M., Rutten, H., Fichtlscherer, S., Martin, H., & Zeiher, A. M. 2001, "HMG-CoA reductase inhibitors (statins) increase endothelial progenitor cells via the PI 3-kinase/Akt pathway", *J.Clin.Invest*, vol. 108, no. 3, pp. 391-397.
- Dimmeler, S., Zeiher, A. M., & Schneider, M. D. 2005, "Unchain my heart: the scientific foundations of cardiac repair", *J.Clin.Invest*, vol. 115, no. 3, pp. 572-583.
- Dobson, J. 2006, "Magnetic nanoparticles for drug delivery", *Drug Development Research*, vol. 67, no. 1, pp. 55-60.
- Duncombe, A. 1997, "ABC of clinical haematology. Bone marrow and stem cell transplantation", *BMJ*, vol. 314, no. 7088, pp. 1179-1182.

- Embury, S. H., Mohandas, N., Paszty, C., Cooper, P., & Cheung, A. T. 1999, "In vivo blood flow abnormalities in the transgenic knockout sickle cell mouse", *J.Clin.Invest*, vol. 103, no. 6, pp. 915-920.
- Erbs, S., Linke, A., Adams, V., Lenk, K., Thiele, H., Diederich, K. W., Emmrich, F., Kluge, R., Kendziorra, K., Sabri, O., Schuler, G., & Hambrecht, R. 2005, "Transplantation of blood-derived progenitor cells after recanalization of chronic coronary artery occlusion: first randomized and placebo-controlled study", *Circ.Res.*, vol. 97, no. 8, pp. 756-762.
- Fahlvik, A. K., Klaveness, J., & Stark, D. D. 1993, "Iron oxides as MR imaging contrast agents", *J.Magn Reson.Imaging*, vol. 3, no. 1, pp. 187-194.
- Fay, J. A. 1994, *Introduction to fluid mechanics*, 2nd edn, MIT Press.
- Fischman, D. L., Leon, M. B., Baim, D. S., Schatz, R. A., Savage, M. P., Penn, I., Detre, K., Veltri, L., Ricci, D., Nobuyoshi, M., & . 1994, "A randomized comparison of coronary-stent placement and balloon angioplasty in the treatment of coronary artery disease. Stent Restenosis Study Investigators", *N.Engl.J.Med.*, vol. 331, no. 8, pp. 496-501.
- Fons, P., Herault, J. P., Delesque, N., Tuyaret, J., Bono, F., & Herbert, J. M. 2004, "VEGF-R2 and neuropilin-1 are involved in VEGF-A-induced differentiation of human bone marrow progenitor cells", *J.Cell Physiol*, vol. 200, no. 3, pp. 351-359.
- Forbes, Z. G., Yellen, B. B., Barbee, K. A., & Friedman, G. 2003, "An approach to targeted drug delivery based on uniform magnetic fields", *Magnetics, IEEE Transactions on*, vol. 39, no. 5, pp. 3372-3377.
- Forbes, Z. G., Yellen, B. B., Halverson, D. S., Fridman, G., Barbee, K. A., & Friedman, G. 2008, "Validation of high gradient magnetic field based drug delivery to magnetizable implants under flow", *IEEE Trans.Biomed.Eng*, vol. 55, no. 2, pp. 643-649.
- Fox, K. A. 2009, "COURAGE to change practice? Revascularisation in patients with stable coronary artery disease", *Heart*.
- Frank, J. A., Miller, B. R., Arbab, A. S., Zywicke, H. A., Jordan, E. K., Lewis, B. K., Bryant, L. H., Jr., & Bulte, J. W. 2003, "Clinically applicable labeling of mammalian and stem cells by combining superparamagnetic iron oxides and transfection agents", *Radiology*, vol. 228, no. 2, pp. 480-487.
- Frank, J. A., Zywicke, H., Jordan, E. K., Mitchell, J., Lewis, B. K., Miller, B., Bryant, L. H., Jr., & Bulte, J. W. 2002, "Magnetic intracellular labeling of mammalian cells by combining (FDA-approved) superparamagnetic iron oxide MR contrast agents and commonly used transfection agents", *Acad.Radiol.*, vol. 9 Suppl 2:S484-7., p. S484-S487.
- Frasca, G., Gazeau, F., & Wilhelm, C. 2009, "Formation of a three-dimensional multicellular assembly using magnetic patterning", *Langmuir*, vol. 25, no. 4, pp. 2348-2354.

- Freedman, S. B. 2002, "Clinical trials of gene therapy for atherosclerotic cardiovascular disease", *Curr.Opin.Lipidol.*, vol. 13, no. 6, pp. 653-661.
- Friedrich, E. B., Walenta, K., Scharlau, J., Nickenig, G., & Werner, N. 2006, "CD34-/CD133+/VEGFR-2+ endothelial progenitor cell subpopulation with potent vasoregenerative capacities", *Circ.Res.*, vol. 98, no. 3, p. e20-e25.
- Fujiyama, S., Amano, K., Uehira, K., Yoshida, M., Nishiwaki, Y., Nozawa, Y., Jin, D., Takai, S., Miyazaki, M., Egashira, K., Imada, T., Iwasaka, T., & Matsubara, H. 2003, "Bone marrow monocyte lineage cells adhere on injured endothelium in a monocyte chemoattractant protein-1-dependent manner and accelerate reendothelialization as endothelial progenitor cells", *Circ.Res.*, vol. 93, no. 10, pp. 980-989.
- Furlani, E. J. & Furlani, E. P. 2007, "A model for predicting magnetic targeting of multifunctional particles in the microvasculature", *Journal of Magnetism and Magnetic Materials*, vol. 312, no. 1, pp. 187-193.
- Garcia-Villalon, A. L., Roda, J. M., Alvarez, F., Gomez, B., & Dieguez, G. 1992, "Carotid blood flow in anesthetized rats: effects of carotid ligation and anastomosis", *Microsurgery*, vol. 13, no. 5, pp. 258-261.
- Gehling, U. M., Ergun, S., Schumacher, U., Wagener, C., Pantel, K., Otte, M., Schuch, G., Schafhausen, P., Mende, T., Kilic, N., Kluge, K., Schafer, B., Hossfeld, D. K., & Fiedler, W. 2000, "In vitro differentiation of endothelial cells from AC133-positive progenitor cells", *Blood.*, vol. 95, no. 10, pp. 3106-3112.
- Gill, M., Dias, S., Hattori, K., Rivera, M. L., Hicklin, D., Witte, L., Girardi, L., Yurt, R., Himel, H., & Rafii, S. 2001, "Vascular trauma induces rapid but transient mobilization of VEGFR2(+)AC133(+) endothelial precursor cells", *Circ.Res.*, vol. 88, no. 2, pp. 167-174.
- Gimbrone, M. A., Topper, J. N., Nagel, T., Anderson, K. R., & Garcia-Cardena, G. 2000, "Endothelial dysfunction, hemodynamic forces, and atherogenesis", *Ann.N.Y.Acad.Sci.*, vol. 902, pp. 230-239.
- Goldman, S. A. & Windrem, M. S. 2006, "Cell replacement therapy in neurological disease", *Philos.Trans.R.Soc.Lond B Biol.Sci.*, vol. 361, no. 1473, pp. 1463-1475.
- Goldschmidt-Clermont, P. J., Creager, M. A., Losordo, D. W., Lam, G. K., Wassef, M., & Dzau, V. J. 2005, "Atherosclerosis 2005: recent discoveries and novel hypotheses", *Circulation*, vol. 112, no. 21, pp. 3348-3353.
- Gotoh, A., Ritchie, A., Takahira, H., & Broxmeyer, H. E. 1997, "Thrombopoietin and erythropoietin activate inside-out signaling of integrin and enhance adhesion to immobilized fibronectin in human growth-factor-dependent hematopoietic cells", *Ann.Hematol.*, vol. 75, no. 5-6, pp. 207-213.
- Green, C. R., Holloway, H., & Walker, M. M. 2001, "Detection of submicroscopic magnetite particles using reflectance mode confocal laser scanning microscopy", *Cell Biol.Int.*, vol. 25, no. 10, pp. 985-990.

- Grief, A. D. & Richardson, G. 2005, "Mathematical modelling of magnetically targeted drug delivery", *Journal of Magnetism and Magnetic Materials*, vol. 293, no. 1, pp. 455-463.
- Griese, D. P., Ehsan, A., Melo, L. G., Kong, D., Zhang, L., Mann, M. J., Pratt, R. E., Mulligan, R. C., & Dzau, V. J. 2003, "Isolation and transplantation of autologous circulating endothelial cells into denuded vessels and prosthetic grafts: implications for cell-based vascular therapy", *Circulation*, vol. 108, no. 21, pp. 2710-2715.
- Gulati, R., Jevremovic, D., Peterson, T. E., Witt, T. A., Kleppe, L. S., Mueske, C. S., Lerman, A., Vile, R. G., & Simari, R. D. 2003, "Autologous culture-modified mononuclear cells confer vascular protection after arterial injury", *Circulation*, vol. 108, no. 12, pp. 1520-1526.
- Gulati, R., Lerman, A., & Simari, R. D. 2005, "Therapeutic uses of autologous endothelial cells for vascular disease", *Clin.Sci.(Lond)*, vol. 109, no. 1, pp. 27-37.
- Gulati, R. & Simari, R. D. 2004, "Autologous cell-based therapies for vascular disease", *Trends Cardiovasc.Med.*, vol. 14, no. 7, pp. 262-267.
- Gunn, J. & Taggart, D. P. 2003, "Revascularisation for acute coronary syndromes: PCI or CABG?", *Heart*, vol. 89, no. 9, pp. 967-970.
- Gupta, V., Aravamuthan, B. R., Baskerville, S., Smith, S. K., Gupta, V., Lauer, M. A., & Fischell, T. A. 2004, "Reduction of subacute stent thrombosis (SAT) using heparin-coated stents in a large-scale, real world registry", *J.Invasive.Cardiol.*, vol. 16, no. 6, pp. 304-310.
- Häfeli, U. O., Gilmour, K., Zhou, A., Lee, S., & Hayden, M. E. 2007, "Modeling of magnetic bandages for drug targeting: Button vs. Halbach arrays", *Journal of Magnetism and Magnetic Materials*, vol. 311, no. 1, pp. 323-329.
- Häfeli, U. O., Gilmour, K., Zhou, A., Lee, S., & Hayden, M. E. 2007, "Modeling of magnetic bandages for drug targeting: Button vs. Halbach arrays", *Journal of Magnetism and Magnetic Materials*, vol. 311, no. 1, pp. 323-329.
- Hamasaki, T., Tanaka, N., Ishida, O., Yanada, S., Kamei, N., Fujiwara, Y., Nishida, K., Nakanishi, K., Sharman, P., Kawamata, S., & Ochi, M. 2005, "Characterization of labeled neural progenitor cells for magnetic targeting", *Neuroreport*, vol. 16, no. 15, pp. 1641-1645.
- Haudenschild, C. C. & Schwartz, S. M. 1979, "Endothelial regeneration. II. Restitution of endothelial continuity", *Lab Invest*, vol. 41, no. 5, pp. 407-418.
- Hautot, D., Pankhurst, Q. A., & Dobson, J. 2005, "Superconducting quantum interference device measurements of dilute magnetic materials in biological samples", *Rev.Sci.Instrum.*, vol. 76, no. 4, p. 045101.
- Hawrylak, N., Ghosh, P., Broadus, J., Schlueter, C., Greenough, W. T., & Lauterbur, P. C. 1993, "Nuclear Magnetic Resonance (NMR) Imaging of Iron Oxide-Labeled Neural Transplants", *Experimental Neurology*, vol. 121, no. 2, pp. 181-192.

- Hayden, M. E. & Hafeli, U. O. 2006, "'Magnetic bandages' for targeted delivery of therapeutic agents", *Journal of Physics: Condensed Matter*, vol. 18, no. 38, p. S2877-S2891.
- Hill, J. M., Zalos, G., Halcox, J. P., Schenke, W. H., Waclawiw, M. A., Quyyumi, A. A., & Finkel, T. 2003, "Circulating endothelial progenitor cells, vascular function, and cardiovascular risk", *N.Engl.J.Med.*, vol. 348, no. 7, pp. 593-600.
- Hinds, K. A., Hill, J. M., Shapiro, E. M., Laukkanen, M. O., Silva, A. C., Combs, C. A., Varney, T. R., Balaban, R. S., Koretsky, A. P., & Dunbar, C. E. 2003, "Highly efficient endosomal labeling of progenitor and stem cells with large magnetic particles allows magnetic resonance imaging of single cells", *Blood.*, vol. 102, no. 3, pp. 867-872.
- Ho, V. H., Muller, K. H., Darton, N. J., Darling, D. C., Farzaneh, F., & Slater, N. K. 2009, "Simple magnetic cell patterning using streptavidin paramagnetic particles", *Exp.Biol.Med.(Maywood.)*, vol. 234, no. 3, pp. 332-341.
- Hoffmann, R. & Mintz, G. S. 2000, "Coronary in-stent restenosis - predictors, treatment and prevention", *Eur.Heart J.*, vol. 21, no. 21, pp. 1739-1749.
- Hofmann, A., Wenzel, D., Becher, U. M., Freitag, D. F., Klein, A. M., Eberbeck, D., Schulte, M., Zimmermann, K., Bergemann, C., Gleich, B., Roell, W., Weyh, T., Trahms, L., Nickenig, G., Fleischmann, B. K., & Pfeifer, A. 2009, "Combined targeting of lentiviral vectors and positioning of transduced cells by magnetic nanoparticles", *Proc.Natl.Acad.Sci.U.S.A.*, vol. 106, no. 1, pp. 44-49.
- Hofmann, M., Wollert, K. C., Meyer, G. P., Menke, A., Arseniev, L., Hertenstein, B., Ganser, A., Knapp, W. H., & Drexler, H. 2005, "Monitoring of bone marrow cell homing into the infarcted human myocardium", *Circulation*, vol. 111, no. 17, pp. 2198-2202.
- Hou, D., Youssef, E. A., Brinton, T. J., Zhang, P., Rogers, P., Price, E. T., Yeung, A. C., Johnstone, B. H., Yock, P. G., & March, K. L. 2005, "Radiolabeled cell distribution after intramyocardial, intracoronary, and interstitial retrograde coronary venous delivery: implications for current clinical trials", *Circulation*, vol. 112, no. 9 Suppl, p. I150-I156.
- Hristov, M. & Weber, C. 2006, "The therapeutic potential of progenitor cells in ischemic heart disease--Past, present and future", *Basic Res.Cardiol.*, vol. 101, no. 1, pp. 1-7.
- Hristov, M. & Weber, C. 2008, "Endothelial progenitor cells in vascular repair and remodeling", *Pharmacol.Res.*, vol. 58, no. 2, pp. 148-151.
- Hristov, M. & Weber, C. 2004, "Endothelial progenitor cells: characterization, pathophysiology, and possible clinical relevance", *J.Cell Mol.Med.*, vol. 8, no. 4, pp. 498-508.
- Hristov, M., Zerneck, A., Bidzhekov, K., Liehn, E. A., Shagdarsuren, E., Ludwig, A., & Weber, C. 2007a, "Importance of CXC chemokine receptor 2 in the homing of human peripheral blood endothelial progenitor cells to sites of arterial injury", *Circ.Res.*, vol. 100, no. 4, pp. 590-597.

- Hristov, M., Zerneck, A., Liehn, E. A., & Weber, C. 2007b, "Regulation of endothelial progenitor cell homing after arterial injury", *Thromb.Haemost.*, vol. 98, no. 2, pp. 274-277.
- Iacob, G., Rotariu, O., Strachan, N. J., & Hafeli, U. O. 2004, "Magnetizable needles and wires--modeling an efficient way to target magnetic microspheres in vivo", *Biorheology*, vol. 41, no. 5, pp. 599-612.
- Inaba, S., Egashira, K., & Komori, K. 2002, "Peripheral-blood or bone-marrow mononuclear cells for therapeutic angiogenesis?", *Lancet*, vol. 360, no. 9350, p. 2083.
- Ince, H., Valgimigli, M., Petzsch, M., de Lezo, J. S., Kuethe, F., Dunkelmann, S., Biondi-Zoccai, G., & Nienaber, C. A. 2008, "Cardiovascular events and re-stenosis following administration of G-CSF in acute myocardial infarction: systematic review and meta-analysis", *Heart*, vol. 94, no. 5, pp. 610-616.
- Ino, K., Ito, A., & Honda, H. 2007, "Cell patterning using magnetite nanoparticles and magnetic force", *Biotechnology and Bioengineering*, vol. 97, no. 5, p. 1309.
- Iwaguro, H., Yamaguchi, J., Kalka, C., Murasawa, S., Masuda, H., Hayashi, S., Silver, M., Li, T., Isner, J. M., & Asahara, T. 2002, "Endothelial progenitor cell vascular endothelial growth factor gene transfer for vascular regeneration", *Circulation*, vol. 105, no. 6, pp. 732-738.
- Jaffe, R. & Strauss, B. H. 2007, "Late and very late thrombosis of drug-eluting stents: evolving concepts and perspectives", *J.Am.Coll.Cardiol.*, vol. 50, no. 2, pp. 119-127.
- Jiang, G., Giannone, G., Critchley, D. R., Fukumoto, E., & Sheetz, M. P. 2003, "Two-piconewton slip bond between fibronectin and the cytoskeleton depends on talin", *Nature*, vol. 424, no. 6946, pp. 334-337.
- Jiles, D. 1998, "Magnetization and magnetic moment," in *Magnetism and magnetic materials*, 2nd edn, Chapman & Hall, London.
- Jin, H., Aiyer, A., Su, J., Borgstrom, P., Stupack, D., Friedlander, M., & Varner, J. 2006, "A homing mechanism for bone marrow-derived progenitor cell recruitment to the neovasculature", *J.Clin.Invest*, vol. 116, no. 3, pp. 652-662.
- Josephson, L., Tung, C. H., Moore, A., & Weissleder, R. 1999, "High-efficiency intracellular magnetic labeling with novel superparamagnetic-Tat peptide conjugates", *Bioconjug.Chem.*, vol. 10, no. 2, pp. 186-191.
- Kalish, H., Arbab, A. S., Miller, B. R., Lewis, B. K., Zywicke, H. A., Bulte, J. W., Bryant, L. H., Jr., & Frank, J. A. 2003, "Combination of transfection agents and magnetic resonance contrast agents for cellular imaging: relationship between relaxivities, electrostatic forces, and chemical composition", *Magn Reson.Med.*, vol. 50, no. 2, pp. 275-282.
- Kalka, C., Masuda, H., Takahashi, T., Kalka-Moll, W. M., Silver, M., Kearney, M., Li, T., Isner, J. M., & Asahara, T. 2000, "Transplantation of ex vivo expanded endothelial progenitor cells for therapeutic neovascularization", *Proc.Natl.Acad.Sci.U.S.A.*, vol. 97, no. 7, pp. 3422-3427.

- Kawamoto, A., Gwon, H. C., Iwaguro, H., Yamaguchi, J. I., Uchida, S., Masuda, H., Silver, M., Ma, H., Kearney, M., Isner, J. M., & Asahara, T. 2001, "Therapeutic potential of ex vivo expanded endothelial progenitor cells for myocardial ischemia", *Circulation*, vol. 103, no. 5, pp. 634-637.
- Kawamoto, A. & Losordo, D. W. 2008, "Endothelial progenitor cells for cardiovascular regeneration", *Trends Cardiovasc.Med.*, vol. 18, no. 1, pp. 33-37.
- Khakoo, A. Y. & Finkel, T. 2005, "Endothelial progenitor cells", *Annu.Rev.Med.*, vol. 56, pp. 79-101.
- Khan, A. R. & Richardson, J. F. 1987, "The resistance to motion of a solid sphere in a fluid", *Chemical Engineering Communications*, vol. 62, no. 1, pp. 135-150.
- Kipshidze, N., Dangas, G., Tsapenko, M., Moses, J., Leon, M. B., Kutryk, M., & Serruys, P. 2004, "Role of the endothelium in modulating neointimal formation: vasculoprotective approaches to attenuate restenosis after percutaneous coronary interventions", *J.Am.Coll.Cardiol.*, vol. 44, no. 4, pp. 733-739.
- Klimanskaya, I., Rosenthal, N., & Lanza, R. 2008, "Derive and conquer: sourcing and differentiating stem cells for therapeutic applications", *Nat.Rev.Drug Discov.*, vol. 7, no. 2, pp. 131-142.
- Kocher, A. A., Schuster, M. D., Szabolcs, M. J., Takuma, S., Burkhoff, D., Wang, J., Homma, S., Edwards, N. M., & Itescu, S. 2001, "Neovascularization of ischemic myocardium by human bone-marrow-derived angioblasts prevents cardiomyocyte apoptosis, reduces remodeling and improves cardiac function", *Nat.Med.*, vol. 7, no. 4, pp. 430-436.
- Kong, D., Melo, L. G., Mangi, A. A., Zhang, L., Lopez-Illasaca, M., Perrella, M. A., Liew, C. C., Pratt, R. E., & Dzau, V. J. 2004, "Enhanced inhibition of neointimal hyperplasia by genetically engineered endothelial progenitor cells", *Circulation*, vol. 109, no. 14, pp. 1769-1775.
- Korbling, M., Reuben, J. M., Gao, H., Lee, B. N., Harris, D. M., Cogdell, D., Giralt, S. A., Khouri, I. F., Saliba, R. M., Champlin, R. E., Zhang, W., & Estrov, Z. 2006, "Recombinant human granulocyte-colony-stimulating factor-mobilized and apheresis-collected endothelial progenitor cells: a novel blood cell component for therapeutic vasculogenesis", *Transfusion*, vol. 46, no. 10, pp. 1795-1802.
- Kostura, L., Kraitchman, D. L., Mackay, A. M., Pittenger, M. F., & Bulte, J. W. 2004, "Feridex labeling of mesenchymal stem cells inhibits chondrogenesis but not adipogenesis or osteogenesis", *NMR Biomed.*, vol. 17, no. 7, pp. 513-517.
- Kraitchman, D. L., Heldman, A. W., Atalar, E., Amado, L. C., Martin, B. J., Pittenger, M. F., Hare, J. M., & Bulte, J. W. 2003, "In vivo magnetic resonance imaging of mesenchymal stem cells in myocardial infarction", *Circulation.*, vol. 107, no. 18, pp. 2290-2293.
- Kubo, T., Sugita, T., Shimose, S., Nitta, Y., Ikuta, Y., & Murakami, T. 2000, "Targeted delivery of anticancer drugs with intravenously administered magnetic liposomes in osteosarcoma-bearing hamsters", *Int J.Oncol.*, vol. 17, no. 2, pp. 309-315.

- Laflamme, M. A. & Murry, C. E. 2005, "Regenerating the heart", *Nat.Biotechnol.*, vol. 23, no. 7, pp. 845-856.
- Lam, A. C., Li, K., Zhang, X. B., Li, C. K., Fok, T. F., Chang, A. M., James, A. E., Tsang, K. S., & Yuen, P. M. 2001, "Preclinical ex vivo expansion of cord blood hematopoietic stem and progenitor cells: duration of culture; the media, serum supplements, and growth factors used; and engraftment in NOD/SCID mice", *Transfusion.*, vol. 41, no. 12, pp. 1567-1576.
- Lee, J. M., Kim, C. S., Youk, J. H., & Lee, M. S. 2003, "Characterization of focal liver lesions with superparamagnetic iron oxide-enhanced MR imaging: value of distributional phase T1-weighted imaging", *Korean J.Radiol.*, vol. 4, no. 1, pp. 9-18.
- Lemesle, G., Delhaye, C., Bonello, L., de, L. A., Waksman, R., & Pichard, A. 2008, "Stent thrombosis in 2008: definition, predictors, prognosis and treatment", *Arch.Cardiovasc.Dis.*, vol. 101, no. 11-12, pp. 769-777.
- Lerou, P. H. & Daley, G. Q. 2005, "Therapeutic potential of embryonic stem cells", *Blood Rev.*, vol. 19, no. 6, pp. 321-331.
- Lewin, M., Carlesso, N., Tung, C. H., Tang, X. W., Cory, D., Scadden, D. T., & Weissleder, R. 2000, "Tat peptide-derivatized magnetic nanoparticles allow in vivo tracking and recovery of progenitor cells", *Nat.Biotechnol.*, vol. 18, no. 4, pp. 410-414.
- Lin, Y., Weisdorf, D. J., Solovey, A., & Hebbel, R. P. 2000, "Origins of circulating endothelial cells and endothelial outgrowth from blood", *J.Clin.Invest*, vol. 105, no. 1, pp. 71-77.
- Lindvall, O. & Kokaia, Z. 2006, "Stem cells for the treatment of neurological disorders", *Nature*, vol. 441, no. 7097, pp. 1094-1096.
- Losordo, D. W., Schatz, R. A., White, C. J., Udelson, J. E., Veereshwarayya, V., Durgin, M., Poh, K. K., Weinstein, R., Kearney, M., Chaudhry, M., Burg, A., Eaton, L., Heyd, L., Thorne, T., Shturman, L., Hoffmeister, P., Story, K., Zak, V., Dowling, D., Traverse, J. H., Olson, R. E., Flanagan, J., Sodano, D., Murayama, T., Kawamoto, A., Kusano, K. F., Wollins, J., Welt, F., Shah, P., Soukas, P., Asahara, T., & Henry, T. D. 2007, "Intramyocardial transplantation of autologous CD34+ stem cells for intractable angina: a phase I/IIa double-blind, randomized controlled trial", *Circulation*, vol. 115, no. 25, pp. 3165-3172.
- Lowe, H. C., Oesterle, S. N., & Khachigian, L. M. 2002, "Coronary in-stent restenosis: current status and future strategies", *J.Am.Coll.Cardiol.*, vol. 39, no. 2, pp. 183-193.
- Lübbe, A. S., Alexiou, C., & Bergemann, C. 2001, "Clinical Applications of Magnetic Drug Targeting", *Journal of Surgical Research*, vol. 95, no. 2, pp. 200-206.
- Lucerna, M., Zerneck, A., de, N. R., de Jager, S. C., Bot, I., van der, L. C., Kholova, I., Liehn, E. A., van Berkel, T. J., Yla-Herttuala, S., Weber, C., & Biessen, E. A. 2007, "Vascular endothelial growth factor-A induces plaque expansion in ApoE knock-out mice by promoting de novo leukocyte recruitment", *Blood*, vol. 109, no. 1, pp. 122-129.

- Luciani, A., Wilhelm, C., Bruneval, P., Cunin, P., Autret, G., Rahmouni, A., Clement, O., & Gazeau, F. 2009, "Magnetic targeting of iron-oxide-labeled fluorescent hepatoma cells to the liver", *Eur.Radiol.*, vol. 19, no. 5, pp. 1087-1096.
- Lusis, A. J. 2000, "Atherosclerosis", *Nature*, vol. 407, no. 6801, pp. 233-241.
- Maiellaro, K. & Taylor, W. R. 2007, "The role of the adventitia in vascular inflammation", *Cardiovasc.Res.*, vol. 75, no. 4, pp. 640-648.
- Mallinson, J. 1973, "One-sided fluxes - A magnetic curiosity?", *IEEE Transactions on Magnetism*, vol. 9, no. 4, pp. 678-682.
- Marrink, S. J., Berger, O., Tieleman, P., & Jahnig, F. 1998, "Adhesion forces of lipids in a phospholipid membrane studied by molecular dynamics simulations", *Biophys.J.*, vol. 74, no. 2 Pt 1, pp. 931-943.
- Massberg, S., Konrad, I., Schurzinger, K., Lorenz, M., Schneider, S., Zohlhoefer, D., Hoppe, K., Schiemann, M., Kennerknecht, E., Sauer, S., Schulz, C., Kerstan, S., Rudelius, M., Seidl, S., Sorge, F., Langer, H., Peluso, M., Goyal, P., Vestweber, D., Emambokus, N. R., Busch, D. H., Frampton, J., & Gawaz, M. 2006, "Platelets secrete stromal cell-derived factor 1alpha and recruit bone marrow-derived progenitor cells to arterial thrombi in vivo", *J.Exp.Med.*, vol. 203, no. 5, pp. 1221-1233.
- Matuszewski, L., Persigehl, T., Wall, A., Schwindt, W., Tombach, B., Fobker, M., Poremba, C., Ebert, W., Heindel, W., & Bremer, C. 2005, "Cell tagging with clinically approved iron oxides: feasibility and effect of lipofection, particle size, and surface coating on labeling efficiency", *Radiology*, vol. 235, no. 1, pp. 155-161.
- McKay, R. 2000, "Stem cells--hype and hope", *Nature.*, vol. 406, no. 6794, pp. 361-364.
- Meyer, H. W. 1972, *A history of electricity and magnetism* Burndy Library.
- Michalopoulos, G. K. & DeFrances, M. C. 1997, "Liver regeneration", *Science*, vol. 276, no. 5309, pp. 60-66.
- Min-Cheol, K., Do-Kyung, K., Se-Hee, L., Amin, M. S., Il-Han, P., Charn-Jung, K., & Zahn, M. 2006, "Dynamic characteristics of superparamagnetic iron oxide nanoparticles in a viscous fluid under an external magnetic field", *Magnetism, IEEE Transactions on*, vol. 42, no. 4, pp. 979-982.
- Miyashiro, J. K., Poppa, V., & Berk, B. C. 1997, "Flow-induced vascular remodeling in the rat carotid artery diminishes with age", *Circ.Res.*, vol. 81, no. 3, pp. 311-319.
- Mourino, M. R. 1991, "From Thales to Lauterbur, or from the lodestone to MR imaging: magnetism and medicine", *Radiology*, vol. 180, no. 3, pp. 593-612.
- Murohara, T. 2001, "Therapeutic vasculogenesis using human cord blood-derived endothelial progenitors", *Trends Cardiovasc.Med.*, vol. 11, no. 8, pp. 303-307.
- Murohara, T., Ikeda, H., Duan, J., Shintani, S., Sasaki, K., Eguchi, H., Onitsuka, I., Matsui, K., & Imaizumi, T. 2000, "Transplanted cord blood-derived endothelial

precursor cells augment postnatal neovascularization", *J.Clin.Invest*, vol. 105, no. 11, pp. 1527-1536.

Murry, C. E., Soonpaa, M. H., Reinecke, H., Nakajima, H., Nakajima, H. O., Rubart, M., Pasumarthi, K. B., Virag, J. I., Bartelmez, S. H., Poppa, V., Bradford, G., Dowell, J. D., Williams, D. A., & Field, L. J. 2004, "Haematopoietic stem cells do not transdifferentiate into cardiac myocytes in myocardial infarcts", *Nature*, vol. 428, no. 6983, pp. 664-668.

Muthana, M., Scott, S. D., Farrow, N., Morrow, F., Murdoch, C., Grubb, S., Brown, N., Dobson, J., & Lewis, C. E. 2008, "A novel magnetic approach to enhance the efficacy of cell-based gene therapies", *Gene Ther.*, vol. 15, no. 12, pp. 902-910.

Nakayama, Y. & Boucher, R. F. 1999, *Introduction to fluid mechanics* Butterworth-Heinemann.

Nelson, K. L. & Runge, V. M. 1995, "Basic principles of MR contrast", *Top.Magn Reson.Imaging*, vol. 7, no. 3, pp. 124-136.

Nussbaum, J., Minami, E., Laflamme, M. A., Virag, J. A., Ware, C. B., Masino, A., Muskheli, V., Pabon, L., Reinecke, H., & Murry, C. E. 2007, "Transplantation of undifferentiated murine embryonic stem cells in the heart: teratoma formation and immune response", *FASEB J.*, vol. 21, no. 7, pp. 1345-1357.

Oliver, M., Entman, M., & Jacob, S. The human cardiovascular system. Encyclopedia Britannica Online . 2009. 14-3-2009.

Ref Type: Electronic Citation

Orive, G., Hernandez, R. M., Gascon, A. R., Igartua, M., & Pedraz, J. L. 2003, "Controversies over stem cell research", *Trends Biotechnol.*, vol. 21, no. 3, pp. 109-112.

Orlic, D. 2005, "BM stem cells and cardiac repair: where do we stand in 2004?", *Cytotherapy.*, vol. 7, no. 1, pp. 3-15.

Orlic, D., Kajstura, J., Chimenti, S., Jakoniuk, I., Anderson, S. M., Li, B., Pickel, J., McKay, R., Nadal-Ginard, B., Bodine, D. M., Leri, A., & Anversa, P. 2001, "Bone marrow cells regenerate infarcted myocardium", *Nature*, vol. 410, no. 6829, pp. 701-705.

Panizzo, R. A., Kyrtatos, P. G., Price, A. N., Gadian, D. G., Ferretti, P., & Lythgoe, M. F. 2009, "In vivo magnetic resonance imaging of endogenous neuroblasts labelled with a ferumoxide-polycation complex", *Neuroimage.*, vol. 44, no. 4, pp. 1239-1246.

Pankhurst, Q., Connolly, J., Jones, S., & Dobson, J. 2003, "Applications of magnetic particles in biomedicine", *J.Phys.D: Appl.Phys.*, vol. 36, pp. 167-181.

Patel, M. I., Tuckerman, R., & Dong, Q. 2005, "A Pitfall of the 3-(4,5-dimethylthiazol-2-yl)-5(3-carboxymethoxyphenol)-2-(4-sulfophenyl)-2H-tetra zolium (MTS) assay due to evaporation in wells on the edge of a 96 well plate", *Biotechnol.Lett.*, vol. 27, no. 11, pp. 805-808.

Peichev, M., Naiyer, A. J., Pereira, D., Zhu, Z., Lane, W. J., Williams, M., Oz, M. C., Hicklin, D. J., Witte, L., Moore, M. A., & Rafii, S. 2000, "Expression of VEGFR-2 and

AC133 by circulating human CD34(+) cells identifies a population of functional endothelial precursors", *Blood*, vol. 95, no. 3, pp. 952-958.

Pislaru, S. V., Harbuzariu, A., Agarwal, G., Witt, T., Gulati, R., Sandhu, N. P., Mueske, C., Kalra, M., Simari, R. D., & Sandhu, G. S. 2006a, "Magnetic forces enable rapid endothelialization of synthetic vascular grafts", *Circulation*, vol. 114, no. 1 Suppl, p. I314-I318.

Pislaru, S. V., Harbuzariu, A., Gulati, R., Witt, T., Sandhu, N. P., Simari, R. D., & Sandhu, G. S. 2006b, "Magnetically targeted endothelial cell localization in stented vessels", *J.Am.Coll.Cardiol.*, vol. 48, no. 9, pp. 1839-1845.

Polyak, B., Fishbein, I., Chorny, M., Alferiev, I., Williams, D., Yellen, B., Friedman, G., & Levy, R. J. 2008, "High field gradient targeting of magnetic nanoparticle-loaded endothelial cells to the surfaces of steel stents", *Proc.Natl.Acad.Sci.U.S.A*, vol. 105, no. 2, pp. 698-703.

Pompilio, G., Capogrossi, M. C., Pesce, M., Alamanni, F., DiCampli, C., Achilli, F., Germani, A., & Biglioli, P. 2009, "Endothelial progenitor cells and cardiovascular homeostasis: clinical implications", *Int J.Cardiol.*, vol. 131, no. 2, pp. 156-167.

Power, C. & Rasko, J. E. 2008, "Whither prometheus' liver? Greek myth and the science of regeneration", *Ann.Intern.Med.*, vol. 149, no. 6, pp. 421-426.

Quaini, F., Urbanek, K., Beltrami, A. P., Finato, N., Beltrami, C. A., Nadal-Ginard, B., Kajstura, J., Leri, A., & Anversa, P. 2002, "Chimerism of the transplanted heart", *N.Engl.J.Med.*, vol. 346, no. 1, pp. 5-15.

Quirici, N., Soligo, D., Caneva, L., Servida, F., Bossolasco, P., & Deliliers, G. L. 2001, "Differentiation and expansion of endothelial cells from human bone marrow CD133(+) cells", *Br.J.Haematol.*, vol. 115, no. 1, pp. 186-194.

Rad, A. M., Iskander, A., Janic, B., Knight, R. A., Arbab, A. S., & Soltanian-Zadeh, H. 2009, "AC133+ progenitor cells as gene delivery vehicle and cellular probe in subcutaneous tumor models: a preliminary study", *BMC.Biotechnol.*, vol. 9, no. 1, p. 28.

Rad, A. M., Janic, B., Iskander, A. S., Soltanian-Zadeh, H., & Arbab, A. S. 2007, "Measurement of quantity of iron in magnetically labeled cells: comparison among different UV/VIS spectrometric methods", *Biotechniques*, vol. 43, no. 5, pp. 627-8, 630, 632.

Rafii, D. C., Psaila, B., Butler, J., Jin, D. K., & Lyden, D. 2008, "Regulation of vasculogenesis by platelet-mediated recruitment of bone marrow-derived cells", *Arterioscler.Thromb.Vasc.Biol.*, vol. 28, no. 2, pp. 217-222.

Ratajczak, M. Z., Zuba-Surma, E. K., Wysoczynski, M., Wan, W., Ratajczak, J., Wojakowski, W., & Kucia, M. 2008, "Hunt for pluripotent stem cell -- regenerative medicine search for almighty cell", *J.Autoimmun.*, vol. 30, no. 3, pp. 151-162.

Raynal, I., Prigent, P., Peyramaure, S., Najid, A., Rebuzzi, C., & Corot, C. 2004, "Macrophage endocytosis of superparamagnetic iron oxide nanoparticles: mechanisms and comparison of ferumoxides and ferumoxtran-10", *Invest Radiol.*, vol. 39, no. 1, pp. 56-63.

- Rehman, J., Li, J., Orschell, C. M., & March, K. L. 2003, "Peripheral blood "endothelial progenitor cells" are derived from monocyte/macrophages and secrete angiogenic growth factors", *Circulation*, vol. 107, no. 8, pp. 1164-1169.
- Reimer, P. & Tombach, B. 1998, "Hepatic MRI with SPIO: detection and characterization of focal liver lesions", *Eur.Radiol.*, vol. 8, no. 7, pp. 1198-1204.
- Reyes, M., Dudek, A., Jahagirdar, B., Koodie, L., Marker, P. H., & Verfaillie, C. M. 2002, "Origin of endothelial progenitors in human postnatal bone marrow", *J.Clin.Invest*, vol. 109, no. 3, pp. 337-346.
- Ribatti, D. 2007, "The discovery of endothelial progenitor cells. An historical review", *Leuk.Res.*, vol. 31, no. 4, pp. 439-444.
- Rippon, H. J. & Bishop, A. E. 2004, "Embryonic stem cells", *Cell Prolif.*, vol. 37, no. 1, pp. 23-34.
- Ritter, J. A., Ebner, A. D., Daniel, K. D., & Stewart, K. L. 2004, "Application of high gradient magnetic separation principles to magnetic drug targeting", *Journal of Magnetism and Magnetic Materials*, vol. 280, no. 2-3, pp. 184-201.
- Rohde, E., Bartmann, C., Schallmoser, K., Reinisch, A., Lanzer, G., Linkesch, W., Guelly, C., & Strunk, D. 2007, "Immune cells mimic the morphology of endothelial progenitor colonies in vitro", *Stem Cells*, vol. 25, no. 7, pp. 1746-1752.
- Rohde, E., Malischnik, C., Thaler, D., Maierhofer, T., Linkesch, W., Lanzer, G., Guelly, C., & Strunk, D. 2006, "Blood monocytes mimic endothelial progenitor cells", *Stem Cells*, vol. 24, no. 2, pp. 357-367.
- Roncalli, J. G., Tongers, J., Renault, M. A., & Losordo, D. W. 2008, "Endothelial progenitor cells in regenerative medicine and cancer: a decade of research", *Trends Biotechnol.*, vol. 26, no. 5, pp. 276-283.
- Ross, R. 1995, "Cell biology of atherosclerosis", *Annu.Rev.Physiol*, vol. 57, pp. 791-804.
- Ross, R. 1999, "Atherosclerosis--an inflammatory disease", *N.Engl.J.Med.*, vol. 340, no. 2, pp. 115-126.
- Ross, R., Glomset, J., & Harker, L. 1977, "Response to injury and atherogenesis", *Am.J.Pathol.*, vol. 86, no. 3, pp. 675-684.
- Rossi, M. L., Zavalloni, D., Gasparini, G. L., Mango, R., Belli, G., & Presbitero, P. 2009, "The first report of late stent thrombosis leading to acute myocardial infarction in patient receiving the new endothelial progenitor cell capture stent", *Int J.Cardiol.*
- Rotmans, J. I., Heyligers, J. M., Verhagen, H. J., Velema, E., Nagtegaal, M. M., de Kleijn, D. P., de Groot, F. G., Stroes, E. S., & Pasterkamp, G. 2005, "In vivo cell seeding with anti-CD34 antibodies successfully accelerates endothelialization but stimulates intimal hyperplasia in porcine arteriovenous expanded polytetrafluoroethylene grafts", *Circulation*, vol. 112, no. 1, pp. 12-18.

Santiago, F. S., Ishii, H., Shafi, S., Khurana, R., Kanellakis, P., Bhindi, R., Ramirez, M. J., Bobik, A., Martin, J. F., Chesterman, C. N., Zachary, I. C., & Khachigian, L. M. 2007, "Yin Yang-1 inhibits vascular smooth muscle cell growth and intimal thickening by repressing p21WAF1/Cip1 transcription and p21WAF1/Cip1-Cdk4-cyclin D1 assembly", *Circ.Res.*, vol. 101, no. 2, pp. 146-155.

Schachinger, V., Assmus, B., Britten, M. B., Honold, J., Lehmann, R., Teupe, C., Abolmaali, N. D., Vogl, T. J., Hofmann, W. K., Martin, H., Dimmeler, S., & Zeiher, A. M. 2004, "Transplantation of progenitor cells and regeneration enhancement in acute myocardial infarction: final one-year results of the TOPCARE-AMI Trial", *J.Am.Coll.Cardiol.*, vol. 44, no. 8, pp. 1690-1699.

Schillinger, U., Brill, T., Rudolph, C., Huth, S., Gersting, S., Krötz, F., Hirschberger, J., Bergemann, C., & Plank, C. 2005, "Advances in magnetofection--magnetically guided nucleic acid delivery", *Journal of Magnetism and Magnetic Materials*, vol. 293, no. 1, pp. 501-508.

Schipper, L. F., Brand, A., Reniers, N. C., Melief, C. J., Willemze, R., & Fibbe, W. E. 1998, "Effects of thrombopoietin on the proliferation and differentiation of primitive and mature haemopoietic progenitor cells in cord blood", *Br.J.Haematol.*, vol. 101, no. 3, pp. 425-435.

Schmeisser, A., Garlich, C. D., Zhang, H., Eskafi, S., Graffy, C., Ludwig, J., Strasser, R. H., & Daniel, W. G. 2001, "Monocytes coexpress endothelial and macrophagocytic lineage markers and form cord-like structures in Matrigel under angiogenic conditions", *Cardiovasc.Res.*, vol. 49, no. 3, pp. 671-680.

Schmitt, R. 2002, "Fundamentals of Magnetic Fields," in *Electromagnetics Explained*, S. Ron, ed., Newnes, Burlington, pp. 51-74.

Segers, V. F. & Lee, R. T. 2008, "Stem-cell therapy for cardiac disease", *Nature*, vol. 451, no. 7181, pp. 937-942.

Serruys, P. W., de, J. P., Kiemeneij, F., Macaya, C., Rutsch, W., Heyndrickx, G., Emanuelsson, H., Marco, J., Legrand, V., Materne, P., & . 1994, "A comparison of balloon-expandable-stent implantation with balloon angioplasty in patients with coronary artery disease. Benestent Study Group", *N.Engl.J.Med.*, vol. 331, no. 8, pp. 489-495.

Serruys, P. W., Kutryk, M. J., & Ong, A. T. 2006, "Coronary-artery stents", *N.Engl.J.Med.*, vol. 354, no. 5, pp. 483-495.

Shaughnessy, E. J., Katz, I. M., & Schaffer, J. P. 2005, *Introduction to fluid dynamics* Oxford University Press.

Shi, Q., Rafii, S., Wu, M. H., Wijelath, E. S., Yu, C., Ishida, A., Fujita, Y., Kothari, S., Mohle, R., Sauvage, L. R., Moore, M. A., Storb, R. F., & Hammond, W. P. 1998, "Evidence for circulating bone marrow-derived endothelial cells", *Blood*, vol. 92, no. 2, pp. 362-367.

Shintani, S., Murohara, T., Ikeda, H., Ueno, T., Honma, T., Katoh, A., Sasaki, K., Shimada, T., Oike, Y., & Imaizumi, T. 2001, "Mobilization of endothelial progenitor

cells in patients with acute myocardial infarction", *Circulation*, vol. 103, no. 23, pp. 2776-2779.

Shmelkov, S. V., St, C. R., Lyden, D., & Rafii, S. 2005, "AC133/CD133/Prominin-1", *Int.J.Biochem.Cell Biol.*, vol. 37, no. 4, pp. 715-719.

Smith, B. R. 1990, "Regulation of hematopoiesis", *Yale J.Biol.Med.*, vol. 63, no. 5, pp. 371-380.

Srinivas, G., Anversa, P., & Frishman, W. H. 2009, "Cytokines and myocardial regeneration: a novel treatment option for acute myocardial infarction", *Cardiol.Rev.*, vol. 17, no. 1, pp. 1-9.

Stahli, B. E., Camici, G. G., & Tanner, F. C. 2009, "Drug-eluting stent thrombosis", *Ther.Adv.Cardiovasc.Dis.*, vol. 3, no. 1, pp. 45-52.

Stamm, C., Kleine, H. D., Choi, Y. H., Dunkelmann, S., Lauffs, J. A., Lorenzen, B., David, A., Liebold, A., Nienaber, C., Zurakowski, D., Freund, M., & Steinhoff, G. 2007, "Intramyocardial delivery of CD133+ bone marrow cells and coronary artery bypass grafting for chronic ischemic heart disease: safety and efficacy studies", *J.Thorac.Cardiovasc.Surg.*, vol. 133, no. 3, pp. 717-725.

Stocum, D. L. & Zupanc, G. K. 2008, "Stretching the limits: stem cells in regeneration science", *Dev.Dyn.*, vol. 237, no. 12, pp. 3648-3671.

Strehlow, K., Werner, N., Berweiler, J., Link, A., Dirnagl, U., Priller, J., Laufs, K., Ghaeni, L., Milosevic, M., Bohm, M., & Nickenig, G. 2003, "Estrogen increases bone marrow-derived endothelial progenitor cell production and diminishes neointima formation", *Circulation*, vol. 107, no. 24, pp. 3059-3065.

Sun, R., Dittrich, J., Le-Huu, M., Mueller, M. M., Bedke, J., Kartenbeck, J., Lehmann, W. D., Krueger, R., Bock, M., Huss, R., Seliger, C., Grone, H. J., Misselwitz, B., Semmler, W., & Kiessling, F. 2005, "Physical and biological characterization of superparamagnetic iron oxide- and ultrasmall superparamagnetic iron oxide-labeled cells: a comparison", *Invest Radiol.*, vol. 40, no. 8, pp. 504-513.

Swijnenburg, R. J., Tanaka, M., Vogel, H., Baker, J., Kofidis, T., Gunawan, F., Lebl, D. R., Caffarelli, A. D., de Bruin, J. L., Fedoseyeva, E. V., & Robbins, R. C. 2005, "Embryonic stem cell immunogenicity increases upon differentiation after transplantation into ischemic myocardium", *Circulation*, vol. 112, no. 9 Suppl, p. I166-I172.

Takahashi, H., Letourneur, D., & Grainger, D. W. 2007, "Delivery of large biopharmaceuticals from cardiovascular stents: a review", *Biomacromolecules.*, vol. 8, no. 11, pp. 3281-3293.

Tateishi-Yuyama, E., Matsubara, H., Murohara, T., Ikeda, U., Shintani, S., Masaki, H., Amano, K., Kishimoto, Y., Yoshimoto, K., Akashi, H., Shimada, K., Iwasaka, T., & Imaizumi, T. 2002, "Therapeutic angiogenesis for patients with limb ischaemia by autologous transplantation of bone-marrow cells: a pilot study and a randomised controlled trial", *Lancet*, vol. 360, no. 9331, pp. 427-435.

- Thomson, J. A., Itskovitz-Eldor, J., Shapiro, S. S., Waknitz, M. A., Swiergiel, J. J., Marshall, V. S., & Jones, J. M. 1998, "Embryonic stem cell lines derived from human blastocysts", *Science*, vol. 282, no. 5391, pp. 1145-1147.
- Urbich, C. & Dimmeler, S. 2005, "Risk factors for coronary artery disease, circulating endothelial progenitor cells, and the role of HMG-CoA reductase inhibitors", *Kidney Int.*, vol. 67, no. 5, pp. 1672-1676.
- Urbich, C. & Dimmeler, S. 2004, "Endothelial progenitor cells: characterization and role in vascular biology", *Circ.Res.*, vol. 95, no. 4, pp. 343-353.
- Urbich, C., Heeschen, C., Aicher, A., Dernbach, E., Zeiher, A. M., & Dimmeler, S. 2003, "Relevance of monocytic features for neovascularization capacity of circulating endothelial progenitor cells", *Circulation*, vol. 108, no. 20, pp. 2511-2516.
- van Beusekom, H. M., Saia, F., Zindler, J. D., Lemos, P. A., Swager-Ten Hoor, S. L., van Leeuwen, M. A., de Feijter, P. J., Serruys, P. W., & van der Giessen, W. J. 2007, "Drug-eluting stents show delayed healing: paclitaxel more pronounced than sirolimus", *Eur.Heart J.*, vol. 28, no. 8, pp. 974-979.
- van Beusekom, H. M., Whelan, D. M., Hofma, S. H., Krabbendam, S. C., van, H., V, Verdouw, P. D., & van der Giessen, W. J. 1998, "Long-term endothelial dysfunction is more pronounced after stenting than after balloon angioplasty in porcine coronary arteries", *J.Am.Coll.Cardiol.*, vol. 32, no. 4, pp. 1109-1117.
- Vasa, M., Fichtlscherer, S., Adler, K., Aicher, A., Martin, H., Zeiher, A. M., & Dimmeler, S. 2001a, "Increase in circulating endothelial progenitor cells by statin therapy in patients with stable coronary artery disease", *Circulation*, vol. 103, no. 24, pp. 2885-2890.
- Vasa, M., Fichtlscherer, S., Aicher, A., Adler, K., Urbich, C., Martin, H., Zeiher, A. M., & Dimmeler, S. 2001b, "Number and migratory activity of circulating endothelial progenitor cells inversely correlate with risk factors for coronary artery disease", *Circ.Res.*, vol. 89, no. 1, p. E1-E7.
- Vaughan, C. J., Gotto, A. M., & Basson, C. T. 2000, "The evolving role of statins in the management of atherosclerosis", *J.Am.Coll.Cardiol.*, vol. 35, no. 1, pp. 1-10.
- Vermes, I., Haanen, C., Steffens-Nakken, H., & Reutelingsperger, C. 1995, "A novel assay for apoptosis. Flow cytometric detection of phosphatidylserine expression on early apoptotic cells using fluorescein labelled Annexin V", *J.Immunol.Methods.*, vol. 184, no. 1, pp. 39-51.
- Voltairas, P. A., Fotiadis, D. I., & Michalis, L. K. 2002, "Hydrodynamics of magnetic drug targeting", *Journal of Biomechanics*, vol. 35, no. 6, pp. 813-821.
- Voo, S., Rats, R., Donners, M., & Waltenberger, J. Circulating progenitor cells differentiate into 'foam-cell'-like cells under the influence of oxidized LDL: evidence for a causal involvement of progenitor cells in atherosclerosis development. European Society of Cardiology Congress , 4612. 2008.
- Ref Type: Abstract

W.H.O. Cardiovascular Disease Fact Sheet 317.

<http://www.who.int/mediacentre/factsheets/fs317/en/index.html> . 2007. 14-3-2009.

Ref Type: Electronic Citation

Walter, D. H., Cejna, M., az-Sandoval, L., Willis, S., Kirkwood, L., Stratford, P. W., Tietz, A. B., Kirchmair, R., Silver, M., Curry, C., Wecker, A., Yoon, Y. S., Heidenreich, R., Hanley, A., Kearney, M., Tio, F. O., Kuenzler, P., Isner, J. M., & Losordo, D. W. 2004, "Local gene transfer of phVEGF-2 plasmid by gene-eluting stents: an alternative strategy for inhibition of restenosis", *Circulation*, vol. 110, no. 1, pp. 36-45.

Walter, D. H., Rittig, K., Bahlmann, F. H., Kirchmair, R., Silver, M., Murayama, T., Nishimura, H., Losordo, D. W., Asahara, T., & Isner, J. M. 2002, "Statin therapy accelerates reendothelialization: a novel effect involving mobilization and incorporation of bone marrow-derived endothelial progenitor cells", *Circulation*, vol. 105, no. 25, pp. 3017-3024.

Walter, D. H., Zeiher, A. M., & Dimmeler, S. 2004, "Effects of statins on endothelium and their contribution to neovascularization by mobilization of endothelial progenitor cells", *Coron.Artery Dis.*, vol. 15, no. 5, pp. 235-242.

Wang, C. H., Cherng, W. J., Yang, N. I., Kuo, L. T., Hsu, C. M., Yeh, H. I., Lan, Y. J., Yeh, C. H., & Stanford, W. L. 2008, "Late-outgrowth endothelial cells attenuate intimal hyperplasia contributed by mesenchymal stem cells after vascular injury", *Arterioscler.Thromb.Vasc.Biol.*, vol. 28, no. 1, pp. 54-60.

Wang, S., Liu, H., & Xu, W. 2008, "Hydrodynamic modelling and CFD simulation of ferrofluids flow in magnetic targeting drug delivery", *International Journal of Computational Fluid Dynamics*, vol. 22, no. 10, pp. 659-667.

Wang, Y. X., Hussain, S. M., & Krestin, G. P. 2001, "Superparamagnetic iron oxide contrast agents: physicochemical characteristics and applications in MR imaging", *Eur.Radiol.*, vol. 11, no. 11, pp. 2319-2331.

Weissleder, R., Stark, D. D., Engelstad, B. L., Bacon, B. R., Compton, C. C., White, D. L., Jacobs, P., & Lewis, J. 1989, "Superparamagnetic iron oxide: pharmacokinetics and toxicity", *AJR Am.J.Roentgenol.*, vol. 152, no. 1, pp. 167-173.

Welt, F. G. & Losordo, D. W. 2006, "Cell therapy for acute myocardial infarction: curb your enthusiasm?", *Circulation*, vol. 113, no. 10, pp. 1272-1274.

Werner, N., Junk, S., Laufs, U., Link, A., Walenta, K., Bohm, M., & Nickenig, G. 2003, "Intravenous transfusion of endothelial progenitor cells reduces neointima formation after vascular injury", *Circ.Res.*, vol. 93, no. 2, p. e17-e24.

Werner, N., Kosiol, S., Schiegl, T., Ahlers, P., Walenta, K., Link, A., Bohm, M., & Nickenig, G. 2005, "Circulating endothelial progenitor cells and cardiovascular outcomes", *N.Engl.J.Med.*, vol. 353, no. 10, pp. 999-1007.

Werner, N. & Nickenig, G. 2006, "Influence of cardiovascular risk factors on endothelial progenitor cells: limitations for therapy?", *Arterioscler.Thromb.Vasc.Biol.*, vol. 26, no. 2, pp. 257-266.

- Werner, N., Priller, J., Laufs, U., Endres, M., Bohm, M., Dirnagl, U., & Nickenig, G. 2002, "Bone marrow-derived progenitor cells modulate vascular reendothelialization and neointimal formation: effect of 3-hydroxy-3-methylglutaryl coenzyme a reductase inhibition", *Arterioscler.Thromb.Vasc.Biol.*, vol. 22, no. 10, pp. 1567-1572.
- Westbrook, C., Roth, C. K., & Talbot, J. 2005, "Basic Principles," in *MRI in Practice*, 3rd edn, Blackwell Publishing Ltd, Oxford.
- Wilhelm, C., Billotey, C., Roger, J., Pons, J. N., Bacri, J. C., & Gazeau, F. 2003a, "Intracellular uptake of anionic superparamagnetic nanoparticles as a function of their surface coating", *Biomaterials.*, vol. 24, no. 6, pp. 1001-1011.
- Wilhelm, C., Cebers, A., Bacri, J. C., & Gazeau, F. 2003b, "Deformation of intracellular endosomes under a magnetic field", *Eur.Biophys.J.*, vol. 32, no. 7, pp. 655-660.
- Wilhelm, C., Gazeau, F., & Bacri, J. C. 2002, "Magnetophoresis and ferromagnetic resonance of magnetically labeled cells", *Eur.Biophys.J.*, vol. 31, no. 2, pp. 118-125.
- Wilson, M. W., Kerlan, R. K., Jr., Fidelman, N. A., Venook, A. P., LaBerge, J. M., Koda, J., & Gordon, R. L. 2004, "Hepatocellular carcinoma: regional therapy with a magnetic targeted carrier bound to doxorubicin in a dual MR imaging/ conventional angiography suite--initial experience with four patients", *Radiology*, vol. 230, no. 1, pp. 287-293.
- Yellen, B. B., Forbes, Z. G., Halverson, D. S., Fridman, G., Barbee, K. A., Chorny, M., Levy, R., & Friedman, G. 2005, "Targeted drug delivery to magnetic implants for therapeutic applications", *Journal of Magnetism and Magnetic Materials*, vol. 293, no. 1, pp. 647-654.
- Yin, A. H., Miraglia, S., Zanjani, E. D., meida-Porada, G., Ogawa, M., Leary, A. G., Olweus, J., Kearney, J., & Buck, D. W. 1997, "AC133, a novel marker for human hematopoietic stem and progenitor cells", *Blood*, vol. 90, no. 12, pp. 5002-5012.
- Zammaretti, P. & Zisch, A. H. 2005, "Adult 'endothelial progenitor cells'. Renewing vasculature", *Int.J.Biochem.Cell Biol.*, vol. 37, no. 3, pp. 493-503.
- Zampetaki, A., Kirton, J. P., & Xu, Q. 2008, "Vascular repair by endothelial progenitor cells", *Cardiovasc.Res.*, vol. 78, no. 3, pp. 413-421.
- Zohlhofer, D., Dibra, A., Koppa, T., de, W. A., Ripa, R. S., Kastrup, J., Valgimigli, M., Schomig, A., & Kastrati, A. 2008, "Stem cell mobilization by granulocyte colony-stimulating factor for myocardial recovery after acute myocardial infarction: a meta-analysis", *J.Am.Coll.Cardiol.*, vol. 51, no. 15, pp. 1429-1437.

APPENDIX A

METHODOLOGICAL DEVELOPMENTS

A.1 - Absorbance spectrum of Prussian Blue

There was an increase in absorbance between 560 and 900nm when the PrB solution reacted with the iron in SPIO, with peak absorbance at 690nm, 0.21 absorbance units (au). This was 4-fold higher than PrB (peak = 0.07 au) or SPIO alone (peak = 0.09 au).

Figure A.1 is a summary of the absorbance profile within the range 405-900nm of **i)** PrB staining solution + SPIO, **ii)** SPIO only and **iii)** PrB staining solution only, using the microplate spectrophotometer and available filters.

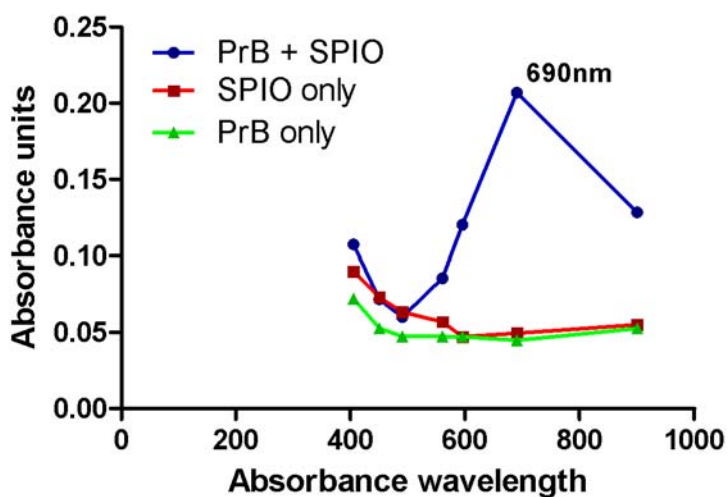


Figure A.1 - Absorbance profile of Prussian Blue

A.2 Effect of cell lysis buffer on the Prussian Blue reaction

Addition of lysis buffer slowed down the production of the PrB colour and led to an approximately 14% decrease in maximum absorbance at 690nm. Figure A.2 demonstrates the increase in absorbance with time immediately following the addition of PrB staining solution to **i)** SPIO + lysis buffer and **ii)** SPIO + PBS. Table A.1 is a summary of the maximum absorbance values and time to reach half-maximum, as estimated from the spline curve coordinates.

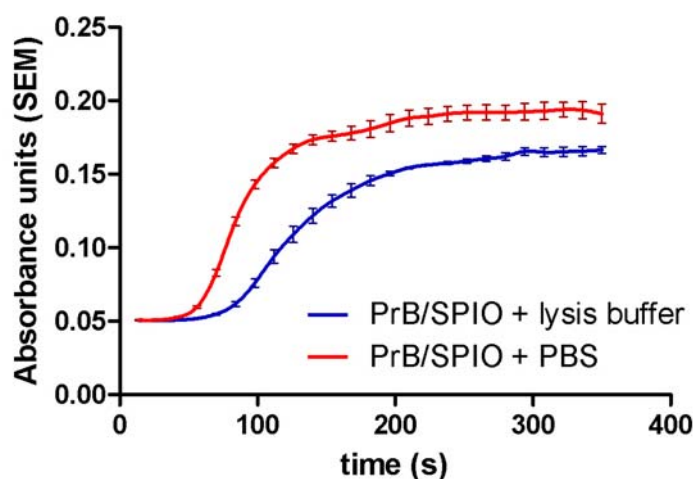


Figure A.2 - Prussian blue with lysis buffer
The solid lines are cubic spline curves connecting the data points.

Table A.1 – Prussian blue with lysis buffer

	(i) PrB / SPIO + lysis buffer (SEM, n=3)	(ii) PrB / SPIO + PBS (SEM, n=3)
Max absorbance units	0.167 (0.003)	0.191 (0.007)
Time to reach max/2	105 seconds	75 seconds

To reduce the resulting error in subsequent experiments, cell lysis buffer was added in equal amounts even in the absence of cells.

Figure A.3 illustrates the absorbance at 690nm following PrB staining of cell lysates.

The data is summarised in Table A.2.

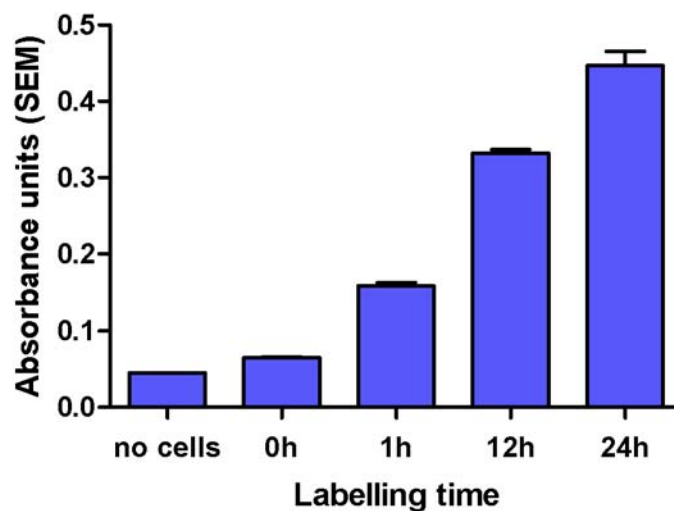


Figure A.3 – Labelling timecourse - absorbance at 690nm

Table A.2 – Labelling timecourse - absorbance at 690nm

Labelling time	Mean absorbance units (SEM $\times 10^{-3}$), n=3
No cells*	0.045 (0.4)
0 h*	0.065 (1)
1 h	0.159 (5)
12 h	0.332 (5)
24 h	0.447 (18)

In the control group (0h), the presence of cells caused a small increase in absorbance by 0.02 au above the no-cells baseline ($0.065 - 0.045 = 0.02$).

Figure A.4 displays a standard curve for the absorbance of Endorem® following the PrB reaction.

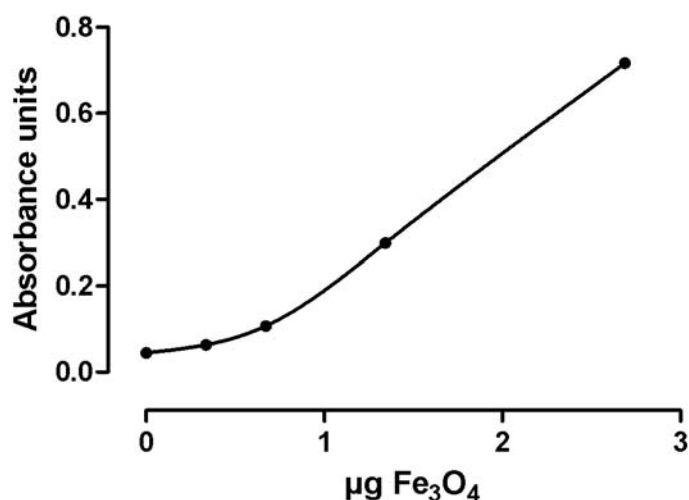


Figure A.4 – Standard curve for iron quantification

The coordinates of the spline curve were used to estimate the Fe₃O₄ content of each well. For a more accurate quantification, the excess 0.02 au due to the presence of the cells was first subtracted to produce a corrected absorbance value. This was then used to estimate the Fe₃O₄ content of each well and, assuming 1.5×10^5 cells / well, the average iron content of adherent cells. These results are summarised in Table A.3 and Figure 4.5.

Table A.3 - Labelling timecourse - estimation of cellular iron content

Labelling time	Corrected absorbance units (SEM), n=3	Fe ₃ O ₄ content / well Mean, µg (SEM), n=3	Fe ₃ O ₄ content / cell Mean, pg (SEM), n=3
0 h	0.045 (0.001)	0.013 (0.013)	0.09 (0.09)
1 h	0.139 (0.005)	0.815 (0.019)	5.4 (0.12)
12 h	0.312 (0.005)	1.384 (0.014)	9.2 (0.09)
24 h	0.427 (0.018)	1.744 (0.059)	11.6 (0.39)

A.3 Water evaporation from 96-well plates

There was marked evaporation of water from 96-well plates. This evaporation was increased in corner wells (exactly where the magnets are placed in the magnetic plate) than centre wells. Filling the rest of the plate with PBS minimised evaporation. Table A.4 and Figure A.5 display the amount of water evaporation in 48h, from 4 corner or 4 centre wells, in the two 96-well plates with/without flooding with PBS.

Table A.4 – Water evaporation in 96-well plates

At 48h	Corner wells (Mean $\mu\text{L} \pm \text{SEM}$)	Centre wells (Mean $\mu\text{L} \pm \text{SEM}$)
Without flooding	56.4 (1.6)	28.7 (0.9)
With flooding	5.5 (2.7)	6 (2.1)

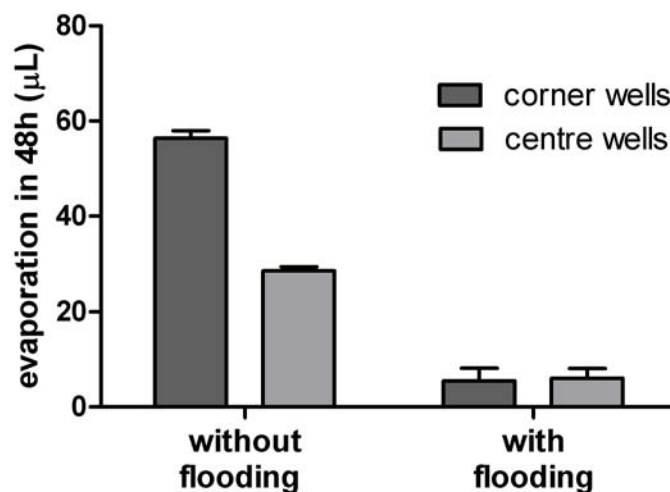


Figure A.5 – Water evaporation in 96-well plates

APPENDIX B

FULL TABLES

B.1 Full tables for Figures 4.5, 5.3 and 5.5.**Table B.1 – Full table for Figure 4.5**

Labelling time (n=3)	Mean Fe ₃ O ₄ (pg, SEM)	Comparison groups ¹	Mean difference	95% CI difference	p-value
0h	0.1 (0.1)	0h vs 1h	-5.4	-6.3 to -4.4	<0.001
1h	5.4 (0.1)	0h vs 12h	-9.1	-10.1 to -8.2	<0.001
12h	9.3 (0.1)	0h vs 24h	-11.5	-12.5 to -10.6	<0.001
24h	11.6 (0.4)	1h vs 12h	-3.8	-4.8 to -2.8	<0.001
		1h vs 24h	-6.2	-7.2 to -5.2	<0.001
		12h vs 24h	-2.4	-3.4 to -1.4	<0.001

¹ One-way ANOVA with Tukey's post-hoc multiple comparison test

Table B.2 – Full table for Figure 5.3

	Early apoptosis				Late apoptosis				Necrosis			
	24 h		72 h		24 h		72 h		24 h		72 h	
	control	DfL	control	DfL	control	DfL	control	DfL	control	DfL	control	DfL
Mean %	6.49	5.70	3.74	4.12	2.13	2.01	2.37	2.23	0.04	0.05	0.09	0.09
SEM (n=8)	0.78	0.90	0.50	0.65	0.41	0.44	0.41	0.41	0.01	0.02	0.03	0.02

Table B.3 – Full table for Figure 5.5

	Early apoptosis						Late apoptosis						Necrosis					
	24 h		48 h		120 h		24 h		48 h		120 h		24 h		48 h		120 h	
	DfL	DfL + magnet	DfL	DfL + magnet	DfL	DfL + magnet	DfL	DfL + magnet	DfL	DfL + magnet	DfL	DfL + magnet	DfL	DfL + magnet	DfL	DfL + magnet	DfL	DfL + magnet
Mean %	9.39	9.03	4.85	5.36	3.14	3.40	3.42	3.27	3.13	3.65	1.54	1.51	0.08	0.05	0.06	0.06	0.08	0.31
SEM (n=6)	1.35	1.73	1.22	1.24	0.37	0.75	0.29	0.30	0.52	0.74	0.18	0.23	0.01	0.01	0.01	0.00	0.01	0.27

Table B.4 – Full table for Figure 5.8

	Mean marker expression (% , SEM)			
	Suspension		Adherent	
	control	DfL	control	DfL
VE-Cad (n=6)	1.82 (0.57)	2.30 (0.89)	10.40 (3.88)	5.70 (1.67)
CD304 (n=6)	4.36 (1.69)	5.08 (1.95)	38.47 (4.95)	29.34 (4.59)
CD14 (n=6)	8.95 (0.99)	12.24 (2.34)	43.78 (5.93)	44.82 (5.54)
CD11b (n=3)	16.26 (10.52)	17.03 (9.99)	3.37 (0.54)	3.21 (0.30)

APPENDIX C

MTS ASSAY

This appendix presents the rationale for removing ascorbic acid from the MTS assay medium. MTS positive controls are also shown.

Figure C.1 displays the absorbance at 490nm, for media only and cells. Media only was left to react with the MTS reagent for 4 hours (left side of graph). The presence of ascorbic acid in the normal growth medium used for cell culture (4.2.2.1) reacted with the MTS reagent and resulted in high absorbance values. Subsequently, the medium used for the MTS assays was the normal medium, less ascorbic acid.

The right side of the graph displays the effect of a 24h serum deprivation on the MTS results absorbance results (1% FBS instead of 20%). There was a significant decrease in 490nm absorbance (mean difference=0.035, 95% CI -0.063 to -0.007, $p=0.03$, unpaired t-test). The same serum deprivation caused a 16% increase in early apoptosis and a 3% increase in late apoptosis (not shown). These values were used as the basis of the equivalence testing in Chapter 5 (section 5.2.9).

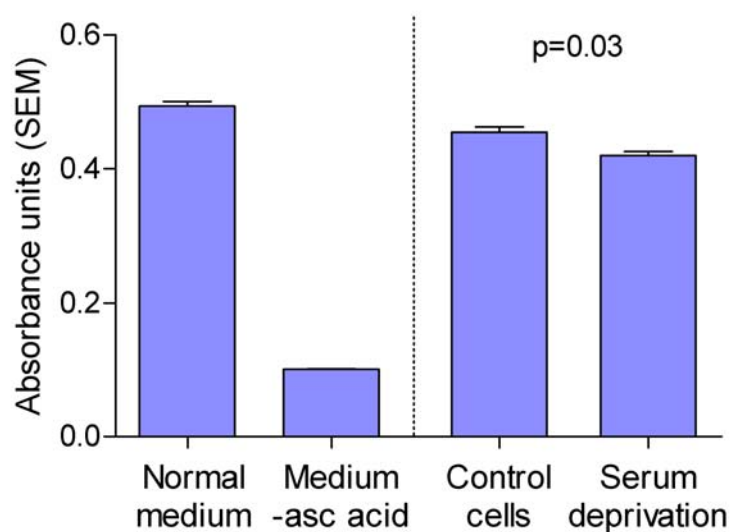


Figure C.1 – MTS assay absorbance at 490nm

(Asahara & Kawamoto 2004) for
Figure 1.2

(Carter et al. 2004) for Figure 1.9

(Thomson et al. 1998)

(Lee et al. 2003) for Figure 2.6